Development of Small Molecules to Target and Modulate Multiple Factors in the Neuropathogenesis of Alzheimer's Disease

by

Akiko Kochi

A dissertation submitted in partial fulfillment
of the requirements for the degree of
Doctor of Philosophy
(Chemistry)
in the University of Michigan
2014

Doctoral Committee:

Associate Professor Mi Hee Lim, Chair
Professor Raoul Kopelman
Assistant Professor Kenichi Kuroda
Assistant Professor Zaneta Nikolovska-Coleska

最愛なる両親へ捧げたいと思います。
自由に伸び伸びと育ててくれて、
何時でも温かく見守ってくれて感謝しています。
To my significant other, Zachery Kirkland and my cats
(Artemis, Apollo, and Toramame)
with the utmost gratitude for their unconditional love and support.
With all my heart, love always.

Acknowledgments

Word cannot express the gratitude for my advisor Professor Mi Hee Lim, for her constant guidance and patience during my Ph.D. Her motivation, enthusiasm, and knowledge for her research are awe-inspiring. The major reason I was able to conduct this research and prepare this dissertation is because of my advisor, who goes above and beyond expectations to help her students succeed. I am truly indebted for the time spent educating me as a researcher, for the opportunity to try everything at the University of Michigan as well as for the experience at Ulsan National Institute of Science and Technology (UNIST) in Ulsan, Korea, and for her belief in me and providing me nonstop support. I am humbled and proud to be graduating from her lab, knowing that this experience has given me the confidence to tackle and overcome any challenges. I am excited to see what kind of outstanding science comes from the Lim lab in the future.

My sincere thanks go to my committee members: Professors Raoul Kopelman, Kenichi Kuroda, and Zaneta Nikolovska-Coleska for their encouragement, insightful comments and critiques during data meetings to better myself as a research scientist.

I would like to extend a great debt of gratitude to my collaborators that I share credit with on my work for various projects. I would like to take the opportunity to thank a few collaborators here, without whom my dissertation would not be complete. I am grateful for Yihong Liu for her support as well as taking the time to teach me cell culture. I would like to thank Dr. Xiaoming He, Dr. Sanghyun Lee, and Dr. Masha Savelieff for their mentorship and collaboration. I have had the opportunity to work with great undergraduates, Yuzhong Liu, who was instrumental in work for tuning the diphenylpropynone derivatives and Lauren Lendzion, a Perrigo Fellowship student from Michigan State University. The past and current members of the Lim group have contributed immensely in my path to becoming a scientist. The group has been an excellent source for scientific to and fro, collaborations, as well as great friendships. I

would like to especially thank a few members who have been influential in my Ph.D.: Dr. Joey Braymer, Dr. Alaina DeToma, Nichole Schmidt, Hyun Min Park, Amit Pithadia, Jin Hoon Kim, Juhye Kang, Michael Beck, Hyuck Jin Lee, Kyle Korshavn, Younwoo Nam, Milim Jang, and Jeffrey Derrick.

My time at the University of Michigan was made enjoyable due to my friends and especially fellow lab members whose friendship went beyond our collaboration. First I would like to thank to extend my upmost gratitude and appreciation to Dr. Alaina DeToma. She has been nothing but encouraging and supportive through the rough times. Without you, I probably would have been able to get through this experience. I truly am blessed with having a friend like you in my life, acknowledging that we are both weird and love Dr. Who! “Good game coach!” Yuzhong Liu, my lovely undergraduate who has shown so much patience. I liked our conversations at 2 am while making revisions on the manuscript. I can’t wait to see your excellent work at UC Berkeley! Jeff Derrick, my “little baby bro” whom I got to know the past year. Thanks for giving me a shoulder to whine on when things are tough overseas. Your support and friendship means more than you’ll ever know and thanks for being such a great buddy! “Time to wake up Jeffrey~” I know you have the brightest future ahead of you! Kyle Korshavn, my other “cat-lady/gentleman-in-training.” First person that I actually opened up to, who sat next to me in lab. Thanks for all the lovely Roz pictures to lift my spirits up. It was weird to find someone with so much in common, but I am glad to have the chance to get to know you better as a lab member and a friend. I am grateful to Hyuck Jin Lee, who has made the transition of doing research at UNIST as easy as possible. Thank you for being my unofficial translator! “I’m just curious…” I know that your curiosity for science will take you far. Thanks to Michael Beck for the laughs and support at UNIST as I finish up my Ph.D. Ah, two great minds do think alike, I’m glad that I was able to become better friends with you in Korea!! Kimbop heaven or Grandma’s house for dinner? Younwoo Nam, thank you for teaching me how to do ITC and being patient and answering all my questions. I know that my first impression wasn’t the best, but I’m really happy that we bonded and talked in the middle of the night when we were both scrambling to make our group presentation. I know that you will be an excellent addition to our Lim group! To my Korean girls, Milim Jang and Juhye Kang, thank you for being

so supportive (especially Milim who has been there at my side through the rough spots in life) and for all the wonderful memories that I made in Korea. I am fortunate to have the opportunity to meet you two and become better friends with guys! 사랑해~

Without the support from family and friends, none of this would have been possible. To everyone I had been blessed to know academically, your support and friendship means the world to me. Thank you all the encouragement!

To Lydia-Ann, thanks for being the rock and my sanity through this process. I'm glad to have stirred up the courage to talk to you about your chucks. From there, an awesome friendship has blossomed. I can't express how much your friendship means to me, I'm proud to have someone like you to call a friend, to hang out for stress relief as well as have in depth discussion about science.

To sisters, Ryoko (よよ姉) and Ayako (ヤーモ), I know that we aren't the closest of siblings, but your support is greatly appreciated. Chats via kakaotalk have been highly entertaining, a welcomed stress relief, and feel it brought us closer together. I hope that we can get all together and go to the hot springs in Japan.

To Zach, how do I express my gratitude to a guy who has been nothing but supportive throughout this whole process. I'm glad to have been able to share this experience with you and can't wait to see what's in the future for us. Thank you for being so understanding (or at least try to be) and putting up with all my shenanigans. I love you so much! To my kids (cats), Artemis, Apollo, and Toramame, thanks for being a sympathetic ear when I just needed to vent. I know you guys are cats, but having you three in my life has made it so much better. Mimi, I know that you're in a better place now, thanks for being a part of my family. You'll always be in my heart. Mama loves you.

Last and certainly not least, I want to thank my parents. Thank you for not being overbearing parents. Because of the freedom that you have given me, I was able to pursue my life path that gotten me to where I am today. Thank you the support and love. I strive to be a better person and model myself to be half the person that both of you are. I love you both more than you know, although I don't express well, and I'm honored to have my mom and dad as my parents. Nothing but gratitude and respect.

Table of Contents

List of Tables

List of Figures

List of Abbreviations

8-HQ	8-Hydroxyquinoline
Aβ	Amyloid-β
ABTS	2,2‘-Azino-bis(3-ethylbenzothiaxoline-6-sulfonic acid
ACh	Acetycholine
AChE	Acetylcholinesterase
AChEi	Acetylcholinesterase inhibitor
AD	Alzheimer’s disease
ALS	Amyotrophic lateral sclerosis
APP	Amyloid precursor protein
ATP	Adenosine triphosphate
ATC	Acetylthiocholine
BBB	Blood-brain barrier
BChE	Butylcholinesterase
BSA	Bovine serum albumin
BSB	Brain sink buffer
BTC	Buturylthiocholine
CAS	Catalytic active site
CcO	Cytochrome *c* oxidase
$CDCl_3$	Deuterated chloroform
$CDCN_3$	Deuterated acetonitrile
CH_2Cl_2	Dichloromethane
CH_3OH	Methanol
clog*P*	Calculated logarithm of octonal-water partition coefficient
CNS	Central nervous system
CO_2	Carbon dioxide
Cp	Ceruloplasmin
CQ	Clioquinol

Cu	Copper
$CuCl_2$	Copper(II) chloride
CuI	Copper(I) iodide
Cur	Curcumin
DCC	Dicyclohexylcarbodiimide
ddH_2O	Double-distilled water
DETAPAC	Diethylenetriaminepentaacetic acid
DMEM	Dulbecco's modified Eagle medium
DPP	Diphenylpropynone
DMAP	Dimethylaminopyridine
DMSO	Dimethyl sulfoxide
DTNB	5,5'-Dithiobis-(2-nitrobenzoic acid)
*Ee*AChE	AChE from *Electrophorus electricus*
*es*BChE	BChE from equine serum
EGCG	(−)-Epigallocatechin-3-gallate
ESI	Electrospray ionization
Et_2O	Diethyl ether
EtOAc	Ethyl acetate
EtOH	Ethanol
FBS	Fetal bovine serum
Fe	Iron
GABA	γ-Aminobutyric acid
Gd^{III}DTPA	Gadolinium(III) diethylenetriaminepentaacetate
H_2O_2	Hydrogen peroxide
HBA	Hydrogen bond acceptor
HBD	Hydrogen bond donor
HBT	2-(2-Hydroxyphenyl)benzothiazole
HCl	Hydrochloric acid
HEPES	(2-[4-(2-Hydroxyethyl)piperazin-1-yl]ethanesulfonic acid)
HO	Hemeoxygenase
K_d	Dissociation constant

KOH	Potassium hydroxide
m/z	Mass-to-charge ratio
M17	SK-N-BE(2)-M17
mAChR	Muscarinic acetylcholine receptor
MEM	Minimal essential media
Metal–Aβ	Metal-associated Aβ
$MgSO_4$	Magnesium(II) sulfate
MRI	Magnetic resonance imaging
MS	Mass spectrometry
MT	Metallothionein
MTT	3-(4,5-Dimethylthiazol-2-yl)-2,5-diphenyltetrazolium bromide
MW	Molecular weight
N2a	Neuro-2a
nAChR	Nicotinic acetylcholine receptor
$NaBH_4$	Sodium borohydride
NaCl	Sodium chloride
$NaHCO_3$	Sodium bicarbonate
NEAA	Non-essential amino acids
nESI	Nanospray ESI
NH_4OH	Ammonium hydroxide
NMDA	*N*-Methyl-D-aspartate
NMR	Nuclear magnetic resonance
NO	Nitric oxide
O_2	Dioxygen
OXPHOS	Oxygen phosphorylation
Pd/C	Palladium on carbon
PAMPA	Parallel Artificial Membrane Permeability Assay
PAGE	Polyacrylamide gel electrophoresis
PAS	Peripheral anionic site
PBS	Phosphate-buffered saline
pI	Isoelectric point

K_a	Acidity constant
PSA	Polar surface area
ROS	Reactive oxygen species
sAPPα/β	Soluble APP α/β fragment
SiO_2	Silica
SOD	Superoxide dismutase
SDS	Sodium dodecyl sulfate
TBS	Tris-buffered saline
TBS-T	Tris-buffered saline containing Tween20
*Tc*AChE	Acetylcholinesterase from *Torpedo californica*
ThT	Thioflavin-T
TEM	Transmission electron microscopy
UV-vis	UV-Visible spectroscopy
Vitamin E	α-Tocopherol
v/v	Volume/volume ratio
w/v	Weight/volume ratio
Zn	Zinc
$ZnCl_2$	Zinc(II) chloride
ZnT	Zinc transporter

Abstract

Alzheimer's disease (AD) is one of the leading cause of death; being the only cause to have increased attribution to death necessitates the understanding of its etiology. Several pathological features, including accumulation of misfolded proteins (*i.e.*, amyloid-β; Aβ), metal ion dyshomeostasis, and loss of acetylcholine (ACh) neurotransmission, are suggested in AD pathogenesis. Current AD therapeutics focus on inhibition of acetylcholinesterase (AChE) for mitigating ACh breakdown. Extensive studies indicate a potential interconnection between Aβ and metal ions (*i.e.*, Cu^{2+}/Zn^{2+}) as well as between Aβ and AChE. Aforementioned factors or their inter-relationships in neuropathogenesis have been unclear, however. To understand the correlation between these factors, efforts have been made toward the development of small molecules as chemical tools, capable of targeting them and subsequently regulating their reactivity.

For such purposes, in this thesis, diphenylpropynone (**DPP**; Aβ imaging probe) derivatives, bioapplicable molecules (*i.e.*, curcumin, found in curry and enediyne, framework used in cancer research), as well as a multifunctional hybrid molecule (hybrid **5**) were developed and investigated toward their targets. **DPP** derivatives are observed to interact with Aβ species and metal ions. The bifunctionality (Aβ interaction and metal chelation) of these derivatives is able to influence the reactivity (metal-induced Aβ aggregation) of metal-associated Aβ (metal–Aβ) species *in vitro*. The Gd^{III}DTPA-curcumin conjugate, a synthesized, Aβ specific MRI agent, is also found to target metal–Aβ species and modulate metal-triggered Aβ aggregation. This study presents the potential to develop a theranostic (diagnostic and therapeutic) agent all-in-one. The enediyne derivative, with its proclivity to generate radicals, is shown to target metal–Aβ species and control the Aβ aggregation possibly *via* multiple properties (*i.e.*, metal chelation, Aβ interaction, radical generation). Lastly, hybrid **5** interacts with

various targets (Aβ, metals, and AChE), is able to inhibit AChE activity with and without Aβ and metals, and modulate metal-induced Aβ aggregation in the absence and presence of AChE. Through this finding, the feasibility of designing a single molecule for multiple functions was indicated. Taken together, the presented studies demonstrate the development of small molecules as chemical tools that can be used to understand the involvement of multiple factors in AD pathogenesis.

Chapter 1: Metals and Proteins in Alzheimer's Disease

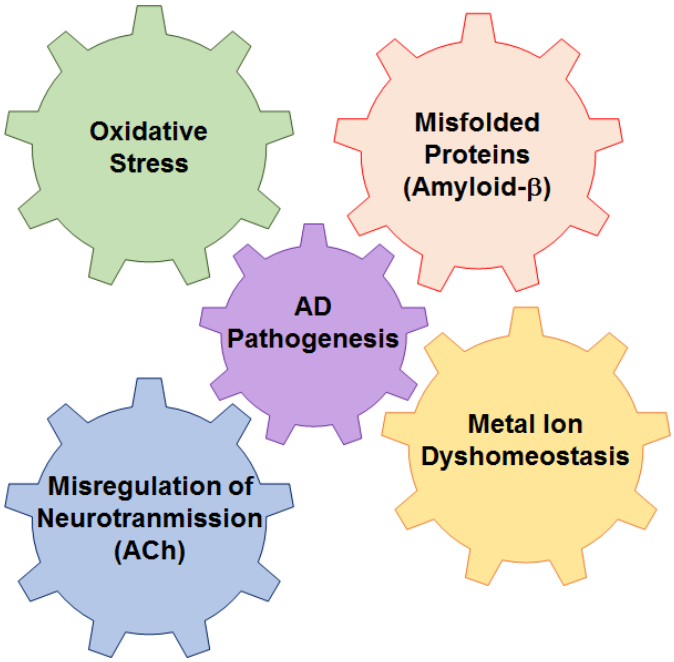

A portion of this chapter was presented in a publication [Lee, H. J.;‡ Korshavn, K.;‡ Kochi, A.; Derrick, J. S.; Lim, M. H. *Chem. Soc. Rev.* **2014** *in press* (‡ Equal contribution)].

1.1. Alzheimer's disease (AD)

AD is currently the most prevalent form of neurodegenerative disease, afflicting over 5 million people, making it the sixth leading cause of death in the United States alone.[1] The symptomatic signs and pathological features of AD have been identified, yet the complete understanding of the disease onset and progression still remains elusive. Due to the complex nature of this disease and limited understanding of AD etiology, the drugs available are able to only offer temporary symptomatic alleviation.[2-6] The hallmarks of AD are the accumulation of misfolded protein aggregates which are

composed mainly of neurofibrillary tangles consisting of hyperphosphorylated tau proteins and senile plaques made up of amyloid-β (Aβ) peptides, as well as morphological changes (*e.g.*, shrinkage) in *post mortem* brain.[2-7] In the Aβ plaques, concentrated metal ions, such as Cu, Zn, and Fe have observed, suggesting metal ion dyshomeostasis/miscompartmentalization may be involved in initiation and progression of AD. Moreover, upon binding of redox active metals to Aβ, excess reactive oxygen species (ROS) is generated, potentially establishing the oxidative stress environment shown in AD brain.[2-6,8] In addition to the possible Aβ and metal ion pathology, synaptic dysfunction in the cholinergic system has been correlated to AD. An inter-relationship between the various factors (*i.e.*, Aβ, metal ion, cholinergic dysfunction) has been suggested toward neurodegeneration, but it still remains to be elucidated.

1.2. Function of metals in the brain

How could metal ion miscompartmentalization and dyshomeostasis potentially influence the neurodegeneration that has been observed in AD-afflicted patients? In order to answer this question, a basic understanding of biologically available metals and their functions is necessary. Metal ions serve many vital roles, including acting as secondary messengers in cellular signaling, stabilizing proteins' structures, catalyzing enzymatic reactions, and transporting dioxygen (O_2) throughout the body.[2,9,10] In order to maintain proper function, metal ion homeostasis is tightly controlled. In particular, three transition metals (*i.e.*, Cu, Zn, Fe) has garnered attention in the AD field, due to the colocalization of the metal ions within senile plaques, consisting of Aβ, observed in AD-afflicted brain.[2,3,6,8]

Copper is the third most abundant transition metal in the body, and the copper in the brain accounts for *ca.* 9% of total copper in the body.[9,10] The major oxidation states of copper are +1 and +2. Cu^{+} is typically found in the intracellular environment while Cu^{2+} is more common in the extracellular environment.[10] Copper in the brain is categorized into two main groups, either bound to proteins, including C*c*O for ATP production, SOD1 for ROS regulation, and Cp for iron metabolism, or unbound in labile, synaptic pools.[2,9,10]

The importance of copper is evident in mitochondrial oxidative phosphorylation (OXPHOS), a multi-step electron transport chain necessary for the formation of the proton gradient utilized for ATP production.[11] C*c*O is the terminal enzyme of OXPHOS and consists of 13 subunits, three of which serve as the catalytic centers (Cox 1-3) containing copper and heme. Electrons transfer between copper and iron centers is coupled to the generation of a proton gradient.[11] Another critical metalloprotein found both in the mitochondrial intermembrane and the cytoplasm is SOD1, a 32 kDa homodimeric copper- and zinc-containing enzyme.[10,12] Through a two-step redox reaction on the copper center at the catalytic site, SOD1 converts harmful superoxide radicals ($O_2^{-\bullet}$) that escape from the mitochondria into O_2 and hydrogen peroxide (H_2O_2).[2,12] Loss of copper results in complete inactivation of the enzyme.[12] Copper is also present in proteins which regulate iron homeostasis. Cp, the major carrier for copper in plasma, is a multicopper oxidase that is paramount for iron metabolism.[2,10]

Zinc is the second most abundant metal in the body, and it is most concentrated in the brain.[10] Like copper, zinc is either protein-bound or labile forms.[10] The majority of the zinc in biology is protein-bound, where it is regulated (*i.e.*, MTs) and transported (*i.e.*, zinc transporters (ZnTs)) to play a role in other biological processes or aid in conformational stability of protein (*e.g.*, SOD1)[2,10] ZnT3-knockout mice studies demonstrated that the accumulation of Zn^{2+} was not associated with synaptic vesicles, suggesting that MTs, not ZnTs, may help maintain an equilibrium between protein-bound and labile Zn^{2+} pools.[2] SOD1 binds zinc to stabilize the active structure, facilitating copper catalyzed antioxidant activity.[13] Studies of amyotrophic lateral sclerosis (ALS) indicate that SOD1 adopts an ALS-linked, mutant-like conformation in the absence of bound zinc.[13] This structural change allows specific protein-protein interactions between SOD1 and Derlin-1 which induces endoplasmic reticulum stress responses, such as protein synthesis inhibition and ZnT induction.[13] The labile zinc pool is also necessary for neuronal transmission; Zn^{2+} is released into the synaptic cleft, along with glutamate, following the excitation of glutamatergic neurons.[2,9,10] Although the role of Zn^{2+} in neurotransmission is not fully understood, it is suggested to be involved in the modulation of neurotransmission through interaction with other

biomolecules, such as *N*-methyl-D-aspartate (NMDA) and γ-aminobutyric acid (GABA) receptors, to regulate their reactivity.[2,9,10,14]

The most abundant transition metal ion in the brain is iron, likely related to the high demand of O_2.[10] Iron is required for many biological processes, including OXPHOS (*vide supra*), neurotransmitter production, and O_2 transport/storage. Iron is physiologically found mainly in two oxidation states, +2 and +3; Fe^{2+} is bound to proteins, such as hemoglobin and HO1, while approximately 25% of the body's iron is chelated to transferrin and ferritin in the Fe^{3+} state.[2,10] Ferritin, a globular protein consisting of 24 subunits, binds up to 4,500 atoms of iron in order to protect cells from iron-mediated oxidative damage and allow for the release of Fe^{3+} when needed.[10,15]

In addition to iron itself being indispensable for diverse critical functions in the body, products generated upon the breakdown of heme, an iron containing cofactor, have physiological roles as antioxidants and anti-inflammatory agents.[16] Heme is degraded by hemeoxygenase (HO) enzymes.[16] Three isoforms of HO have been characterized: HO1 is induced by oxidative stress, HO2 is constitutively active, and HO3 is newly identified (its function is still unclear).[16,17] HO1 is used in a defense mechanism against cellular oxidative stress in concert with SOD1.[16] HO2 is implicated in the maintenance of heme homeostasis and the prevention of nitric oxide (NO)-mediated damage, such as inflammation and glutamate excitotoxicity.[18,19] HO1 and HO2, in conjunction with NADPH and cytochrome P450 reductase, catabolize heme to produce biliverdin, carbon monoxide, and labile Fe^{2+}.[16,17] Some biliverdin can then be further reduced to bilirubin by biliverdin reductase.[16] The products of HO1- and HO2-mediated heme breakdown, biliverdin and bilirubin, may mitigate oxidative stress by acting as antioxidants and remove a potential pro-oxidant source, heme.[16,17] HO3 was found to be a retrotransposition of the HO2 gene and has been suggested to be involved in heme binding and O_2 sensing.[16,17]

As described above, copper, zinc, and iron play critical roles in normal biological processes. Misregulation of these metal ions lead up to detrimental effects in the body, such as the loss of metal ion observed to inactivate SOD1 activity[12] or misconformation of SOD1 in absence of zinc in ALS (*vide supra*).[13] Due to the observations of metal

involvement in neurodegenerative diseases (*e.g.*, AD), metal ion homeostasis has gained attention as a possible underlying cause of disease neuropathology.

1.3. Misfolded proteins in AD

1.3.1. Amyloid precursor protein in AD

A pathological feature of AD, senile plaques, are composed of Aβ peptides, which are initially generated from a transmembrane amyloid precursor protein (APP).[2,4-6,8] Three isoforms exist (APP_{675}, APP_{751}, and APP_{770}), where the most common found in neuronal cells is APP_{695}.[4,6,8,20] The role in which APP plays in normal physiology is still unknown, but possible roles in metal ion homeostatsis[20-22] as well as ferroxidase activity has been suggested.[2,6,8,23] Two possible binding sites of APP have been suggested; E1 (124-189; APP_{695} numbering)[24] and E2 (313-388)[25] with dissociation constant (K_d) of *ca.* 10^{-8} M (Cu^{2+}) and 10^{-6} M (Zn^{2+})[2,8,25,26]

Aβ peptide can be generated by APP cleavage *via* two pathways: non-amyloidogenic and amyloidogenic (Figure 1.1).[2,4-6,8] For the non-amyloidogenic pathway, initial incision is made between K687 and L688 (APP_{770} numbering) by α-secretase, releasing sAPPα, followed by cleavage at either V711/I712 or A713/T714 by γ-secretase to generate $Aβ_{17-40}$ and $Aβ_{17-42}$, respectively.[2,4-6,8] The two common forms of Aβ associated with AD are $Aβ_{40}$ and $Aβ_{42}$, which are produced *via* the amyloidogenic pathway. APP is cleaved between M671 and D672 by β-secretase, releasing sAPPβ. Subsequent cleavage by γ-secretase produces the amyloidogenic peptides.[2,4-6,8]

1.3.2 Amyloid-β in AD

Aggregation of these Aβ peptides occurs *via* a "nucleation-dependent growth mechanism" which consist of two phases: lag phase and elongation phase (Figure 1.2).[6,8,27,28] During the lag phase, monomeric peptides self-associate and aggregate into oligomeric species, which forms thermodynamically unfavorable nuclei.[29] Once the lag phase is surpassed, elongation occurs,[30] where the nucleus acts as a template for Aβ fibril formation.[6,8,29] Various factors (*i.e.*, solution pH (aggregation accelerated near

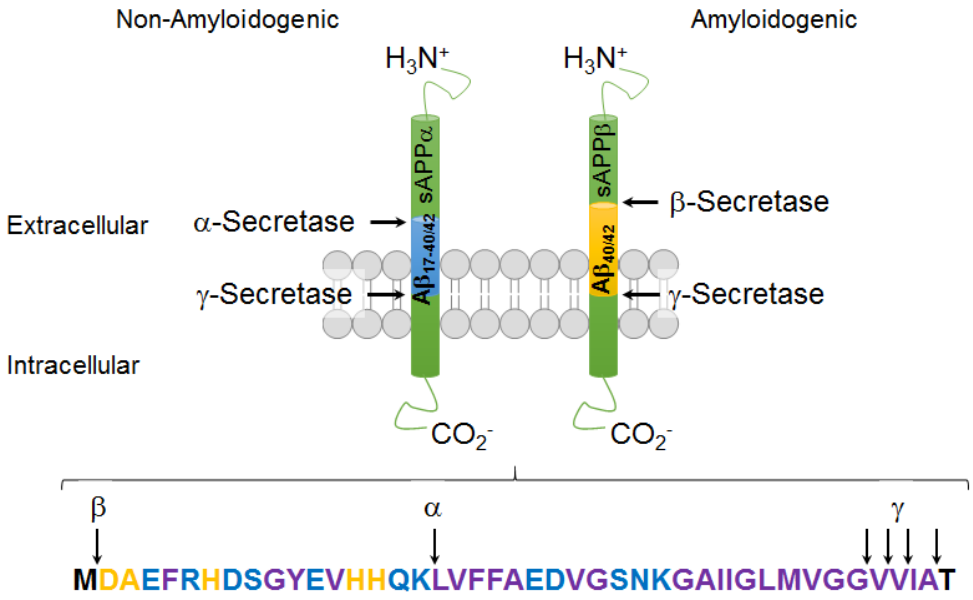

Figure 1.1. Cleavage of APP by α-, β-, and γ-secretases. APP cleavage is initiate by α-secretase followed by γ-secretase to generate $A\beta_{17\text{-}40/42}$ *via* non-amyloidogenic pathway. Proposed pathogenic $A\beta_{40/42}$ is produced upon β-/γ-secretase cleave (amyloidogenic pathway). $A\beta_{42}$ sequence is shown; black: bordering APP amino acids (AA); yellow: proposed metal binding sites; blue: hydrophilic AA residues; purple: hydrophobic AA residues.

protein's isoelectric point); peptide concentration; natural tendency of a peptide to aggregate; exogenous species (proteins, metal ions)) have been shown to influence the initiation and aggregation rate of Aβ peptide.[8] Furthermore, the morphology of

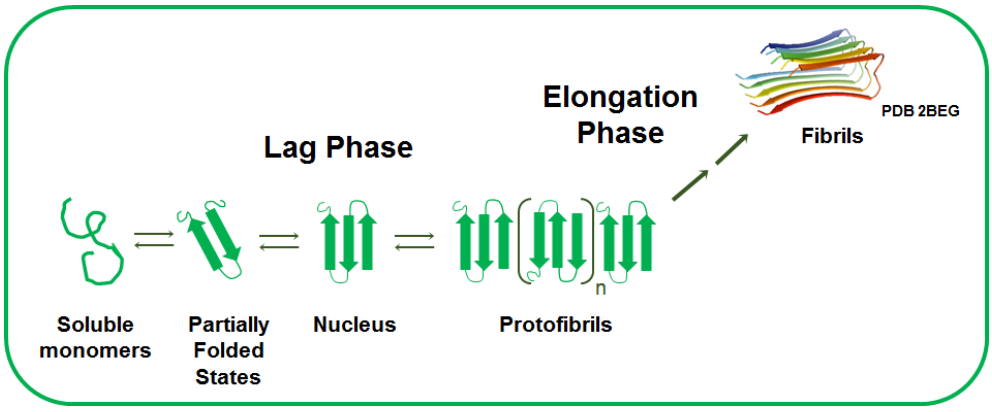

Figure 1.2. Nucleation-dependent growth mechanism for amyloid fibril formation. In the lag phase, the soluble monomers self-aggregate to generate a nucleus and is used as a base for the rapid generation of Aβ fibrils in the elongation phase.

generated Aβ fibrils are impacted by conditions in which aggregation occurs, such as temperature, pH, agitation, or addition of exogenous components (*e.g.*, metal ions, proteins).[8,27,28,30] Though the exact species of Aβ that lead to neurotoxicity is still highly debated, recent studies have implicated oligomeric species, such as dimers, trimers, hexamers, and dodecamers, to exhibit neurotoxicity in AD neurodegeneration.[8,31-35] AD could be classified as either "gain of toxic" function or "loss of function" disease.[6,8] Aggregated Aβ species have been implicated to have detrimental effects, such as interacting with membrane and acting as cation-selective ion channels,[36,37] effecting signaling pathways (*i.e.*, breakdown of signal transduction *via* altering membrane potential or weakening neuroplasticity),[8,38,39] and aiding in the formation of oxidative stress environment observed in AD.[2,8,9,40] In addition to the misfolded proteins displaying toxic effects, Aβ species can also lead to loss of function of many proteins that are essential in normal biological conditions. Aβ fibrils could also act as a possible sink for metal ions, promoting metal ion miscompartmentalization, *vide infra*.[8,9,40]

1.4. Metal ions, proteins, and AD

1.4.1. Effect of metal ion dysregulation on proteins in AD

As described in the section 1.2, metal ions may be critical for the maintenance of proper structure and function for a variety of proteins, including C*c*O, SOD1, Cp, MTs, and HO1 (Figure 1.3). The AD environment (*i.e.*, miscompartmentalized/altered distribution of metal ions and the promotion of oxidative stress) may lead to protein activity disruption[2,10] or the initial misregulation of these proteins may promote the conditions observed in AD environment.[2,10,11] Although it is still debated whether changes in compartmentalization and localization of metal ions are directly involved in AD etiology, the perspective that dysregulated metals could cause oxidative stress (Figure 1.3) is taken for this dissertation, which is believed to be correlated to AD development. In addition, the interaction of metal ions with Aβ and their effects on Aβ aggregation and toxicity have been relatively well characterized.[2,5,40,41]

Copper-/iron-bound Aβ species, along with labile redox-active metal ions, could generate reactive oxygen species (ROS) *via* Fenton-like reactions (eqn 1-5).[2,6,8,40] Aβ

fibrils could also act as a possible sink for metal ions, promoting metal ion miscompartmentalization (Figure 1.3).[8,9,40] Hereafter, how metal ions, both labile and protein-bound, may relate to the generation and clearance of ROS, a possible factor in the onset and progression of AD, will be discussed.

$$A\beta\text{–}Cu^{2+} + \text{reductant} \rightarrow A\beta\text{–}Cu^{+} + \text{reducant}^{+}$$

$$A\beta\text{–}Cu^{+} + O_2 \rightarrow A\beta\text{–}Cu^{2+}\text{–}O_2^{\bullet-} \quad \text{(eqn 1)}$$

$$A\beta\text{–}Cu^{2+}\text{–}O_2^{\bullet-} + e^{-} + H^{+} \rightarrow A\beta\text{–}Cu^{2+}\text{–}HO_2^{\bullet-} \quad \text{(eqn 2)}$$

$$A\beta\text{–}Cu^{2+}\text{–}HO_2^{\bullet-} + H^{+} \rightarrow A\beta\text{–}Cu^{2+} + H_2O_2 \quad \text{(eqn 3)}$$

$$A\beta\text{–}M^{n+} + H_2O_2 \rightarrow A\beta\text{–}M^{(n-1)+} + HOO\bullet + H^{+} \quad \text{(eqn 4)}$$

$$A\beta\text{–}M^{n+} + H_2O_2 \rightarrow A\beta\text{–}M^{(n+1)+} + HO\bullet + OH^{-} \quad \text{(eqn 5)}$$

Organisms have natural antioxidant defense mechanisms that regulate the required amount of ROS present in the body; however, in the diseased state, the system in place for ROS elimination and production (*e.g.*, SOD1 and C*c*O, respectively, *vide supra*) may malfunction, leading to ROS accumulation and oxidative stress.[2,10] High levels of ROS can oxidize lipids and proteins, rendering them unstable and/or nonfunctional, as well as modify DNA which can cause genetic mutations.[2]

In vitro studies have shown that copper, zinc, and iron can coordinate with Aβ, generating metal–Aβ complexes; furthermore, it has been shown that coordination of Aβ to either $Cu^{+/2+}$ or Zn^{2+} can facilitate peptide's aggregation *in vitro*.[2,6,8,9,41] High concentrations of metals have been shown to be colocalized in Aβ plaques: Cu (*ca*. 0.4 mM), Zn (*ca*. 1 mM), and Fe (*ca.* 0.9 mM).[2,6,8,10] The coordination of Cu–Aβ is very dynamic and pH dependent.[2,9,40] The predominant coordination at physiologically relevant pH (*i.e.*, 7.4) for Cu^{2+} and Cu^{+} is 3N1O (three nitrogen donor atoms and one oxygen donor atom; believed to be H6, H13/14, N-terminal amine, and D1 carboxylate) and 2N (two nitrogen donor atoms; suggested to be H13 and H14), respectively. Aβ binds to Cu^{2+} at a 1:1 stoichiometric ratio, with K_d ranging from *ca.* 10^{-11} to 10^{-7} M[2,8,42,43] Aβ also complexes with Cu^{+} at a 1:1 ratio, with K_d of *ca*. 10^{-7} M ($A\beta_{42}$).[6,8,44] Cu–Aβ species have a redox potential = 0.30 V *versus* normal hydrogen electrode

(NHE).[2,9,41] Aβ–Zn^{2+} has been shown to coordinate four to six ligands, with a consensus *via* H6/13/14,[2] while the other ligands (4-6) vary depending on conditions.[2,6]

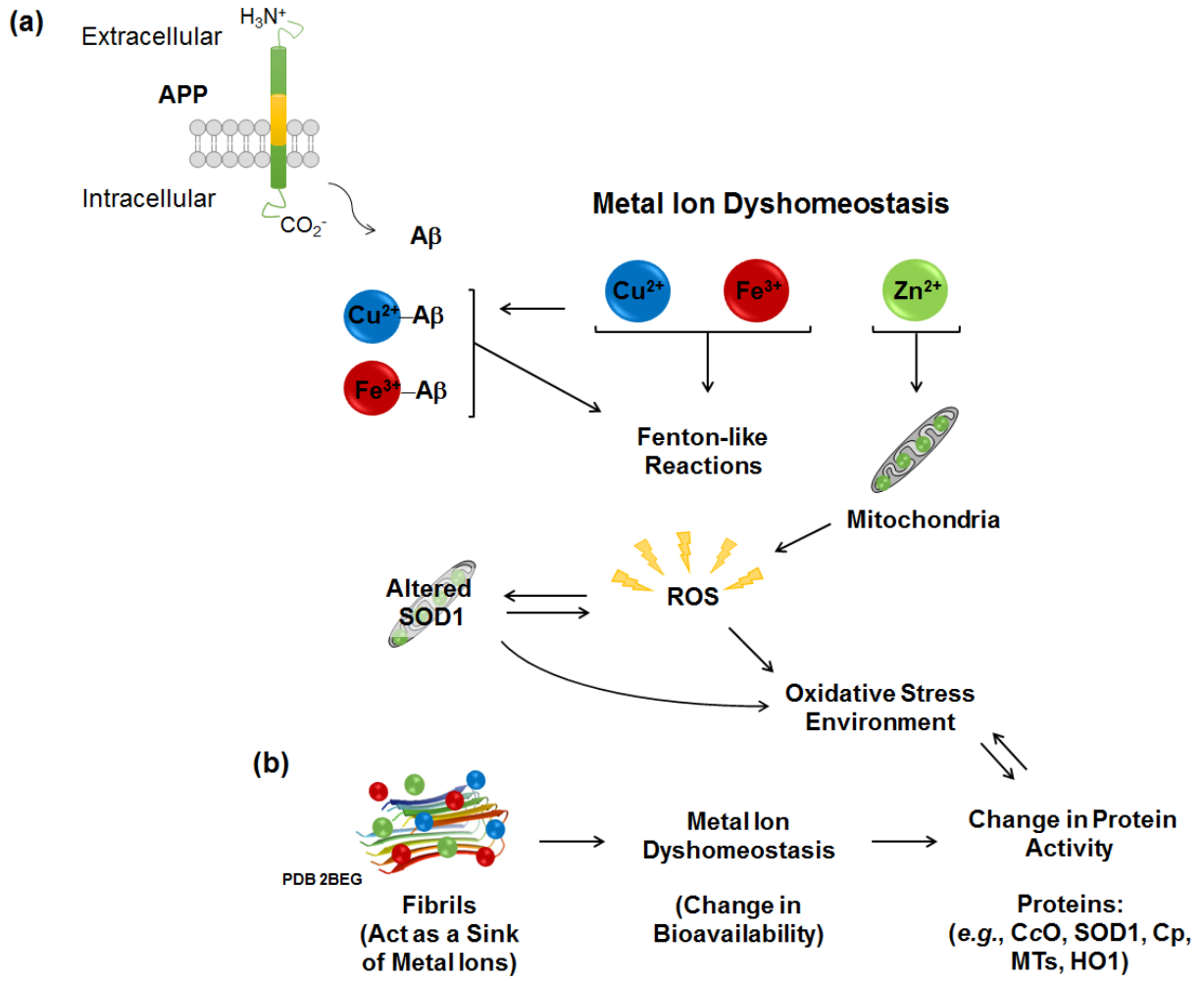

Figure 1.3. Possible interplay of metal ions in inducing oxidative stress and influencing protein activity. (a) Redox active metal ions (*i.e.*, Cu^{2+} (blue spheres), Fe^{3+} (red spheres)) and their complexes with Aβ could produce reactive oxygen species (ROS) through Fenton-like reactions. Zn^{2+} (green spheres) has also been observed to inhibit oxidative phosphorylation (OXPHOS) as well as modify SOD1 structure in mitochondria, leading to Zn^{2+}-triggered ROS production. Imbalance between the formation and removal of ROS could cause oxidative stress. (b) Aggregated Aβ may act as a sink for metal ions, contributing to altered bioavailability of metal ions. Metal ion dyshomeostasis and/or oxidative stress could interfere with critical biological functions (*i.e.*, ATP production, ROS breakdown, maintenance of metal ion homeostasis) of proteins, such as cytochrome *c* oxidase (C*c*O), Cu/Zn superoxide dismutase (SOD1), ceruloplasmin (Cp), metallothioneins (MTs), and hemeoxygenase 1 (HO1).

Aβ complexes with Zn^{2+} at a 1:1 ratio, with K_d from 10^{-9} to 10^{-6} M[2,6,42] Few structural studies have been reported for iron coordination to Aβ due to the propensity of Fe^{2+} to oxidize to Fe^{3+} and precipitate as $Fe(OH)_3$ and other complexes.[41] Preliminary

results proposed D1, E3, and H6/13/14 may be involved in Fe^{2+} coordination by Aβ.[41] The redox potential of Fe^{2+}/Fe^{3+} in the Aβ-iron-nitriloacetic acid complex was determined to be 0.23 V *versus* NHE.[45] Fe^{2+} binds to Aβ with K_d *ca.* 10^{-4} M.[8,46]

Redox inert Zn^{2+} could also take part, indirectly, in ROS generation.[47] Upon subjection of neurons to toxic intracellular zinc concentrations, ROS accumulation as well as lipid peroxidation have occurred.[47] Due to the natural production of ROS during OXPHOS and the natural escape of 1-3% of that ROS, mitochondria are considered a primary contributor to oxidative stress in neurons.[2,48] It has been observed that Zn^{2+} could inhibit OXPHOS at multiple sites (*i.e.*, ubiquinone, glycerol-3-phosphate dehydrogenase, and complex I/II/III/IV(IV; C*c*O), with complex III believed to be the most sensitive to Zn^{2+} inhibition.[47] Zinc was found to inhibit the Q cycle (arresting electron transfer) and a putative zinc binding site was speculated as a part of the proton channel of complex III.[47] In addition, reduced C*c*O activity is consistently found in the diseased brain.[48] C*c*O deficiency in relation to ROS production was assessed in the *COX10* knockout AD mouse model (lacking in one of the hemes in the C*c*O catalytic site), but increased ROS formation was not demonstrated in the presence of decreased C*c*O activity.[49] These findings indicate that the oxidative stress induced by high levels of Zn^{2+} may not arise from C*c*O dysfunction, but rather from a disturbance upstream from C*c*O in OXPHOS, perhaps through Zn^{2+} inhibition of different OXPHOS sites.[47] Zn^{2+} also has been hypothesized to increase ROS formation through interference with the Krebs cycle in the mitochondria.[47] In the Krebs cycle, ROS is generated following NADH oxidation of O_2 by α-ketoglutarate dehydrogenase.[47] Zn^{2+} was shown to accelerate this reaction five-fold through an unknown mechanism, possibly contributing to ROS overproduction.[47]

Along with overproduction of ROS by various metal ions, loss of ROS detoxification machinery could overwhelm the endogenous antioxidant system.[2,10] Current research has found one of the key antioxidant enzymes, SOD1, to be a major target of oxidation.[50] Choi, *et al.* identified four brain SOD1 isoforms from human AD-afflicted brains with different isoelectric points (pI = 6.3, 6.0, 5.7, and 5.0).[50] Relative increase of all isoforms was observed, with a six-fold increase of the acidic (pI 5.0) isoform. In addition, SOD1 was shown to aggregate and associate with Aβ plaques and

neurofibrillary tangles.[50] Moreover, a 7.5–9 fold increase in oxidation of pI 6.0 isoform was determined, with C146 irreversibly oxidized in AD brain.[50] C57 and C146 create an intramolecular disulfide bond with each other that is necessary to maintain proper conformation and enzymatic activity of SOD1; oxidation of one of these prevents the generation of the disulfide bond and hinders enzymatic function.[51] The malfunction of SOD1 may be a factor for the accumulation of ROS, ultimately leading to oxidative stress and neurodegeneration.[10,50]

In AD patients, increased apo-Cp (copper-unbound form without normal function) levels and decreased activity of Cp have been observed.[2] These altered concentrations may exacerbate toxic conditions observed in AD where labile iron promotes oxidative damage.[2] Since Cp has been known to play a central role in cellular homeostasis, including metal and oxidative stress regulation,[2] expression of metalloproteinases that degrade Aβ,[2] ferroxidase activity,[2,52] and H_2O_2 scavenging,[52] diminished presence of the metallated form and lowered protein activity could trigger aberrant pathological events (*e.g.*, Aβ accumulation, oxidative stress, metal ion dyshomeostasis). Due to the iron ion dysregulation that has been observed in AD, a possible relationship between the iron ion dyshomeostasis and disruptions of ferritin has been proposed. No changes in ferritin levels have been observed in the diseased state to date, however.[15]

MTs are another class of proteins affected by oxidative stress.[2] Four isoforms, MT1-4, have been identified. MT1/2 are found in most tissues and MT3/4 are present in specialized tissue, such as the brain and epithelial tissue, respectively.[2,10] MT1/2 in the brain are expressed mainly in the astrocytes which maintain CNS homeostasis, blood-brain barrier (BBB) integrity, and neuronal metabolism, as well as express metalloproteinases that catabolize amyloids.[2] In AD, MT1/2 have been shown to be upregulated and MT3 levels have been shown to be altered, but a consensus has not been reached as to how it changes.[2] MT3 is brain-specific and can coordinate up to nine atoms of zinc under excess Zn^{2+} conditions.[10] Subsequent release of MT-bound Zn^{2+} induced by ROS has been implicated in AD pathogenesis. In the characteristic oxidative stress environment of the AD-affected brain, Zn^{2+} could be released from MTs, which could then induce Zn^{2+} excitotoxicity resulting in cell death by various

mechanisms, such as upregulation of glutamate receptor activity to cytotoxic levels, overstimulation of NO-involved pathways, or generation of ROS (*vide supra*).[10]

HO1 has also been shown to be increased during oxidative stress to mitigate ROS (*vide supra*).[16,17] HO1 has been observed to be overexpressed in neurons and astrocytes, particularly of the parenchyma in AD and is present in senile plaques. It is, however, suppressed in cerebral spinal fluid.[16] HO1 has also been conceptualized as a double-edged sword. The beneficial antioxidant capacity of bilirubin and biliverdin gained after heme metabolism could be nullified by the release of Fe^{2+} which could enter a redox cycle and promote ROS generation.[16]

1.4.2. Cholinergic system in AD

Additionally, the cholinergic system also has been implicated in AD neurodegeneration; initially stemming from the observation of the loss of cholinergic neurons that release acetylcholine (ACh) in basal forebrain in AD.[53-56] ACh is important in many neurological signaling pathways, such as the two major parts of the autonomic nervous system, which are responsible for the regulation of internal organs/glands as well as nerve plasticity, sustainment of attention, and promotion of the rapid eye movement cycle during sleep.[57,58] In the AD-affected brain, ACh release (induced by depolarization) and choline uptake (necessary to recyclize into the ACh pathway of synthesis to produce more ACh) have been shown to be diminished.[55,59-62] Reduced nicotinic ACh receptors (nAChRs) and muscarinic ACh receptors (mAChRs), which bind to the released ACh, in both pre-/postsynaptic neurons have been observed.[53,54,59] Studies indicate Aβ may also interact with both receptors. Aβ specifically has high affinity toward α7nAChR; the interaction showed multiple effects (*i.e.*, impair the release of ACh (presynaptic neuron) and maintenance of long-term potentiation; internalization and accumulation of Aβ in neurons).[53,54,63-65] Current therapeutic efforts have been put forth to increase the reduced levels of ACh by inhibiting acetylcholinesterase, AChE, responsible for cleaving the neurotransmitter.[66-68]

AChE is a serine hydrolase from the esterase family,[69,70] whose primary function is breaking down ACh to terminate cholinergic neurotransmission.[70-72] AChE consists of β-sheet surrounded by α-helices that contains a catalytic triad in the esteric site, located

at the bottom of 20 Å deep cavity composed of aromatic amino acids. (catalytic triad: S200, H440, and E327; *Torpedo californica*; electric eel AChE)[70,72-74] The α-anionic site (W84, Y121, F330), located near the esteric site, interacts with the quaternary ammonium atom of ACh and is responsible for its correct orientation within the enzyme.[70,72,75,76]

Situated on the surface of AChE near the cavity entrance, is the peripheral anionic site (PAS) consisting of amino acids, including Y70, D72, Y121, W279, and Y334.[72,77] Aβ has been correlated to AChE itself, where AChE has been found to be accumulated in Aβ plaques.[78] Studies have suggested that AChE promotes Aβ aggregation *in vitro*[79] and in AD mouse model.[80] It has been shown that Aβ interacts with PAS of the enzyme, which facilitates Aβ fibril formation.[81] Current AD therapeutics (*i.e.*, tacrine, galantamine, donepezil, and rivastigmine) target different binding sites of AChE; tacrine and galantamine binds onto the α-anonic site; donepezil complexes with PAS; rivastigmine binds at the esteric site.[59,72,82] Only modest improvements in disease progression after treatment, as well as low tolerability of treatment in some patients have been observed, however.[2-6,70,72] Therefore, fundamental understanding of how the multiple factors, from the different aspects of AD pathogenesis, must be first illustrated in order to develop effective therapeutics.

1.4.3. Use of small molecules to understand the relationship between Aβ, metal ions, and/or AChE

In order to elucidate the relationship between multiple pathological factors (*i.e.*, Aβ, metal ions, loss of ACh/inhibition of AChE), advances have been focused on the development of small molecules which could be used as chemical tools to gain insight into the interconnection (Figure 1.4).[2,3,83] The basic understanding of each facet to neuropathogenesis in this complex disease will help establish a foundation to which an effective therapeutic could be built upon. Initial findings indicated metal-induced Aβ aggregation could be reversed *in vitro* by the use of metal chelators. Hence metal chelation therapy (*e.g.,* bathophenathroline; Figure 1.4) was examined; however, bioapplicability was low due to BBB impermeability and nonspecific metal binding.[83,84] This investigation resulted in concreting a potential metal correlation to AD pathology

and small molecule framework containing metal chelation have been explored since then.

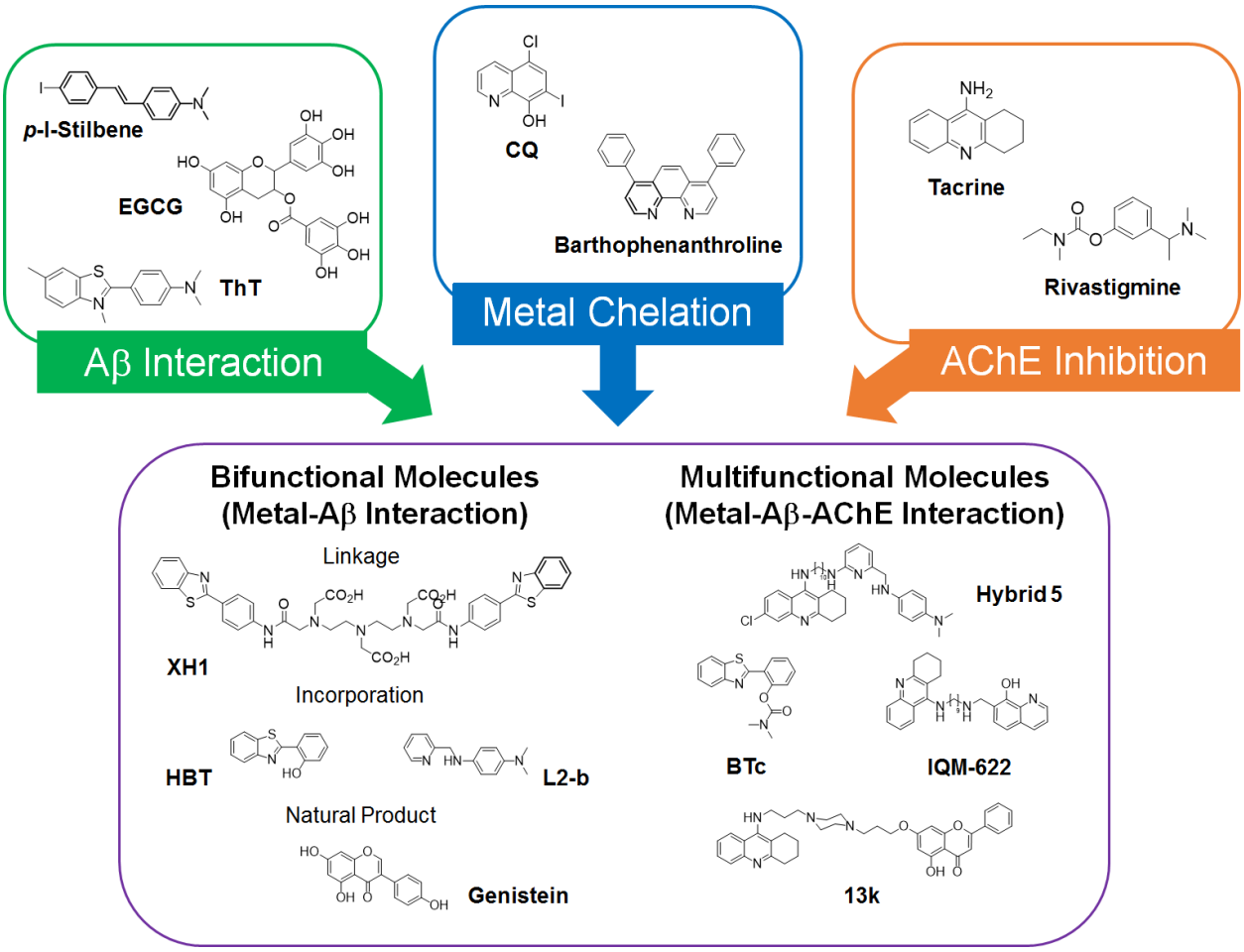

Figure 1.4. Multifunctional small molecules that can be used to investigate Aβ, metal ions and/or AChE inhibtion in AD by combining properties of Aβ interaction (green), metal chelation (blue), and/or AChE inhibition (orange). Multifunctional molecules are shown in the purple box. Abbreviations for compounds: *p*-I-stilbene = *N*,*N*-dimethyl-4-[(1*E*)-2-(4-iodophenyl)ethenyl]benzenamine; EGCG = epigallocatechin-3-gallate; ThT = thioflavin-T, 2-[4-(dimethylamino)phenyl]-3,6-dimethylbenzothiazolium; CQ, clioquinol, = 5-chloro-7-iodo-8-hydroxyquinoline; barthophenanthroline = 4,7-diphenyl-1,10-phenanthroline; tacrine = 1,2,3,4-tetrahydroacridin-9-amine; rivastigmine = 3-(1-(dimethylamino)ethyl)phenyl)ethyl(methyl) carbamate; XH1 = *N*,*N*-bis[2-[[2-[[4-(2-benzothiazolyl)phenyl]amino]-2-oxoethyl](carboxymethyl)amino] ethyl]glycine; HBT = 2-(2-hydroxyphenyl)benzothiazole; L2-b = N^1,N^1-dimethyl-N^4-(pyridin-2-ylmethyl) benzene-1,4-diamine; Genistein = 5,7-dihydroxy-3-(4-hydroxyphenyl)-4*H*-chromen-4-one; Hybrid 5 = 6-{[10-((6-chloro-1,2,3,4-tacrine)amino)decyl]amino}picolinaldehyde; BTc = 2-(benzo[d]thiazol-2-yl)phenyl dimethylcarbamate; IQM-622 : 7-(((((1,2,3,4-tetrahydroacridin-9-yl)amino)methyl)amino)methyl)quinolin-8-ol; 13k = 5-hydroxy-2-phenyl-7-(3-(4-(3-((1,2,3,4-tetrahydroacridin-9-yl)amino)propyl)piperazin-1-yl) propoxy)-4*H*-chromen-4-one.

The exploration of 8-hyrdoxyquniline (8HQ) derivative, clioquinol (CQ; Figure 1.4), a U.S. F.D.A. approved lipophilic small molecule that can permeate through the

BBB, and its derivative PBT2, has shown their ability to disrupt the interaction between metal ions and Aβ, sequester the metal ions and act as an ionophore (transport metal ions across the membrane for redistribution.[3,83,85,86] Although 8HQ derivatives could not directly illustrate the connection between Aβ and metal ions due to the lack of an Aβ interaction moiety, it has lead strides in validating the possible metal ion dyshomeostasis as a possible therapeutic route.[6,85-88]

Advancements in small molecule designs have been made, where a rational structure-based approach has been utilized in order to achieve bifunctional or multifunctional small molecules (Figure 1.4). Bifunctionality in the framework stems from having an Aβ interaction moiety and a metal chelation moiety in one molecule. This desired molecular structure can be achieved either *via* the linkage approach (*i.e.*, chelation moiety is appended onto an Aβ interaction moiety by a linker) or the incorporation approach (*i.e.*, chelation moiety is directly inserted onto the Aβ interacting moiety with minimal change to the core framework) (Figure 1.4). Many chemical tools have been developed using known Aβ contrasting agents (*e.g.*, ThT, stilbene) to garner the high binding affinity of these ligands toward Aβ species.[3,83,87-92] In addition to synthesized compounds, natural products, including myricetin and EGCG, have also been extensively studied as possible molecular structures that have the ability to interact with metal ions and Aβ.[83,88,93-97]

Multifunctional small molecules have been pursued as possible AD therapeutics, which were influenced by the combination of scaffolds that target two hallmarks of AD: Aβ peptides and loss of ACh.[2-4,6,8,98-101] Employing molecular scaffolds inspired by Aβ imaging agents, natural products, or other biologically relevant compounds (bifunctional small molecules, *vide supra*), Aβ targeting moieties have been appended onto molecular framework that demonstrated AChE inhibiting activities, including currently marketed AD drugs (Figure 1.4).[101-104] Further development and investigation of these small molecules would be valuable in elucidating the inter-relationship between the multiple facets observed in AD pathogenesis.

1.5. Conclusion

The intricate collaboration of the different pathological factors in AD adds to the disease complexity and poses a challenge in development in effective therapeutic drugs. Strides in clarifying the relationship between the multiple neuropathological facets have been made; however, only potentially scratching the surface of the enigma of AD etiology. Small molecules, with both bifunctional and multifunctional properties, have been employed to elucidate how the various pathological features impact the onset and progression of AD. The fundamental knowledge gained from these studies may allow to: (1) understand what components (*i.e.*, effects toward a particular pathological feature) are necessary to develop an effective chemical tool to illustrate the interconnection; (2) expedite the discovery of diagnostic tools as well as drugs for AD. To fully achieve these goals, complete insight into the processes of Aβ aggregate formation and the effects of the interaction of other components (*i.e.*, metal ions, proteins) toward disease development is necessary.

1.6. Scope of this thesis

Pursuit of different molecular scaffold using the synthetic approach discussed above, toward targeting and modulating metal–Aβ species, in addition to having other opportune moieties within one compound, has been carried out. Different structural frameworks, such as Aβ imaging agents or natural products, have been employed in understanding AD neuropathogenesis, but their application toward metal-associated Aβ has been minimally pursued. Furthermore, multifunctional molecules designed to understand the correlation between Aβ, metal ions, and/or AChE has recently been investigated. As such, the studies presented in this thesis investigate chemical tools that may help elucidate the interconnection between the different AD pathogenic factors. Chapter 2 details the use of a bifunctional small molecule with diphenylpropynone (**DPP**) scaffold, an Aβ imaging agent, toward metal–Aβ species. Subsequently, Chapter 3 describes modification upon the **DPP** derivatives, examined in Chapter 2, to improve reactivity toward metal–Aβ species, lower cytotoxicity, as well as gain an understanding of a structure-reactivity-cytotoxicity relationship. Chapter 4 encompasses the investigation of the reactivity of Gd^{III}DTPA-curcumin conjugate (**Gd-cur**), shown

previously to interact with Aβ aggregates, toward metal–Aβ species, as a possible theranostic tool. Chapter 5 reports reactivity of enediynes (extensively studied potential anti-cancer drug)[105-107] that contain similar metal chelation moiety to bidentate and tetradentate compounds that demonstrate metal–Aβ reactivity,[88,91,92,108] toward metal–Aβ. Chapter 6 describes the use of a multifunctional small molecule, containing metal–Aβ interaction moiety appended onto an AChE inhibitor, to understand the interconnection between Aβ, metal ions, and/or AChE.

Overall, the designed compounds have demonstrated the ability to control metal-induced Aβ aggregation *in vitro*, as well as being a potent AChE inhibitor (multifunctional small molecule, the hybrid **5**; Chapter 6). These studies, motivated by the use of rational structure-based design, are promising start in the attempt to understand the complex etiology of AD. The present investigations have aided in illustrating a structure-interaction-reactivity-cytotoxicity relationship, in addition to setting a foundation to illustrate the potential role of metal ions in AD pathology.

1.7. References

(1) Thies, W.; Bleiler, L. *Alzheimers Dement.* **2013**, *9*, 208.
(2) Kepp, K. P. *Chem. Rev.* **2012**, *112*, 5193.
(3) Scott, L. E.; Orvig, C. *Chem. Rev.* **2009**, *109*, 4885.
(4) Jakob-Roetne, R.; Jacobsen, H. *Angew. Chem., Int. Ed.* **2009**, *48*, 3030.
(5) Rauk, A. *Chem. Soc. Rev.* **2009**, *38*, 2698.
(6) DeToma, A. S.; Salamekh, S.; Ramamoorthy, A.; Lim, M. H. *Chem. Soc. Rev.* **2012**, *41*, 608.
(7) Hardy, J. A.; Higgins, G. A. *Science* **1992**, *256*, 184.
(8) Savelieff, M. G.; Lee, S.; Liu, Y.; Lim, M. H. *ACS Chem. Biol.* **2013**, *8*, 856.
(9) Faller, P.; Hureau, C. *Chemistry* **2012**, *18*, 15910.
(10) Que, E. L.; Domaille, D. W.; Chang, C. J. *Chem. Rev.* **2008**, *108*, 1517.
(11) Cobine, P. A.; Pierrel, F.; Winge, D. R. *Biochim. Biophys. Acta* **2006**, *1763*, 759.
(12) Noor, R.; Mittal, S.; Iqbal, J. *Med. Sci. Monit.* **2002**, *8*, RA210.
(13) Homma, K.; Fujisawa, T.; Tsuburaya, N.; Yamaguchi, N.; Kadowaki, H.; Takeda, K.; Nishitoh, H.; Matsuzawa, A.; Naguro, I.; Ichijo, H. *Mol. Cell* **2013**, *52*, 75.
(14) Frederickson, C. J.; Koh, J.-Y.; Bush, A. I. *Nat. Rev. Neurosci.* **2005**, *6*, 449.
(15) Friedman, A.; Arosio, P.; Finazzi, D.; Koziorowski, D.; Galazka-Friedman, J. *Parkinsonism Relat. Disord.* **2011**, *17*, 423.
(16) Schipper, H. M.; Song, W.; Zukor, H.; Hascalovici, J. R.; Zeligman, D. *J. Neurochem.* **2009**, *110*, 469.
(17) Bansal, S.; Biswas, G.; Avadhani, N. G. *Redox. Biol.* **2014**, *2*, 273.
(18) Mancuso, C. *Antioxid. Redox Signal.* **2004**, *6*, 878.

(19) Parfenova, H.; Leffler, C. W. *Curr. Pharm. Des.* **2008**, *14*, 443.
(20) Lichtenthaler, S. F.; Haass, C.; Steiner, H. *J. Neurochem.* **2011**, *117*, 779.
(21) Gaggelli, E.; Kozlowski, H.; Valensin, D.; Valensin, G. *Chem. Rev.* **2006**, *106*, 1995.
(22) Ciuculescu, E.-D.; Mekmouche, Y.; Faller, P. *Chem. Eur. J.* **2005**, *11*, 903.
(23) Duce, J. A.; Bush, A. I. *Prog. Neurobiol.* **2010**, *92*, 1.
(24) Barnham, K. J.; McKinstry, W. J.; Multhaup, G.; Galatis, D.; Morton, C. J.; Curtain, C. C.; Williamson, N. A.; White, A. R.; Hinds, M. G.; Norton, R. S.; Beyreuther, K.; Masters, C. L.; Parker, M. W.; Cappai, R. *J. Biol. Chem.* **2003**, *278*, 17401.
(25) Dahms, S. O.; Könnig, I.; Roeser, D.; Gührs, K.-H.; Mayer, M. C.; Kaden, D.; Multhaup, G.; Than, M. E. *J. Mol. Biol.* **2012**, *416*, 438.
(26) Eskici, G.; Axelsen, P. H. *Biochemistry* **2012**, *51*, 6289.
(27) Chiti, F.; Dobson, C. M. *Annu. Rev. Biochem.* **2006**, *75*, 333.
(28) Wilson, M. R.; Yerbury, J. J.; Poon, S. *Mol.Biosyst.* **2008**, *4*, 42.
(29) Butterfield, S. M.; Lashuel, H. A. *Angew. Chem., Int. Ed. Engl.* **2010**, *49*, 5628.
(30) Miller, Y.; Ma, B.; Nussinov, R. *Chem. Rev.* **2010**, *110*, 4820.
(31) Haass, C.; Selkoe, D. J. *Nat. Rev. Mol. Cell Biol.* **2007**, *8*, 101.
(32) Lesné, S.; Koh, M. T.; Kotilinek, L.; Kayed, R.; Glabe, C. G.; Yang, A.; Gallagher, M.; Ashe, K. H. *Nature* **2006**, *440*, 352.
(33) Bernstein, S. L.; Dupuis, N. F.; Lazo, N. D.; Wyttenbach, T.; Condron, M. M.; Bitan, G.; Teplow, D. B.; Shea, J. E.; Ruotolo, B. T.; Robinson, C. V.; Bowers, M. T. *Nat. Chem.* **2009**, *1*, 326.
(34) Ahmed, M.; Davis, J.; Aucoin, D.; Sato, T.; Ahuja, S.; Aimoto, S.; Elliott, J. I.; Van Nostrand, W. E.; Smith, S. O. *Nat. Struct. Mol. Biol.* **2010**, *17*, 561.
(35) Bitan, G.; Vollers, S. S.; Teplow, D. B. *J. Biol. Chem.* **2003**, *278*, 34882.
(36) Demuro, A.; Mina, E.; Kayed, R.; Milton, S. C.; Parker, I.; Glabe, C. G. *J. Biol. Chem.* **2005**, *280*, 17294.
(37) Arispe, N.; Diaz, J. C.; Simakova, O. *Biochimica Et Biophysica Acta-Biomembranes* **2007**, *1768*, 1952.
(38) Sokolov, Y.; Kozak, J. A.; Kayed, R.; Chanturiya, A.; Glabe, C.; Hall, J. E. *J. Gen. Physiol.* **2006**, *128*, 637.
(39) Lambert, M. P.; Barlow, A. K.; Chromy, B. A.; Edwards, C.; Freed, R.; Liosatos, M.; Morgan, T. E.; Rozovsky, I.; Trommer, B.; Viola, K. L.; Wals, P.; Zhang, C.; Finch, C. E.; Krafft, G. A.; Klein, W. L. *Proc. Natl.Acad. Sci. U. S. A.* **1998**, *95*, 6448.
(40) Tiiman, A.; Palumaa, P.; Tougu, V. *Neurochem. Int.* **2013**, *62*, 367.
(41) Hureau, C. *Coord. Chem. Rev.* **2012**, *256*, 2164.
(42) Faller, P.; Hureau, C. *Dalton Trans.* **2009**, 1080.
(43) Telpoukhovskaia, M. A.; Orvig, C. *Chem. Soc. Rev.* **2013**, *42*, 1836.
(44) Feaga, H. A.; Maduka, R. C.; Foster, M. N.; Szalai, V. A. *Inorg. Chem.* **2011**, *50*, 1614.
(45) Jiang, D.; Li, X.; Williams, R.; Patel, S.; Men, L.; Wang, Y.; Zhou, F. *Biochemistry* **2009**, *48*, 7939.
(46) Bousejra-ElGarah, F.; Bijani, C.; Coppel, Y.; Faller, P.; Hureau, C. *Inorg. Chem.* **2011**, *50*, 9024.

(47) Dineley, K. E.; Votyakova, T. V.; Reynolds, I. J. *J. Neurochem.* **2003**, *85*, 563.
(48) Fukui, H.; Moraes, C. T. *Trends Neurosci.* **2008**, *31*, 251.
(49) Pickrell, A. M.; Fukui, H.; Moraes, C. T. *J. Bioenerg. Biomembr.* **2009**, *41*, 453.
(50) Choi, J.; Rees, H. D.; Weintraub, S. T.; Levey, A. I.; Chin, L. S.; Li, L. *J. Biol. Chem.* **2005**, *280*, 11648.
(51) Nagano, S. In *Amyotrophic Lateral Sclerosis*; Maurer, M. H., Ed.; InTech: 2012, p 301.
(52) Loeffler, D. A.; LeWitt, P. A.; Juneau, P. L.; Sima, A. A.; Nguyen, H. U.; DeMaggio, A. J.; Brickman, C. M.; Brewer, G. J.; Dick, R. D.; Troyer, M. D.; Kanaley, L. *Brain Res.* **1996**, *738*, 265.
(53) Pakaski, M.; Kalman, J. *Neurochem. Int.* **2008**, *53*, 103.
(54) Schliebs, R.; Arendt, T. *Behav. Brain Res.* **2011**, *221*, 555.
(55) Contestabile, A. *Behav. Brain Res.* **2011**, *221*, 334.
(56) Whitehouse, P. J.; Price, D. L.; Struble, R. G.; Clark, A. W.; Coyle, J. T.; Delon, M. R. *Science* **1982**, *215*, 1237.
(57) Himmelheber, A. M.; Sarter, M.; Bruno, J. P. *Brain Res.* **2000**, *9*, 313.
(58) Platt, B.; Riedel, G. *Behav. Brain Res.* **2011**, *221*, 499.
(59) Francis, P. T.; Parsons, C. G.; Jones, R. W. *Expert Rev. Neurother.* **2012**, *12*, 1351.
(60) Schifilliti, D.; Santamaria, L. B.; Rosa, G.; Di Nino, G.; Mandal, P. K.; Fodale, V. *J. Alzheimers Dis.* **2010**, *22 Suppl 3*, 35.
(61) Rylett, R. J.; Ball, M. J.; Colhoun, E. H. *Brain Res.* **1983**, *289*, 169.
(62) Bowen, D. M.; Benton, J. S.; Spillane, J. A.; Smith, C. C.; Allen, S. J. *J. Neurol. Sci.* **1982**, *57*, 191.
(63) Querfurth, H. W.; LaFerla, F. M. *N. Eng. J. Med.* **2010**, *362*, 329.
(64) Wang, H. Y.; Lee, D. H.; D'Andrea, M. R.; Peterson, P. A.; Shank, R. P.; Reitz, A. B. *J. Biol. Chem.* **2000**, *275*, 5626.
(65) Nagele, R. G.; D'Andrea, M. R.; Anderson, W. J.; Wang, H. Y. *Neuroscience* **2002**, *110*, 199.
(66) Villarroya, M.; Garcia, A. G.; Marco-Contelles, J.; Lopez, M. G. *Expert Opin. Investig. Drugs* **2007**, *16*, 1987.
(67) Pepeu, G.; Giovannini, M. G. *Curr. Alzheimer Res.* **2009**, *6*, 86.
(68) Smith, D. A. *Am. J. Health Syst. Pharm.* **2009**, *66*, 899.
(69) Aldridge, W. N. *Biochem. J.* **1953**, *53*, 110.
(70) Patocka, J.; Kuca, K.; Jun, D. *Acta Medica* **2004**, *47*, 215.
(71) Schumacher, M.; Camp, S.; Maulet, Y.; Newton, M.; MacPhee-Quigley, K.; Taylor, S. S.; Friedmann, T.; Taylor, P. *Nature* **1986**, *319*, 407.
(72) Pohanka, M. *Biomed. Pap. Med. Fac. Univ. Palacky Olomouc Czech Repub.* **2011**, *155*, 219.
(73) Silman, I.; Sussman, J. L. *Chem. Biol. Interact.* **2008**, *175*, 3.
(74) Sussman, J. L.; Harel, M.; Frolow, F.; Oefner, C.; Goldman, A.; Toker, L.; Silman, I. *Science* **1991**, *253*, 872.
(75) Bartolucci, C.; Haller, L. A.; Jordis, U.; Fels, G.; Lamba, D. *J. Med. Chem.***2010**, *53*, 745.
(76) Kreienkamp, H. J.; Weise, C.; Raba, R.; Aaviksaar, A.; Hucho, F. *Proc. Natl. Acad. Sci. U. S. A.* **1991**, *88*, 6117.

(77) Johnson, G.; Moore, S. W. *Curr. Pharm. Des.* **2006**, *12*, 217.
(78) Schliebs, R.; Arendt, T. *J. Neural. Transm.* **2006**, *113*, 1625.
(79) Inestrosa, N. C.; Alvarez, A.; Perez, C. A.; Moreno, R. D.; Vicente, M.; Linker, C.; Casanueva, O. I.; Soto, C.; Garrido, J. *Neuron* **1996**, *16*, 881.
(80) Rees, T.; Hammond, P. I.; Soreq, H.; Younkin, S.; Brimijoin, S. *Neurobiol. Aging* **2003**, *24*, 777.
(81) De Ferrari, G. V.; Canales, M. A.; Shin, I.; Weiner, L. M.; Silman, I.; Inestrosa, N. C. *Biochemistry* **2001**, *40*, 10447.
(82) Anand, P.; Singh, B. *Arch. Pharm. Res.* **2013**, *36*, 375.
(83) Rodríguez-Rodríguez, C.; Telpoukhovskaia, M.; Orvig, C. *Coord. Chem. Rev.* **2012**, *256*, 2308.
(84) Cherny, R. A.; Legg, J. T.; McLean, C. A.; Fairlie, D. P.; Huang, X.; Atwood, C. S.; Beyreuther, K.; Tanzi, R. E.; Masters, C. L.; Bush, A. I. *J. Biol. Chem.* **1999**, *274*, 23223.
(85) Bush, A. I.; Tanzi, R. E. *Neurotherapeutics* **2008**, *5*, 421.
(86) Bonda, D. J.; Lee, H. G.; Blair, J. A.; Zhu, X.; Perry, G.; Smith, M. A. *Metallomics* **2011**, *3*, 267.
(87) Hureau, C.; Sasaki, I.; Gras, E.; Faller, P. *ChemBioChem* **2010**, *11*, 950.
(88) Braymer, J. J.; Choi, J.-S.; DeToma, A. S.; Wang, C.; Nam, K.; Kampf, J. W.; Ramamoorthy, A.; Lim, M. H. *Inorg. Chem.* **2011**, *50*, 10724.
(89) Dedeoglu, A.; Cormier, K.; Payton, S.; Tseitlin, K. A.; Kremsky, J. N.; Lai, L.; Li, X.; Moir, R. D.; Tanzi, R. E.; Bush, A. I.; Kowall, N. W.; Rogers, J. T.; Huang, X. *Exp. Gerontol.* **2004**, *39*, 1641.
(90) Rodríguez-Rodríguez, C.; Sánchez de Groot, N.; Rimola, A.; Álvarez-Larena, Á.; Lloveras, V.; Vidal-Gancedo, J.; Ventura, S.; Vendrell, J.; Sodupe, M.; Gonzalez-Duarte, P. *J. Am. Chem. Soc.* **2009**, *131*, 1436.
(91) Hindo, S. S.; Mancino, A. M.; Braymer, J. J.; Liu, Y.; Vivekanandan, S.; Ramamoorthy, A.; Lim, M. H. *J. Am. Chem. Soc.* **2009**, *131*, 16663.
(92) Choi, J. S.; Braymer, J. J.; Nanga, R. P.; Ramamoorthy, A.; Lim, M. H. *Proc. Natl. Acad. Sci. U. S. A.* **2010**, *107*, 21990.
(93) Weinreb, O.; Mandel, S.; Amit, T.; Youdim, M. B. *J. Nutr. Biochem.* **2004**, *15*, 506.
(94) Zaveri, N. T. *Life Sci.* **2006**, *78*, 2073.
(95) Hirohata, M.; Hasegawa, K.; Tsutsumi-Yasuhara, S.; Ohhashi, Y.; Ookoshi, T.; Ono, K.; Yamada, M.; Naiki, H. *Biochemistry* **2007**, *46*, 1888.
(96) Mira, L.; Fernandez, M. T.; Santos, M.; Rocha, R.; Florencio, M. H.; Jennings, K. R. *Free Radic. Res.* **2002**, *36*, 1199.
(97) Cao, S.; Jiang, X.; Chen, J. *J. Inorg. Biochem.* **2010**, *104*, 146.
(98) Reyes, A. E.; Chacon, M. A.; Dinamarca, M. C.; Cerpa, W.; Morgan, C.; Inestrosa, N. C. *Am. J. Pathol.* **2004**, *164*, 2163.
(99) Castro, A.; Martinez, A. *Curr. Pharm. Des.* **2006**, *12*, 4377.
(100) Mao, F.; Huang, L.; Luo, Z.; Liu, A.; Lu, C.; Xie, Z.; Li, X. *Bioorg. Med. Chem.* **2012**, *20*, 5884.
(101) Fernandez-Bachiller, M. I.; Perez, C.; Gonzalez-Munoz, G. C.; Conde, S.; Lopez, M. G.; Villarroya, M.; Garcia, A. G.; Rodriguez-Franco, M. I. *J. Med. Chem.* **2010**, *53*, 4927.

(102) Kochi, A.; Eckroat, T. J.; Green, K. D.; Mayhoub, A. S.; Lim, M. H.; Garneau-Tsodikova, S. *Chem. Sci.* **2013**, *4*, 4137.
(103) Telpoukhovskaia, M. A.; Patrick, B. O.; Rodriguez-Rodriguez, C.; Orvig, C. *Mol. Biosyst.* **2013**, *9*, 792.
(104) Li, S. Y.; Wang, X. B.; Xie, S. S.; Jiang, N.; Wang, K. D.; Yao, H. Q.; Sun, H. B.; Kong, L. Y. *Eur. J. Med. Chem.* **2013**, *69*, 632.
(105) Jones, G. B.; Fouad, F. S. *Curr. Pharm. Des.* **2002**, *8*, 2415.
(106) Joshi, M. C.; Rawat, D. S. *Chem. Biodivers.* **2012**, *9*, 459.
(107) Zein, N.; Sinha, A. M.; McGahren, W. J.; Ellestad, G. A. *Science* **1988**, *240*, 1198.
(108) Lee, S.; Zheng, X.; Krishnamoorthy, J.; Savelieff, M. G.; Park, H. M.; Brender, J. R.; Kim, J. H.; Derrick, J. S.; Kochi, A.; Lee, H. J.; Kim, C.; Ramamoorthy, A.; Bowers, M. T.; Lim, M. H. *J. Am. Chem. Soc.* **2014**, *136*, 299.

Chapter 2: Reactivity of Diphenylpropynone Derivatives Toward Metal-Associated Amyloid-β Species

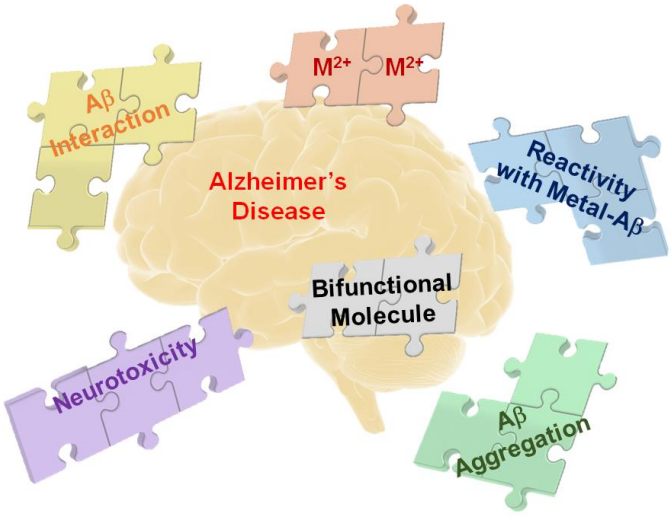

The results presented in this chapter for diphenylpropynone derivatives were previously published (Pithadia, A. S.;‡ Kochi, A.;‡ Soper, M. T.; Beck, M. W.; Liu, Y.; Lee, S.; DeToma, A. S.; Ruotolo, B. T.; Lim, M. H. *Inorg. Chem.* **2012**, *51*, 12959-12967. ‡Equal contribution.). We thank Professor Brandon Ruotolo and Molly Soper for ESI-MS experiments. Dr. Xiaoming He, Amit Pithadia, and Yuzhong Liu synthesized compounds. Amit Pithadia conducted metal binding and selectivity and solution speciation studies. Nate Merrill conducted zinc binding studies. Michael Beck performed the docking studies. Dr. Alaina DeToma conducted the *in vitro* PAMPA assay Dr. Sanghyun Lee conducted the cell experiments. I was involved in the experiments of copper binding studies of **DPP2** in the absence and presence of Aβ, the gel and TEM investigations for all Aβ aggregation studies in the present work, as well as manuscript writing with Amit Pithadia and Michael Beck.

2.1. Introduction

Alzheimer's disease (AD) is a fatal neurodegenerative disease that affects more than 5 million people in the United States.[1,2] A pathological hallmark of the diseased brain is an accumulation of misfolded amyloid-β (Aβ) aggregates.[2-8] Monomeric Aβ peptides, generated from the proteolytic cleavage of the transmembrane amyloid precursor protein, can further aggregate to produce oligomers, protofibrils, and eventually fibrils. It is still not completely understood which conformation of Aβ is associated with AD neuropathogenesis; however, recent evidence has proposed that soluble oligomers might be the toxic species due to their ability to interrupt neurotransmission.[4,5,9] In addition to Aβ species, elevated concentrations of transition metals, such as Fe, Cu, and Zn, have been observed within the deposits of Aβ aggregates.[2,7,8,10-15] The possible relationship between metal-associated Aβ species (metal–Aβ species) and neurotoxicity has been suggested based on observations that upon binding to Aβ, metal ions facilitate peptide aggregation as well as enhance oxidative stress caused by overproduction of reactive oxygen species;[2,4,5,7,8,12-21] however, this connection has not been clearly revealed.

To gain a better understanding of the involvement of metal–Aβ species in AD pathogenesis, recent advancements in the development of chemical reagents to specifically target metal–Aβ species and modulate their interaction and reactivity have been made.[2,7,8,21-33] Among them, rationally designed small molecules with both metal chelation and Aβ interaction properties (defined as bifunctionality) have been devised. Some of the compounds have been fashioned based on the incorporation approach (Figure 2.1), where a metal chelation site is directly inserted into a known Aβ imaging agent with minimal structural modifications, along with consideration of criteria for possible brain uptake.[8,21-25,27-35] These molecules have been shown to be able to control the interactions and reactivity of metal–Aβ species *in vitro* and/or in living cells, suggesting that the incorporation approach (Figure 2.1) could be considered as a promising design strategy to fashion suitable chemical reagents for uncovering the potential role of metal–Aβ species in AD development.

Herein, we report the design and preparation of a new class of bifunctional small molecules (**DPP1** and **DPP2**, Figure 2.1), composed of a diphenylpropynone framework, as chemical reagents for targeting and regulating metal–Aβ species, the characterization of their interactions with metal ions and Aβ species, as well as the investigation of their *in vitro* reactivity with metal–Aβ species. From our overall results and observations, the diphenylpropynone scaffold could be a structural feature for constructing chemical reagents for investigating metal–Aβ species. Moreover, the dimethylamino functionality in **DPP2** was observed to be an important moiety for potentially enhancing Aβ interaction of the compound, as reported previously,[29,31,36] offering noticeable reactivity with metal–Aβ species.

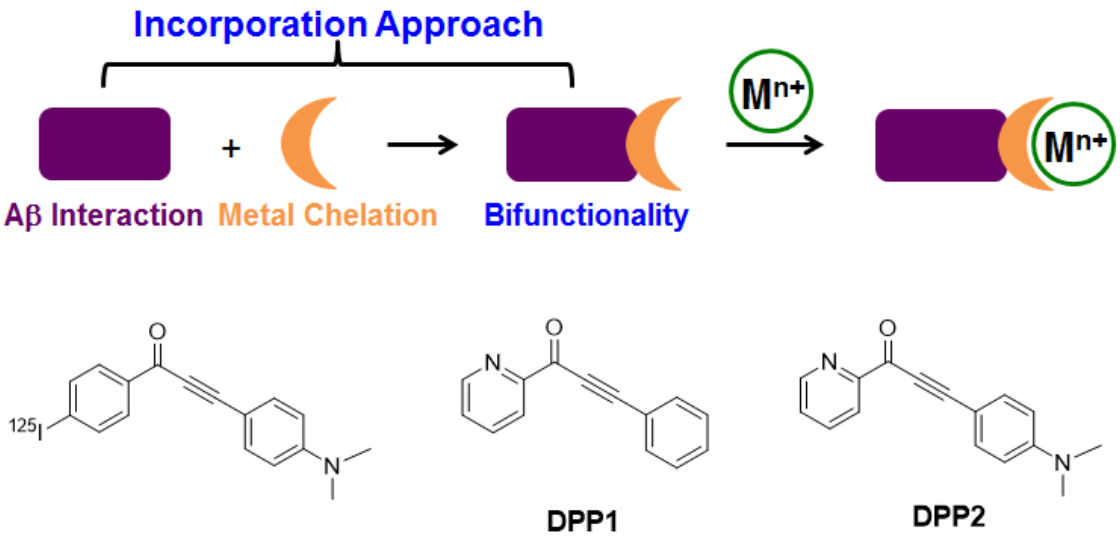

Figure 2.1. Incorporation approach (top) and structures of small molecules (bottom). Left to right: 3-(4-(dimethylamino)phenyl)-1-(4-iodophenyl)prop-2-yn-1-one; **DPP1** = 3-phenyl-1-(pyridin-2-yl)prop-2-yn-1-one; **DPP2** = 3-(4-(dimethylamino)phenyl)-1-(pyridin-2-yl)prop-2-yn-1-one.

2.2. Results and discussion

2.2.1. Design consideration, preparation, and characterization of diphenylpropynone derivatives for targeting and modulating metal–Aβ species

The diphenylpropynone scaffold was shown to have high binding affinity (*ca*. 6 nM) for Aβ aggregates; thus it has been utilized for the design of an Aβ plaque imaging probe (Figure 2.1).[37] Based on the incorporation approach, a nitrogen donor atom was

installed into this framework to generate a metal chelation site with an oxygen donor atom from the carbonyl group, which afforded two bifunctional molecules (**DPP1** and **DPP2**, Figure 2.1). Furthermore, a minor structural difference between **DPP1** and **DPP2** (*i.e.*, a dimethylamino functionality, suggested to be critical for Aβ interaction)[29,31,36] was included to understand a structure-reactivity relationship. **DPP1** was synthesized as previously established.[38-40] The new compound, **DPP2**, was prepared by slight modifications to a previously report method (Scheme 2.1).[40]

Scheme 2.1. Synthesis of **DPP2**

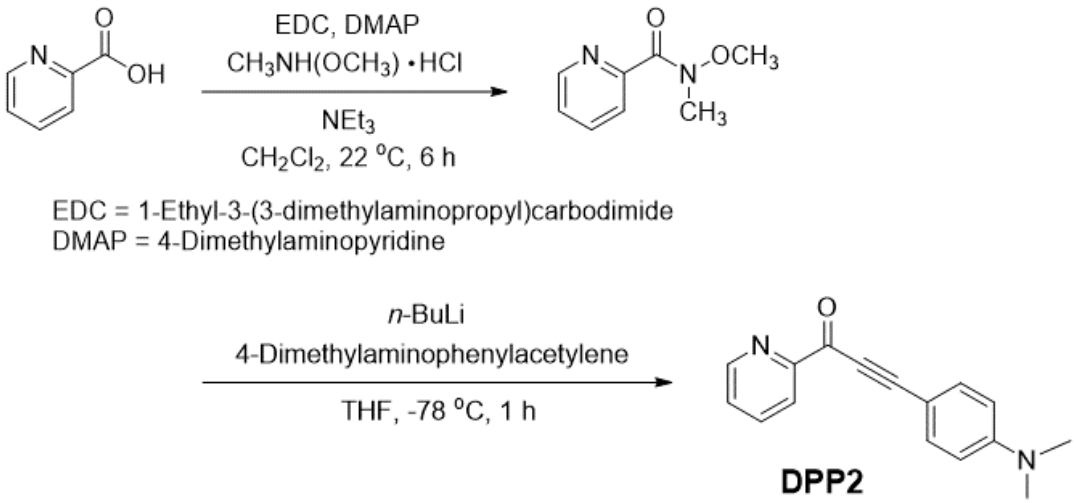

To predict potential druglike and BBB penetration properties of the structural scaffolds of **DPP1** and **DPP2**, we calculated values of Lipinski's rules and logBB.[7,34,35,41,42] As shown in Table 2.1, the theoretical values indicate that both compounds are druglike and possibly BBB permeable. To verify this prediction for BBB penetration of compounds, we performed *in vitro* PAMPA-BBB following a previously reported procedure.[29,41-43] Permeability values ($-\log P_e$) was measured to be 4.2 (± 0.1) for both **DPP1** and **DPP2** (Table 2.1). On the basis of empirical classification of BBB-permeable molecules (*i.e.*, verapamil),[29,41-43] **DPP1** and **DPP2** would also be likely to cross the BBB.

Table 2.1. Values (MW, *c*logP, HBA, HBD, PSA, logBB, and –logP_e) of **DPP1** and **DPP2**.

Calculation[a]	**DPP1**	**DPP2**	Lipinski's rules & others
MW	207	250	≤ 450
*c*logP	2.47	2.63	≤ 5.0
HBA	2	3	≤ 10
HBD	0	0	≤ 5
PSA	30.0	33.2	≤ 90
logBB	0.0618	0.0390	< –1.0 (poorly distributed in the brain.
–logP_e[b]	4.2 ± 0.01	4.2 ± 0.01	
CNS +/– Prediction[c]	CNS+	CNS+	–logP_e < 5.4 (CNS+) > 5.7 (CNS–)

[a] MW, molecular weight; *c*logP, calculated logarithm of the octonal-water partition coefficient; HBA, hydrogen-bond acceptor atoms; HBD, hydrogen-bond donor atoms; PSA, polar surface area; logBB = –0.0148 x PSA + 0.152 x *c*logP + 0.130. [b] The values of –logP_e were measured by the Parallel Artificial Membrane Permeability Assay for BBB (PAMPA-BBB). [c] Compounds categorized as central nervous system, CNS+ have the ability to permeate through the BBB and target the CNS. In the case of compounds assigned as CNS– they have poor permeability through the BBB and therefore, their bioavailability into the CNS is considered to be minimal.

Along with BBB permeability, the solution speciation of **DPP1** and **DPP2** was determined through UV-vis variable-pH titration experiments (I = 0.10 M NaCl; room temperature; pH 2–10).[27,29-33,44,45] As summarized in Figure 2.2, titration results indicated a single acidity constant (pK_a) for **DPP1** (pK_a = 2.035(5)) and two pK_a values for **DPP2** (pK_{a1} = 7.106(1) and pK_{a2} = 2.959(4)). These pK_a values suggest that monoprotonated, diprotonated, and neutral species exist in solution of **DPP2** depending on pH (from 2 to 10), while the monoprotonated and neutral forms of **DPP1** are present in this pH range (Figure 2.2). In addition, the generated solution speciation diagrams of **DPP1** and **DPP2** exhibit that their neutral forms are relatively predominant at physiologically relevant pH (*i.e.*, 7.4) (**DPP1**, 100%; **DPP2**, *ca*. 65%).

2.2.2. Metal binding properties of DPP1 and DPP2

Metal binding properties of **DPP1** and **DPP2** (specifically, Cu^{2+} and Zn^{2+}) were studied by UV-vis and NMR spectroscopy. Upon the addition of $CuCl_2$ (1–20 equiv) to a solution of **DPP1** and **DPP2** in EtOH, new optical bands were observed, indicative of Cu^{2+} binding to the ligand (Figure 2.3a). In particular, in the presence of Cu^{2+}, **DPP2**,

which has a dimethylamino group, showed a distinguishable optical shift from 407 nm to 525 nm. NMR was employed to investigate the interaction of **DPP1** or **DPP2** with Zn^{2+}. When 1 equiv of $ZnCl_2$ was introduced in a solution of **DPP1** or **DPP2** (in CD_3CN), noticeable downfield chemical shifts of the pyridyl protons were recorded (Figure 2.3b), demonstrating that Zn^{2+} binding to the ligand occurred through the pyridyl N-donor

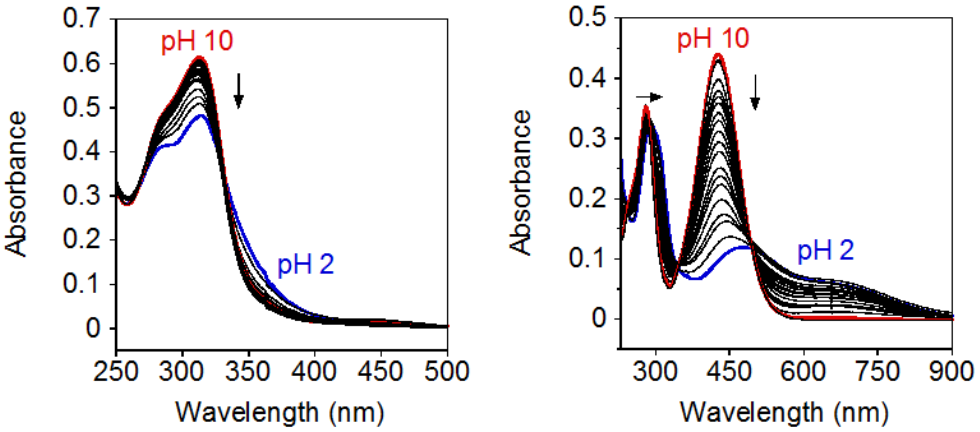

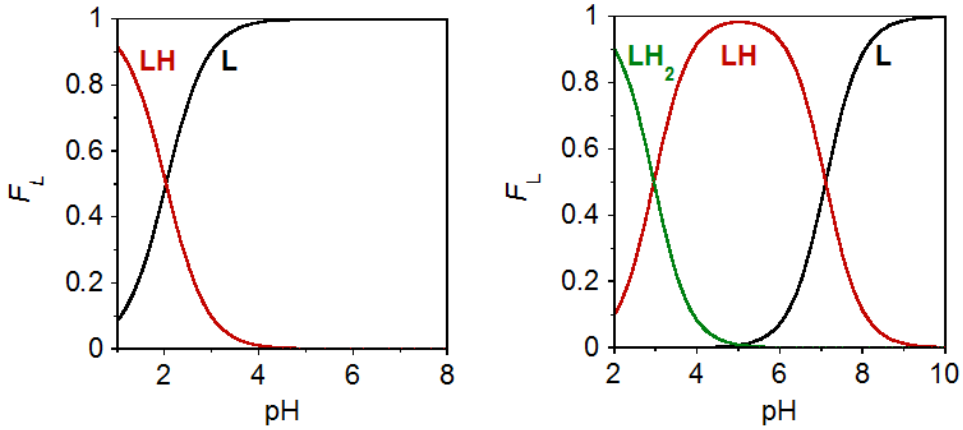

			pK_a[a]	
			DPP1	**DPP2**
LH_2	⇌ LH + H	(pK_{a1})	–	7.106(1)
LH	⇌ L + H	(pK_{a2})	2.035(5)	2.959(4)

Figure 2.2. Solution speciation studies of **DPP1** and **DPP2**. Top: UV-vis spectra of **DPP1** (40 μM, left) and **DPP2** (20 μM, right) in the range of pH 2–10. Middle: Solution speciation diagrams for **DPP1** (left) and **DPP2** (right) (F_L = fraction of compound with given protonation). Bottom: Acidity constants (pK_a) of L (L = **DPP1** or **DPP2**). Charges are omitted for clarity. [a] Error in the parentheses is shown in the last digit. Conditions: I = 0.10 M NaCl; room temperature.

atom.[45] Overall, both UV-vis and NMR studies confirmed Cu^{2+} and Zn^{2+} binding to **DPP1** and **DPP2**.To further identify binding stoichiometry and affinity, the solution speciation investigation of Cu^{2+}–**DPP2** complexes was carried out through UV-vis variable-pH titration experiments (1:2 [Cu^{2+}]/[**DPP2**]; I = 0.10 M NaCl, room temperature). Based onthe pK_a values of **DPP2** and these titration results, stability constants for the Cu^{2+}–**DPP2** complexes were obtained (Figure 2.4, M + LH ⇆ M(LH) ($\log\beta_1$ = 12.99(9)); M + L ⇆ ML ($\log\beta_2$ = 5.85(3)); M = Cu^{2+}, L = **DPP2**). A solution speciation diagram was

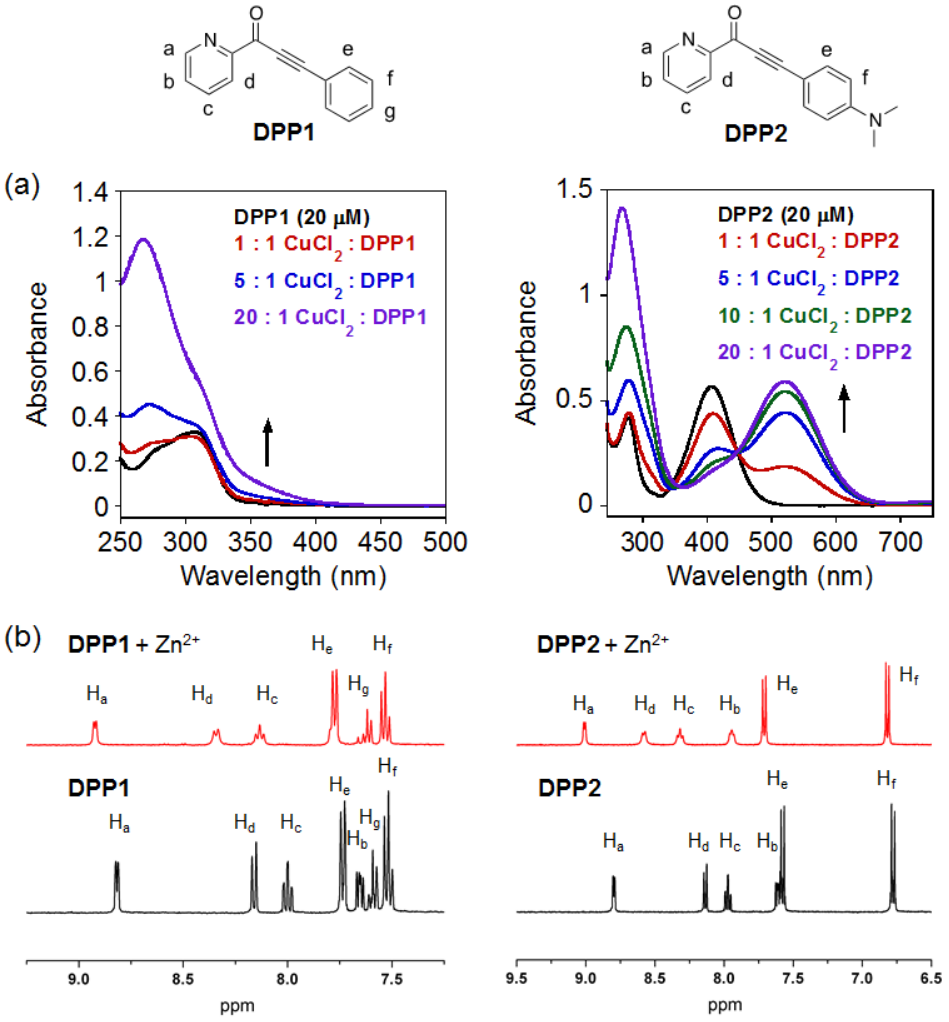

Figure 2.3. Cu^{2+} or Zn^{2+} binding of **DPP1** and **DPP2**. (a) UV-vis spectra of **DPP1** (left) and **DPP2** (right) with $CuCl_2$ (1–20 equiv) in EtOH at room temperature (incubation for 2.5 h (for **DPP1**) and 5 min (for **DPP2**)). (b) ^{1}H NMR spectra of **DPP1** (left, black) or **DPP2** (right, black) with $ZnCl_2$ (red) in CD_3CN at room temperature ([compound] = 4 mM; [$ZnCl_2$] = 4 mM).

generated from these stability constants, suggesting that the major species at pH 7 are a mixture of Cu(LH) and CuL complexes in a ratio of 3:2. Free Cu^{2+} was shown up to pH 7, indicating pCu = 6.6 at pH 6.6 (pCu = –log[$Cu_{unchelated}$]) (Figure 2.4).[27,29,31-33,44,45] The pCu value suggests the approximate dissociation constant (K_d) of Cu^{2+}–**DPP2** to be *ca.* high nanomolar. When compared to the reported K_d values of Cu^{2+}–Aβ (picomolar to nanomolar),[2,5,7,8,12,14,21] **DPP2** may interact with Cu^{2+} from soluble Cu^{2+}–Aβ species. In order to test if Cu^{2+} binding of ligand occurs in the presence of Aβ, a solution containing **DPP2** with Cu^{2+}-treated Aβ was monitored by UV-vis. The new spectral features that coincided with those of the Cu^{2+}–**DPP2** complex without Aβ were observed, suggesting

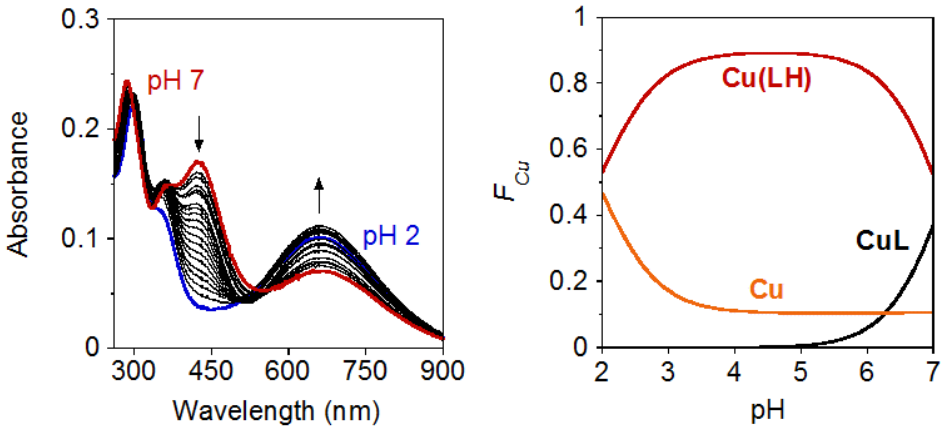

			$\log\beta^{a,b}$
Cu + LH	⇌	Cu(LH)	12.99(9)
Cu + L	⇌	CuL	5.85(3)
Cu + 2L	⇌	CuL_2	1.7(6)

Figure 2.4. Solution speciation investigation of the Cu^{2+}–**DPP2** complexes. Top left: UV-vis spectra (pH 2–7) of Cu^{2+}–**DPP2** complexes. ([Cu^{2+}]/[L] = 1:2; $[Cu^{2+}]_{total}$ = 10 μM; 7 h incubation with ligand (L) prior to pH titration, L = **DPP2**; room temperature). Top right: Solution speciation diagram of the Cu^{2+}–**DPP2** complexes (F_{Cu} = fraction of free Cu and Cu complexes). Bottom: Stability constants ($\log\beta$) of the Cu^{2+}–**DPP2** complexes. Charges are omitted for clarity. [a] Error in the parentheses is shown in the last digit. [b] The species containing CuL_2 was introduced into the calculation model yielding a good fit to the data.

an interaction of **DPP2** with Cu^{2+} in the presence of Aβ (Figure 2.5), Cu^{2+} binding of **DPP2** with Aβ occurred more slowly than that without Aβ, proposing that Aβ might interfere with metal binding to the ligand. Taken together, our spectroscopic studies

present the capability of **DPP1** and **DPP2** to chelate Cu^{2+} and Zn^{2+}, as well as the potential interaction of **DPP2** with Cu^{2+} in the presence of Aβ species, which may be associated with its noticeable reactivity toward metal–Aβ species (*vide infra*).

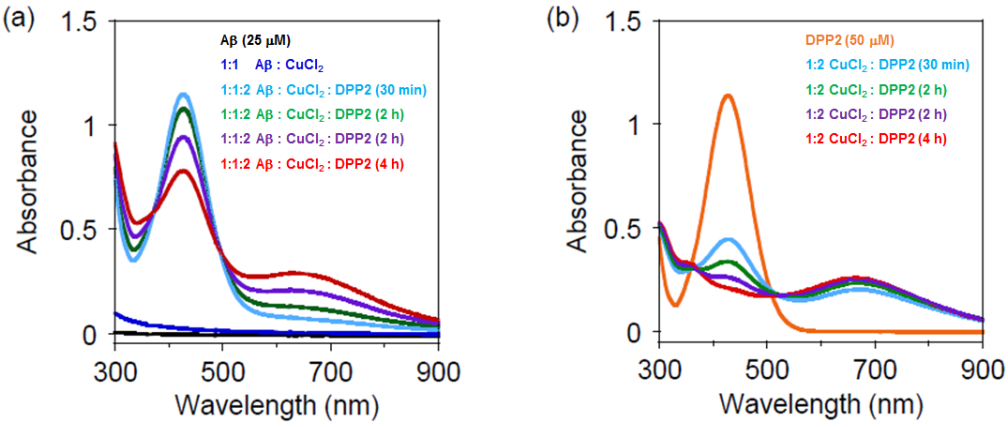

Figure 2.5. Cu^{2+} binding studies of **DPP2** in the absence and presence of Aβ at pH 6.6. (a) UV-vis spectra of Aβ (black), [Aβ + $CuCl_2$] (blue), and [Aβ + $CuCl_2$ + **DPP2**] (1:1:2 ratio, 30 min to 4h incubation; various colors). (b) UV-vis spectra of **DPP2** without (orange) and with $CuCl_2$ (green). Conditions: [Aβ] = 25 μM; [$CuCl_2$] = 25 μM; [**DPP2**] = 50 μM; 20 mM HEPES, pH 6.6, 150 mM NaCl; room temperature.

The metal selectivity of **DPP1** and **DPP2** was also determined by competitive reactions with Cu^{2+} over biologically relevant divalent metal ions (Mg^{2+}, Ca^{2+}, Mn^{2+}, Fe^{2+}, Co^{2+}, Ni^{2+}, and Zn^{2+}), which was monitored by UV-vis. As depicted in Figure 2.6, **DPP1** and **DPP2** displayed selectivity for Cu^{2+} over Mg^{2+}, Ca^{2+}, Mn^{2+}, and Zn^{2+}. Binding of both ligands to Co^{2+} and Ni^{2+} was also observed. Considering the lower abundance of Co^{2+} and Ni^{2+} than Cu^{2+} in biological systems,[46,47] the overall selectivity of **DPP1** and **DPP2** may be sufficient to be used for targeting and interacting with Cu^{2+}–Aβ species in heterogeneous biological environments like the brain.

2.2.3. Aβ interaction with DPP1 and DPP2 studied by MS and docking studies

The interaction of **DPP1** and **DPP2** with $Aβ_{40}$ in the absence of metal ions were probed by ESI-MS, tuned to preserve noncovalent protein-ligand interactions.[48] At a low Aβ concentration (10 μM), a small signal corresponding to the interaction between **DPP2** (30 μM) and the Aβ monomer in the 3^+ charge state could be detected, whereas no interaction between **DPP1** (60 μM) and the peptide was observed under these

conditions (Figure 2.7). At high concentrations of the peptide (100 μM) and compounds (600 μM), both **DPP1** and **DPP2** interacted with Aβ species to different extents (Figure 2.8a). Data for **DPP1** indicated that the molecule interacted broadly with Aβ monomers and oligomers in 1:1, 2:1, and 3:1 Aβ to ligand ratios. In the case of **DPP2**, a stronger preference toward larger Aβ oligomers was shown, but with similar stoichiometries as **DPP1**. The total bound intensities recorded from MS data, and those from individual oligomeric species were shown in Figure 2.8b and Table 2.2.

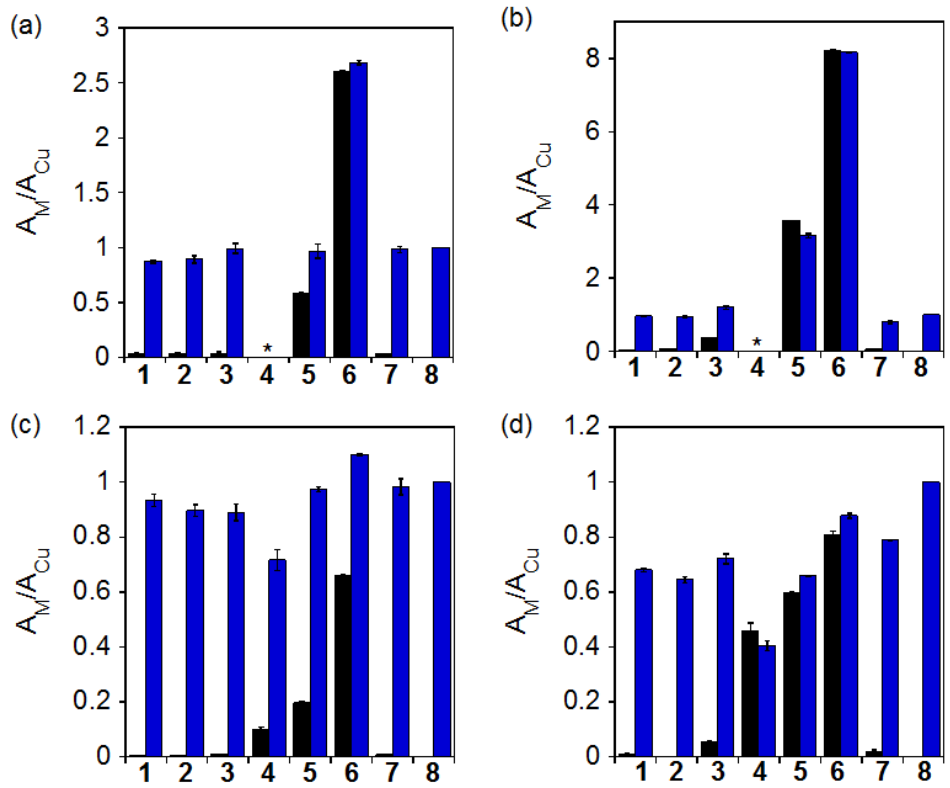

Figure 2.6. Metal selectivity studies of **DPP1** (a and b; 40 μM) and **DPP2** (c and d; 20 μM) in EtOH. Blue bars represent the addition of $CuCl_2$ (**8**) to solutions of the ligand with other divalent metal ions (black bars; **1**, $MgCl_2$; **2**, $CaCl_2$; **3**, $MnCl_2$; **4**, $FeCl_2$; **5**, $CoCl_2$; **6**, $NiCl_2$; **7**, $ZnCl_2$) in a ratio of 1:1 (a and c) or 1:25 (b and d) Cu^{2+} to M^{2+} followed by 5 min incubation at room temperature. The absorbance at 360 nm (for **DPP1**) and 580 nm (for **DPP2**) was used for the calculation of A_M/A_{Cu}. * Indicates that precipitation was observed in the solution.

The intensities shown were normalized for both nonspecific interactions and artifactual complexes formed during the electrospray process using Aβ:ThT binding data as a control, and ion mobility separation was used to separate oligomers that overlapped in *m*/*z*.[6,48,49] From these data, it was clear that, at high concentrations, a

higher proportion of **DPP1** was bound to Aβ species than **DPP2**, but that both could be classified as having weak Aβ affinity in solution (low mM K_d). Therefore, a weak Aβ/compound interaction was captured by MS. Normalized intensity MS data suggest that **DPP2** binding was almost exclusively driven through Aβ multimer interactions (Figure 2.8b). Overall our MS results suggest that although both compounds could interact with Aβ species at high concentrations, **DPP2** was able to bind Aβ species at both low and high concentrations.

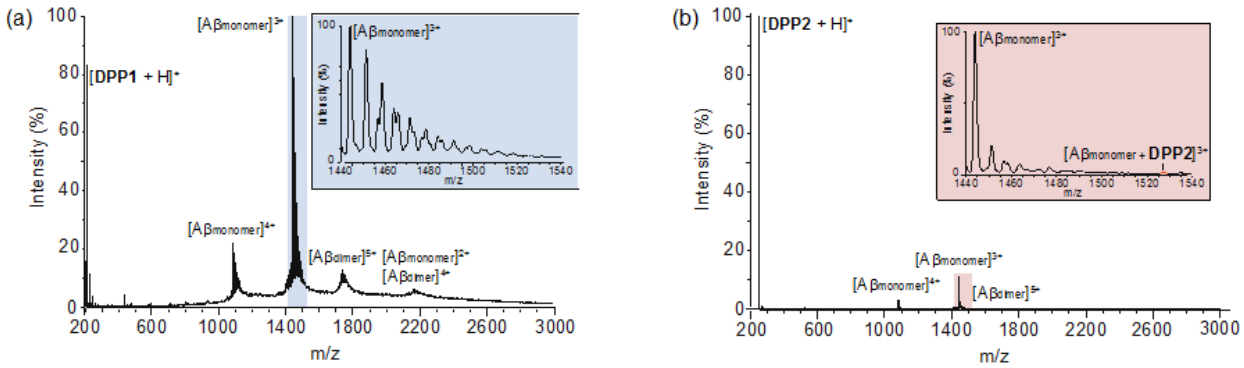

Figure 2.7. Interactions of (a) **DPP1** (60 μM) and (b) **DPP2** (30 μM) with $A\beta_{40}$ (10 μM) determined by nano-electrospray ionization-mass spectrometry (nESI-MS). Binding of **DPP2** to Aβ monomer was observed in a ratio of 3:1 in the 3^+ charge state (incubation = 2 h on ice).

To visualize the potential interaction between Aβ and **DPP1**/**DPP2**, docking studies by AutoDock Vina[50] were performed using the previously determined NMR structure (PDB 2LFM)[51] of $A\beta_{40}$ monomer. Typically, both compounds were positioned between the α-helix and the unstructured *N*-terminal side of Aβ (Figure 2.8c and 2.9). Most docked structures showed a nonspecific orientation of the ligand with respect to the surface features of Aβ. Our preliminary docking studies support the potential interaction of the compounds with Aβ monomer.

2.2.4. Effects of DPP1 and DPP2 on metal-free and metal-induced Aβ aggregation *in vitro*

Confirming metal binding and Aβ interaction properties (bifunctionality) of **DPP1** and **DPP2**, their influence on *in vitro* metal-free and metal-induced Aβ aggregation was

studied.[26-33] Two different experiments (inhibition and disaggregation) were performed to investigate whether **DPP1**/**DPP2** can control the formation of metal-free and metal-induced Aβ aggregates (inhibition, Figure 2.10) or transform preformed metal-free and metal-induced Aβ aggregates (disaggregation, Figure 2.11). Various-sized Aβ species from both studies were monitored by gel electrophoresis and SDS-PAGE followed by

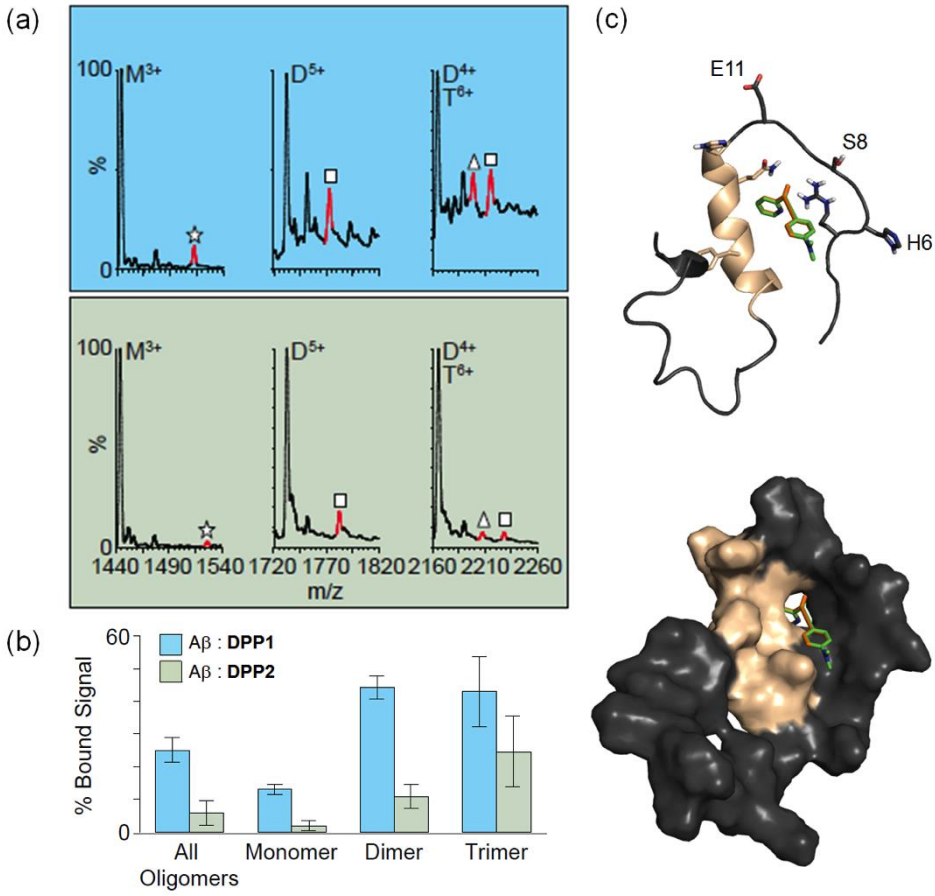

Figure 2.8. Interactions of **DPP1** and **DPP2** with Aβ. (a) MS data for the complexes of $A\beta_{40}$ and **DPP1** or **DPP2** ([Aβ] = 100 μM; [compound] = 600 μM; M = monomer, D = dimer, and T = trimer). Many binding stoichiometries were detected, including 1:1 (star), 2:1 (square), and 3:1 (triangle). (b) A histogram showing the total bound MS signal intensity, normalized for nonspecific interactions and ESI-MS artifacts, for each binding stoichiometry observed in (a). (c) Docking studies of **DPP1** (orange) and **DPP2** (green) with $A\beta_{40}$ (PDB 2LFM) by AutoDock Vina. Poses for both compounds were overlapped in this conformation (other conformations, see Figure 2.9). The helical region of Aβ (H13-D23) is highlighted in color (tan) in both the cartoon (top) and surface (bottom) representation.

Western blot with an anti-Aβ antibody (6E10), whereas morphological changes were identified by transmission electron microscopy (TEM).[26,28-33,52]

Table 2.2. Raw MS signal intensity data for the interaction of **DPP1** or **DPP2** with $A\beta_{40}$.

	DPP1					
	Avg Unbound Signal	*Avg Bound Signal*	*Total Signal for Bound/Unbound*	*% Bound*	*% ThT Bound*	*Normalized % Bound*
Monomer	20966.82	4336.01	25302.84	17.14	0.26	16.88
Dimer	2527.24	1386.40	3913.64	35.42	0.00	35.42
Trimer	444.05	450.33	894.38	50.35	5.71	44.64
All Oligomers	23938.12	6172.74	30110.86	20.50	0.43	20.07
	DPP2					
	Avg .Unbound Signal	*Avg. Bound Signal*	*Total Signal for Bound/Unbound*	*% Bound*	*% ThT Bound*	*Normalized % Bound*
Monomer	4386.14	230.22	4616.37	4.89	0.26	4.63
Dimer	929.44	251.82	1181.26	20.37	0.00	20.37
Trimer	520.65	238.58	759.23	29.71	5.71	24.00
All Oligomers	5836.23	720.63	6556.86	10.60	0.43	10.18

The inhibition studies, as shown in Figure 2.10, demonstrated a different reactivity of **DPP1** or **DPP2** toward metal-induced Aβ species over metal-free Aβ species. In the case of metal-involved Aβ aggregation, Aβ species with a wide range of MW were indicated with **DPP2** for both Cu^{2+}- and Zn^{2+}-treated samples upon longer incubation (Figure 2.10a, lanes 6 and 9). In the samples containing **DPP1** (lanes 5 and 8), less intense gel bands were detected across the longer incubation time, suggesting that further Aβ aggregation may have occurred. The reaction of **DPP1** or **DPP2** with metal-free Aβ also exhibited a different distribution of various-sized Aβ species (Figure 2.10a, lanes 2 and 3). Aβ species formed with compounds in both metal-mediated and metal-free conditions were not completely denatured by SDS implying that these molecules may generate different Aβ assemblies (Figure 2.10b). TEM images of metal-induced Aβ species incubated with **DPP2** for 24 h revealed smaller amorphous aggregates compared to **DPP1**; some of the metal-free Aβ species treated with **DPP1** and **DPP2** presented similar morphology to those untreated with compounds (Figure 2.10c). Overall, **DPP1** and **DPP2** displayed their ability to recognizably modulate metal-induced Aβ aggregation to different extents.

Furthermore, for the disaggregation experiment (Figure 2.11), **DPP2**-treated metal-triggered Aβ aggregates presented different-sized Aβ species than **DPP1**-treated samples, indicating that **DPP2** could alter the properties of preformed Aβ aggregates to a greater extent than **DPP1** (Figure 2.11). In the metal-free conditions, more various-sized Aβ species were indicated in the presence of **DPP2** than **DPP1** (in particular, at 4 h, Figure 2.11, lanes 2 and 3). The Aβ species generated with compounds in both

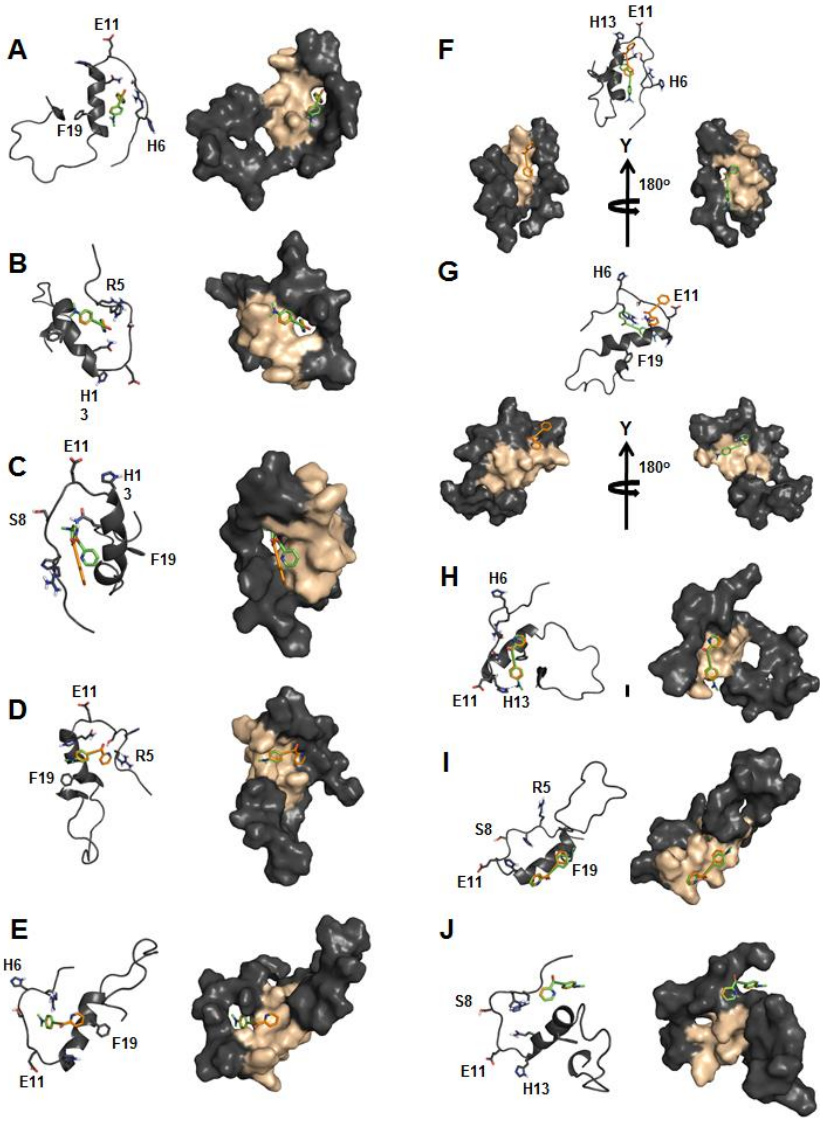

Conformation (PDB 2LFM)	DPP1 (kcal/mol)	DPP2 (kcal/mol)
A	-6.3	-6.5
B	-6.1	-6.1
C	-5.6	-5.8
D	-5.5	-5.7
E	-5.6	-5.7
F	-5.9	-5.5
G	-5.4	-5.5
H	-5.4	-5.3
I	-5.4	-5.3
J	-5.2	-5.3

Figure 2.9. Docking studies of **DPP1** and **DPP2**. Cartoon (left) and surface (right) versions of possible conformations of **DPP1** (orange) and **DPP2** (green) docked with $A\beta_{40}$ (PDB 2LFM) by AutoDock Vina. The helical region of Aβ (H13-D23) in the surface representation is highlighted in color (tan) and hydrogen bonding is indicated with dashed lines (2.5-2.8 Å). Conformation A is also depicted in Figure 2.8c. Bottom: Calculated binding energies of **DPP1** and **DPP2** to Aβ.

metal-triggered and metal-free conditions were relatively stable in the presence of SDS (Figure 2.11b). As shown in Figure 2.11c, **DPP2** was able to reorganize preformed structured metal–Aβ aggregates to amorphous species more noticeably than **DPP1**. Taken together, the results from both inhibition and disaggregation experiments presented that **DPP1** and **DPP2** could regulate metal-involved Aβ aggregation over metal-free aggregation *in vitro* differently. Moreover, the structural variation (*i.e.*, dimethylamino functionality) may enhance the contact with Aβ species *via* hydrogen bonding and/or hydrophobic interactions,[29,31,36] which may afford greater reactivity toward metal–Aβ species.

2.3. Conclusion

Following the incorporation approach, we have developed two bifunctional small molecules (**DPP1** and **DPP2**) composed of a metal chelation site and diphenylpropynone framework (for Aβ interaction), which could possible serve as chemical reagents to target and modulate metal–Aβ species *in vitro*. Their bifunctionality (metal-chelation and Aβ interaction) was confirmed by physical methods and preliminary docking studies. Biochemical and TEM studies revealed that **DPP1** and **DPP2** could modulate metal-induced Aβ aggregation *in vitro*. Notably, **DPP2**, which has a dimethylamino group, exhibited more apparent reactivity toward metal–Aβ species, compared to **DPP1**. This suggests that the interaction and reactivity of molecules with metal–Aβ species can be tuned by such structural variations, proposing a structure-interaction-reactivity relationship. **DPP1** and **DPP2**, however, would be limited in their biological applications since they displayed cytotoxicity in living cells at low micromolar concentrations (Figure 2.12). Overall, the promising *in vitro* reactivity of these potentially BBB-permeable molecules toward metal–Aβ species warrants pursuit of structural modifications that would improve the viability of diphenylpropynone derivatives in biological settings, followed by more detailed characterization by MS and molecular modeling. Our studies have demonstrated the capability of two diphenylpropynone derivatives to target metal–Aβ species and modulate their interaction and reactivity *in vitro*, which can be further optimized toward the development of future chemical

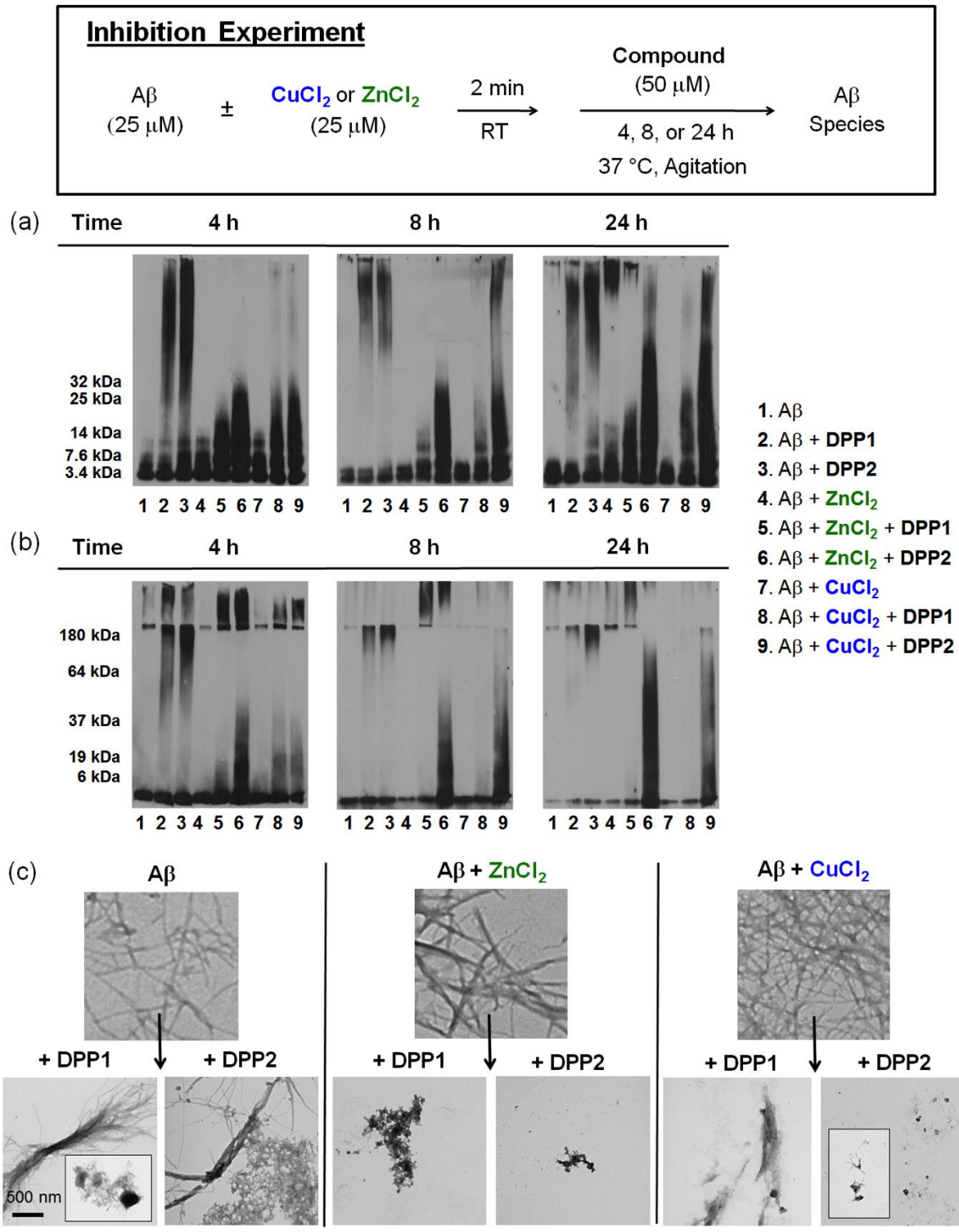

Figure 2.10. Inhibition experiment (scheme, top). Analysis of various-sized Aβ species by (a) gel electrophoresis and (b) SDS-PAGE (nonreducing conditions) with Western blot using an anti-Aβ antibody (6E10). (c) TEM images of the 24 h incubated samples. Conditions: [Aβ] = 25 μM; [$CuCl_2$ or $ZnCl_2$] = 25 μM; [compound] = 50 μM; pH 6.6 (for Cu^{2+} samples) or 7.4 (for metal-free and Zn^{2+} samples); 4, 8, or 24 h incubation; 37 °C; constant agitation.

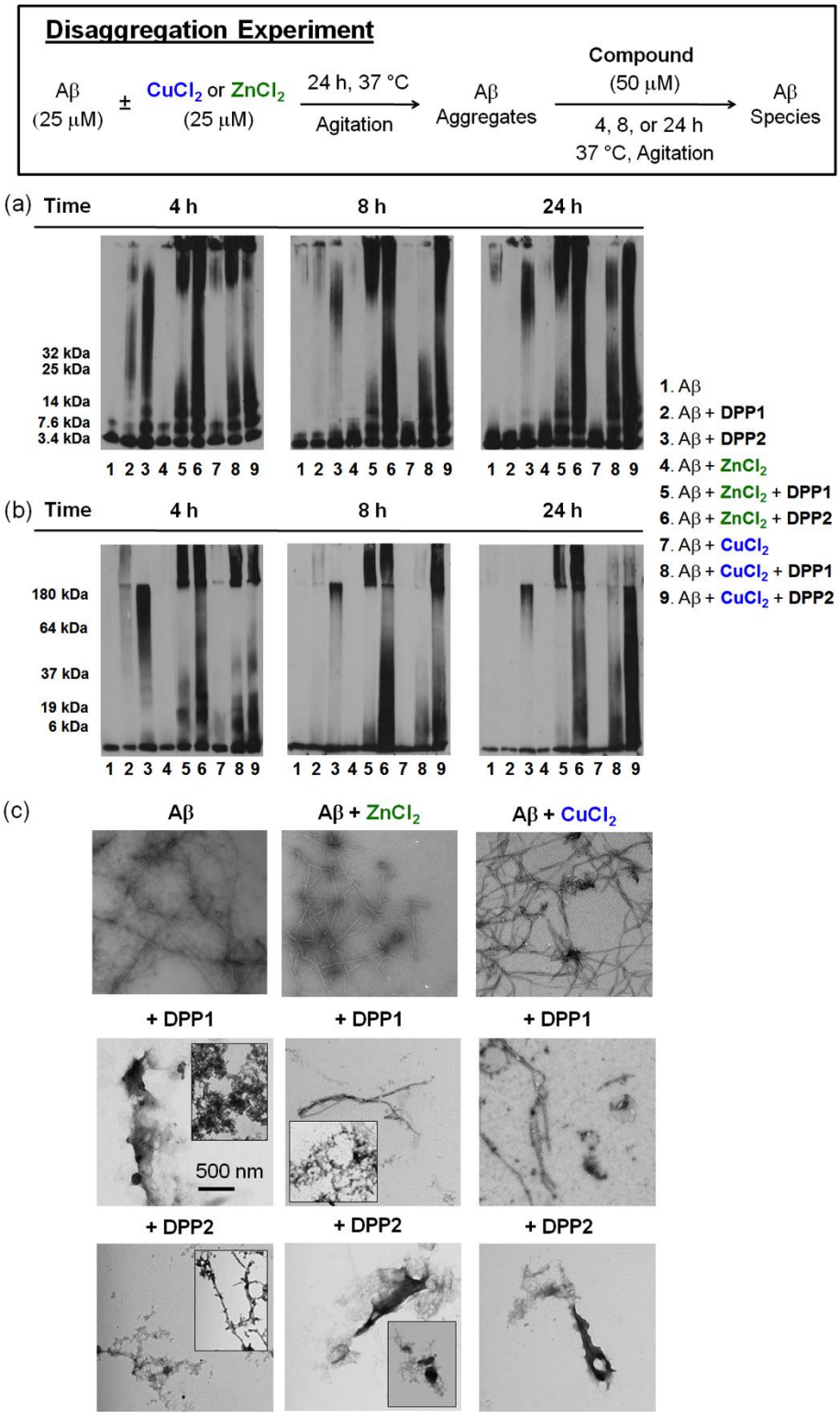

Figure 2.11. Disaggregation experiment (scheme, top). Analysis of various-sized Aβ species by (a) gel electrophoresis and (b) SDS-PAGE (nonreducing conditions) with Western blot using an anti-Aβ antibody (6E10). (c) TEM images of the 24 h incubated samples. Conditions: [Aβ] = 25 μM; [$CuCl_2$ or $ZnCl_2$] = 25 μM; [compound] = 50 μM; pH 6.6 (for Cu^{2+} samples) or 7.4 (for metal-free and Zn^{2+} samples); 4, 8, or 24 h incubation; 37 °C; constant agitation.

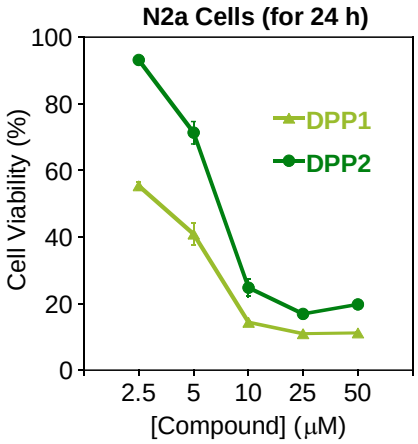

Figure 2.12. Cytotoxicity of **DPP1** and **DPP2** at various concentrations (24 h incubation) in murine Neuro-2a neuroblastoma cells, which was determined by a MTT assay. Values of cell viability (%) were calculated relative to cells treated with 1% v/v DMSO.

reagents for investigating metal–Aβ species in biological systems.

2.4. Experimental section

2.4.1. Materials and procedures

All reagents were purchased from commercial suppliers and used as received unless otherwise stated. The compound, 3-phenyl-1-(pyridin-2-yl)prop-2-yn-1-one (**DPP1**) was prepared following previously reported methods.[38-40] $A\beta_{40}$ (DAEFRHDSGYEVHHQKLV-FFAEDVGSNKGAIIGLMVGGVV) was purchased from AnaSpec (Fremont, CA). An Agilent 8453 UV-visible (UV-vis) spectrophotometer was used to measure the optical spectra. Transmission electron microscopy (TEM) images were recorded with a Philips CM-100 transmission electron microscope. A SpectraMax M5 microplate reader (Molecular Devices, Sunnyvale, CA) was employed for the measurement of absorbance for 3-(4,5-dimethylthiazol-2-yl)-2,5-diphenyltetrazolium bromide (MTT) and Parallel Artificial Membrane Permeability adapted for the BBB (PAMPA-BBB) assays. Nuclear magnetic resonance (NMR) spectra of small molecules and for Zn^{2+} binding studies were obtained by a Varian 400 MHz NMR spectrometer. Mass spectrometric measurements for compounds were conducted by a Micromass LCT Electrospray time-of-flight mass spectrometer. Mass spectrometric studies for investigating the interaction

of **DPP1** and **DPP2** with the peptide were carried out on a Waters Synapt G2 ion-mobility mass spectrometer (Milford, MA).

2.4.2. Preparation of 3-(4-(dimethylamino)phenyl)-1-(pyridin-2-yl)-2-propyn-1-one (DPP2)

DPP2 was synthesized by slight modifications to a previously reported procedure (Scheme 2.1).[40] To a solution of 4'-dimethylaminophenyl acetylene (0.42 g, 2.9 mmol) in dry tetrahydrofuran (THF, 5 mL) was added *n*-butyllithium (0.72 mL, 2.9 mmol, 2.5 M solution in hexanes) dropwise by a syringe over 5 min at −40 °C. The reaction mixture was allowed to stir at −40 °C for 10 min and then warmed to −15 °C. After 30 min, the mixture was cooled to −78 °C (dry ice/acetone) and a solution of Weinreb's amide (0.40 g, 2.4 mmol in 9 mL of dry THF) was introduced through a syringe. The reaction mixture was allowed to react at −78 °C for 10 min and then warmed to room temperature and followed by 1 h stirring. The reaction was quenched by adding saturated aqueous $NaHCO_3$ (2 mL), diluted with EtOAc (10 mL), and washed with brine (2 x 25 mL). The aqueous layer was extracted with EtOAc (2 x 15 mL), and the combined organic solutions were dried over $MgSO_4$ and filtered, followed by removal of the solvent *in vacuo*. The crude product was purified by silica gel chromatography (CH_2Cl_2:EtOAc = 9:1) to yield an orange product (202 mg, 0.81 mmol, 28%). ^{1}H NMR (400 MHz, $CDCl_3$)/δ (ppm): 8.77 (d, *J* = 4.8 Hz, 1 H), 8.14 (d, *J* = 7.6 Hz, 1 H), 7.82 (td, *J* = 7.6, 1.6 Hz, 1 H), 7.57 (d, *J* = 8.4 Hz, 2 H), 7.44 (m, 1 H), 6.59 (d, *J* = 8.4 Hz, 2 H), 2.98 (s, 6 H). ^{13}C NMR (100 MHz, $CDCl_3$)/δ (ppm): 177.6, 153.7, 151.8, 149.7, 136.8, 135.6, 126.9, 123.3, 111.4, 105.5, 100.2, 89.3, 39.9. HRMS: Calcd for $[M+H]^+$, 251.1179; Found, 251.1176.

2.4.3. Parallel Artificial Membrane Permeability Assay adapted for blood-brain barrier (PAMPA-BBB)

PAMPA-BBB experiments were carried out using the PAMPA Explorer kit (Pion Inc. Billerica, MA) with modification to previously reported protocols.[29,41-43] Each stock solution was diluted with pH 7.4 Prisma HT buffer (Pion) to a final concentration of 25 μM (1% v/v final DMSO concentration) and 200 μL were added to the wells of the donor plate (number of replicates = 12). BBB-1 lipid formulation (5 μL, Pion) was used to coat

the polyvinylidene fluoride (PVDF, 0.45 μM) filter membrane on the acceptor plate. The acceptor plate was placed on top of the donor plate forming a sandwich and the brain sink buffer (BSB, 200 μL, Pion) was added to each well of the acceptor plate. The sandwich was incubated for 4 h at ambient temperature without stirring. UV-vis spectra of the solutions in the reference, acceptor, and donor plates were measured using a microplate reader. The PAMPA Explorer software v. 3.5 (Pion) was used to calculate the $-\log P_e$ for each compound. CNS± designations were assigned by comparison to compounds that were identified in previous reports.[29,41-43]

2.4.4. Determination of solution speciation for DPP1, DPP2, and the Cu^{2+}–DPP2 complex

The pK_a values for **DPP1** and **DPP2** were determined by UV-vis variable-pH titrations based on a previously reported procedure.[27,29,31-33,44,45] To establish the pK_a values, a solution (100 mM NaCl, 10 mM NaOH, pH 12) of **DPP1** (40 μM) or **DPP2** (20 μM) was titrated with small aliquots of HCl. At least 30 spectra were recorded in the range of pH 2–10. Similarly, a solution containing **DPP2** (20 μM) and $CuCl_2$ in a ratio of 2:1 was titrated with small additions of HCl and at least 30 spectra were recorded over the range of pH 2–7. The acidity and stability constants were calculated by using the HypSpec program (Protonic Software, UK).[53] Speciation diagrams for **DPP1**, **DPP2**, and Cu^{2+}**–DPP2** complexes were modeled using the HySS2009 program (Protonic Software).[54]

2.4.5. Metal binding studies

The interaction of **DPP1** and **DPP2** with Cu^{2+} and Zn^{2+} was determined by UV-vis and ^{1}H NMR spectroscopy, respectively, based on previously reported procedures.[28-33,45] A solution of ligand (20 μM in EtOH) was prepared, treated with 1 to 20 equiv of $CuCl_2$, and incubated at room temperature for 2.5 h (for **DPP1**) or 5 min (for **DPP2**). The optical spectra of the resulting solutions were measured by UV-vis. The interaction of **DPP1** or **DPP2** with $ZnCl_2$ was observed by ^{1}H NMR. $ZnCl_2$ (1 equiv) was added to a solution of **DPP1** or **DPP2** (4 mM) in CD_3CN. The metal selectivity of both compounds was investigated by measuring the optical changes upon addition of 1 equiv of $CuCl_2$ to

a solution of ligand (**DPP1** = 40 μM; **DPP2** = 20 μM in EtOH) containing 1 equiv or 25 equiv of a divalent metal chloride salt ($MgCl_2$, $CaCl_2$, $MnCl_2$, $FeCl_2$, $CoCl_2$, $NiCl_2$, or $ZnCl_2$). The Fe^{2+} samples were prepared anaerobically (all solutions were purged with N_2). Quantification of the metal selectivity was calculated by comparing and normalizing the absorption values of metal–ligand complexes at λ = 360 nm (for **DPP1**) or 580 nm (for **DPP2**) to the absorption at this wavelength before and after the addition of $CuCl_2$ (A_M/A_{Cu}). Cu^{2+} binding of **DPP2** in the presence of Aβ was examined by UV-vis. Aβ (25 μM) was treated with $CuCl_2$ (25 μM) in 20 mM HEPES (2-[4-(2-hydroxyethyl)piperazin-1-yl]ethanesulfonic acid), pH 6.6, 150 mM NaCl for 2 min at room temperature. **DPP2** (50 μM) was added to the resulting solution, followed by 0.5–4 h incubation. For comparison, the optical spectra of **DPP2** (50 μM) were measured in the absence and presence of $CuCl_2$ (25 μM; 0.5–4 h incubation) without Aβ at pH 6.6.

2.4.6. Aβ interaction of DPP1 and DPP2 by mass spectrometry

The interaction of **DPP1** or **DPP2** with $A\beta_{40}$ was investigated by nanoelectrospray ionization-mass spectrometry (nESI-MS) that was carried out on a Synapt G2 quadrupole-ion mobility-mass spectrometry system. Samples were prepared by mixing stock solutions of **DPP1** or **DPP2** (prepared in DMSO) and $A\beta_{40}$ (dissolved in 100 mM ammonium acetate, pH 6.8) to generate desired final concentrations of the peptide and the compound. Mixtures were incubated on ice or at room temperature for 2 or 4 h, respectively and then analyzed. To produce protein complex ions, an aliquot of the sample (*ca.* 5 μL) was sprayed from the nESI emitter using a capillary voltage of 1.4 kV, with the source operating in positive ion mode and the sample cone operated at 50 V. In order to normalize nESI-MS data for non-specific and electrospray artifact interactions which could occur at high concentrations, data were acquired for Aβ samples containing thioflavin-T (ThT), a compound known to have no affinity for soluble forms of the Aβ peptide,[55] under identical concentration conditions as our **DPP1** and **DPP2** experiments. Any ThT binding observed was assumed to be due to either non-specific binding or the electrospray process, and subtracted from the intensities of the **DPP1** and **DPP2** interactions observed.[56] This procedure was performed over a broad range of

concentrations. The mass spectra were acquired with the following settings and tuned to avoid ion activation and to preserve non-covalent protein–ligand complexes:[48] backing pressure, 7.3 mbar; IMS pressure reading, 3.09 mbar; ToF analyzer pressure, 1.14×10^{-6} mbar.

2.4.7. Docking studies

Flexible ligand docking studies using AutoDock Vina[50] for **DPP1** and **DPP2** were conducted against the $A\beta_{40}$ monomer from the previously determined aqueous solution NMR structure (PDB 2LFM).[51] Ten conformations were selected from 20 conformations within the PDB file (1, 3, 5, 8, 10, 12, 13, 16, 17, and 20). The MMFF94 energy minimization in ChemBio3D Ultra 11.0 was used to optimize the structures of the ligands for the docking studies. The structural files of **DPP1**, **DPP2**, and the peptide were generated by AutoDock Tools and imported into PyRx,[57] which was used to run AutoDock Vina. The search space dimensions were set to contain the entire peptide. The exhaustiveness for the docking runs was set at 1024. Docked poses of the ligands were visualized with Aβ using Pymol.

2.4.8. Amyloid-β (Aβ) peptide

$A\beta_{40}$ was used in all Aβ experiments. $A\beta_{40}$ peptide (1 mg) was dissolved with ammonium hydroxide (NH_4OH, 1% v/v, aq), aliquoted, lyophilized, and stored at –80 °C. A stock solution (*ca*. 200 μM) was prepared by redissolving Aβ with NH_4OH (1% v/v, aq, 10 μL) followed by dilution with ddH_2O. All Aβ solutions were prepared following previously reported procedures.[28-32] The buffered solutions (20 μM HEPES, pH 6.6 (for Cu^{2+} samples) or pH 7.4 (for metal-free and Zn^{2+} samples), 150 μM NaCl) were used for both inhibition and disaggregation studies. For the inhibition experiment, Aβ (25 μM) was first treated with a metal chloride salt ($CuCl_2$ or $ZnCl_2$, 25 μM) for 2 min followed by addition of a compound (**DPP1** or **DPP2**, 50 μM in DMSO, 1% v/v final DMSO concentration). The resulting samples were incubated at 37 °C for 4, 8, or 24 h with constant agitation. For the disaggregation experiment, Aβ and a metal chloride salt ($CuCl_2$ or $ZnCl_2$) were initially incubated at 37 °C for 24 h with steady agitation. The

compound was added afterwards followed by additional 4, 8, or 24 h incubation at 37 °C with constant agitation.

2.4.9. Gel electrophoresis/sodium dodecyl sulfate-polyacrylamide gel electrophoresis (SDS-PAGE) with Western blot

The Aβ peptide experiments (as described above) were analyzed by both gel electrophoresis and SDS-PAGE with Western blot using an anti-Aβ antibody (6E10).[28-32,52] Each sample containing 25 μM Aβ (10 μL) was separated using either a 10–20% gradient Tris-tricine gel (Invitrogen, Grand Island, NY) or SDS gel (4% stacking gel; 10% resolving gel; non-reducing conditions). The gel was transferred to a nitrocellulose membrane and blocked overnight with bovine serum albumin (BSA, 3% w/v, Sigma, St. Louis, MO) dissolved in Tris-buffered saline (TBS, Fisher, Pittsburg, PA) containing 0.1% Tween-20 (TBS-T, Sigma). The membrane was treated with 6E10 (1:2,000; 2% BSA in TBS-T, Covance, Princeton, NJ) for 4 h at room temperature. The membrane was probed with a horseradish peroxidase-conjugated goat anti-mouse secondary antibody (1:5,000; Cayman Chemical, Ann Arbor, MI) in 2% BSA in TBS-T solution for 1 h at room temperature. The protein bands were visualized using the Thermo Scientific Supersignal West Pico Chemiluminescent Subtrate (Rockford, IL).

2.4.10. Transmission electron microscopy (TEM)

Samples for TEM were prepared following a previously reported method.[28-31,33,52] Glow-discharged grids (Formar/Carbon 300-mesh, Electron Microscopy Sciences, Hatfield, PA) were treated with samples from either inhibition or disaggregation experiments (5 μL) for 2 min at room temperature. Excess sample was removed with filter paper and washed with ddH_2O five times. Each grid was stained with uranyl acetate (1% w/v, ddH_2O, 5 μL) for 1 min. Uranyl acetate was blotted off and grids were dried for 15 min at room temperature. Images of samples were taken by a Philips CM-100 transmission electron microscope (80 kV, 25,000x magnification).

2.4.11. Cytotoxicity (MTT Assay)

The murine neuro-2a (N2a) neuroblastoma cell line was purchased from the

American Type Culture Collection (ATCC, Manassas, VA). The cell line was maintained in media containing 45% Dulbecco's modified Eagle's medium (DMEM) and 50% OPTI-MEM (GIBCO), supplemented with 5% fetal bovine serum (FBS, Sigma), 2 mM glutamine, 100 U/ml penicillin, and 100 mg/ml streptomycin (GIBCO). The cells were grown and maintained at 37 °C in a humidified atmosphere with 5% CO_2. Cell viability upon treatment of compounds was determined using the MTT assay (Sigma). N2a cells were seeded in a 96 well plate (15,000 cells in 100 μL per well) and treated with various concentrations of **DPP1** and **DPP2** (2–50 μM, final 1% v/v DMSO). After 24 h incubation at 37 °C, 25 μL MTT (5 mg/mL in phosphate buffered saline, PBS, GIBCO, pH 7.4) was added to each well and the plates were incubated for 4 h at 37 °C. Formazan produced by the cells was dissolved by addition of a solution (100 μL) containing *N,N*-dimethylformamide (DMF, 50% v/v, aq, pH 4.5) and sodium dodecyl sulfate (SDS, 20% w/v) overnight at room temperature. A microplate reader was used to measure the absorbance (A_{600}).

2.5. Acknowledgment

This study was supported by the Alzheimer's Art Quilt Initiative, the Alzheimer's Association (NIRG-10-172326), and the Ruth K. Broad Biomedical Foundation (to M.H.L.), as well as start-up funding from the University of Michigan (to B.T.R.). A.K., M.T.S., and A.S.D. are grateful for the Research Excellence Fellowship from the Department of Chemistry at the University of Michigan, the NIH Training Grant (T32CA140044), and the NSF Graduate Research fellowship, respectively. We thank Dr. Xiaoming He for synthetic assistance and Nathan Merrill for the NMR measurements for Zn^{2+} binding studies.

2.6. References

(1) Thies, W.; Bleiler, L. *Alzheimers Dement.* **2013**, *9*, 208.
(2) Kepp, K. P. *Chem. Rev.* **2012**, *112*, 5193.
(3) Hardy, J. A.; Higgins, G. A. *Science* **1992**, *256*, 184.
(4) Jakob-Roetne, R.; Jacobsen, H. *Ang. Chem., Int. Ed.* **2009**, *48*, 3030.
(5) Rauk, A. *Chem. Soc. Rev.* **2009**, *38*, 2698.
(6) Teplow, D. B.; Lazo, N. D.; Bitan, G.; Bernstein, S.; Wyttenbach, T.; Bowers, M. T.; Baumketner, A.; Shea, J. E.; Urbanc, B.; Cruz, L.; Borreguero, J.; Stanley, H. E. *Acc. Chem. Res.* **2006**, *39*, 635.

(7) Scott, L. E.; Orvig, C. *Chem. Rev.* **2009**, *109*, 4885.
(8) DeToma, A. S. S., S.; Ramamoorthy, A.; Lim, M. H. *Chem. Soc. Rev.* **2012**, *41*, 608.
(9) Haass, C.; Selkoe, D. J. *Nat. Rev. Mol. Cell Biol.* **2007**, *8*, 101.
(10) Lovell, M. A.; Robertson, J. D.; Teesdale, W. J.; Campbell, J. L.; Markesbery, W. R. *J. Neurol. Sci.* **1998**, *158*, 47.
(11) Frederickson, C. J.; Koh, J.-Y.; Bush, A. I. *Nat. Rev. Neurosci.* **2005**, *6*, 449.
(12) Gaggelli, E.; Kozlowski, H.; Valensin, D.; Valensin, G. *Chem. Rev.* **2006**, *106*, 1 995.
(13) Faller, P.; Hureau, C. *Dalton Trans.* **2009**, 1080.
(14) Faller, P. *ChemBioChem* **2009**, *10*, 2837.
(15) Bourassa, M. W.; Miller, L. M. *Metallomics* **2012**, *4*, 721.
(16) Zhu, X.; Su, B.; Wang, X.; Smith, M. A.; Perry, G. *Cell. Mol. Life Sci.* **2007**, *64*, 2202.
(17) Zatta, P.; Drago, D.; Bolognin, S.; Sensi, S. L. *Trends Pharmacol. Sci.* **2009**, *30*, 346.
(18) Hureau, C.; Faller, P. *Biochimie* **2009**, *91*, 1212.
(19) Bonda, D. J. L., H. -g.; Blair, J. A.; Zhu, X.; Perry, G.; Smith, M. A. *Metallomics* **2011**, *3*, 267.
(20) Jomova, K. V., M. *Toxicology* **2011**, *283*, 65.
(21) Pithadia, A. S.; Lim, M. H. *Curr. Opin. Chem. Biol.* **2012**, *16*, 67.
(22) Hureau, C.; Sasaki, I.; Gras, E.; Faller, P. *ChemBioChem* **2010**, *11*, 950.
(23) Braymer, J. J. D., A. S.; Choi, J.-S.; Ko, K. S.; Lim, M. H. *Int. J. Alzheimers Dis.* **2011**, *2011*, Article ID 623051.
(24) Perez, L. R.; Franz, K. J. *Dalton Trans.* **2010**, *39*, 2177.
(25) Rodríguez-Rodríguez, C.; Telpoukhovskaia, M.; Orvig, C. *Coord. Chem. Rev.* **2012**, *256*, 2308.
(26) Sharma, A. K.; Pavlova, S. T.; Kim, J.; Finkelstein, D.; Hawco, N.; Rath, N. P.; Kim, J.; Mirica, L. M. *J. Am. Chem. Soc.* **2012**, *134*, 6625.
(27) Rodríguez-Rodríguez, C.; Sanchez de Groot, N.; Rimola, A.; Alvarez-Larena, A.; Lloveras, V.; Vidal-Gancedo, J.; Ventura, S.; Vendrell, J.; Sodupe, M.; Gonzalez-Duarte, P. J. *J. Am. Chem. Soc.* **2009**, *131*, 1436.
(28) Hindo, S. S.; Mancino, A. M.; Braymer, J. J.; Liu, Y.; Vivekanandan, S.; Ramamoorthy, A.; Lim, M. H. *J. Am. Chem. Soc.* **2009**, *131*, 16663.
(29) Choi, J.-S.; Braymer, J. J.; Nanga, R. P.; Ramamoorthy, A.; Lim, M. H. *Proc. Natl. Acad. Sci.* **2010**, *107*, 21990.
(30) Choi, J.-S.; Braymer, J. J.; Park, S. K.; Mustafa, S.; Chae, J.; Lim, M. H. *Metallomics* **2011**, *3*, 284.
(31) Braymer, J. J.; Choi, J.-S.; DeToma, A. S.; Wang, C.; Nam, K.; Kampf, J. W.; Ramamoorthy, A.; Lim, M. H. *Inorg. Chem.* **2011**, *50*, 10724.
(32) He, X.; Park, H. M.; Hyung, S.-J.; Detoma, A. S.; Kim, C.; Ruotolo, B. T.; Lim, M. H. *Dalton Trans.* **2012**, *41*, 6558.
(33) Jones, M. R.; Service, E. L.; Thompson, J. R.; Wang, M. C.; Kimsey, I. J.; DeToma, A. S.; Ramamoorthy, A.; Lim, M. H.; Storr, T. *Metallomics* **2012**, *4*, 910.
(34) Lipinski, C. A.; Lombardo, F.; Dominy, B. W.; Feeney, P. J. *Adv. Drug Delivery Rev.* **2001**, *46*, 3.

(35) Clark, D. E.; Pickett, S. D. *Drug Discovery Today* **2000**, *5*, 49.
(36) Leuma Yona, R.; Mazères, S.; Faller, P.; Gras, E. *ChemMedChem* **2008**, *3*, 63.
(37) Ono, M.; Watanabe, H.; Watanabe, R.; Haratake, M.; Nakayama, M.; Saji, H. *Bioorg. Med. Chem. Lett.* **2011**, *21*, 117.
(38) Seregin, I. V.; Schammel, A. W.; Gevorgyan, V. *Org. Lett.* **2007**, *9*, 3433.
(39) Harkat, H.; Blanc, A.; Weibel, J. M.; Pale, P. *J. Org. Chem.* **2008**, *73*, 1620.
(40) Friel, D. K.; Snapper, M. L.; Hoveyda, A. H. *J. Am. Chem. Soc.* **2008**, *130*, 9942.
(41) Di, L.; Kerns, E. H.; Fan, K.; McConnell, O. J.; Carter, G. T. *Eur. J. Med. Chem.* **2003**, *38*, 223.
(42) Avdeef, A.; Bendels, S.; Di, L.; Faller, B.; Kansy, M.; Sugano, K.; Yamauchi, Y. *J. Pharm. Sci.* **2007**, *96*, 2893.
(43) Pion *Inc. BBB protocol and test compounds*, **2009**.
(44) Storr, T.; Merkel, M.; Song-Zhao, G. X.; Scott, L. E.; Green, D. E.; Bowen, M. L.; Thompson, K. H.; Patrick, B. O.; Schugar, H. J.; Orvig, C. *J. Am. Chem. Soc.* **2007**, *129*, 7453.
(45) Braymer, J. J.; Merrill, N. M.; Lim, M. H. *Inorg. Chim. Acta* **2012**, *380*, 261.
(46) Lippard, S. J.; Berg, J. M. *Principles of Bioinorganic Chemistry*; University Science Books: California, 1994.
(47) Gray, H. B.; Stiefel, E. I.; Valentine, J. S.; Bertini, I. *Biological Inorganic Chemistry: Structure and Reactivity*; University Science Books: California, 2007.
(48) Hernandez, H.; Robinson, C. V. *Nat. Protoc.* **2007**, *2*, 715.
(49) Bernstein, S. L.; Dupuis, N. F.; Lazo, N. D.; Wyttenbach, T.; Condron, M. M.; Bitan, G.; Teplow, D. B.; Shea, J. E.; Ruotolo, B. T.; Robinson, C. V.; Bowers, M. T. *Nat. Chem.* **2009**, *1*, 326.
(50) Trott, O.; Olson, A. J. *J. Comput.Chem.* **2010**, *31*, 455.
(51) Vivekanandan, S.; Brender, J. R.; Lee, S. Y.; Ramamoorthy, A. *Biochem. Biophys. Res. Commun.*, **2011**, *411*, 312.
(52) Reinke, A. A.; Seh, H. Y.; Gestwicki, J. E. *Bioorg. Med. Chem. Lett.* **2009**, *19*, 4952.
(53) Gans, P.; Sabatini, A.; Vacca, A. *Ann. Chim.* **1999**, *89*, 45.
(54) Alderighi, L.; Gans, P.; Ienco, A.; Peters, D.; Sabatini, A.; Vacca, A. *Coord. Chem. Rev* **1999**, *184*, 311.
(55) Reinke, A. A.; Gestwicki, J. E. *Chem. Biol. Drug Des.* **2011**, *77*, 399.
(56) Sun, J.; Kitova, E. N.; Wang, W.; Klassen, J. S. *Anal. Chem.* **2006**, *78*, 3010.
(57) Wolf, L. K. *Chem. Eng. News* **2009**, *87*, 31.

Chapter 3: Tuning Reactivity of Diphenylpropynone Derivatives with Metal-Associated Amyloid-β Species *via* Structural Modifications

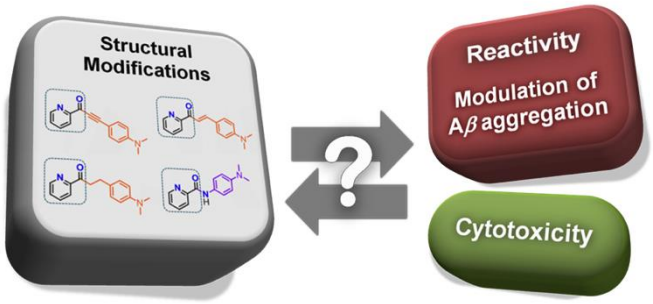

The results presented in this chapter for diphenylpropynone derivatives were previously published (Liu, Y.;‡ Kochi, A.;‡ Pithadia, A. S.; Lee, S.; Nam, Y.; Beck, M. W.; He, X.; Lee, D.; Lim, M. H. *Inorg. Chem.* **2013**, *52*, 8121-8130. ‡ Equal contribution.). We thank Professor Dongkuk Lee and Younwoo Nam for ITC experiments. Dr. Xiaoming He, Amit Pithadia, Yuzhong Liu, and Whitney Smith synthesized compounds. Yuzhong Liu, Amit Pithadia, and Michael Beck conducted metal binding studies. Michael Beck performed the docking studies. Dr. Alaina DeToma conducted the *in vitro* PAMPA assay. Dr. Sanghyun Lee conducted cell studies. Yuzhong Liu and Amit Pithadia contributed to manuscript writing. I contributed to the gel and TEM analyses for Aβ aggregation studies for this present work. In addition to that, I wrote the manuscript with Yuzhong Liu and Amit Pithadia.

3.1. Introduction

Alzheimer's disease (AD) is a global economic and social issue, currently affecting 5.4 million Americans and an estimated 24 million people worldwide.[1] To date, there is no known cure for AD and prevailing treatments only offer symptomatic relief for a short duration of time.[2-6] Recently, a particular emphasis has been placed on therapeutics for misfolded amyloidogenic peptides, amyloid-β (Aβ) peptides, commonly found in AD brains.[2-7] The etiology of AD, however, remains elusive due to the complexity emerging from the limited understanding of pathological features. The role of Aβ itself and its potential inter-relationships with other multiple factors, such as metal ion dyshomeostatsis and oxidative stress, have been suggested.[2-4,5,6,8] Interactions between metal ions (*e.g.*, Cu^{2+} and Zn^{2+}) and Aβ have been demonstrated to facilitate peptide aggregation and enhance oxidative stress *via* generation of reactive oxygen species.[2,3,6,8,9] The involvement of metal-associated Aβ (metal–Aβ) species in the onset and progression of AD, however, has been unclear and contentious, due to the limited availability of suitable chemical reagents to target metal–Aβ species and probe their link to neurotoxicity.

In order to elucidate potential associations of metal–Aβ species with AD pathogenesis, recent efforts have been made toward the development of chemical reagents to target metal–Aβ species, control the interactions between metal ions and Aβ species, and alter their reactivities (*e.g.*, metal-triggered Aβ aggregation).[3,6,9,10] The structures of these reagents are rationally selected to achieve both metal chelation and Aβ interaction (bifunctionality).[11-16] Recently, a diphenylpropynone derivative (**DPP2**) was constructed through a rational structure-based design principle (incorporation approach), where a metal chelation site was directly installed into an Aβ interacting framework with minimal structural modifications (Figure 3.1).[16] **DPP2**, with a dimethylamino functionality, has demonstrated the ability to control both metal-free and metal-induced Aβ aggregation *in vitro* to different extents; however, due to its cytotoxicity, it could be only implemented for *in vitro* applications.[16] Further investigations on the structural modifications of **DPP2** would be valuable to improve its reactivity toward metal-free and metal-associated Aβ species and cytotoxicity, as well

as to establish a relationship between chemical structures, reactivity with Aβ and metal–Aβ species, and toxicity in cells. Thus, we present the design, preparation, characterization, and *in vitro* metal-free and metal-associated Aβ reactivity of a structurally modified **DPP2** series (**C1**/**C2**, **P1**/**P2**, and **PA1**/**PA2**, Figure 3.1). The results and observations presented in this study illustrate that our structural variations on **DPP2** were shown to (i) tune metal binding and Aβ interaction properties of small molecules, thus altering their influence on both metal-free and metal-induced Aβ aggregation *in vitro*; (ii) reduce their cytotoxicity; and (iii) maintain their potential BBB permeability.

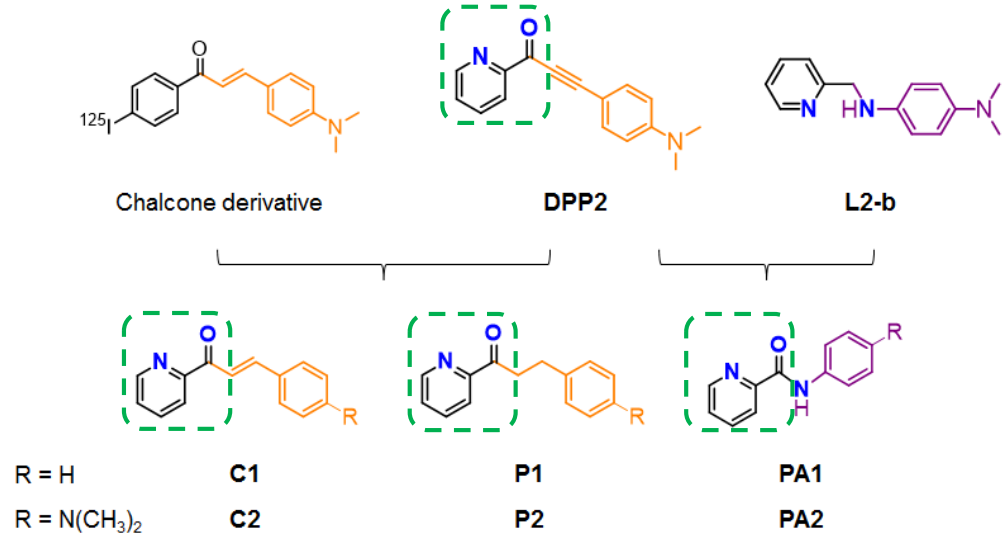

Figure 3.1. A class of **DPP** derivatives (**C1/2**, **P1/2**, and **PA1/2**). Chemical structures of chalcone derivative ([^{125}I]-(*E*)-3-(4-(dimethylamino)phenyl)-1-(4-iodophenyl)prop-2-en-1-one), **DPP2** (3-(4-(dimethylamino)phenyl)-1-(pyridin-2-yl)prop-2-yn-1-one), **L2-b** (*N*^{1},*N*^{1}-dimethyl-*N*^{4}-(pyridin-2-ylmethyl) benzene-1,4-diamine), **C1** ((*E*)-3-phenyl-1-(pyridin-2-yl)prop-2-en-1-one), **C2** ((*E*)-3-(4-(dimethylamino) phenyl)-1-(pyridine-2-yl)prop-2-en-1-one), **P1** (3-phenyl-1-(pyridin-2-yl)propan-1-one), **P2** (3-(4-(dimethyl amino)phenyl)-1-(pyridin-2-yl)propan-1-one), **PA1** (*N*-phenylpicolinamide), and **PA2** (*N*-(4-(dimethyl amino)phenyl)picolinamide). Atoms for potential metal binding are highlighted in blue. The green box indicates metal chelation site from **DPP2**.

3.2. Results and discussion

3.2.1. Design consideration and preparation of C1/2, P1/2, and PA1/2

A small molecule, **DPP2**, has been observed to target Aβ and metal–Aβ species and noticeably modulate metal-free and metal-induced Aβ aggregation *in vitro* to

different extents; however, it presented cytotoxicity at low micromolar concentrations.[16] A series of compounds (**C1**/**C2**, **P1**/**P2**, and **PA1**/**PA2**, Figure 3.1) were designed based on the structural modifications of **DPP2** in order to improve its reactivity with Aβ and metal–Aβ species, mitigate its cytotoxicity, as well as to establish a structure-reactivity-cytotoxicity relationship. For the design of the compounds, the structural portion of **DPP2** for metal chelation, 2-pyridyl ketone,[16] was first retained in these frameworks (Figure 3.1). Metal chelation of **C1**/**C2** and **P1**/**P2** could occur through nitrogen and oxygen (N/O) donor atoms from 2-pyridyl ketone, while in **PA1**/**PA2**, N/O (2-pyridyl ketone) or N/N (pyridine and amide) donor atoms may be involved in metal binding.[17] Secondly, the triple bond with a carbonyl group (ynone) in **DPP2**, which may act as a Michael acceptor and cause cytotoxicity,[18-20] was modified (*i.e.,* reduction or derivation of the triple bond; Figure 3.1).

Scheme 3.1. Synthetic routes of **C1/2**, **P1/2**, and **PA1/2**

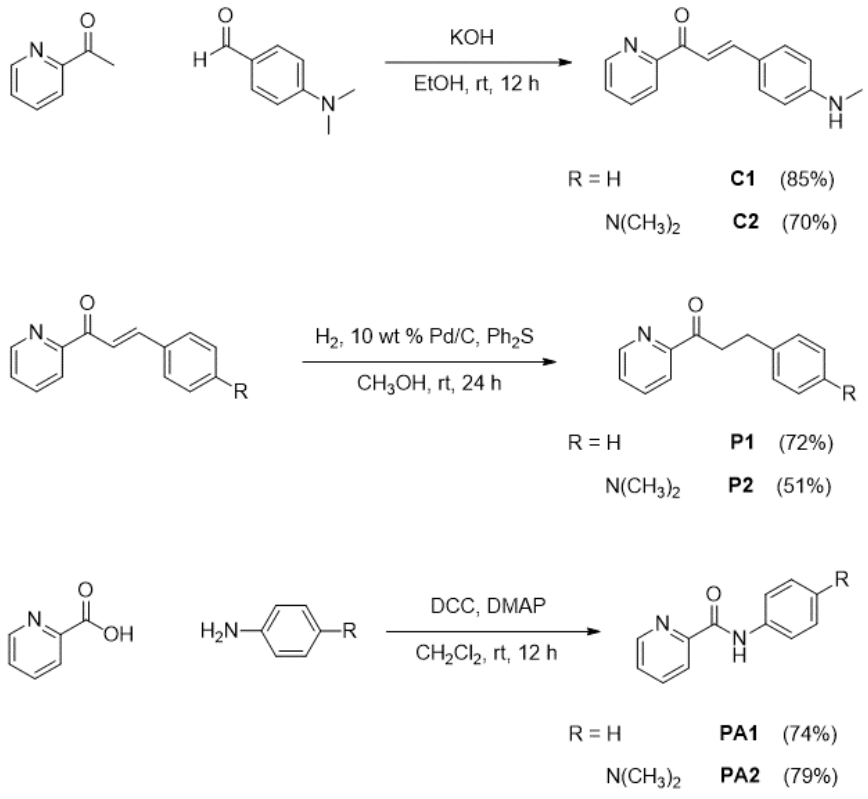

This structural alteration could vary overall structural rigidity. **C1**/**C2** were produced by reduction of the triple bond to a double bond; the backbone of **C1**/**C2** was also found in the framework of an Aβ imaging agent, which is a chalcone derivative (Figure 3.1).[21] For **P1**/**P2**, the double bond was further reduced to a single bond. **PA1**/**PA2** were fashioned through combining the 2-pyridyl ketone moiety from **DPP2** and the aniline portion from **L2-b** *via* an amide moiety instead of the carbon linker shown in **DPP2**, **C1**/**C2**, and **P1**/**P2**. Similar to **DPP2**, **L2-b** (Figure 3.1) was previously designed to serve as a potential chemical reagent to investigate metal–Aβ species *in vitro* and in living cells.[13] Lastly, a dimethylamino group, suggested to be important for Aβ interaction,[13,16,22] was incorporated into the frameworks of **C2**, **P2**, and **PA2**. For preparation, **C1**/**C2** and **PA1**/**PA2** were synthesized based on previously reported methods with modifications (Scheme 3.1).[23-26] **P1**/**P2** were generated through the selective hydrogenation of **C1**/**C2** in the presence of 10 wt % Pd/C (Scheme 3.1).

3.2.2. Effects of C1/2, P1/2, and PA1/2 on metal-free and metal-induced Aβ aggregation *in vitro*

In order to understand the effect of structural variations on compound reactivity toward metal-free and metal-induced Aβ aggregation, inhibition (Figure 3.2) and disaggregation (Figure 3.3) studies were conducted. Size distributions and morphologies of the resulting Aβ species from the two experiments were monitored by gel electrophoresis followed by Western blot with an anti-Aβ antibody (6E10) and TEM, respectively.[12-16,27]

The influence of **C1**/**C2**, **P1**/**P2**, and **PA1**/**PA2** on formation of metal-free and metal-treated Aβ aggregates was first examined (inhibition studies, Figure 3.2). Among these compounds, **C2** demonstrated the greatest reactivity with metal-free and metal-associated Aβ species to different extents, as confirmed by gel analysis. From metal-free Aβ aggregation with **C2** treatment, a wide molecular weight (MW) distribution of Aβ species was observed (Figure 3.2a, left, lane 3), which was also enhanced with prolonged incubation. Moreover, TEM images, obtained from the sample incubated with **C2** for 24 h (without metal ions), revealed thinner fibrils with diverse lengths compared

to those generated under compound-free conditions (Figure 3.2b). In the case of metal-induced Aβ aggregation, **C2** presented differences in control of Aβ aggregate formation in the reaction with Cu^{2+}–Aβ over that with Zn^{2+}–Aβ. Upon treating Cu^{2+}–Aβ species with **C2**, various-sized Aβ species were visualized by gel electrophoresis (Figure 3.2a, lane 6); while species (MW ≤ 25 kDa) were exhibited from the sample containing Aβ, Zn^{2+}, and **C2** (Figure 3.2a, lane 9). The modulation of Aβ aggregation by **C2** in the absence and presence of metal ions was also distinguished by TEM. A mixture of fibrils and

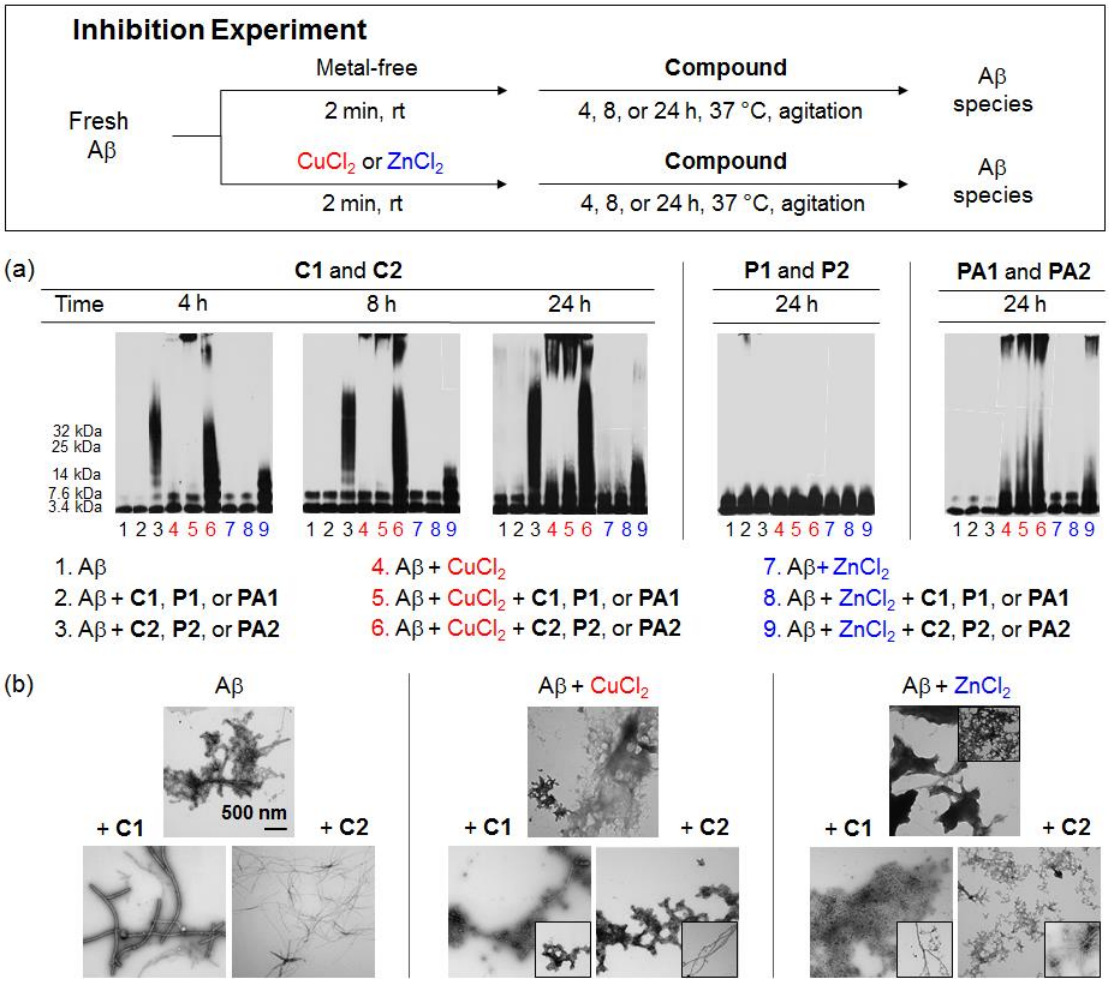

Figure 3.2. Inhibition experiment: modulation of Aβ aggregate formation in the absence and presence of metal ions (scheme, top) by **C1/2**, **P1/2**, and **PA1/2**. (a) Analysis of the size distribution of the resulting Aβ species by gel electrophoresis with Western blot using an anti-Aβ antibody (6E10). (b) Visualization of the morphologies of the Aβ species from samples that were incubated with **C1** or **C2** for 24 h by TEM. Conditions: [Aβ] = 25 μM; [$CuCl_2$ or $ZnCl_2$] = 25 μM; [compound] = 50 μM (compound = **C1/2**, **P1/2**, or **PA1/2**; pH 6.6 (for Cu^{2+} samples) or 7.4 (for metal-free and Zn^{2+} samples); various inhibition time; 37 °C; constant agitation.

amorphous aggregates (mainly, unstructured Aβ species) was detected in metal-treated conditions, whereas fibrils were mostly indicated from metal-free analogues.

As shown in Figure 3.2, alterations in structural scaffold differentiated reactivity toward Aβ aggregation (with and without metal ions). First, **C1**, which does not contain a dimethylamino group on the backbone compared to that of **C2** (Figure 3.1), did not significantly regulate the generation of Aβ aggregates (Figure 3.2a, left, lanes 2, 5, and 8). Second, as the carbon–carbon triple bond (C≡C) between two structural moieties (2-pyridyl ketone and dimethylaniline) in **DPP2**[16] was reduced to a double bond (C=C) in **C2** (Figure 3.1), reactivity was changed toward Aβ aggregation in the absence and presence of metal ions. Under metal-free conditions, **C2** afforded Aβ species with a diverse range of MW starting from 4 h–24 h, while **DPP2** exhibited less control on Aβ aggregation as time progressed.[16] Cu^{2+}-containing samples presented Aβ species with a various distribution of MW after 24 h with **C2** and **DPP2**.[16] Notably, this reactivity was more apparent with **C2** at early time period. Aβ aggregates < 25 kDa were indicated over time when treated with Zn^{2+} and **C2**. Aβ species (MW ≤ 25 kDa) were also observed in the case of **DPP2** at a short incubation time (*e.g.*, 4 h), yet species showing different sizes were yielded after 24 h.[16] Third, upon substitution of the double bond in **C2** to a single bond in **P1**/**P2** (Figure 3.1), reactivity toward metal-free and metal-triggered Aβ aggregation disappeared (Figure 3.2a, middle). Lastly, for **PA1**/**PA2**, composed of 2-pyridyl ketone and an aniline portion *via* an amide linkage (Figure 3.1), some reactivity was detected toward Cu^{2+}-treated Aβ species after 24 h incubation (Figure 3.2a, right, lanes 5 and 6). In addition, **PA2**, which has a dimethylamino functionality, showed slight modulation of Zn^{2+}-induced Aβ aggregation after 24 h (Figure 3.2a, right, lanes 9). In contrast to their reactivity toward metal–Aβ, **PA1**/**PA2** did not display any significant influence on metal-free Aβ species even with longer incubation time. This general reactivity of **PA1**/**PA2** was distinct from that of **DPP2**[16] or **C2**.

Moreover, transformation of preformed metal-free and metal-induced Aβ aggregates by **C1**/**C2**, **P1**/**P2**, or **PA1**/**PA2** was also investigated (disaggregation studies, Figure 3.3). Upon incubation of these compounds, similar size distributions of

resulting Aβ aggregates were confirmed by gel electrophoresis in comparison to those shown in the inhibition experiment (Figures 3.2 and 3.3). In particular, **C2** was able to noticeably disassemble preformed metal-free and metal-mediated Aβ aggregates (Figure 3.3a). Aβ species generated from the disaggregation experiment employing **C2** displayed an array of MW and morphologies analogous to those in the inhibition studies

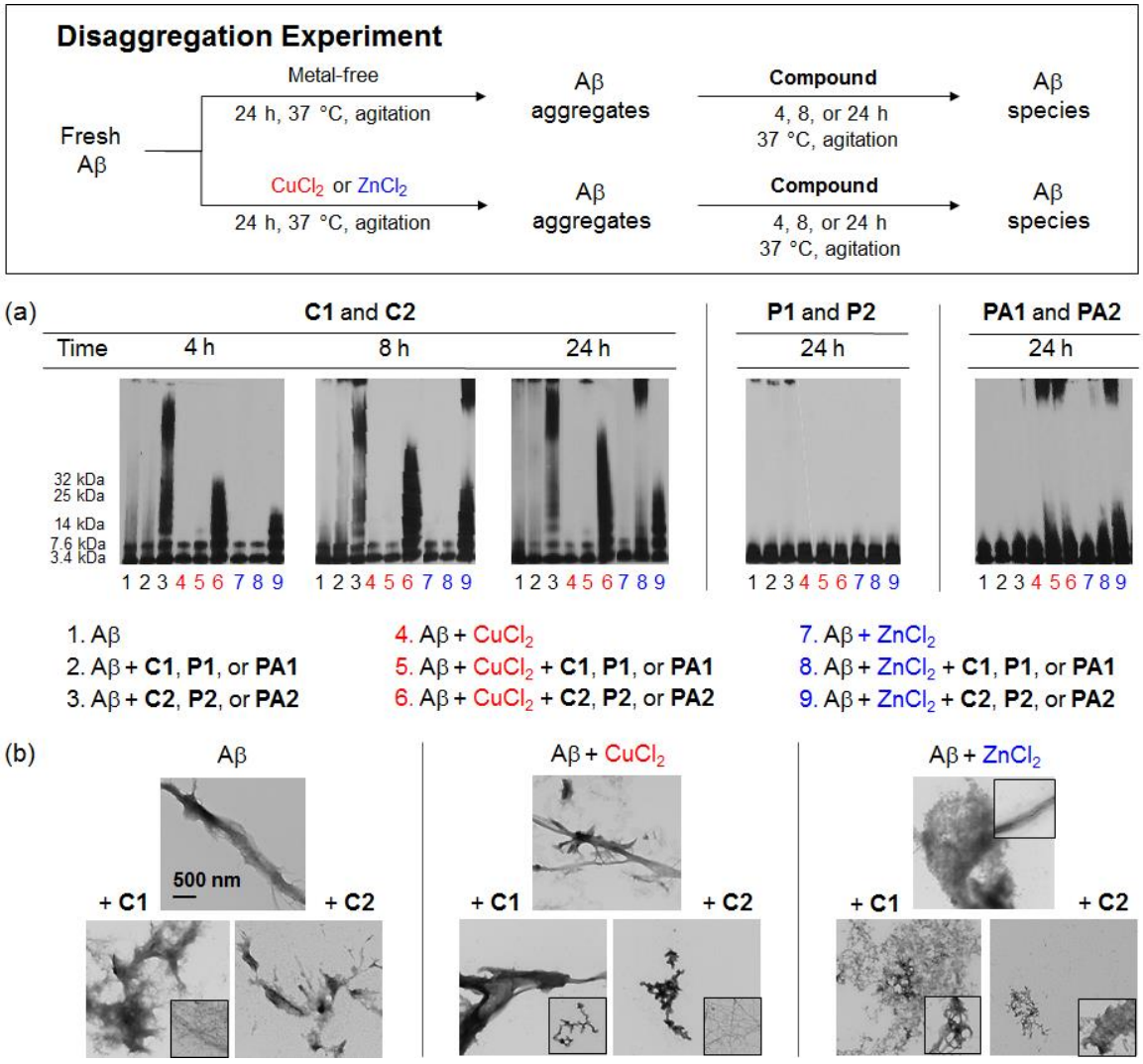

Figure 3.3. Disaggregation experiment: disassembly of preformed, metal-free or metal-induced Aβ aggregates by **C1/2**, **P1/2**, or **PA1/2** (scheme, top). (a) Analysis of the size distribution of resulting Aβ species by gel electrophoresis with Western blot (anti-Aβ antibody, 6E10). (b) TEM images of the 24 h samples containing **C1** or **C2** from (a). Conditions: [Aβ] = 25 μM; [$CuCl_2$ or $ZnCl_2$] = 25 μM; [compound] = 50 μM (compound = **C1/2**, **P1/2**, or **PA1/2**); pH 6.6 (for Cu^{2+} samples) or 7.4 (for metal-free and Zn^{2+} samples); various inhibition time; 37 °C; constant agitation.

(Figures 3.2 and 3.3). The samples containing metal-treated Aβ species followed by addition of **DPP2**[16] were visualized to have relatively more dispersion in MW than those with **C2**. In the metal-free condition, however, diverse-sized Aβ species were exhibited over longer incubation only in the presence of **C2**. As observed in inhibition studies, **C1** and **P1**/**P2** were not able to influence the disassembly of preformed Aβ aggregates in both metal-absent or metal-present cases; the modulation of these peptide aggregates was indicated with **PA1**/**PA2** only after 24 h. Thus, structural variations, such as the introduction of flexibility into the framework and/or incorporation of a dimethylamino moiety, afforded altered reactivity with metal-free and metal-treated Aβ species in both inhibition and disaggregation studies. Both experiments suggest that **C2**, with a double bond replacing the triple bond in **DPP2**,[16] displayed the greatest control in regulating Aβ aggregate generation as well as disassembling preformed Aβ aggregates (in both absence and presence of metal ions) to varying degrees *in vitro*. Furthermore, the backbones of **P** and **PA**, designed by further modification of the double bond in **C2** to a single bond and an amide bond, respectively, presented no or slight modulation on the formation or disaggregation of metal-free or metal-induced Aβ aggregates. Taken together, results and observations from both inhibition and disaggregation experiments imply that structural features, such as scaffold rigidity and substituents, may be essential for directing *in vitro* reactivity of small molecules toward metal-free and metal-induced Aβ aggregation.

3.2.3. Metal binding properties of C1/2, P1/2, and PA1/2

To investigate the effect of structural variation on metal binding properties of **C1**/**C2**, **P1**/**P2**, and **PA1**/**PA2** (containing a similar putative metal chelation site as **DPP2**, 2-pyridyl ketone[16]), the ability of **C1**/**C2**, **P1**/**P2**, or **PA1**/**PA2** to bind Cu^{2+} and Zn^{2+} was first examined by UV-vis and ^{1}H NMR spectroscopy, respectively (Figures 3.4 and 3.5). As shown in Figure 3.4, changes in UV-vis spectra (*i.e.*, new optical bands and/or change in absorbance intensity) were exhibited upon treatment of $CuCl_2$ (1–5 equiv) with **C1**/**C2**, **P1**/**P2**, or **PA1**/**PA2** in EtOH, indicating Cu^{2+} interaction of these compounds. Noticeable optical shifts from *ca*. 431 nm and 332 nm to 564 nm and 408

nm were detected after $CuCl_2$ treatment of **C2** and **PA2**, respectively. In addition to Cu^{2+} coordination, Zn^{2+} binding of **C1**/**C2**, **P1**/**P2**, and **PA1**/**PA2** were studied by ^1H NMR

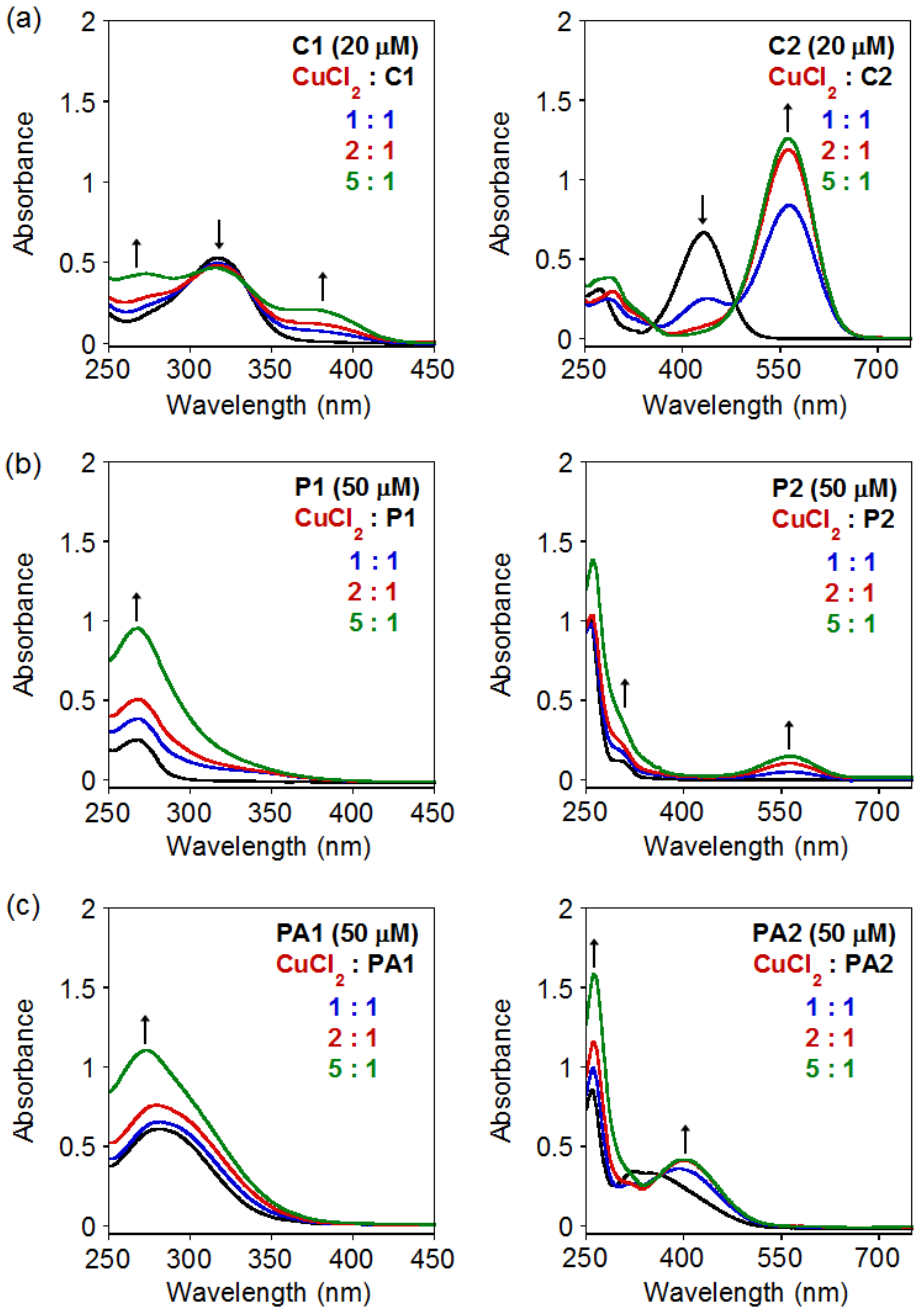

Figure 3.4. Cu^{2+} binding studies of **C1/2**, **P1/2**, and **PA1/2**. UV-vis spectra of (a) **C1** and **C2**, (b) **P1** and **P2**, and (c) **PA1** and **PA2** with $CuCl_2$ (1-5 equiv) in EtOH. Conditions: [**C1** or **C2**] = 20 μM; [**P1**/**P2** or **PA1**/**PA2**] = 50 μM; room temperature; incubation for 2 or 10 min.

(Figure 3.5). NMR was employed for Zn^{2+} binding studies due to the lack of significant optical changes of these ligands with $ZnCl_2$. The introduction of 1–3 equiv of Zn^{2+} to a

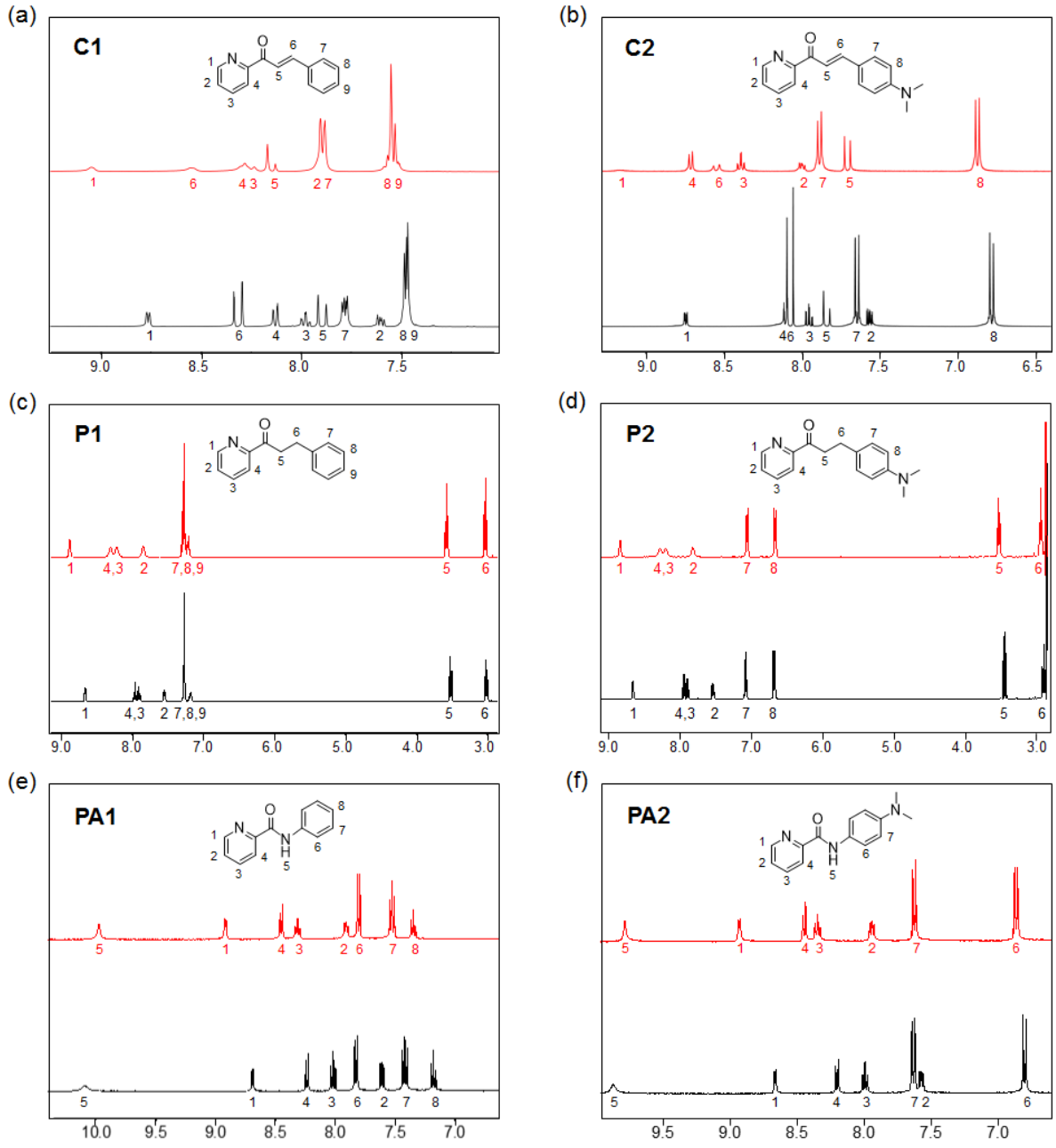

Figure 3.5. Zn^{2+} binding studies of **C1/2**, **P1/2**, and **PA1/2** by ^1H NMR spectroscopy in CD_3CN at room temperature. NMR spectra of (a) **C1** (black, 2 mM) with $ZnCl_2$ (red, 5 mM), (b) **C2** (black, 4 mM) with $ZnCl_2$ (red, 12 mM), (c) **P1** (black, 4 mM) with $ZnCl_2$ (red, 8 mM), (d) **P2** (black, 4 mM) with $ZnCl_2$ (red, 8 mM), (e) **PA1** (black, 8 mM) with $ZnCl_2$ (red, 14 mM), and (f) **PA2** (black, 8 mM) with $ZnCl_2$ (red, 13 mM).

CD_3CN solution of **C1**/**C2**, **P1**/**P2**, or **PA1**/**PA2** resulted in downfield chemical shifts of the pyridyl protons, demonstrating the involvement of the N donor atom from the pyridine ring (Figure 3.1) for Zn^{2+} binding. Moreover, the α and β protons of **C1**/**C2** and **P1**/**P2** displayed chemical shifts with Zn^{2+} treatment, which indicated that the O donor atom of the carbonyl group may also be associated in Zn^{2+} binding. In **PA1**/**PA2**, the

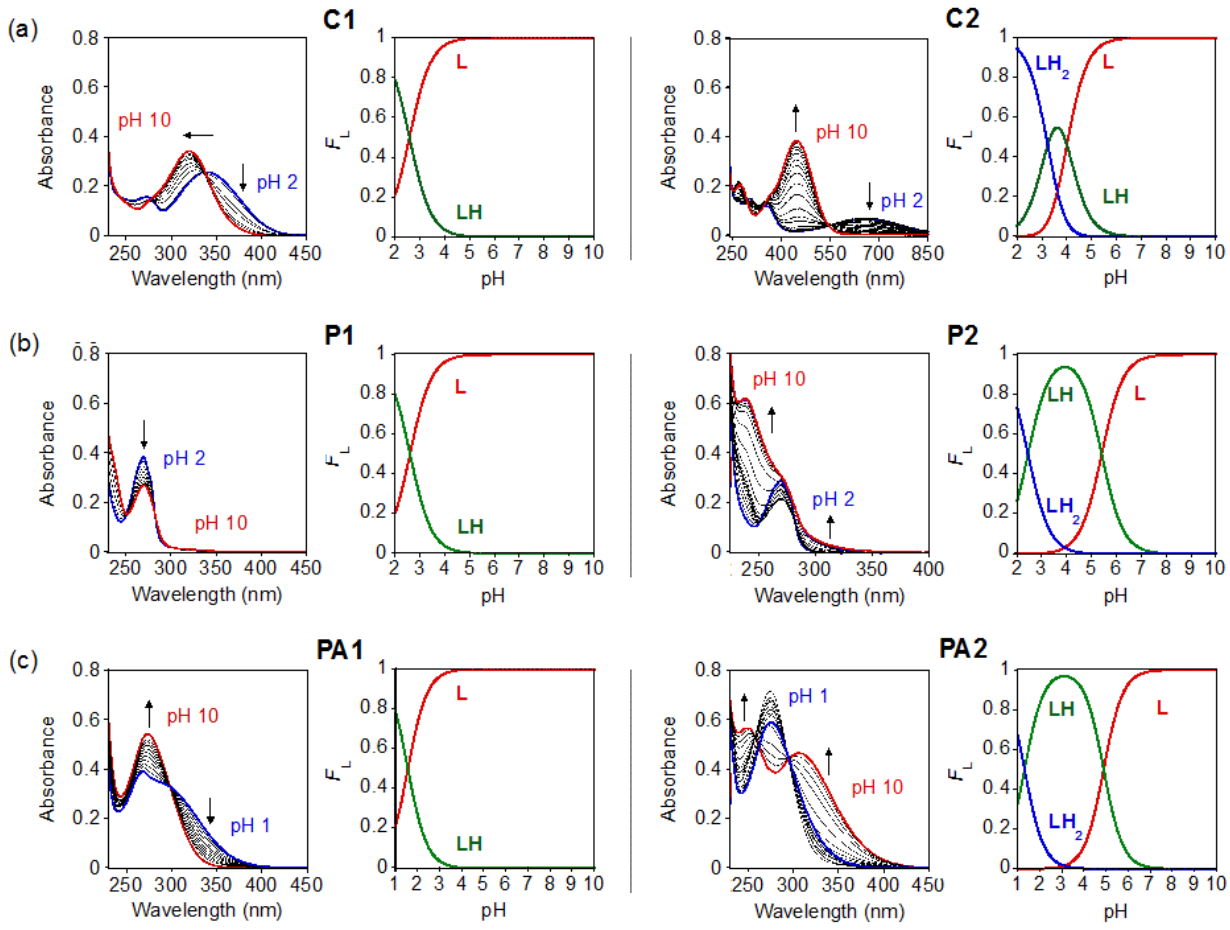

						pK$_a$[a]					
				L =		**C1**	**C2**	**P1**	**P2**	**PA1**	**PA2**
LH_2	⇌	LH	+ H	(pK_{a1})		–	3.23(1)	–	2.44(2)	–	1.38(5)
LH	⇌	L	+ H	(pK_{a2})		2.57(4)	4.00(1)	2.59(5)	5.40(4)	1.69(9)	4.91(8)

Figure 3.6. Solution speciation studies of **C1/2**, **P1/2**, and **PA1/2**. UV-vis variable-pH titration spectra (left) and solution speciation diagrams (right) of (a) **C1** and **C2** (pH 2–10), (b) **P1** and **P2** (pH 2–10), (c) **PA1** and **PA2** (pH 1–10) (F_L = fraction of species at the given pH). Acidity constants (pK_a) of L (L = **C1/2**, **P1/2**, or **PA1/2**) are summarized in the table. Conditions: [L] = 20 μM (L = **C1** or **C2**) or 50 μM (L = **P1**, **P2**, **PA1**, or **PA2**); I = 0.10 M NaCl; room temperature. Charges are omitted for clarity. [a] The error in the last digit is shown in the parentheses.

amide proton shifted upfield and sharpened in the presence of Zn^{2+}, suggesting that the N donor atom of the amide moiety may be involved in metal coordination.[28,29] Overall, **C1**/**C2**, **P1**/**P2**, and **PA1**/**2**, generated via structural modification from **DPP2**, were able to bind to metal ions, such as Cu^{2+} and Zn^{2+}, possibly through the N and/or O donor atoms, similar to **DPP2**.[16]

To understand solution speciation of our chemical series in the absence and presence of Cu^{2+}, UV-vis variable-pH titration experiments were conducted.[11,13,16] Spectrophotometric titrations of compounds, **C1**/**C2**, **P1**/**P2**, and **PA1**/**PA2**, were first performed to estimate the acidity constant (pK_a) values (Figure 3.6; **C1**, pK_a = 2.57(4); **C2**, pK_{a1} = 3.23(1), pK_{a2} = 4.00(1); **P1**, pK_a = 2.59(5); **P2**, pK_{a1} = 2.44(2), pK_{a2} = 5.40(4); **PA1**, pK_a = 1.69(9); **PA2**, pK_{a1} = 1.38(5), pK_{a2} = 4.91(8)). The diagrams depicted based on acidity constants indicated the presence of two forms of ligand (neutral and monoprotonated species; L and LH; L = **C1**, **P1**, and **PA1**; pK_a: protonation of the pyridyl N), as well as three forms of ligand (neutral, monoprotonated, and diprotonated species; L, LH, and LH_2; L = **C2**, **P2**, and **PA2**; pK_{a1}: protonation of the pyridyl N, pK_{a2}: protonation of the dimethylamino N) (Figure 3.6). The pK_{a2} values of **C2**, **P2**, and **PA2** are lower than that of **DPP2** (pK_{a2} = 7.01(6)),[16] which implies that neutral species would be present in a greater magnitude at a physiologically relevant pH (*i.e.,* 7.4). Overall, all six compounds are expected to mainly exist in the neutral form at pH 7.4, suggesting their potential penetration through the blood-brain barrier (BBB; *vide infra*).[13,16,30-32]

Through solution speciation experiments of **C2**/**P2**/**PA2** in the presence of $CuCl_2$, their Cu^{2+} binding stochiometries, affinities, and the distribution of Cu^{2+}–ligand species were investigated (Figure 3.7).[11,13,16] Based on the measured pK_a values of ligands above, the stability constants (logβ) of Cu^{2+}–**C2**/**P2**/**PA2** complexes were first determined (Figure 3.7; Cu + LH $\rightleftharpoons$ Cu(LH) (logβ_1); Cu + L $\rightleftharpoons$ CuL (logβ_2); Cu + 2L $\rightleftharpoons$ CuL_2 (logβ_3); for **C2**, logβ_1 = 8.73(0), logβ_2 = 5.62(8); for **P2**, logβ_1 = 6.50(1), logβ_2 = 3.76(9); for **PA2**, logβ_1 =7.76(9), logβ_2 = 4.17(7), logβ_3 = 3.86(5)). Based on logβ values, greater stability of Cu^{2+}–ligand complexes was shown in the order of **C2**, **PA2**, and **P2**. Second, solution speciation diagrams were also modeled using these stability constants, indicating that (i) complexation occurred between Cu^{2+} and ligand in mainly

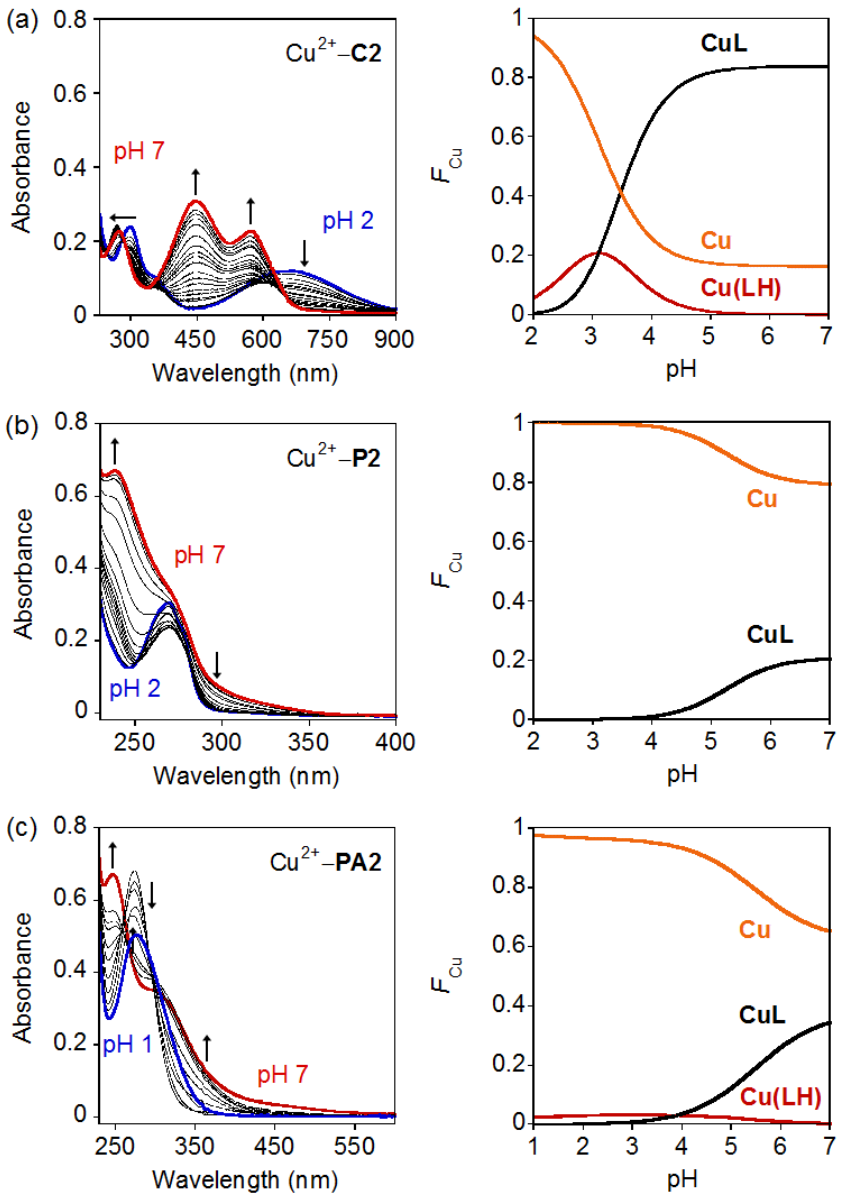

							logβ^a		
					L =		**C2**	**P2**	**PA2**
Cu	+	LH	⇌	Cu(LH)			8.73(0)	6.50(1)	7.76(9)
Cu	+	L	⇌	CuL			5.62(8)	3.76(9)	4.17(7)
Cu	+	2L	⇌	CuL_2			–	–	3.86(5)
pCu (= $-\log[Cu^{2+}]_{unchelated}$; pH 6.6)							5.79	4.70	4.81

Figure 3.7. Solution speciation studies of the Cu^{2+}–**C2**, Cu^{2+}–**P2**, and Cu^{2+}–**PA2** complexes. UV-vis variable-pH spectra (left) and solution speciation diagrams (right) of (a) Cu^{2+}–**C2** (pH 2–7), (b) Cu^{2+}–**P2** (pH 2–7), and (c) Cu^{2+}–**PA2** (pH 1–7) (F_{Cu} = fraction of free Cu and Cu–L complexes at the given pH). Conditions: $[Cu^{2+}]/[L]$ = 1:2, [L] = 20 μM (L = **C2**) or 50 μM (L = **P2** or **PA2**); incubation of ligand with Cu^{2+} for 30 min (L = **C2** and **PA2**) or 2 h (L = **P2**) prior to pH titration; room temperature. Stability constants (logβ) of Cu–L complexes are summarized in the table. Charges are omitted for clarity. [a] The error in the last digit is shown in the parentheses.

1:1 ratio (Cu:L; L = **C2**, **P2**, or **PA2**), (ii) free Cu^{2+}, CuL and Cu(LH) complexes were present in the solution containing Cu^{2+} and L (L = **C2** or **PA2**), and (iii) free Cu^{2+} and CuL complexes were shown in the sample of **P2**. At pH 7,[33] the complexes of CuL were present in solution at *ca*. 80%, 20%, and 40% for **C2**, **P2**, and **PA2**, respectively. From the diagrams, the values of pCu (pCu = $-\log[Cu_{unchelated}]$) of these compounds were also calculated to be 5.79, 4.70, and 4.81 at pH 6.6[34-36] for **C2**, **P2**, and **PA2**, respectively. Thus, the approximate dissociation constants ($K_d \approx [Cu_{unchelated}]$) for **C2**, **P2**, and **PA2** with Cu^{2+} were predicted to be in the micromolar range, making them slightly weaker metal chelators compared to **DPP**2 (pCu = 6.6, *ca.* low micromolar).[16]

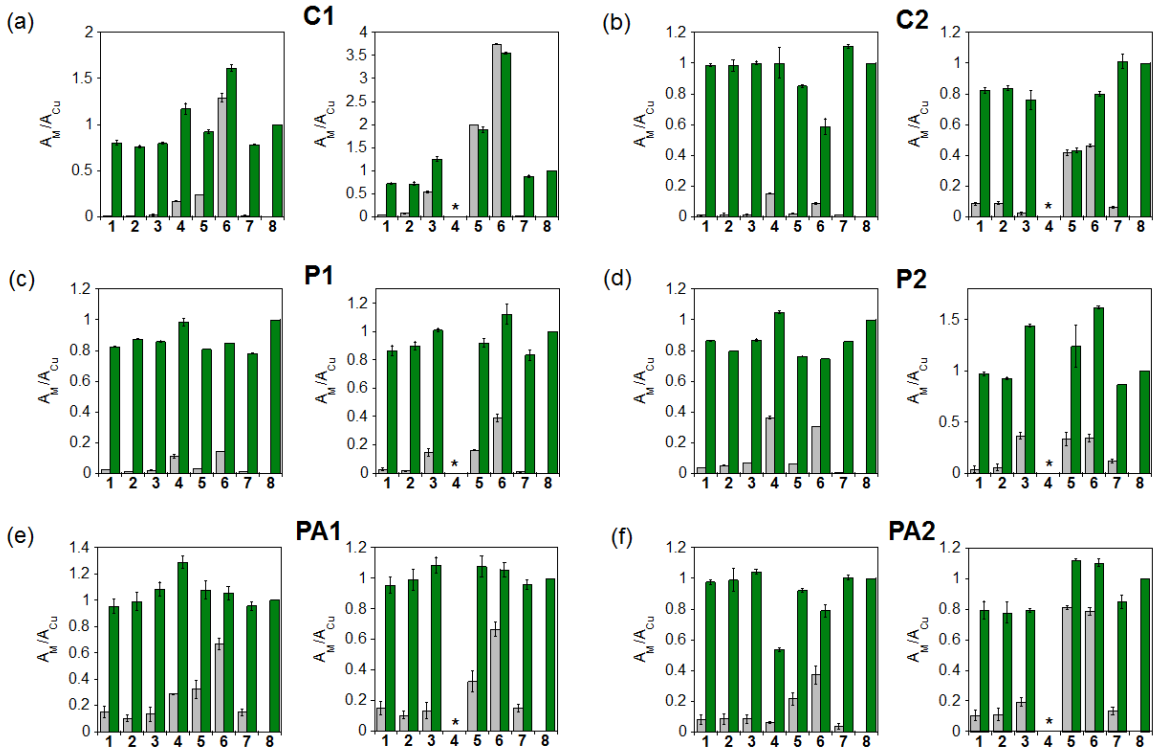

Figure 3.8. Metal selectivity studies of **C1** (a, 20 μM), **C2** (b, 20 μM), **P1** (c, 50 μM), (d) **P2** (50 μM), (e) **PA1** (50 μM), and **PA2** (f, 50 μM) in EtOH. Green bars represent the addition of $CuCl_2$ (**8**) to solutions containing the ligand and another divalent metal ion (grey bars; **1**, $MgCl_2$; **2**, $CaCl_2$; **3**, $MnCl_2$; **4**, $FeCl_2$; **5**, $CoCl_2$; **6**, $NiCl_2$; **7**, $ZnCl_2$) in a ratio of 1:1 (left) and 25:1 (right) MCl_2:$CuCl_2$ followed by 5 min incubation at room temperature. Absorbance at 400 nm (for **C1**), 650 nm (for **C2**), 320 nm (for **P1**), 300 nm (for **P2**), 350 nm (for **PA1**), and 480 nm (for **PA2**) were used for the calculation of A_M/A_{Cu}. The observed higher absorbance after Cu^{2+} addition to solution containing ligand and another metal ion compared to that of the control (ligand and Cu^{2+} only) may be due to the absorbance from ligand binding to another metal ion at the wavelength selected for analysis. * Indicates precipitation in the solution or interference with unidentified species in spectra.

Different Cu^{2+} binding affinities of our ligands could be resulted from the influence of electron density on the donor atoms for metal binding through structural variations (*e.g.*, structural moieties between the 2-pyridyl ketone and aniline portions). Higher binding ability of **DPP2** and **C2** for Cu^{2+} in comparison with those of **P2** and **PA2** as well as Aβ interaction properties may direct their ability to modulate Cu^{2+}-induced Aβ aggregation.

Furthermore, potential selectivity of **C2**, **P2**, and **PA2** for Cu^{2+} over other biologically relevant divalent metal ions (Mg^{2+}, Ca^{2+}, Mn^{2+}, Fe^{2+}, Co^{2+}, Ni^{2+}, and Zn^{2+}) was studied by competition reactions which were monitored by UV-vis. As depicted in Figure 3.8, at an equimolar concentration of another metal ion and Cu^{2+}, the spectral changes after Cu^{2+} addition indicated possible binding of compounds to Cu^{2+} in the presence of other divalent metal ions, similar to **DPP2**.[16] Moreover, these results may suggest a slightly higher selectivity for Cu^{2+} by **C2**, **P2**, and **PA2** in the solution containing $CoCl_2$ or $NiCl_2$, compared to **DPP2**.[16] At a supramolar ratio of another divalent metal ion to Cu^{2+} (25:1), **P2** appeared to be more selective for Cu^{2+} than **C2** and **PA2**.

3.2.4. Interaction of C1/2 with Aβ species monitored by isothermal titration calorimetry (ITC)

In order to shed some light on possible interactions of **C1**/**C2**, **P2**, **PA2**, and **DPP2** with $A\beta_{40}$, ITC experiments were performed following previously reported methods.[37] Measured heat changes during the titration indicated potential interaction of our compounds with Aβ.[38] The titration data for **C1** and **C2** were fitted using a one-site binding model, while the data for **DPP2** were fitted with a sequential binding model (Figure 3.9). Based on the binding models, the best-fit values [binding stoichiometries (*N*), binding constants (K_A), enthalpy changes (Δ*H*), and Gibbs free energy (Δ*G*)] of these molecules were determined (Table 3.1). The binding affinities of all three ligands with Aβ were estimated to be in the same range (*ca.* 10^4–10^5 M^{-1}). The higher binding stoichiometry of **C2** to Aβ, compared to that of **C1**, however, implied that **C2** may be able to interact with Aβ to a greater extent (Table 3.1). This may explain the better reactivity of **C2** toward Aβ species over **C1** observed from Aβ aggregation studies (*vide*

supra, Figures 3.2 and 3.3). **DPP2** also presented similar binding affinity toward Aβ as **C2**. Overall **C2** and **DPP2** were shown to interact with Aβ in an energetically favorabable manner (Table 3.1).

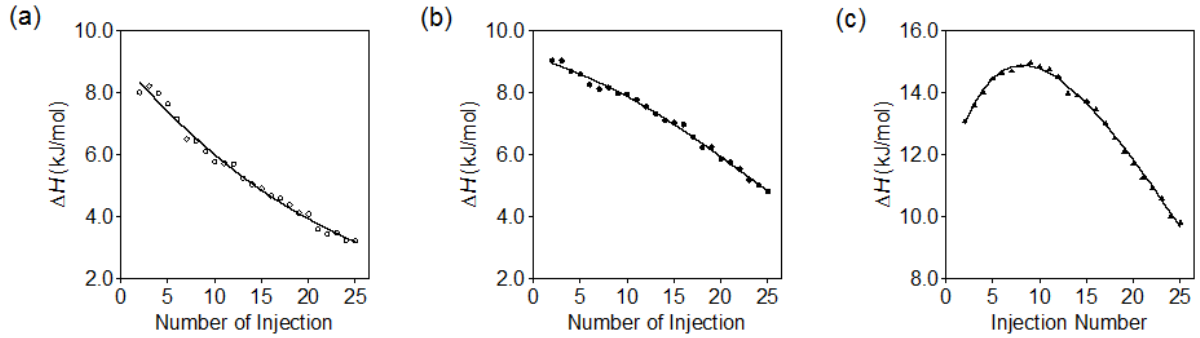

Figure 3.9. Integrated enthalpy change (Δ*H*) upon injection of (a) **C1**, (b) **C2**, and (c) **DPP2** into a solution of Aβ ([compound] = 200 μM; [Aβ] = 20 μM; 20 μM HEPES, pH 7.4, 150 μM NaCl; 10% v/v DMSO; 25 °C). Solid lines were generated by fitting the experimental data employing the one-site binding (for **C1** and **C2**) or sequential binding model (for **DPP2**).

Table 3.1. Thermodynamic parameters (binding stoichiometry (*N*), binding constants (K_A), enthalpy change (Δ*H*), and Gibbs free energy (Δ*G*)) of interactions between **C1/2** or **DPP2** with $A\beta_{40}$ at 25 °C.

	C1	**C2**	**DPP2**[a]
N	0.88 ± 0.27	2.12 ± 0.06	–
K_A (M^{-1})	2.38 ± 0.56 x 10^5	1.61 ± 0.26 x 10^5	4.06 ± 1.00 x 10^5 7.27 ± 1.26 x 10^4 3.97 ± 0.80 x 10^4
Δ*H* (kJ/mol)	15.48 ± 9.16	10.93 ± 0.58	12.87 ± 0.21 x 10^5 33.70 ± 2.52 x 10^4 −15.18 ± 3.70 x 10^4
Δ*G* (kJ/mol)	−0.69 ± 0.58	−29.72 ± 0.40	−32.01 ± 0.61 −27.75 ± 0.43 −26.25 ± 0.50

[a] Themodynamic values for **DPP2** were calculated using a sequential binding mode.

3.2.5. Docking studies for possible conformations of C1/2 with Aβ

To visualize and further explore the possible interaction between Aβ and **C1** or **C2**, docking studies were carried out using AutoDock Vina[39] utilizing the previously

determined NMR structure (PDB 2LFM)[40] of monomeric $A\beta_{40}$ (Figure 3.10). Aβ and **C1**/**C2** were observed to interact with each other through nonspecific and/or direct intermolecular interactions (*e.g.*, hydrogen bonding, π–π stacking), with most conformations that exhibited **C1**/**C2** docking between the α-helix and the *N*-terminal random coil, similar to **DPP2**.[16] These interactions were calculated to have binding energies ranging from −5.8 to −4.9 kcal/mol and −5.9 to −4.8 kcal/mol for **C1** and **C2**, respectively (Figure 3.10). As shown in all conformations, **C1** and **C2** did not dock at the same sites on Aβ and were situated offset from each other when docked at similar sites (Figure 3.10). The observations from preliminary docking studies suggest that **C1** and **C2** could interact differently with Aβ, possibly related to the presence of a dimethylamino group in **C2**. This may further support the different reactivity toward Aβ aggregation of **C1** and **C2** *in vitro* (*vide supra*, Figures 3.2 and 3.3).

3.2.6. Cell toxicity of C1/2, P1/2, and PA1/2

Cytotoxicity studies of **C1**/**C2**, **P1**/**P2**, and **PA1**/**PA2** illustrated a potential relationship between molecular scaffold and cytotoxicity. Human neuroblastoma SK-N-BE(2)-M17 cells were treated with various concentrations of compounds and cell viability was measured using the MTT assay (Figure 3.11).[13,16,27] Overall, through reduction of the conjugated triple bond to a double bond in **C1**/**C2**, cell viability (*ca.* 60% viability at 50 μM) was improved compared to that of **DPP2** (*ca.* 20% viability at 50 μM).[16] Furthermore, complete removal of the α,β-unsaturated moiety in **P1**/**P2** and **PA1**/**PA2** significantly mitigated cytotoxicity of compounds (*ca*. 80% cell viability up to 200 μM concentration). Through structural modifications, we were able to improve the cytotoxicity of **DPP2**.[16]

3.2.7. Predicted blood-brain barrier (BBB) permeability of C1/2, P1/2, and PA1/2

To probe whether the scaffold modifications in the six compounds could alter structural parameters required for BBB permeability predicted with **DPP2**,[16] the values of Lipinski's rules and logBB were first calculated.[30,31,41,42] Based on the calculated values (Table 3.2), all six compounds indicated drug-likeness and possible brain uptake.

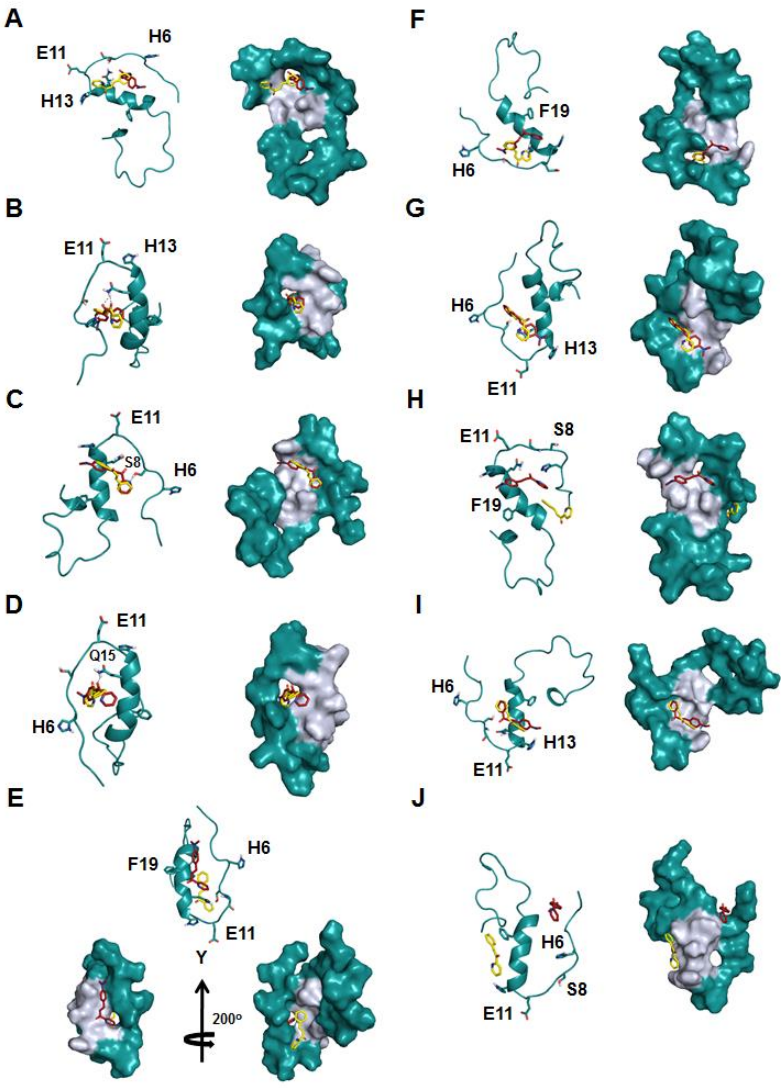

Conformation	C1 (kcal/mol)	C2 (kcal/mol)
A	-6.1	-6.6
B	-6.5	-6.4
C	-5.3	-5.9
D	-5.9	-5.8
E	-6.8	-5.7
F	-5.9	-5.6
G	-5.9	-5.5
H	-5.1	-5.5
I	-6.0	-5.5
J	-6.1	-5.4

Figure 3.10. Docking studies of **C1** and **C2** with $A\beta_{40}$ monomer. Top: conformation of **C1** (yellow) and **C2** (red) with cartoon (left) and surface (right) depictions of $A\beta_{40}$ (PDB 2LFM) by AutoDock Vina. The helical region of Aβ in the surface representation is depicted in light grey. Hydrogen bonding is indicated with dashed lines (2.0-2.7 Å). Bottom: summary of calculated binding energies of **C1** and **C2** to each Aβ conformation.

To confirm the potential BBB penetration prediction, an *in vitro* PAMPA-BBB assay was performed, following a previously reported method.[16,30-32] Based on the empirical classification of BBB-permeable molecules (*e.g.*, verapamil),[16,30-32] the measured permeability values (–logP_e), along with neutral speciation state at a physiologically relevant pH (*vide supra*, Figure 3.6), suggest that **C1**/**C2**, **P1**/**P2**, and **PA1**/**PA2** could potentially permeate through the BBB and be available in the central nervous system (CNS+). Taken together, our structural alterations to **DPP2** did not seem to change the structural properties necessary for BBB permeability.

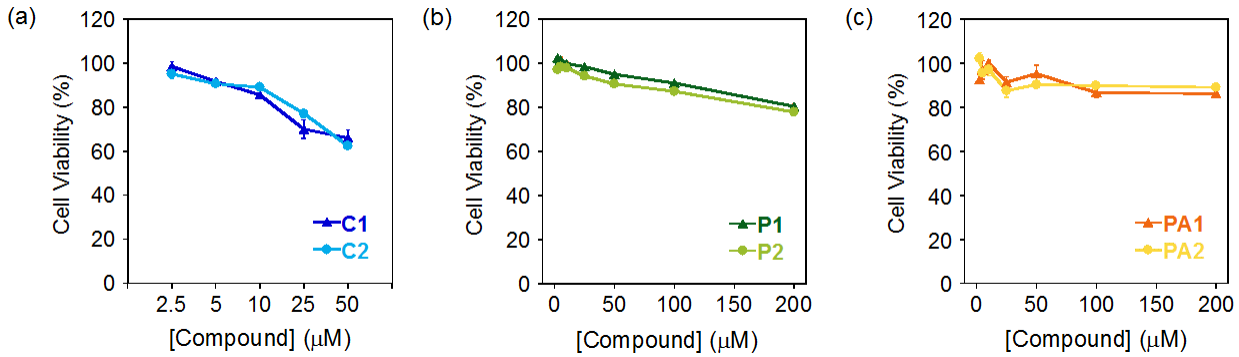

Figure 3.11. Cytotoxicity studies of **C1**/**2**, **P1**/**2**, and **PA1**/**2** in human neuroblastoma SK-N-BE(2)-M17 cells. Cells were treated with various concentrations of (a) **C1**/**2** (2.5–50 μM), (b) **P1**/**2** (2.5–200 μM), and (c) **PA1**/**PA2** (2.5–200 μM) for 24 h incubation. Cell viability was determined by the MTT assay. Values of cell viability (%) were calculated relative to that of cells incubated only with 1% v/v DMSO. Error bars represent the standard deviation from at least three independent experiments.

3.3. Conclusion

DPP2 derivatives, **C1**/**C2**, **P1**/**P2**, and **PA1**/**PA2**, were synthesized in order to improve reactivity of **DPP2** toward Aβ and metal–Aβ species and lower its cytotoxicity, as well as to establish a structure-reactivity-cytotoxicity relationship. The ability of these structurally modified compounds to modulate *in vitro* metal-free and metal-induced Aβ aggregation was significantly distinct. Particularly, **C2**, having a double bond between two structural moieties (2-pyridyl ketone and dimethylaniline) and a dimethylamino group, displayed noticeable reactivity with both metal-free and metal-treated Aβ species. The difference in reactivity was associated with metal binding and Aβ interaction properties of our compounds, which were confirmed by solution speciation and ITC studies. In addition, an increase in cell viability was indicated with **C1**/**C2**, **P1**/**P2**, and

PA1/**PA2**, relative to that with **DPP2**, possibly due to the alteration of the α,β-ynone moiety. Taken together, through structural modifications of **DPP2**, we demonstrate a relationship between structures, reactivity with Aβ and metal–Aβ, and cytotoxicity.

Table 3.2. Values (MW, *c*logP, HBA, HBD, PSA, logBB, and −logP_e) of **C1**/**2**, **P1**/**2** and **PA1**/**2**.

Calculation[a]	**C1/C2**	**P1/P2**	**PA1/PA2**	**DPP2**[c]	Lipinski's rules & others
MW	209/252	211/254	198/241	250	≤ 450
*c*log*P*	2.92/3.09	2.98/3.14	1.26/1.43	2.63	≤ 5.0
HBA	2/3	2/3	3/4	3	≤ 10
HBD	0/0	0/0	1/1	0	≤ 5
PSA	30.0/33.2	30.0/33.2	42.0/45.2	33.2	≤ 90 Å^2
logBB	0.131/0.108	0.139/0.116	−0.300/−0.323	0.0390	< −1.0 (poorly distributed in the brain)
−logP_e	4.3 ± 0.1 4.2 ± 0.1	4.4 ± 0.1 4.3 ± 0.1	4.2 ± 0.1 4.2 ± 0.1	4.2 ± 0.1	
CNS+/− prediction[b]	CNS+ CNS+	CNS+ CNS+	CNS+ CNS+	CNS+	−logP_e < 5.4 (CNS+) −logP_e > 5.7 (CNS–)

[a] MW: Molecular weight; *c*log*P*: Calculated logarithm of the octanol-water partition coefficient; HBA: Hydrogen-bond acceptor atoms; HBD: Hydrogen-bond donor atoms; PSA: Polar surface area; logBB = −0.0148 × PSA + 0.152 × *c*log*P* + 0.130; −logP_e values were determined using the Parallel Artificial Membrane Permeability Assay adapted for BBB (PAMPA-BBB). [b] Prediction of the ability of the compound to penetrate the central nervous system (CNS). Compounds categorized as CNS+ have the ability to permeate through the BBB and target the CNS. In the case of compounds assigned as CNS–, they have poor permeability through the BBB and therefore, their bioavailability into the CNS is considered to be minimal. [c] The values for DPP2 have been previously reported.[16]

The reactivity of our compounds with Aβ and metal–Aβ species, however, is shown to be limited *in vitro*;[43] therefore, further structural optimization for interacting with metal ions and/or Aβ species is desirable to accomplish their use in biological systems. Especially, the metal binding affinity of **C**, **P**, and **PA** could be improved through substitution of the carbonyl group in their backbones with a stronger metal binding group such as an amino or hydroxyl moiety, as well as variation of denticity.

3.4. Experimental section

3.4.1. Materials and procedures

All reagents were purchased from commercial suppliers and used as received unless otherwise stated. The compounds (**C1**/**C2** and **PA1**/**PA2**) were synthesized following previously reported methods with modifications.[23-26] $A\beta_{40}$ (DAEFRHDSGYEVHHQKLVFFAEDVGSNKGAIIGLMVGGVV) was purchased from Anaspec (Fremont, CA). Optical spectra for metal binding and solution speciation studies were recorded on an Agilent 8453 UV-visible (UV-vis) spectrophotometer. Nuclear magnetic resonance (NMR) spectra for the characterization of small molecules and Zn^{2+} binding studies were acquired on a Varian 400 MHz NMR spectrometer. Isothermal calorimetric titrations of $A\beta_{40}$ with compounds were carried out with a MicroCal VP-ITC isothermal titration calorimeter (Northampton, MA). Transmission electron microscopy (TEM) images were recorded on a Philips CM-100 transmission electron microscope. A SpectraMax M5 microplate reader (Molecular Devices, Sunnyvale, CA) was used to measure the absorbance for MTT (3-(4,5-dimethylthiazol-2-yl)-2,5-diphenyltetrazolium bromide) and Parallel Artificial Membrane Permeability Assay adapted for Blood-Brain Barrier (PAMPA-BBB) assays.

3.4.2. Preparation of (*E*)-3-phenyl-1-(pyridin-2-yl)prop-2-en-1-one (C1)

A flask was charged with a mixture of 2-acetylpyridine (300 mg, 2.5 mmol) and benzaldehyde (285 mg, 2.7 mmol) in H_2O (15 mL). To the stirring mixture was added a 10 % solution of NaOH (1.5 mL) dropwise. The mixture was stirred overnight at room temperature. The precipitates formed were filtered, washed with H_2O (3 x 10 mL), and dried over anhydrous $MgSO_4$. The product was concentrated *in vacuo* and purified by column chromatography (SiO_2, 100% CH_2Cl_2) to afford a yellow solid (450 mg, 2.2 mmol, 85%). ^{1}H NMR (400 MHz, $CDCl_3$)/δ (ppm): 7.42 (3H, m), 7.49 (1H, m), 7.73 (2H, m), 7.88 (1 H, dt, *J* = 7.6 and 1.6), 7.95 (1H, d, *J* = 16.0 Hz), 8.20 (1H, d, *J* = 8.0 Hz), 8.32 (1H, d, *J* = 16.0 Hz), 8.75 (1 H, m). ^{13}C NMR (100 MHz, $CDCl_3$)/δ (ppm): 189.4, 154.1, 148.8, 144.8, 137.0, 135.1, 130.5, 128.8, 126.9, 122.9, 120.8. HRMS: Calcd for $[M+H]^+$, 210.0841; found for $[M+H]^+$, 210.0913.

3.4.3. Preparation of (*E*)-3-(4-(dimethylamino)phenyl)-1-(pyridin-2-yl)prop-2-en-1-one (C2)

A flask was charged with a mixture of 2-acetylpyridine (242 mg, 2.0 mmol) and 4-dimethylaminobenzaldehyde (300 mg, 2.0 mmol) in EtOH (5 mL). To the stirring mixture was added a 20% solution of KOH (3 mL) dropwise. After stirring the mixture for overnight at room temperature, H_2O (5 mL) was added to the flask before the red precipitates were filtered and washed with H_2O (5 mL) and cold EtOH (5 mL). The product was concentrated *in vacuo* and purified by recrystallization from CH_2Cl_2 and hexanes to afford dark orange crystals (352 mg, 1.4 mmol, 70 %). ^{1}H NMR (400 MHz, $CDCl_3$)/δ (ppm): 3.05 (6H, s), 6.07 (2H, *J* = 9.2 Hz), 7.46 (1H, m), 7.64 (2 H, *J* = 9.2 Hz), 7.86 (1H, td, *J* = 7.6 and 2.0 Hz), 7.94 (1H, d, *J* = 16.0 Hz), 8.08 (1H, d, *J* = 16.0 Hz), 8.19 (1 H, d, *J* = 8.0 Hz), 8.73 (1 H, m). ^{13}C NMR (100 MHz, $CDCl_3$)/δ (ppm): 189.2, 155.0, 152.1, 148.7, 146.0, 136.9, 130.9, 126.4, 123.0, 122.8, 115.5, 111.7, 40.1. HRMS: Calcd for $[M+H]^+$, 253.1263; found for $[M+H]^+$, 253.1335.

3.4.4. Preparation of 3-phenyl-1-(pyridin-2-yl)propan-1-one (P1)

A flame dried flask was charged with (*E*)-3-phenyl-1-(pyridin-2-yl)prop-2-en-1-one (300 mg, 0.71 mmol) and purged for 5 min prior to addition of dry CH_3OH (9 mL). To the stirring solution was added 10 wt % Pd/C (30 mg, 10 mol%) and Ph_2S (2.5 μL, 7.0 μmol). The reaction was allowed to stir under H_2 at room temperature for 24 h. The solution was then filtered through a 25 mm syringe filter, washed with CH_3OH (3 x 10 mL), and dried over anhydrous $MgSO_4$. The product was concentrated in vacuo and purified by column chromatography (SiO_2, 100% CH_2Cl_2) to afford an orange oil (108 mg, 0.51 mmol, 72%). ^{1}H NMR (400 MHz, $CDCl_3$)/δ (ppm): 3.07 (2H, t, *J* = 7.6 Hz), 3.57 (2H, t, *J* = 7.6 Hz), 7.18 (1H, q), 7.25-7.26 (4H, br), 7.45-7.42 (1H, m), 7.81 (1H, td, *J* = 9.2, 1.6 Hz), 8.02 (1H, dt, *J* = 8.0, 1.2 Hz), 8.64 (1H, d, *J* = 4.8 Hz). ^{13}C NMR (100 MHz, $CDCl_3$)/δ (ppm): 200.8, 153.4, 148.9, 141.7, 136.9, 128.4, 128.3, 127.1, 125.9, 121.5, 39.2, 29.8. HRMS: Calcd for $[M+H]^+$, 212.1070; found for $[M+H]^+$, 212.1070.

3.4.5. Preparation of 3-(4-(dimethylamino)phenyl)-1-(pyridin-2-yl)propan-1-one (P2)

A flame dried flask was charged with (*E*)-3-(4-(dimethylamino)phenyl)-1-(pyridin-2-yl)prop-2-en-1-one (300 mg, 0.72 mmol) and purged for 5 min prior to addition of dry CH_3OH (9 mL). To the stirring solution was added 10 wt % Pd/C (30 mg, 10 mol%) and Ph_2S (2.5 μL, 7.0 μmol). The reaction was allowed to stir under H_2 at room temperature for 24 h. The solution was then filtered through a 25 mm syringe filter, washed with CH_3OH (3 x 10 mL), and dried over anhydrous $MgSO_4$. The product was concentrated *in vacuo* and purified by column chromatography (SiO_2, 1:1 ethyl acetate:hexanes) and washed several times with hexanes to afford the final product as a light green solid (93 mg, 0.37 mmol, 51%). ^{1}H NMR (400 MHz, CD_2Cl_2)/δ (ppm): 2.89 (6H, s), 2.93 (2H, t, *J* = 8.0 Hz), 3.48 (2H, t, *J* = 8.0 Hz), 6.67 (2H, d, *J* = 8.0 Hz), 7.11 (2H, d, *J* = 8.0 Hz), 7.47 (1H, ddd, *J* = 12.0, 4.0, 1.0 Hz), 7.83 (1H, td, *J* = 7.6, 1.6 Hz), 7.99 (1H, dt, *J* = 7.6, 0.8 Hz), 8.65 (1H, dd, *J* = 4.5, 1.2 Hz). ^{13}C NMR (100 MHz, CD_2Cl_2)/δ (ppm): 201.2, 153.5, 149.2, 148.9, 136.8, 129.8, 128.9, 127.1, 121.5, 112.9, 40.7, 39.6, 28.9. HRMS: Calcd for $[M+H]^+$, 255.1492; found for $[M+H]^+$, 255.1496.

3.4.6. Preparation of *N*-phenylpicolinamide (PA1)

A dried flask was charged with picolinic acid (123 mg, 1.0 mmol) followed by addition of dry CH_2Cl_2 (10 mL). To the stirring mixture was added dicyclohexylcarbodiimide (DCC, 230 mg, 2.2 mmol), aniline (0.2 mL, 2.2 mmol) and 4-dimethylaminopyridine (DMAP, 50 mg, 0.45 mmol). After the mixture was stirred overnight at room temperature, H_2O (5 mL) was added to the flask before the white precipitates were filtered. The organic mixture was washed with H_2O (3 x 10 mL) and dried over anhydrous $MgSO_4$. The product was concentrated *in vacuo* and purified by column chromatography (SiO_2, 6:1 CH_2Cl_2:ethyl acetate) to afford a white solid (147 mg, 0.74 mmol, 74 %). ^{1}H NMR (400 MHz, $CDCl_3$)/δ (ppm): 7.13 (1H, t, *J* = 7.4 Hz), 7.40 (2H, dd, *J* = 7.8, 8.1 Hz), 7.46 (1H, m), 7.78 (2H, d, *J* = 7.8 Hz), 7.89 (2H, dt, *J* = 1.8, 7.8 Hz), 8.29 (1H, d, *J* = 7.8 Hz), 8.60 (1H, d, *J* = 4.8 Hz). ^{13}C NMR (100 MHz, $CDCl_3$)/δ (ppm): 161.9, 149.8, 147.9, 137.7, 129.1, 126.4, 124.3, 122.4, 119.7. HRMS: Calcd for $[M+H]^+$, 199.0793; found for $[M+H]^+$, 199.0866.

3.4.7. Preparation of *N*-(4-(dimethylamino)phenyl)picolinamide (PA2)

A dried flask was charged with picolinic acid (123 mg, 1.0 mmol) followed by addition of dry CH_2Cl_2 (10 mL). To the stirring mixture was added DCC (230 mg, 2.2 mmol), N^1,N^1-dimethylbenzene-1,4-diamine (149 mg, 2.2 mmol), and DMAP (50 mg, 0.45 mmol). After the mixture was stirred overnight at room temperature, H_2O (5 mL) was added to the flask before the white precipitates were filtered. The organic mixture was washed with water (3 x 10 mL) and dried over anhydrous $MgSO_4$. The product was concentrated in vacuo and purified by column chromatography (SiO_2, 5:1 CH_2Cl_2:ethyl acetate) to afford a yellow solid (190 mg, 0.79 mmol, 79 %). ^{1}H NMR (400 MHz, $CDCl_3$)/δ (ppm): 2.93 (6H, s), 6.75 (2H, d, J = 9.0 Hz), 7.43 (1H, m), 7.63 (2H, d, J = 9.0 Hz), 7.86 (1H, dt, J = 1.7, 7.7 Hz), 8.27 (1H, d, J = 7.8 Hz), 8.58 (1H, d, J = 4.8 Hz), 9.82 (1H, s). ^{13}C NMR (100 MHz, DMSO)/δ(ppm): 162.0, 150.7, 148.7, 147.9, 138.5, 128.5, 127.0, 122.5, 121.8, 112.9, 40.9. HRMS: Calcd for $[M+H]^+$, 242.1205; found for $[M+H]^+$, 242.1292.

3.4.8. Amyloid-β (Aβ) peptide experiments

$A\beta_{40}$ peptide was dissolved with ammonium hydroxide (NH_4OH, 1% v/v, aq), aliquoted, lyophilized, and stored at −80 °C. A stock solution (*ca*. 200 μM) was prepared by redissolving Aβ with NH_4OH (1% w/v, aq, 10 μL) followed by dilution with ddH_2O, as reported previously.[13,16,27] Buffered solutions (20 μM HEPES (4-(2-hydroxyethyl)-1-piperazineethanesulfonic acid), pH 6.6 or 7.4, 150 μM NaCl) were used for both inhibition and disaggregation studies (pH 6.6 for Cu^{2+} samples;[34-36] pH 7.4 for metal-free and Zn^{2+} samples). For the inhibition experiment, Aβ (25 μM) was first treated with or without a metal chloride salt ($CuCl_2$ or $ZnCl_2$, 25 μM) for 2 min followed by addition of **C1**/**C2**, **P1**/**P2**, or **PA1**/**PA2** (50 μM, 1% v/v final DMSO concentration). The resulting samples were incubated at 37 °C for 4, 8, or 24 h with constant agitation. For the disaggregation experiment, Aβ in the absence or presence of a metal chloride salt ($CuCl_2$ or $ZnCl_2$) were initially incubated at 37 °C for 24 h with steady agitation. Compound was added afterwards followed by additional 4, 8, or 24 h incubation at 37 °C with constant agitation.

3.4.9. Gel electrophoresis with Western blot

The Aβ peptide experiments described above were analyzed by gel electrophoresis followed by Western blotting using an anti-Aβ antibody (6E10).[13,16,27] Each sample (10 μL, [Aβ] = 25 μM) was separated using a 10-20% gradient Tris-tricine gel (Invitrogen, Grand Island, NY). The gel was transferred to a nitrocellulose membrane and blocked overnight with a bovine serum albumin solution (BSA, 3% w/v, Sigma, St. Louis, MO) in Tris-buffered saline (TBS, Fisher, Pittsburgh, PA) containing 0.1% Tween-20 (Sigma; TBS-T). The membrane was treated with the Aβ monoclonal antibody (6E10, Covance, Princeton, NJ; 1:2,000; BSA, 2% w/v, in TBS-T) for 4 h at room temperature and then probed with a horseradish peroxidase-conjugated goat anti-mouse secondary antibody (1:5,000; Cayman Chemical, Ann Arbor, MI) in 2% BSA in TBS-T solution for 1 h at room temperature. The protein bands were visualized using Thermo Scientific Supersignal West Pico Chemiluminescent Subtrate (Rockford, IL).

3.4.10. Transmission electron microscopy (TEM)

Samples for TEM were prepared following a previously reported method.[13,16,27] Glow-discharged grids (Formar/Carbon 300-mesh, Electron Microscopy Sciences, Hatfield, PA) were treated with samples from either inhibition or disaggregation experiments (5 μL) for 2 min at room temperature. Excess sample was removed with filter paper and the grids were washed with ddH_2O five times. Each grid was stained with uranyl acetate (1% w/v ddH_2O, 5 μL) for 1 min. Uranyl acetate was blotted off and grids were dried for 15 min at room temperature. Images of samples were taken by a Philips CM-100 transmission electron microscope (80 kV, 25,000x magnification).

3.4.11. Metal binding studies

The interactions of **C1**/**C2**, **P1**/**P2**, and **PA1**/**PA2** with Cu^{2+} and Zn^{2+} were investigated by UV-vis and ^{1}H NMR spectroscopy, respectively, based on previously reported procedures.[13,16,27] A solution of **C1**/**C2** (20 μM), **P1**/**P2** (50 μM), or **PA1**/**PA2** (50 μM) in EtOH was treated with 1 to 5 equiv of $CuCl_2$ with incubation of 2 min (for **C1**/**2**) or 10 min (for **P1**/**P2** or **PA1**/**PA2**) at room temperature and was monitored by UV-vis. The interaction of **C1**/**C2**, **P1**/**P2**, or **PA1**/**PA2** with $ZnCl_2$ was observed by ^{1}H

NMR spectroscopy upon addition of 1 to 3 equiv of $ZnCl_2$ to a solution of **C1** (2 mM), **C2** (4 mM), **P1**/**P2** (4 mM), or **PA1**/**PA2** (8 mM) in acetonitrile-d_3 (CD_3CN). In addition, metal selectivity of **C1**/**C2**, **P1**/**P2**, and **PA1**/**PA2** was examined by measuring the optical changes upon addition of 1 equiv of $CuCl_2$ to a solution of ligand ([**C1**/**C2**] = 20 μM or [**P1**/**P2**] = [**PA1**/**PA2**] = 50 μM in EtOH) containing 1 or 25 equiv of another divalent metal chloride salt ($MgCl_2$, $CaCl_2$, $MnCl_2$, $FeCl_2$, $CoCl_2$, $NiCl_2$, or $ZnCl_2$). The Fe^{2+} samples were prepared by purging the solutions with N_2. Quantification of metal selectivity was calculated by comparing and normalizing the absorption values of metal–ligand complexes at 400 nm (for **C1**), 650 nm (for **C2**), 320 nm (for **P1**), 300 nm (for **P2**), 350 nm (for **PA1**), or 480 nm (for **PA2**) to the absorption at these wavelengths before and after the addition of $CuCl_2$ (A_M/A_{Cu}).

3.4.12. Solution speciation studies

The pK_a values for **C1**/**C2**, **P1**/**P2**, and **PA1**/**PA2** were determined by UV-vis variable-pH titrations following previously reported methods.[13,16] To obtain the pK_a values, a solution (10 mM NaOH, pH 12, 100 mM NaCl) of **C1**/**C2** (20 μM), **P1**/**P2** (50 μM), or **PA1**/**PA2** (50 μM) was titrated with small aliquots of HCl to obtain at least 30 spectra in the range of pH 2–10 (for **C1**/**C2** and **P1**/**P2**) or pH 1–12 (for **PA1**/**PA2**). In order to investigate the binding properties of ligands to Cu^{2+} at various pH values, a solution containing a compound ([**C2**] = 20 μM, [**P2**] = 50 μM, or [**PA2**] = 50 μM) and $CuCl_2$ in a ratio of 2:1 was incubated for 30 min, 2 h, and 30 min, respectively, and titrated with additions of HCl in a similar manner. At least 30 spectra were obtained over the range of pH 2–7 (for **C2** and **P2**) or pH 1–7.5 (for **PA2**). The acidity (pK_a) and stability (logβ) constants were calculated by using the HypSpec program (Protonic Software, UK).[44] The speciation diagrams for **C1**/**C2**, **P1**/**P2**, **PA1**/**PA2**, Cu^{2+}–**C2**, Cu^{2+}–**P2**, and Cu^{2+}–**PA2** complexes were modeled by the HySS2009 program (Protonic Software).[45]

3.4.13. Isothermal titration calorimetry (ITC)

Solutions of ligand (200 μM) and $A\beta_{40}$ (20 μM) in 20 μM HEPES buffer, pH 7.4, 150 μM NaCl (10% v/v DMSO) were prepared and degassed for 10 min prior to titration. The ligand solution (10 μL per injection) was injected over 1 sec (25 times, with an interval of 200 sec between each injection) into a solution of $A\beta_{40}$ (1.4 mL) using a motor-driven 250 μL syringe rotating at 310 rpm at 25 °C. As the control experiment, the ligand solution was injected into buffer solution without Aβ to measure the heat of dilution. Heat values of binding were measured by subtracting the heat of dilution value from the experimental results. Titration data were analyzed by an evaluation software, MicroCal Origin, Version 7.0. The binding curves were fitted with one-site binding or sequential model affording the overall heat values of thermodynamic parameters.[37]

3.4.14. Docking studies

Flexible ligand docking studies for **C1**/**C2** against the $A\beta_{40}$ monomer from the previously determined aqueous solution NMR structure (PDB 2LFM)[40] were conducted using AutoDock Vina.[39] Ten conformations were selected from 20 conformations within the PDB file (1, 3, 5, 8, 10, 12, 13, 16, 17, and 20). The MMFF94 energy minimization in ChemBio3D Ultra 11.0 was used to optimize the ligand structures for docking studies. The structural files of **C1**/**C2** and the peptide were generated by AutoDock Tools and imported into PyRx,[46] which were used to run AutoDock Vina.[39] The search space dimensions were set to contain the entire peptide. The exhaustiveness for the docking runs was set at 1024. Docked poses of the ligands with Aβ were visualized using Pymol.

3.4.15. Cytotoxicity (MTT Assay)

The human neuroblastoma SK-N-BE(2)-M17 cell line was purchased from the American Type Culture Collection (ATCC, Manassas, VA). The cell line was maintained in media containing 1:1 Minimum Essential Media (MEM, GIBCO, Grand Island, NY) and Ham's F12K Kaighn's Modification Media (F12K, GIBCO), 10% (v/v) fetal bovine serum (FBS, Sigma), 100 U/mL penicillin (GIBCO), and 100 mg/mL streptomycin (GIBCO). The cells were grown and maintained at 37 °C in a humidified atmosphere

with 5% CO_2. M17 cells were seeded in a 96 well plate (15,000 cells in 100 μL per well) according to previously reported methods.[13,16,27] These cells were treated with various concentrations of **C1**/**C2**, **P1**/**P2**, or **PA1**/**PA2** (2.5–50 μM for **C1**/**C2**, 2.5–200 μM for **P1**/**P2** and **PA1**/**PA2**, final 1% v/v DMSO). After 24 h incubation at 37 °C, 25 μL MTT (5 mg/mL in phosphate buffered saline (PBS), pH 7.4, GIBCO) was added to each well and the plates were incubated for 4 h at 37 °C. Formazan produced by the cells was dissolved in a solution containing *N*,*N*-dimethylformamide (DMF, 50% v/v aq, pH 4.5) and sodium dodecyl sulfate (SDS, 20% w/v) overnight at room temperature. The absorbance (A_{600}) was subsequently measured on a microplate reader.

3.4.16. Parallel Artificial Membrane Permeability Assay adapted for blood-brain barrier (PAMPA-BBB)

PAMPA-BBB experiments of compounds were carried out using the PAMPA Explorer kit (Pion, Inc. Billerica, MA) with modification to previously reported protocols.[16,30-32] Each stock solution was diluted with pH 7.4 Prisma HT buffer (Pion) to a final concentration of 25 μM (1% v/v DMSO) and was added to the wells of the donor plate (200 μL, number of replicates = 12). BBB-1 lipid formulation (5 μL, Pion) was used to coat the polyvinylidene fluoride (PVDF, 0.45 μM) filter membrane on the acceptor plate. The acceptor plate was placed on top of the donor plate forming a sandwich and brain sink buffer (BSB, 200 μL, Pion) was added to each well of the acceptor plate. The sandwich was incubated for 4 h at ambient temperature without stirring. UV-vis spectra of the solutions in the reference, acceptor, and donor plates were measured on a microplate reader. The PAMPA Explorer software v. 3.5 (Pion) was used to calculate the value of $-\log P_e$ for each compound. CNS+/− designations were assigned by comparison to compounds that were identified in previous reports.[30-32]

3.5. Acknowledgment

This study was supported by the Ruth K. Broad Biomedical Foundation, American Heart Association, and National Science Foundation (CHE-1253155) (to M.H.L.). D.L. thanks the Basic Science Program through the National Research Foundation of Korea (NRF) funded by the Ministry of Education, Science and

Technology (2009-0087836) for the support. A.K. is grateful for the Research Excellence Fellowship from the Department of Chemistry at the University of Michigan. We thank Dr. Alaina DeToma and Whitney Smith for assistance of the PAMPA-BBB assay and the synthesis of **C1** and **C2**, respectively.

3.6. References

(1) Thies, W.; Bleiler, L. *Alzheimers Dement.* **2013**, *9*, 208.
(2) Kepp, K. P. *Chem. Rev.* **2012**, *112*, 5193.
(3) Scott, L. E.; Orvig, C. *Chem. Rev.* **2009**, *109*, 4885.
(4) Jakob-Roetne, R.; Jacobsen, H. *Angew. Chem., Int. Ed.* **2009**, *48*, 3030.
(5) Rauk, A. *Chem. Soc. Rev.* **2009**, *38*, 2698.
(6) DeToma,A.S.; Salamekh, S.; Ramamoorthy, A.; Lim, M. H. *Chem. Soc. Rev.* **2012***, 44*, 608.
(7) Hardy, J. A.; Higgins, G. A. *Science* **1992**, *256*, 184.
(8) Savelieff, M. G.; Lee, S.; Liu, Y.; Lim, M. H. *ACS Chem. Biol.* **2013**, *8*, 856.
(9) Pithadia, A. S.; Lim, M. H. *Curr. Opin. Chem. Biol.* **2012**, *16*, 67.
(10) Rodríguez-Rodríguez, C.; Telpoukhovskaia, M.; Orvig, C. *Coord. Chem. Rev.* **2012**, *256*, 2308.
(11) Rodríguez-Rodríguez, C.; Sánchez de Groot, N.; Rimola, A.; Álvarez-Larena, Á.; Lloveras, V.; Vidal-Gancedo, J.; Ventura, S.; Vendrell, J.; Sodupe, M.; Gonzalez-Duarte, P. *J. Am. Chem. Soc.* **2009**, *131*, 1436.
(12) Hindo, S. S.; Mancino, A. M.; Braymer, J. J.; Liu, Y.; Vivekanandan, S.; Ramamoorthy, A.; Lim, M. H. *J. Am. Chem. Soc.* **2009**, *131*, 16663.
(13) Choi, J. S.; Braymer, J. J.; Nanga, R. P.; Ramamoorthy, A.; Lim, M. H. *Proc. Natl. Acad. Sci. U. S. A.* **2010**, *107*, 21990.
(14) Braymer, J. J.; Choi, J.-S.; DeToma, A. S.; Wang, C.; Nam, K.; Kampf, J. W.; Ramamoorthy, A.; Lim, M. H. *Inorg. Chem.* **2011**, *50*, 10724.
(15) Sharma, A. K.; Pavlova, S. T.; Kim, J.; Finkelstein, D.; Hawco, N.; Rath, N. P.; Kim, J.; Mirica, L. M. *J. Am. Chem. Soc.* **2012**, *134*, 6625.
(16) Pithadia, A. S.; Kochi, A.; Soper, M. T.; Beck, M. W.; Liu, Y.; Lee, S.; DeToma, A. S.; Ruotolo, B. T.; Lim, M. H. *Inorg. Chem.* **2012**, *51*, 12959.
(17) Gomes, L.; Low, J. N.; Valente, M. A. D. C.; Freire, C.; Castro, B. *Acta Cryst.* **2007**, *C63*, m293.
(18) Schultz, T. W.; Yarbrough, J. W. *SAR QSAR Environ. Res.* **2004**, *15*, 139.
(19) Koleva, Y. K.; Madden, J. C.; Cronin, M. T. D. *Chem. Res. Toxicol.* **2008**, *21*, 2300.
(20) Sakagami, H.; Kawase, M.; Wakabayashi, H.; Kunihara, T. *Autophagy* **2007**, *3*, 493.
(21) Cui, M.; Ono, M.; Kimura, H.; Liu, B. L.; Saji, H. *Bioorg. Med. Chem. Lett.* **2011**, *21*, 980.
(22) Leuma Yona, R.; Mazères, S.; Faller, P.; Gras, E. *ChemMedChem* **2008**, *3*, 63.
(23) Zakharychev, V. V.; Kuzenkov, A. V. *Chem. Heterocycl. Compd.* **2007**, *43*, 1167.
(24) Singh, P. K.; Singh, V. K. *Org. Lett.* **2008**, *10*, 4121.

(25) Carpino, L. A.; El-Faham, A. *J. Org. Chem.* **1995**, *60*, 3561.
(26) Sasaki, K.; Crich, D. *Org. Lett.* **2011**, *13*, 2256.
(27) Hyung, S.-J.; DeToma, A. S.; Brender, J. R.; Lee, S.; Vivekanandan, S.; Kochi, A.; Choi, J.-S.; Ramamoorthy, A.; Ruotolo, B. T.; Lim, M. H. *Proc. Natl. Acad. Sci. U. S. A.* **2013**, *110*, 3743.
(28) Xu, Z.; Baek, K.-H.; Kim, H. N.; Cui, J.; Qian, X.; Spring, D. R.; Shin, I.; Yoon, J. *J. Am. Chem. Soc.* **2010**, *132*, 601.
(29) Braymer, J. J.; Merrill, N. M.; Lim, M. H. *Inorg. Chim. Acta* **2012**, *380*, 261.
(30) Di, L.; Kerns, E. H.; Fan, K.; McConnell, O. J.; Carter, G. T. *Eur. J. Med. Chem.* **2003**, *38*, 223.
(31) Avdeef, A.; Bendels, S.; Di, L.; Faller, B.; Kansy, M.; Sugano, K.; Yamauchi, Y. *J. Pharm. Sci.* **2007**, *96*, 2893.
(32) *BBB Protocol and Test Compounds*; Pion, Inc.: Woburn, MA, 2009.
(33) Because of the limited optical feartures at high pH (>8), solution speciation studies of Cu^{2+}–ligand complexes were conducted up to pH 7.
(34) Physiological acidosis was observed in the AD brain (*i.e.*, pH 6.6). To correlate diseased conditions, experiments were performed at the relevant pH. In addition, Aβ aggregation in the presence of Cu^{2+} has been also suggested to be facilitated in slightly acidic environment (see refs 35 and 36).
(35) Yates, C. M.; Butterworth, J.; Tennant, M. C.; Gordon, A. *J. Neurochem.* **1990**, *55*, 1624.
(36) Atwood, C. S.; Moir, R. D.; Huang, X.; Scarpa, R. C.; Bacarra, N. M.; Romano, D. M.; Hartshorn, M. A.; Tanzi, R. E.; Bush, A. I. *J. Biol. Chem.* **1998**, *273*, 12817.
(37) Wang, S.-H.; Liu, F.-F.; Dong, X.-Y.; Sun, Y. *J. Phys. Chem. B* **2010**, *114*, 11576.
(38) The titration data for **P2** and **PA2** could not be fitted with any binding model.
(39) Trott, O.; Olson, A. J. *J. Comput. Chem.* **2010**, *31*, 455.
(40) Vivekanandan, S.; Brender, J. R.; Lee, S. Y.; Ramamoorthy, A. *Biochem. Biophys. Res. Commun.* **2011**, *411*, 312.
(41) Lipinski, C. A.; Lombardo, F.; Dominy, B. W.; Feeney, P. J. *Adv. Drug Delivery Rev.* **2001**, *46*, 3.
(42) Clark, D. E.; Pickett, S. D. *Drug Discov. Today* **2000**, *5*, 49.
(43) Mitigation of Aβ or metal–Aβ-induced toxicity by our compounds was further investigated; however, no noticeable influence on cell viability was observed (data not shown).
(44) Gans, P.; Sabatini, A.; Vacca, A. *Ann. Chim.* **1999**, *89*, 45.
(45) Alderighi, L.; Gans, P.; Ienco, A.; Peters, D.; Sabatini, A.; Vacca, A. *Coord. Chem. Rev.* **1999**, *184*, 311.
(46) Wolf, L. K. *Chem. Eng. News* **2009**, *87*, 31.

Chapter 4: Reactivity of a Gd^{III}DTPA-Curcumin Conjugate with Metal-Free and Associated Amyloid-β Species

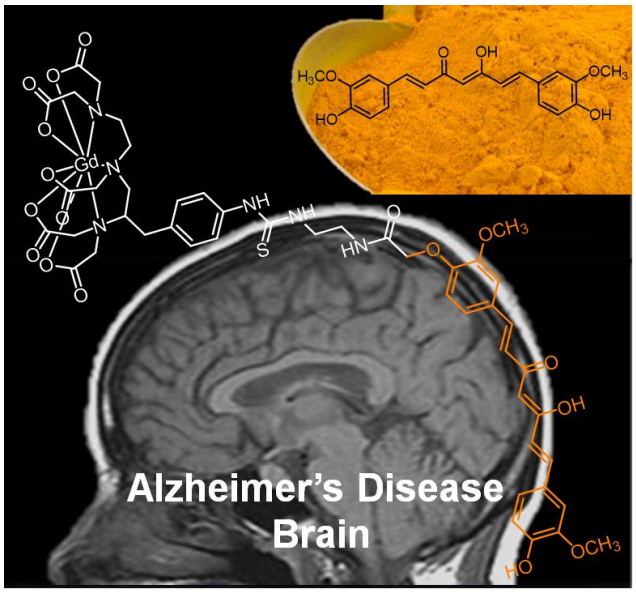

Image by Akiko Kochi, courtesy of iStockphoto.

We thank Professor Matthew Allen and Dr. Sashiprabha Vithanarachchi for providing the Gd^{III}DTPA-curcumin (**Gd-cur**) conjugate and its derivatives. I have been investigating metal binding, modulation of Aβ aggregation and Aβ morphological changes, antioxidant activity, cytotoxicity, and BBB permeability of compounds presented in the entire chapter.

4.1. Introduction

Alzheimer's disease (AD) is the most common, incurable neurodegenerative disease that is currently projected to affect approximately 14 million Americans by the year 2050.[1] Several pathological features, such as accumulation of amyloid-β (Aβ) peptide aggregates, metal ion dyshomeostasis, and oxidatie stress, have been observed and suggested to have potential link to AD onset and progression.[2-8] An inter-relationship between these factors have been indicated (*e.g.*, upon binding to Aβ, metal ions (*i.e.*, $Cu^{+/2+}$) have been shown to facilitate peptide aggregation, as well as generate reactive oxygen species (ROS) *in vitro*), which proposes the elusive, complex etiology of the disease.[2,4,5,7,8]

In order to elucidate the interconnection between multiple pathological factors, small molecules, designs based on a rational structure-based approach where a metal binding site was incorporated into an Aβ interacting framework, have been investigated.[8-15] In addition, natural products, such as curcumin[16-20] and (–)-epigallocatechin-3-gallate (EGCG; green tea extract),[21-24] have been studied to possibly target and modulate metal-free and/or metal-associated Aβ species, as well as reactive oxygen species (ROS). Senile plaques, composed of Aβ peptide, have been used as disease diagnostic confirmation *post mortem*;[2,4,5,25] making Aβ plaques a viable detection marker for AD.[26,27] Efforts have been put forth to develop magnetic resonance imaging (MRI) contrast agents to potentially overcome the limitations (*e.g.*, limited resolution, bioavailability) of current Aβ probes.[28-32] In addition, Aβ-targeting moieties (*e.g.*, Aβ peptides,[33-36] antibodies[37-41] and Aβ-binding dye[31]) have been to appended to the framework of MRI contrast agents to gain Aβ-targeting ability; however, their practical biological applications may be restricted due to possible blood-brain barrier (BBB) impermeability, amyloidogenic properties, and/or toxicity.

A conjugate (**Gd-cur**) of Gd^{III}DTPA (DTPA = diethyleneaminepentaacetate), a clinically approved contrast agent, and curcumin (**cur**) was fashioned for as a potential MRI contrast agent specific for Aβ plaques (Figure 4.1).[42] Curcumin is a natural principal phenol in turmeric, a popular Indian spice in curry.[43,44] Curcumin has been observed to inhibit the formation of Aβ oligomers and fibrils,[17,45] as well as aid in the reduction of

neuronal damage[46] and oxidative stress,[47-49] and amyloid accumulation[17] in an AD transgenic mouse model. Additionally, curcumin has been used as a fluoresent dye for Aβ plaque imaging.[17,50,51] The conjugate, **Gd-cur**, was demonstrated as a potential multimodal contrasting agent to detect Aβ plaques, applicable to MRI and fluorescence microscopy,[42] which warrants further investigations of its reactivity toward metal-free and metal-associated Aβ species. Herein, the influence of **Gd-cur** on metal-free and metal-induced Aβ aggregation was studied *in vitro*, compared to individual structural components, [Gd^{III}DTPA (**Gd^{III}DPTA**), curcumin, (**cur**), and curcumin linker (**cur-L**)]. Our present results and observations indicate that **Gd-cur** could modulate Cu^{2+}-induced Aβ aggregation, showing greater reactivity toward $Aβ_{42}$ over $Aβ_{40}$. Moreover, the antioxidant activity of this series was assessed and **Gd-cur** was observed to have similar antioxidant capacity in comparison to Trolox, a vitamin E analogue.

4.2. Results and discussion

4.2.1. Rationale and characterization of Gd-cur

As mentioned above, the conjugate, **Gd-cur**, was designed based on a rational structure-based design, where a clinically approved MRI contrast agent (Gd^{III}DTPA) was linked to curcumin,[42] a nontoxic natural product which has been shown to have anti-amyloidogenic activity.[17,45] Although curcumin has many advantageous aspects, such as anti-inflammatory effects and mediation of neuropathogenic factors of AD (*vide supra*), the use of curcumin as a potential therapeutic has been severely hindered by its lack of solubility and stability in physiologically relevant conditions.[52-54] Thus, **Gd-cur** was investigated to determine if its curcumin moiety would retain curcumin's auspicious characteristics (*i.e.*, nontoxicity, antioxidant activity, control of Aβ aggregation), along with solubility improvements, after the conjugation to Gd^{III}DTPA. Curcumin's insolubility in water has been previously reported.[52-55] Linkage of the Gd^{III}DTPA to curcumin (**Gd-cur**, Figure 4.1) vastly improved the solubility of curcumin (**cur**; Figure 4.1) in buffered solution. The stock solution (high mM concentration) of **Gd-cur** was made only using 20 mM HEPES (4-(2-hydroxylethyl)-1-piperazineethane-sulfonic acid), pH 7.4, 150 mM NaCl).

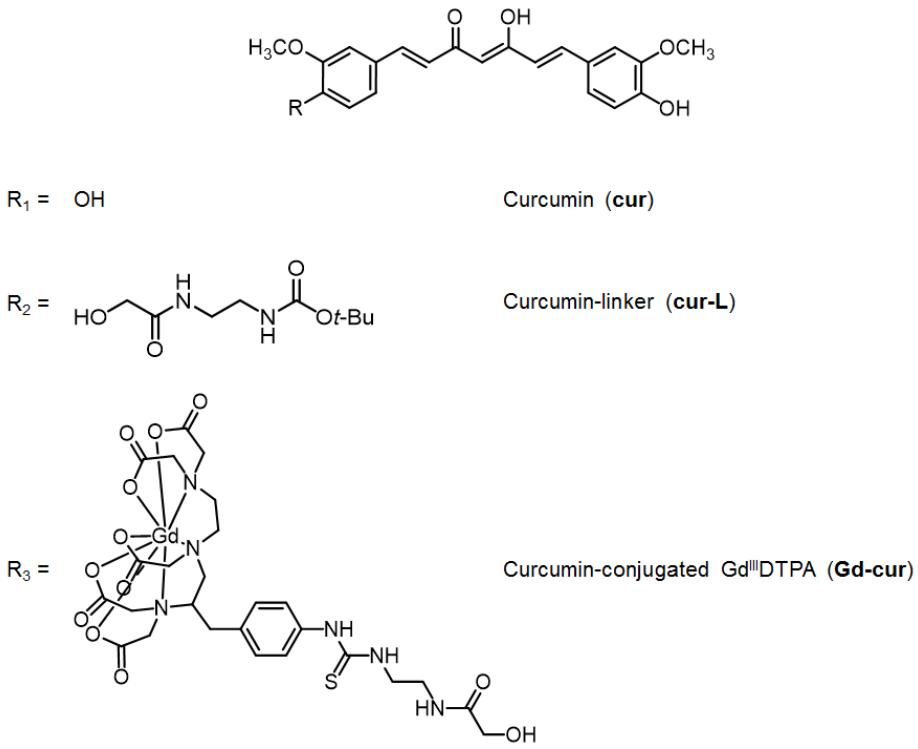

Figure 4.1. Structures of curcumin derivatives. Top to bottom: Curcumin (**cur**) = (1*E*,4*Z*,6*E*)-5-hydroxy-1,7-bis(4-hydroxy-3-methoxyphenyl)hepta-1,4,6-trien-3-one; curcumin-linker (**cur-L**) = *tert*-butyl(2-(2-(4-((1*E*,4*Z*,6*E*)-5-hydroxy-7-(4-hydroxy-3-methoxyphenyl)-3oxohepta-1,4,6-trien-1-yl)-2-methoxyphenoxy) acetoamido)ethyl)carbamate; Gd^{III}DTPA conjugated curcumin (**Gd-cur**) = Gd^{III}diethylenetriaminepenta-acetate-complexed-2-(4-((1*E*,4*Z*,6*E*)-5-hydroxy-7-(4-hydroxy-3-methoxyphenyl)-3-oxohepta-1,4,6-trien-1-yl)-2-methoxyphenoxy)-*N*-(2-(3-(*p*-tolyl)ethyl)acetamide.

The ability of **cur**, **cur-L**, and **Gd-cur** to bind Cu^{2+} and Zn^{2+} was investigated by UV-visible (UV-vis) spectroscopy (Figure 4.2). Changes in UV-vis spectra, such as new optical bands and/or change in absorbance intensity were observed upon $CuCl_2$ or $ZnCl_2$ treatment (1 to 2 equiv) with **cur**, **cur-L**, or **Gd-cur** in EtOH, indicating interaction between metal ions and these compounds. Optical shifts were detected from *ca.* 430 and 455 nm (for **cur**), 427 nm and 450 nm (for **cur-L**), and 424 and 452 nm (for **Gd-cur**) (Figure 4.2a) after $CuCl_2$ treatment. Upon introduction of $ZnCl_2$, optical shifts were observed *ca*. 430 nm (for **cur**), 423 and 450 nm (for **cur-L**), and 424 and 459 nm (for **Gd-cur**) (Figure 4.2b). It should be noted that very minimal optical shift was observed for **cur** and **cur-L** upon the addition of $ZnCl_2$. Overall, Cu^{2+} and Zn^{2+} binding **cur**, **cur-L**, and **Gd-cur** was confirmed by UV-vis.

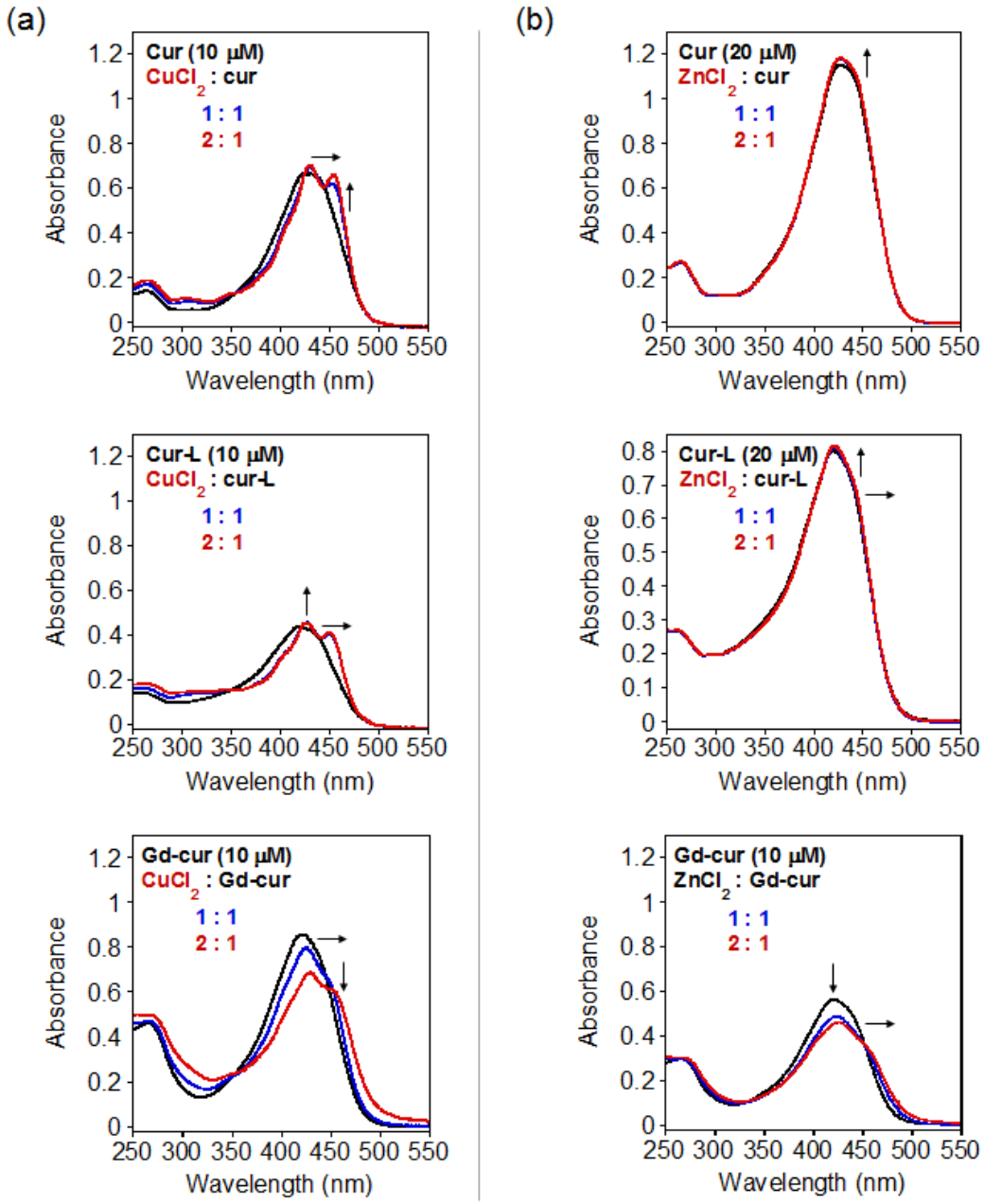

Figure 4.2. Cu^{2+} and Zn^{2+} binding studies of **cur**, **cur-L**, and **Gd-cur**. UV-vis spectra of **cur**, **cur-L**, and **Gd-cur** with (a) $CuCl_2$ (1-2 equiv) in EtOH or (b) $ZnCl_2$ (1-2 equiv) in EtOH. Conditions: [**cur**, **cur-L**, or **Gd-cur**] = 10 μM for Cu^{2+} binding studies; [**cur** or **cur-L**] = 20 μM or [**Gd-cur**] = 10 μM for Zn^{2+} binding studies; room temperature; incubation for 5 min.

4.2.2. Influence of Gd^{III}DTPA, cur, cur-L, and Gd-cur on metal-free and metal-triggered Aβ aggregation *in vitro*

The control of **Gd^{III}DTPA**, **cur**, **cur-L**, and **Gd-cur** upon *in vitro* metal-free and metal-induced Aβ aggregation was investigated through two experiments: inhibition

(modulation of Aβ aggregate formation) and disaggregation (transformation of preformed Aβ aggregates) (Figures 4.3 and 4.4).[10,11,15] The generated Aβ species from both experiments were monitored *via* gel electrophoresis followed by Western blot with an anti-Aβ antibody (6E10) for distribution of molecular weight (MW) and transmission electron microscopy (TEM) for identification of morphological changes.[10,11,15]

As shown in Figure 4.3, the inhibition studies demonstrated different reactivity of **Gd^{III}DTPA**, **cur**, **cur-L**, and **Gd-cur** toward formation of metal-free and metal-induced Aβ aggregates consisting of either $Aβ_{40}$ or $Aβ_{42}$. In the case of samples containing $Aβ_{40}$, reactivity was only observed with Cu^{2+} treatment, where slight reactivity was visualized with **cur** and **cur**-**L** and none with **Gd^{III}DTPA** (Figure 4.3a, left, lanes 2, 3, and 5). $Aβ_{40}$ species with a wide distribution of MW was indicated with **Gd-cur**. TEM images of Cu^{2+}-treated $Aβ_{40}$ species incubates with **cur**, **cur-L**, or **Gd-cur** revealed smaller amorphous aggregates compared to untreated with compounds; while the resulting Cu^{2+}-added $Aβ_{40}$ species from compound-free and **Gd^{III}DTPA**-incubated samples presented similar size and morphology to compound-free conditions (Figure 4.3b, left).

Treatment of $Aβ_{42}$ with **cur**, **cur**-**L**, or **Gd-cur** showed distinct reactivity relative to $Aβ_{40}$ samples (Figure 4.3a, lanes 3, 4, and 5). In both metal-free and metal-associated $Aβ_{42}$ aggregation, various-sized Aβ species were present with **cur-L** (lane 4). Moreover, samples consisting of $Aβ_{42}$, Cu^{2+}, and **cur**, **cur**-**L**, or **Gd-cur** were visualized to have a different gel band pattern of varying MW (lanes 3, 4, and 5) in reference to compound-free samples (lane 1). Similar to $Aβ_{40}$, the ability of **Gd^{III}DTPA** to control either metal-free or metal-induced Aβ aggregation was not demonstrated (lane 2).

In addition, disaggregation studies indicated a similar pattern of reactivity for compounds with $Aβ_{40}$ samples (Figure 4.4). Minimal reactivity of **Gd^{III}DTPA**, **cur**, **cur**-**L**, or **Gd-cur** was visualized with metal-free and Zn^{2+}-treated Aβ species (Figure 4.4a, left, lanes 2, 3, 4, and 5), while a $Aβ_{40}$ aggregates with a wide distribution of MW was observed with **cur**, **cur**-**L**, or **Gd-cur** in the in presence of Cu^{2+} (lanes 3, 4, and 5). Morphological changes of Cu^{2+}-treated $Aβ_{40}$ species upon compound incubation was distinguished by TEM. Unstructured $Aβ_{40}$ species were detected in the sample containing **cur**, **cur-L**, or **Gd-cur** (Figure 4.4b). In the case of metal-free $Aβ_{42}$, a slightly

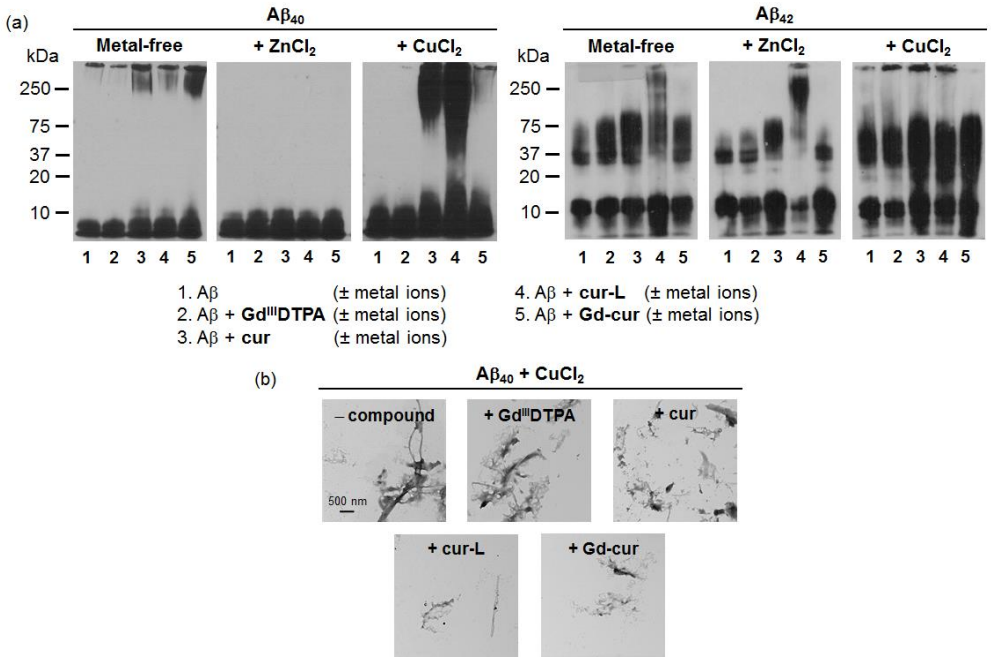

Figure 4.3. *In vitro* inhibition experiments of **Gd^{III}DTPA**, **cur**, **cur-L**, and **Gd-cur**. (a) Visualization of various-sized Aβ_{40} species (left) or Aβ_{42} species (right) by gel electrophoresis with Western blot (anti-Aβ antibody, 6E10). (c) TEM images of the 24 h incubated samples. Conditions: [Aβ] = 25 μM; [$CuCl_2$ or $ZnCl_2$] = 25 μM; [compound] = 50 μM; pH 6.6 (for Cu^{2+} samples) or 7.4 (for metal-free and Zn^{2+} samples); 24 h incubation; 37 °C; constant agitation.

different smearing pattern was visualized for **cur**, **cur-L**, and **Gd-cur** (Figure 4.4a, right, lanes 3, 4, and 5) in comparison to that of compound-untreated Aβ_{42} (lane 1). **Cur** and **Gd-cur** demonstrated distinct reactivity with Zn–Aβ_{42} (lanes 3 and 5). Interestingly, Aβ_{42} species having a wide range of MW was observed with **cur-L** with both metal-free and Zn^{2+}-added samples (lane 4). As expected, the treatment of **cur**, **cur-L**, or **Gd-cur** with preformed Cu^{2+}-induced Aβ aggregates was shown to generate various-sized Aβ_{42} species (lanes 3, 4, and 5). Surprisingly, reactivity was observed with the addition of **Gd^{III}DTPA** in samples containing Aβ_{42} and Cu^{2+} (lane 2).

4.2.3. Antioxidant activity of cur, cur-L, and Gd-cur

The ability of **cur**, **cur-L**, and **Gd-cur** to scavange free radicals was evaluated by the Trolox equivalent antioxidant capacity (TEAC) assay with cell lysates[15] which measures the ability of the compounds to inhibit the oxidation of ABTS to ABTS cation radicals ($ABTS^{\bullet+}$; ABTS = 2,2‘-azino-bis(3-ethylbenzothiaxoline-6-sulfonic acid) in the

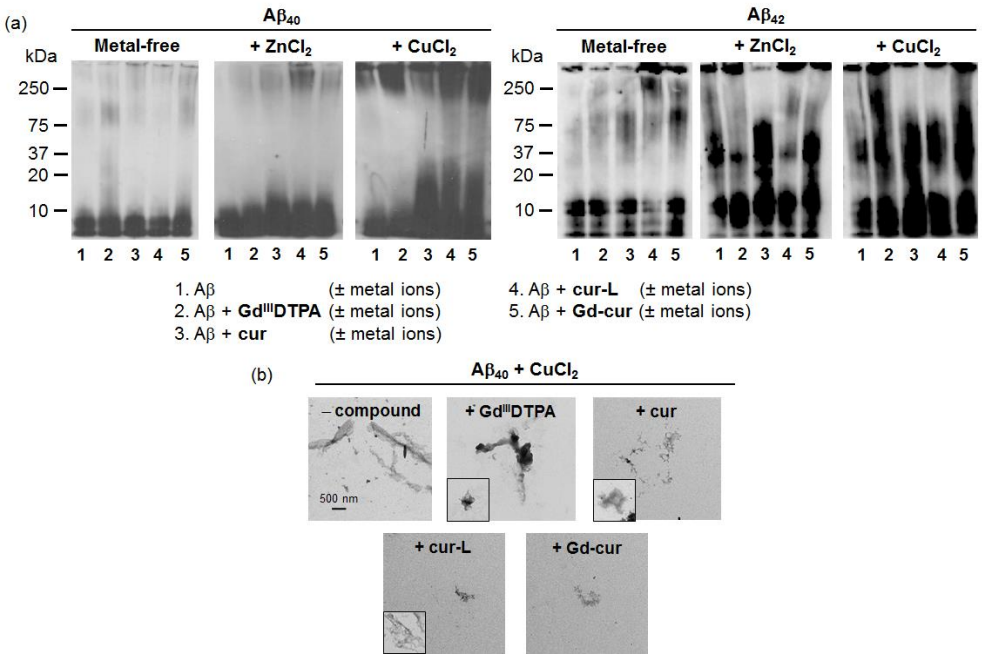

Figure 4.4. *In vitro* disaggregation experiments of **Gd^{III}DTPA**, **cur**, **cur-L**, and **Gd-cur**. (a) Visualization of various-sized $A\beta_{40}$ species (left) or $A\beta_{42}$ species (right) by gel electrophoresis with Western blot (anti-Aβ antibody, 6E10). (c) TEM images of the 24 h incubated samples. Conditions: [Aβ] = 25 μM; [$CuCl_2$ or $ZnCl_2$] = 25 μM; [compound] = 50 μM; pH 6.6 (for Cu^{2+} samples) or 7.4 (for metal-free and Zn^{2+} samples); 24 h incubation; 37 °C; constant agitation.

presence of metmyoglobin and H_2O_2. As shown in Figure 4.5, **Gd^{III}DTPA** and **Gd-cur** has similar antioxidant capacity as Trolox (vitamin E analogue) (1.2 ± 0.27 for **Gd^{III}DTPA**; 0.99 ± 0.12 for **Gd-cur**). The compounds **cur** and **cur-L** showed distinct differences in antioxidant activity in comparison to Trolox (TEAC value = 0.27 ± 0.15 and 3.72 ± 1.69, respectively, Figure 4.5). Note that precipitation was observed with **cur** and **cur-L** in the cell lysate assay conditions (owing to their poor solubility in aqueous media).

4.2.4. Cyotoxocity of Gd^{III}DTPA and Gd-cur in living cells

The cytoxicity of **Gd^{III}DTPA** and **Gd-cur**, in the absence and presence of metal salt ($CuCl_2$ or $ZnCl_2$) were determined using an MTT assay[8,11,14,15,21] (Figure 4.6). Due to the insolubility of **cur** and **cur-L** in aqueous environment, the cytotoxicity of the two compounds was not assessed at this time. Murine Neuro-2a (N2a) neuroblastoma cells were treated with various concentrations of compounds (2.5–25 μM). No toxicity was

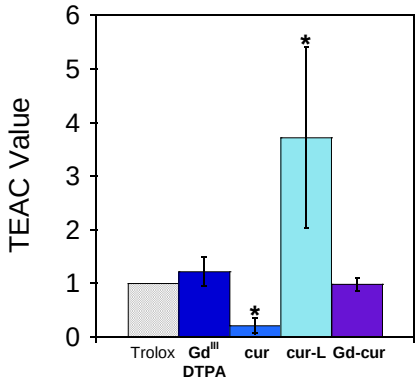

Figure 4.5. Antioxidant activity of **Gd^{III}DTPA**, **cur**, **cur-L**, and **Gd-cur** determined by the TEAC assay with cell lysates. TEAC values are relative to Trolox (vitamine E analogue; 6-hydroxy-2,5,7,8-tetramethlchroman-2-carboxylic acid). * Indicates precipitation in cell lysate assay conditions.

observed for both **Gd^{III}DTPA** and **Gd-cur**. (Figure 4.6a). Upon the addition of either $CuCl_2$ or $ZnCl_2$ (2.5–25 μM) with compound (M^{2+}: compound ratio = 1:1 or 1:2), **Gd^{III}DPTA** and **Gd-cur** showed relatively low cytotoxicity in the presence of either Cu^{2+} or Zn^{2+} (*ca.* 80% cell viability; Figure 4.6b). Overall, **Gd-cur** exhibited relatively high cell viability, indicating its potential use for biological application.

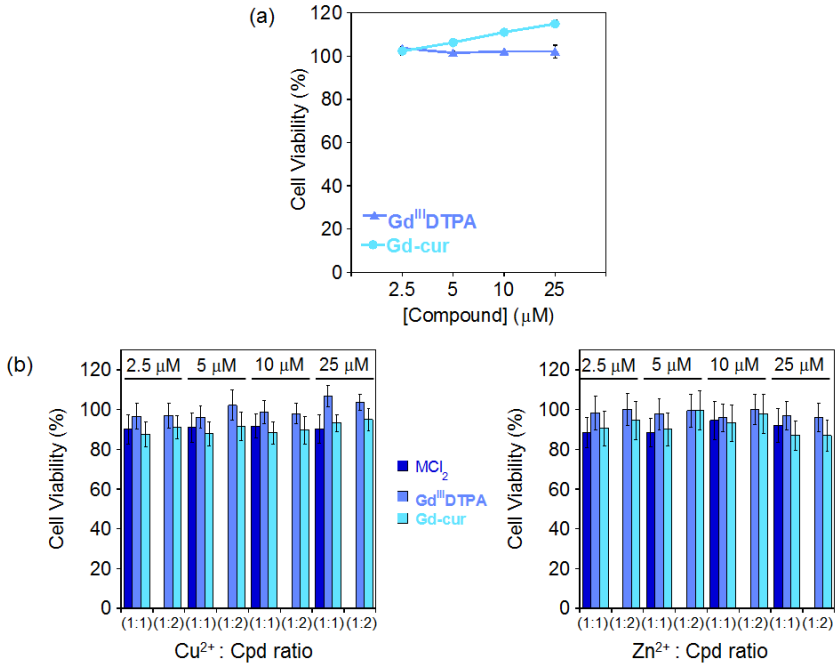

Figure 4.6. Cytotoxicity of **Gd^{III}DTPA**, **cur**, **cur-L**, and **Gd-cur** in the absence and presence of $CuCl_2$ or $ZnCl_2$ (a) Treatment of N2a cells with various concentrations of compounds (2.5–25 μM) for 24 h incubation. (b) Treatment of N2a cells with compound:M^{2+} ratio at 1:1 or 1:2. [M^{2+}] and [compound] = 2.5–50 μM.

4.2.5. Blood-brain barrier permeability

To assess the biological applicability of **cur**, **cur**-**L**, or **Gd-cur**, BBB permeability, initially predicted by Lipinski's rules and logBB[56-59] (Table 4.1), was verified by an *in vitro* Parallel Artificial Membrane Permeability Assay adapted for BBB (PAMPA-BBB), following a previously reported method.[8,14,56,57,60] Based on the empirical classification of molecules known to be BBB-permeable (*e.g.*, verapamil) [56,57,60] and the measured permeability values ($-\log P_e$) indicate that **cur**, **cur**-**L** may potentially diffuse through the BBB, while **Gd-cur** may or may not passively permeate through the BBB.

4.3. Conclusion

A synthesized hybrid of Gd^{III}DTPA and curcumin (**Gd-cur**) was previously determined to be a viable contrast agent with the ability to target Aβ fibrils.[42] Therefore, the potential diagnostic tool was investigated to determine if **Gd-cur** could be used for therapeutic means. **Gd-cur** was examined to observe whether the curcumin moeity appended to the Gd^{III}DTPA still retained the advantageous aspects of curcumin, such as antioxidant activity and control Aβ aggregation, after conjugation, as well as having the ability to target metal-free and metal-associated Aβ species and modulate Aβ aggregation. **Gd-cur** presented improved solubility aquous solution, while **cur** and **cur-L** was shown to be relatively insoluble in aquous environments. **Gd-cur** was found to slightly modulate the assembly of Cu^{2+}-associated $A\beta_{40}$ species, while in the case of $A\beta_{42}$, distinct reactivity was observed in the presence of Cu^{2+}. Furthermore, **Gd-cur** was indicated to transform preformed Cu^{2+}–$A\beta_{40}$ aggregates, although, interestingly, reactivity was observed in both metal-free and metal-added conditions for $A\beta_{42}$ samples, suggesting that **Gd-cur** may be more preferential to $A\beta_{42}$ in comparison to $A\beta_{40}$. For biological ultilization, **Gd-cur** has similar antioxidant capability as Trolox and shows relatively no toxicity in living cells. It, however, may be limited to applications in the brain due to its BBB permeability property. Overall, the promising increase in solubility of **Gd-cur** and its *in vitro* reactivity toward Aβ and metal–Aβ species makes this conjugate worthy of further structural modifications for improvement of BBB permeability. Our studies, along with the previous report,[42] have demonstrated the feasibility to potentially develop a thernostic agent (both diagnostic and therapeutic) in AD.

Table 4.1. Values (MW, *c*log*P*, HBA, HBD, PSA, logBB, and –logP_e) for **cur**, **cur-L**, or **Gd-cur**.

Calculation[a]	cur	cur-L	Gd-cur	Lipinski's rules and others
MW	368	569	1161	500
*c*log*P*	2.94	3.73	3.32	≤ 5.0
HBA	6	11	20	≤ 10
HBD	3	4	5	≤ 5.0
PSA	96.2	153	270	≤ 90
logBB	−0.838	−1.56	−3.36	< −1.0 (poor distribution in the brain)
–logP_e[b]	4.7 ± 0.1	4.7 ± 0.1	5.7 ± 0.1	
CNS+/– prediction[c]	CNS+	CNS+	CNS+/–	–logP_e < 5.4 (CNS+) –logP_e > 5.7 (CNS–)

[a] MW, molecular weight; *c*logP, calculated logarithm of the octonal-water partition coefficient; HBA, hydrogen-bond acceptor atoms; HBD, hydrogen-bond donor atoms; PSA, polar surface area; logBB = −0.0148 x PSA + 0.152 x *c*logP + 0.130. [b] The values of –logP_e were measured by the Parallel Artificial Membrane Permeability Assay adapted for blood-brain barrier (PAMPA-BBB). [c] CNS+/– prediction: prediction of compound to penetrate to the central nervous system (CNS). CNS+: compounds have the ability to permeate through the BBB and be bioavailable in the CNS. CNS–: poor permeability through the BBB and therefore, compound bioavailability into the CNS is considered to be minimal.

4.4. Experimental section

4.4.1. Materials and methods

All reagents were purchased from commercial suppliers and used as received unless otherwise stated. The compound, gadolinium-conjugated 2-(4-((1*E*,4*Z*,6*E*)-5-hydroxy-7-(4-hydroxy-3-methoxyphenyl)-3oxohepta-1,4,6-trien-1-yl)-2-methoxyphenoxy)-*N*-(2-(3-(*p*-tolyl)ethyl)acetamide (**Gd-cur**) was prepared following previously reported methods.[35] Aβ_{40} (DAEFRHDSGYEVHHQKLVFFAEDVGSNKGAIIGLMVGGVV) and Aβ_{42} (DAEFRHDSGYEVHHQKLVFFAEDVGSNKGAIIGLMVGGVVIA) were purchased from AnaSpec (Fremont, CA). Transmission electron microscopy (TEM) images were recorded with a Philips CM-100 transmission electron microscope (Microscopy and Image Analysis Laboratory, University of Michigan, Ann Arbor, MI). A SpectraMax M5 microplate reader (Molecular Devices, Sunnyvale, CA) was employed for the measurement of absorbance for TEAC, MTT, and PAMPA-BBB assays.

4.4.2. Metal binding studies

The interactions of **Gd^{III}DTPA**, **cur**, **cur-L**, and **Gd-cur** with Cu^{2+} and Zn^{2+} were

investigated by UV-vis, based on previously reported procedures.[11,15,21] A solution of **cur** (10 μM for Cu^{2+} binding studies; 20 μM for Zn^{2+} binding studies), **cur-L** (10 μM for Cu^{2+} binding studies; 20 μM for Zn^{2+} binding studies), or **Gd-cur** (10 μM for either Cu^{2+} or Zn^{2+} binding studies) in EtOH was treated with 1 to 2 equiv of a metal chloride salt ($CuCl_2$ or $ZnCl_2$) with incubation of 5 min at room temperature.

4.4.3. Amyloid-β (Aβ) peptide experiments

Aβ experiments were performed according to previously published procedures.[10,11,15] $Aβ_{40}$ or $Aβ_{42}$ was dissolved in ammonium hydroxide (NH_4OH, 1% v/v, aq), aliquoted, lyophilized overnight, and stored at −80 °C. A stock solution was prepared by dissolving Aβ in 1% NH_4OH and diluted with ddH_2O. For the inhibition experiment, Aβ (25 μM) was treated with or without metal ions ($CuCl_2$ or $ZnCl_2$; 25 μM) for 2 min, followed by addition of a compound (50 μM; 1% v/v final DMSO concentration). The resulting samples were incubated for 24 h at 37 °C with constant agitation. For the disaggregation experiment, Aβ (25 μM) with and without metal ions ($CuCl_2$ or $ZnCl_2$, 25 μM) was first incubated for 24 h at 37 °C with constant agitation. Afterward, a compound (50 μM, 1% v/v final DMSO concentration for **cur** and **cur-L**) was added and followed by an additional 24 h incubation at 37 °C with constant agitation. Both studies were performed using a buffered solution (20 μM HEPES, pH 6.6 (for $CuCl_2$) or pH 7.4 (metal-free and $ZnCl_2$), 150 μM NaCl).

4.4.4. Gel electrophoresis with Western blot

The Aβ peptide experiments described above were analyzed using gel electrophoresis followed by Western blotting with an anti-Aβ antibody (6E10, Covance, Princeton, NJ).[10,11,15] Each sample (10 μL) was separated using a 10–20% Tris-tricine gel (Invitrogen, Grand Island, NY). After the separation. the proteins were transferred onto a nitrocellulose membrane and blocked with bovine serum albumin (BSA, 3% w/v, Sigma-Aldrich) in Tris-buffered saline (TBS) containing 0.1% Tween-20 (TBS-T) for 2–3 h at ambient temperature. The membranes were incubated with an anti-Aβ antibody (1:2000) in 2% BSA (w/v in TBS-T) for overnight at 4 °C. After washing, membranes

were probed with the horseradish peroxidase-conjugated goat anti-mouse antibody (1:10,000) in 2% BSA for 1 h at ambient temperature. Thermo Scientific Supersignal West Pico Chemiluminescent Substrate (Thermo Scientific, Rockford, IL) was used to visualize protein bands.

4.4.5. Transmission electron microscopy (TEM)

TEM samples were prepared following a previously reported method.[10,11,15] Glow-discharged grids (Formar/Carbon 300-mesh, Electron Microscopy Sciences, Hatfield, PA) were treated with the samples (5 μL) from either the inhibition or disaggregation experiment for 2 min at room temperature. Excess sample was removed with filter paper. The grids were washed 3 times with ddH_2O, stained with uranyl acetate (1% w/v, ddH_2O, 5 μL) for 1 min, and dried for 15 min at room temperature. A Philips CM-100 transmission electron microscope (80 kV, 25,000x magnification; Microscopy and Image Analysis Laboratory, University of Michigan, Ann Arbor, MI) was used for obtaining TEM images of the samples.

4.4.6. Trolox Equivalent Antioxidant Capacity Assay with cell lysate

The antioxidant activity of **Gd^{III}DTPA**, **cur**, **cur-L**, and **Gd-cur** was determined by the TEAC assay employing cell lysate following the protocol of the antioxidant assay kit purchased from Cayman Chemical Company (Ann Arbor, MI) with modifications. The N2a cells were used for this assay. This cell line purchased from ATCC was maintained in media containing 50% Dulbecco's modified Eagle's medium (DMEM) and 50% OPTI-MEM (GIBCO), supplemented with 10% fetal bovine serum (FBS, Sigma), 1% Non-essential Amino Acids (NEAA, GIBCO), 2 mM glutamine, 100 U/ml penicillin, and 100 mg/ml streptomycin (GIBCO). The cells were grown and maintained at 37 °C in a humidified atmosphere with 5% CO_2. For the antioxidant assay using cell lysates, cells were seeded in a 6 well plate and grown to approximately 80-90% confluence. Cell lysates were prepared following the previously reported method with modifications.[61] N2a cells were washed once with cold PBS (pH 7.4, GIBCO) and harvested by gently pipetting off adherent cells with cold PBS. The cell pellet was generated by centrifugation (2,000 x g for 10 min at 4 °C). This cell pellet was sonicated on ice (5 sec

pulses, 5 times with 20 sec intervals between each pulse) in 2 mL of cold Assay Buffer (5 mM potassium phosphate, pH 7.4, containing 0.9% NaCl and 0.1% glucose). The cell lysates were centrifuged at 5,000 x g for 10 min at 4 °C. The supernatant was removed and stored on ice until use. To standard and sample 96 wells, 10 μL of the supernatant of cell lysates was delivered followed by addition of compound, metmyoglobin, ABTS, and H_2O_2 in order. After 5 min incubation at room temperature on a shaker, absorbance values at 750 nm were recorded. The final concentrations (0.045, 0.090, 0.135, 0.180, 0.225, and 0.330 mM) of **Gd^{III}DTPA**, **cur**, **cur-L**, **Gd-cur**, and Trolox (Sigma-Aldrich; Trolox = 6-hydroxy-2,5,7,8-tetramethylchroman-2-carboxylic acid; dissolved in DMSO) were used. The percent inhibition was calculated according to the measured absorbance (% Inhibition = $(A_0 - A)/A_0$, where A_0 is absorbance of the supernatant of cell lysates) and was plotted as a function of compound concentration. The TEAC value of ligands was calculated as a ratio of the slope of the standard curve of the compound to that of Trolox. The measurements were conducted in triplicate.

4.4.7. Cell viability (MTT Assay)

The N2a neuroblastoma cell line was purchased from the American Type Culture Collection (ATCC, Manassas, VA). The cell line was maintained in media containing 50% DMEM and 50% OPTI-MEM (GIBCO), supplemented with 10% FBS (Sigma), 1% NEAA (GIBCO), 2 mM glutamine, 100 U/ml penicillin, and 100 mg/ml streptomycin (GIBCO). The cells were grown and maintained at 37 °C in a humidified atmosphere with 5% CO_2. Cell viability upon treatment of compounds was determined using the MTT assay. N2a cells were seeded in a 96 well plate (15,000 cells in 100 μL per well). The cells were treated with various concentrations (2.5–25 μM) with or without $CuCl_2$ or $ZnCl_2$ (2.5–50 μM; either 1:1 or 1:2 compound:M^{2+} ratio), and incubated for 24 h. After incubation, 25 μL MTT (5 mg/mL (Sigma) in phosphate buffered saline (PBS, pH 7.4, Gibco, Grand Island, NY, USA) was added to each well and the plate was incubated for 4 h at 37 °C. Formazan produced by the cells was solubilized using an acidic solution of *N*,*N*-dimethylformamide (50%, v/v aq) and sodium dodecyl sulfate (SDS, 20%, w/v) overnight at room temperature in the dark. The absorbance was measured at 600 nm using a microplate reader. Cell viability was calculated relative to cells containing an

equivalent amount of HEPES.

4.4.8. Parallel Artificial Membrane Permeability Assay adapted for blood-brain barrier (PAMPA-BBB)

Previously reported protocols with modification using the PAMPA Explorer kit (Pion, *Inc*.) were applied to our PAMPA-BBB experiment.[11,56,57,60] Each stock solution of the compounds was diluted to a final concentration of 10 μM (1% v/v final DMSO concentration) with pH 7.4 Prisma HT buffer (Pion). The resulting solution (200 μL) was added to each of the wells of the donor plate (number of replicates per sample = 12). The BBB-1 lipid (Pion formulation, 5 μL) was used to coat the polyvinylidene fluoride (PDVF, 0.45 μM) filter membrane on the acceptor plate. The acceptor plate was placed on the top of the donor plate generating a "sandwich" and each well of the acceptor plate was filled with the brain sink buffer (200 μL, Pion). The sandwich was incubated at rt for 4 h without stirring. A microplate reader was used to obtain the optical spectra (250-500 nm) of the solutions in the reference, acceptor, and donor plates. The $-\log P_e$ for each compound was calculated using the PAMPA Explorer software c. 3.5 (Pion). CNS+/– assignment was determined in comparison to compounds identified previously.[5656,57,60] Compounds categorized as CNS+ have the ability to permeate through the BBB and target the CNS. Compounds assigned as CNS– have poor permeability through the BBB and therefore, their bioavailability into the CNS is considered to be minimal.

4.5. References

(1) Thies, W.; Bleiler, L. *Alzheimers Dement.* **2013**, *9*, 208.
(2) Kepp, K. P. *Chem. Rev.* **2012**, *112*, 5193.
(3) Scott, L. E.; Orvig, C. *Chem. Rev.* **2009**, *109*, 4885.
(4) Jakob-Roetne, R.; Jacobsen, H. *Angew. Chem., Int. Ed.* **2009**, *48*, 3030.
(5) DeToma, A. S.; Salamekh, S.; Ramamoorthy, A.; Lim, M. H. *Chem. Soc. Rev.* **2012**, *41*, 608.
(6) Hardy, J. A.; Higgins, G. A. *Science* **1992**, *256*, 184.
(7) Savelieff, M. G.; Lee, S.; Liu, Y.; Lim, M. H. *ACS Chem. Biol.* **2013**, *8*, 856.
(8) Pithadia, A. S.; Kochi, A.; Soper, M. T.; Beck, M. W.; Liu, Y.; Lee, S.; DeToma, A. S.; Ruotolo, B. T.; Lim, M. H. *Inorg. Chem.* **2012**, *51*, 12959.

(9) Rodríguez-Rodríguez, C.; Sánchez de Groot, N.; Rimola, A.; Álvarez-Larena, Á.; Lloveras, V.; Vidal-Gancedo, J.; Ventura, S.; Vendrell, J.; Sodupe, M.; Gonzalez-Duarte, P. *J. Am. Chem. Soc.* **2009**, *131*, 1436.
(10) Hindo, S. S.; Mancino, A. M.; Braymer, J. J.; Liu, Y.; Vivekanandan, S.; Ramamoorthy, A.; Lim, M. H. *J. Am. Chem. Soc.* **2009**, *131*, 16663.
(11) Choi, J. S.; Braymer, J. J.; Nanga, R. P.; Ramamoorthy, A.; Lim, M. H. *Proc. Natl. Acad. Sci. U. S. A.* **2010**, *107*, 21990.
(12) Braymer, J. J.; Choi, J.-S.; DeToma, A. S.; Wang, C.; Nam, K.; Kampf, J. W.; Ramamoorthy, A.; Lim, M. H. *Inorg. Chem.* **2011**, *50*, 10724.
(13) Sharma, A. K.; Pavlova, S. T.; Kim, J.; Finkelstein, D.; Hawco, N.; Rath, N. P.; Kim, J.; Mirica, L. M. *J. Am. Chem. Soc.* **2012**, *134*, 6625.
(14) Liu, Y.; Kochi, A.; Pithadia, A. S.; Lee, S.; Nam, Y.; Beck, M. W.; He, X.; Lee, D.; Lim, M. H. *Inorg. Chem.* **2013**, *52*, 8121.
(15) Lee, S.; Zheng, X.; Krishnamoorthy, J.; Savelieff, M. G.; Park, H. M.; Brender, J. R.; Kim, J. H.; Derrick, J. S.; Kochi, A.; Lee, H. J.; Kim, C.; Ramamoorthy, A.; Bowers, M. T.; Lim, M. H. *J. Am. Chem. Soc.* **2014**, *136*, 299.
(16) Zhang, X.; Tian, Y.; Li, Z.; Tian, X.; Sun, H.; Liu, H.; Moore, A.; Ran, C. *J. Am. Chem. Soc.* **2013**, *135*, 16397.
(17) Yang, F.; Lim, G. P.; Begum, A. N.; Ubeda, O. J.; Simmons, M. R.; Ambegaokar, S. S.; Chen, P. P.; Kayed, R.; Glabe, C. G.; Frautschy, S. A.; Cole, G. M. *J. Biol. Chem.* **2005**, *280*, 5892.
(18) Reinke, A. A.; Gestwicki, J. E. *Chem. Biol. Drug Des.* **2007**, *70*, 206.
(19) Narlawar, R.; Pickhardt, M.; Leuchtenberger, S.; Baumann, K.; Krause, S.; Dyrks, T.; Weggen, S.; Mandelkow, E.; Schmidt, B. *ChemMedChem* **2008**, *3*, 165.
(20) Airoldi, C.; Zona, C.; Sironi, E.; Colombo, L.; Messa, M.; Aurilia, D.; Gregori, M.; Masserini, M.; Salmona, M.; Nicotra, F.; La Ferla, B. *J. Biotechnol.* **2010**, *156*, 317.
(21) Hyung, S. J.; DeToma, A. S.; Brender, J. R.; Lee, S.; Vivekanandan, S.; Kochi, A.; Choi, J. S.; Ramamoorthy, A.; Ruotolo, B. T.; Lim, M. H. *Proc. Natl. Acad. Sci. U. S. A.* **2013**, *110*, 3743.
(22) Porat, Y.; Abramowitz, A.; Gazit, E. *Chem. Biol. Drug Des.* **2006**, *67*, 27.
(23) Ehrnhoefer, D. E.; Bieschke, J.; Boeddrich, A.; Herbst, M.; Masino, L.; Lurz, R.;Engemann, S.; Pastore, A.; Wanker, E. E. *Nat. Struct. Mol. Biol.* **2008**, *15*, 558.
(24) Bieschke, J.; Russ, J.; Friedrich, R. P.; Ehrnhoefer, D. E.; Wobst, H.; Neugebauer, K.; Wanker, E. E. *Proc. Natl. Acad. Sci. U. S. A.* **2010**, *107*, 7710.
(25) Rauk, A. *Chem. Soc. Rev.* **2009**, *38*, 2698.
(26) Gorman, P. M.; Yip, C. M.; Fraser, P. E.; Chakrabartty, A. *J. Mol. Biol.* **2003**, *325*, 743.
(27) Naslund, J.; Haroutunian, V.; Mohs, R.; Davis, K. L.; Davies, P.; Greengard, P.; Buxbaum, J. D. *JAMA, J. Am. Med. Assoc.* **2000**, *283*, 1571.
(28) Klunk, W. E.; Lopresti, B. J.; Ikonomovic, M. D.; Lefterov, I. M.; Koldamova, R. P.; Abrahamson, E. E.; Debnath, M. L.; Holt, D. P.; Huang, G. F.; Shao, L.; DeKosky, S. T.; Price, J. C.; Mathis, C. A. *J. Neurosci.* **2005**, *25*, 10598.
(29) Lockhart, A.; Lamb, J. R.; Osredkar, T.; Sue, L. I.; Joyce, J. N.; Ye, L.; Libri, V.; Leppert, D.; Beach, T. G. *Brain* **2007**, *130*, 2607.

(30) Toyama, H.; Ye, D.; Ichise, M.; Liow, J. S.; Cai, L.; Jacobowitz, D.; Musachio, J. L.; Hong, J.; Crescenzo, M.; Tipre, D.; Lu, J. Q.; Zoghbi, S.; Vines, D. C.; Seidel, J.; Katada, K.; Green, M. V.; Pike, V. W.; Cohen, R. M.; Innis, R. B. *Eur. J. Nucl. Med. Mol. Imaging* **2005**, *32*, 593.
(31) Li, S.; He, H.; Cui, W.; Gu, B.; Li, J.; Qi, Z.; Zhou, G.; Liang, C. M.; Feng, X. Y. *Anat. Rec. (Hoboken)* **2010**, *293*, 2136.
(32) Kung, H. F.; Lee, C. W.; Zhuang, Z. P.; Kung, M. P.; Hou, C.; Plossl, K. *J. Am. Chem. Soc.* **2001**, *123*, 12740.
(33) Poduslo, J. F.; Wengenack, T. M.; Curran, G. L.; Wisniewski, T.; Sigurdsson, E. M.; Macura, S. I.; Borowski, B. J.; Jack, C. R., Jr. *Neurobiol. Dis.* **2002**, *11*, 315.
(34) Poduslo, J. F.; Curran, G. L.; Peterson, J. A.; McCormick, D. J.; Fauq, A. H.; Khan, M. A.; Wengenack, T. M. *Biochemistry* **2004**, *43*, 6064.
(35) Scholtzova, H.; Wadghiri, Y. Z.; Douadi, M.; Sigurdsson, E. M.; Li, Y. S.; Quartermain, D.; Banerjee, P.; Wisniewski, T. *J. Neurosci. Res.* **2008**, *86*, 2784.
(36) Yang, J.; Wadghiri, Y. Z.; Hoang, D. M.; Tsui, W.; Sun, Y.; Chung, E.; Li, Y.; Wang, A.; de Leon, M.; Wisniewski, T. *NeuroImage* **2011**, *55*, 1600.
(37) Majocha, R. E.; Reno, J. M.; Friedland, R. P.; VanHaight, C.; Lyle, L. R.; Marotta, C. A. *J. Nucl. Med.* **1992**, *33*, 2184.
(38) Friedland, R. P.; Shi, J.; Lamanna, J. C.; Smith, M. A.; Perry, G. *Ann. N. Y. Acad. Sci.* **2000**, *903*, 123.
(39) Lee, H. J.; Zhang, Y.; Zhu, C.; Duff, K.; Pardridge, W. M. *J Cereb. Blood Flow Metab.* **2002**, *22*, 223.
(40) Tamura, Y.; Hamajima, K.; Matsui, K.; Yanoma, S.; Narita, M.; Tajima, N.; Xin, K. Q.; Klinman, D.; Okuda, K. *Neurobiol. Dis.* **2005**, *20*, 541.
(41) Ramakrishnan, M.; Wengenack, T. M.; Kandimalla, K. K.; Curran, G. L.; Gilles, E. J.; Ramirez-Alvarado, M.; Lin, J.; Garwood, M.; Jack, C. R., Jr.; Poduslo, J. F. *Pharm. Res.* **2008**, *25*, 1861.
(42) Vithanarachchi, S. M.; Allen, M. J. *Chem. Commun. (Camb)* **2013**, *49*, 4148.
(43) Aggarwal, B. B.; Sundaram, C.; Malani, N.; Ichikawa, H. *Adv. Exp. Med. Biol.* **2007**, *595*, 1.
(44) Mishra, S.; Palanivelu, K. *Ann. Indian Acad. Neurol.* **2008**, *11*, 13.
(45) Ono, K.; Hasegawa, K.; Naiki, H.; Yamada, M. *J. Neurosci. Res.* **2004**, *75*, 742.
(46) Shukla, P. K.; Khanna, V. K.; Khan, M. Y.; Srimal, R. C. *Hum. Exp. Toxicol.* **2003**, *22*, 653.
(47) Lim, G. P.; Chu, T.; Yang, F.; Beech, W.; Frautschy, S. A.; Cole, G. M. *J. Neurosci.* **2001**, *21*, 8370.
(48) Frautschy, S. A.; Hu, W.; Kim, P.; Miller, S. A.; Chu, T.; Harris-White, M. E.; Cole, G. M. *Neurobiol. Aging* **2001**, *22*, 993.
(49) Sandur, S. K.; Ichikawa, H.; Pandey, M. K.; Kunnumakkara, A. B.; Sung, B.; Sethi, G.; Aggarwal, B. B. *Free Radic. Biol. Med.* **2007**, *43*, 568.
(50) Garcia-Alloza, M.; Borrelli, L. A.; Rozkalne, A.; Hyman, B. T.; Bacskai, B. J. *J. Neurochem.* **2007**, *102*, 1095.
(51) Koronyo-Hamaoui, M.; Koronyo, Y.; Ljubimov, A. V.; Miller, C. A.; Ko, M. K.; Black, K. L.; Schwartz, M.; Farkas, D. L. *NeuroImage* **2011**, *54 Suppl 1*, S204.
(52) Bernabe-Pineda, M.; Ramirez-Silva, M. T.; Romero-Romo, M.; Gonzalez-Vergara, E.; Rojas-Hernandez, A. *Spectrochim. Acta, Part A* **2004**, *60*, 1091.

(53) Wang, Y. J.; Pan, M. H.; Cheng, A. L.; Lin, L. I.; Ho, Y. S.; Hsieh, C. Y.; Lin, J. K. *J. Pharm. Biomed. Anal.* **1997**, *15*, 1867.
(54) Tonnesen, H. H.; Karlsen, J. *Z. Lebensm. Unters. Forsch.* **1985**, *180*, 402.
(55) Kaewnopparat, N.; Kaewnopparat, S.; Jangwang, A.; Maneenaun, D.; Chuchrome, T.; Panichayapakaranant, P. *World Academy of Science, Engineering and Technology* **2009**, *55*, 229.
(56) Di, L.; Kerns, E. H.; Fan, K.; McConnell, O. J.; Carter, G. T. *Eur. J. Med. Chem.* **2003**, *38*, 223.
(57) Avdeef, A.; Bendels, S.; Di, L.; Faller, B.; Kansy, M.; Sugano, K.; Yamauchi, Y. *J. Pharm. Sci.* **2007**, *96*, 2893.
(58) Lipinski, C. A.; Lombardo, F.; Dominy, B. W.; Feeney, P. J. *Adv. Drug Delivery Rev.* **2001**, *46*, 3.
(59) Clark, D. E.; Pickett, S. D. *Drug Discovery Today* **2000**, *5*, 49.
(60) *BBB Protocol and Test Compounds; Pion Inc.; Wolburn, MA, 2009*.
(61) Spencer, V. A.; Sun, J. M.; Li, L.; Davie, J. R. *Methods* **2003**, *31*, 67.

Chapter 5: *In Vitro* Influence of Enediyne Derivatives on Metal-Free and Metal-Induced Amyloid-β Aggregation

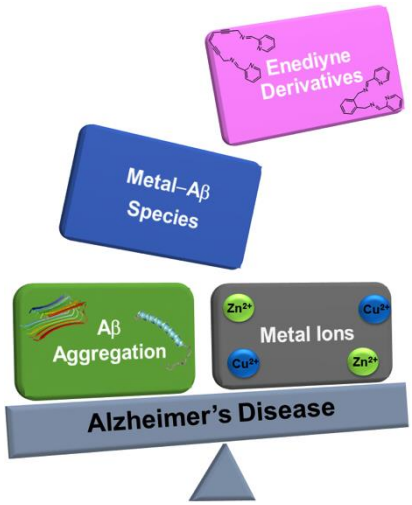

We thank Professor Jeffrey Zaleski and Meghan Porter for the synthesis, metal binding studies, solution speciation studies, and $A\beta_{40}$ gel analysis and TEM of the enediyne derivatives. For the work presented in this chapter, I have been contributing to the gel (Western blot) and TEM analyses for all $A\beta_{42}$ aggregation studies and *in vitro* PAMPA-BBB assay.

5.1. Introduction

Alzhiemer's disease (AD) is a crippling and fatal neurodegenerative disease that is the sixth leading cause of death, making it the only cause within the top 10 in the US that has no preventative or therapeutic measures, or any means to impede the progression of the disease.[1] AD is characterized by pathological features, including aggregation of misfolded proteins, (*e.g.*, amyloid-β (Aβ)), miscompartmentalization and dyshomeostasis of metal ions, and environment of oxidative stress.[2-8] A relationship between dysregulation of metal ions and Aβ-related toxicity has been suggested. High concentrations of metals (*i.e.*, Cu, Zn) have found in Aβ plaques; these metals can interact with Aβ species influencing aggregation and conformation of Aβ peptides and/or formation of reactive oxygen species (ROS).[2,6-9] The role of Aβ as well as metal-bound Aβ (metal–Aβ) in AD onset and progression still remains to be clearly elucidated.

In order to understand the involvement of metal–Aβ in the AD etiology, chemical tools designed to specifically target metal–Aβ species and modulate their reactivity (*i.e.*, Aβ aggregation and ROS generation) is therefore necessary. Current studies have enlisted the use of a rational structure-based approach to develop bifunctional small molecules for such chemical tool development (in particular, incorporation approach: insertion of a metal chelating site into an Aβ interacting framework, which can generate a single entity for metal chelation and Aβ interaction (bifunctionality)).[10-17] These molecules have demonstrated to the ability to control the interaction between metal ions and Aβ, consequently altering its reactivity *in vitro* and/or in living cells. In addition to synthesized small molecules, natural products, including EGCG (green tea extract) [18-20] and curcumin (spice in Indian curry),[21-23] have been explored as well, as viable framework for the same purposes.

Naturally occurring enediynes (*e.g.*, calicheamicin) have been extensively studied as a potential anti-cancer drugs.[24-26] Upon activation (through normal biological redox events), these compounds have the ability to undergo Bergman cyclization which could perform a H-atom abstraction.[27] Metal coordination to compounds has been shown to promote thermal Bergman cyclization, indicated in systems, including enediynes.[28-32] Due to its biological relevancy and metal binding property, the enediyne

framework was investigated as a chemical tool for studying metal–Aβ related to AD. Herein, we report the reactivity of enediyne derivatives (**PyED** (uncyclized) and **PyBD** (cyclized)) toward metal-free and metal-induced Aβ aggregation, employing both $A\beta_{40}$ and $A\beta_{42}$, along with their metal binding properties (metal ions: Cu^{2+} and Zn^{2+}).

5.2. Results and discussion

5.2.1. Rationale and characterization of PyED and PyBD investigated for modulating Aβ aggregation in the absence and presence of metal ions

PyED was selected as a potential chemical tool to be utilized for targeting and modulating metal–Aβ species, due to its proclivity to bind metal ions (*i.e.*, Cu^{2+}, Zn^{2+}) and undergo a subsequent radical generation event leading to an H-atom abstraction under physiologically relevant conditions.[27-32] In addition, the tetradentate ligand, **PyED** or **PyBD,** bears resemblance to previous bidentate and tetradentate compounds containing nitrogen and/or oxygen donor atoms that demonstrate the ability to control the formation of metal-triggered Aβ aggregates as well as dissemble preformed metal-treated Aβ aggregates.[10,11,13-17] For the purposes of an unreactive model for metal binding studies and differentiating compound activity due solely to metal chelation, as opposed to metal chelation and radical generation event, a fully cyclized structure (**PyBD**; Figure 5.1) with a binding site analogous to **PyED** was employed. Both **PyED** and **PyBD** were synthesized from previously reported procedures.[33]

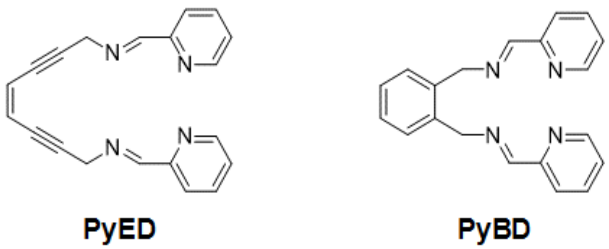

Figure 5.1. Structures of enediyne derivatives. **PyED** (1*E*,1'*E*)-*N*,*N*'-((*Z*)-octa-4-en-2,6-diyne-1,8-diyl)bis(1-(pyridin-2-yl)methanimine) (left) and **PyBD** (1*E*,1'*E*)-*N*,*N*'-(1,2-phenylenebis(methylene))bis(1-(pyridine-2-yl)methanimine) (right).

Variable-pH UV-visible (UV-vis) titrations were conducted to evaluate the ligand

species in solution, particularly at physiologically relevant pH (*e.g.*, 7.4).[10,12,15-17] Speciation was determined using **PyBD** due the fact that **PyED** undergoes Bergman cyclization in the presence of metal ions (referred to as the reactivity of **PyED** in the all metal binding experiments; *vide infra*). Given the structural similarities between **PyED** and **PyBD**, **PyBD** should serve as a good model for both ligand systems. Titration results indicated a single acid ionization constant (pK_a) for **PyBD** (pK_a = 3.81(2)), suggesting that neutral and monoprotonated form may exist depending on pH. Furthermore, the generated solution speciation diagram depicted **PyBD** as expected to exist mainly in the neutral from at pH 7.4. (Figure 5.2).

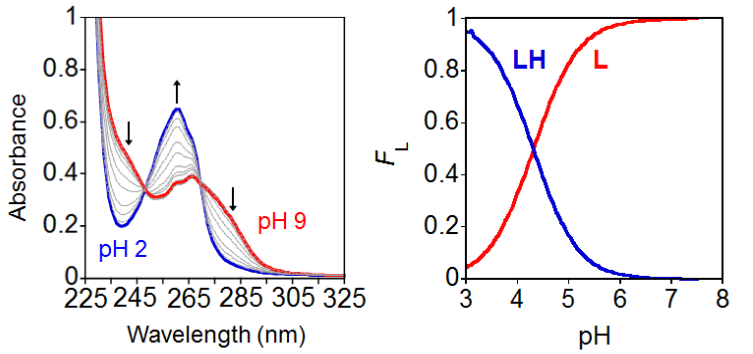

					PyBD
LH	⇌	L	+	H	pK_a[a] 3.78(2)

Figure 5.2. Solution speciation studies of **PyBD**. UV-vis variable-pH titration spectra (left) and solution speciation diagrams (right) of **PyBD** (pH 2–8) (F_L = fraction of species at the given pH). Acidity constants (pK_a) of **PyBD** is summarized in the table. Conditions: [**PyBD**] = 50 μM; I = 0.10 M NaCl; room temperature. Charges are omitted for clarity. [a] The error in the last digit is shown in the parentheses.

5.2.2. Metal binding properties of PyED and PyBD

The divalent metal binding properties of **PyED** and **PyBD** were investigated by UV-vis. Addition of one equiv of $ZnCl_2$ or $CuCl_2$ to **PyED** or **PyBD** in EtOH, bathochromic shifts in all samples are observed for optical bands at 264 and 272 nm, respectively (Figure 5.3). The shifts observed in response to Cu^{2+} binding by **PyED** and **PyBD** are more noticeable than those seen upon Zn^{2+} binding. The optical changes shown in the spectra following metal addition indicated occurrence of metal binding by **PyED** and **PyBD** in the presence of either Zn^{2+} or Cu^{2+}.

The neutral form of **PyBD** is the major species in solution at experimental pH

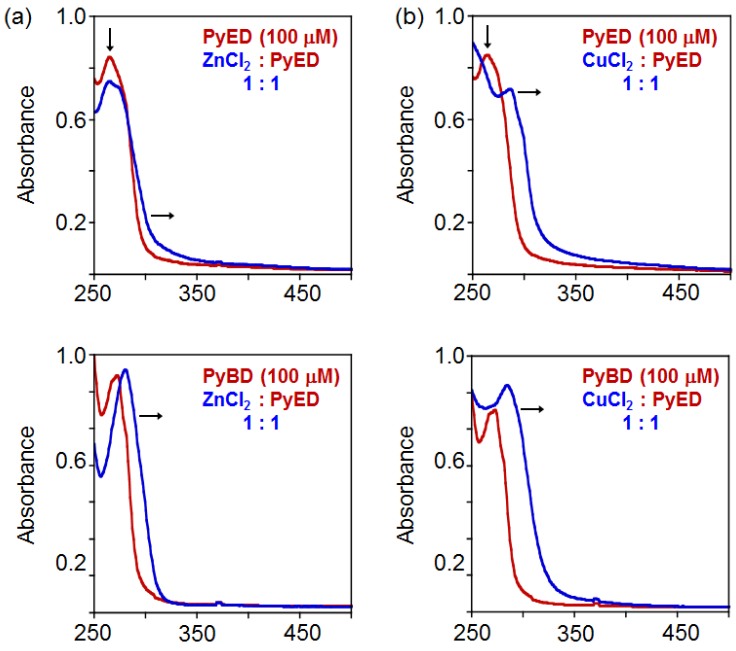

Figure 5.3. Zn^{2+} and Cu^{2+} binding of **PyED** and **PyBD**, monitored by UV-vis. UV-vis spectra of (a) **PyED** and **PyBD** with $ZnCl_2$ (1 equiv). (b) **PyED** and **PyBD** with $CuCl_2$ (1 equiv) in EtOH. Conditions: [**PyED** or **PyBD**] = 100 μM; room temperature; incubation for 10 min.

(*vide supra*) and variable-pH UV-vis titrations[10,12,15-17] were also conducted to elucidate complexation and binding properties of **PyBD** with Cu^{2+} in solution (Figure 5.4). Based the pK_a value determined for **PyBD** above and these titration results, the stability constants (logβ) for the these complexes were determined to be 12.2(8) and 16.6(8) for CuL and Cu(LH), respectively. A solution speciation diagram was modeled using these stability constants, suggests complexation of **PyBD** with Cu^{2+} occurred in a ratio of 1:1 metal to ligand, as well as neutral and protonated form of the Cu^{2+}**−PyBD** complex may exist at different pH. The data implicates neutral Cu^{2+}**−PyBD** form is the major species at pH 6.6 (Figure 5.4). The concentration of free Cu^{2+} in solution at pH 6.6 yielded a pCu value of 8.3(4) (pCu = $-\log[Cu^{2+}]_{unbound}$). This value suggested an approximate dissociation constant (K_d) for Cu^{2+}**−PyBD** to be *ca.* nanomolar range. When taken in consideration with the reported K_d values for Cu^{2+}−Aβ species (picomolar to nanomolar range),[2,4,6-8,34] **PyBD** could interact with Cu^{2+} in Cu^{2+}–Aβ species.

To assess the ability of **PyED** and **PyBD** to bind Cu^{2+} in a heterogeneous biological environment, metal selectivity studies were performed using **PyBD** as a model for both compounds due to the reactivity exhibited by **PyED** in the presence of

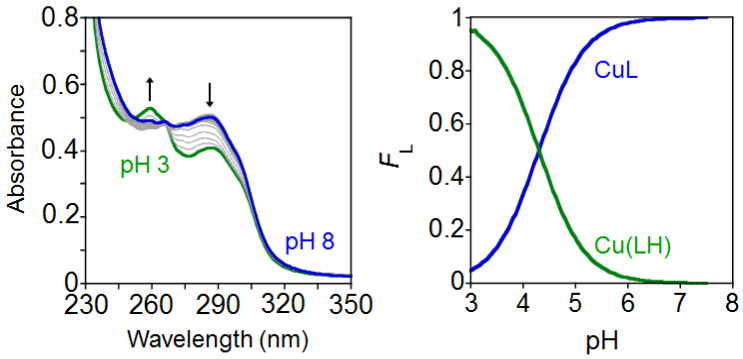

					Logβ [a]
Cu	+	LH	⇌	Cu(LH)	16.6(8)
Cu	+	L	⇌	CuL	12.2(8)

Figure 5.4. Solution speciation studies of the Cu^{2+}–**PyBD** complex. UV-vis variable-pH spectra (left) and solution speciation diagrams (right) of Cu^{2+}–**PyBD** (pH 3–8) (F_{Cu} = fraction of free Cu and Cu–L complexes at the given pH). Conditions: [Cu^{2+}]/[**PyBD**] = 1:1, [**PyBD**] = 50 μM; room temperature. Stability constant (logβ) of Cu–**PyBD** complexes are summarized in the table. Charges are omitted for clarity. [a] The error in the last digit is shown in the parentheses.

metal ions. The selectivity of **PyBD** for Cu^{2+} compared to other biologically relevant metal ions (*i.e.*, Ca^{2+}, Co^{2+}, Fe^{2+}, Fe^{3+}, Mg^{2+}, Mn^{2+}, Ni^{2+}, and Zn^{2+}) was investigated using UV-vis (Figure 5.5). Even in the presence of a large excess of a competing metal ion, **PyBD** displays relative moderate selectivity for Cu^{2+} over Ca^{2+}, Co^{2+}, Mg^{2+}, Mn^{2+}, Ni^{2+}, and Zn^{2+}. In the presence of Fe^{2+} and Fe^{3+} in solution, **PyBD** binding to these metal ions was also observed (Figure 5.5). This binding is likely due to the preferred octahedral binding geometry of the iron center and the structure of the binding moiety. Overall, these metal selectivity results demonstrate that the tetradentate pyridine-imine binding moiety of **PyBD** and **PyED** may be selective toward Cu^{2+} over other divalent metal ions found in biological environments, such as the brain.

5.2.3. Effects of PyED and PyBD on metal-free and metal-induced Aβ aggregation *in vitro*

In order to assess the ability of **PyED** to modulate metal-induced $A\beta_{40}$ and $A\beta_{42}$ aggregation pathways, *in vitro* disaggregation and inhibition experiments were conducted.[10-17] For comparison to **PyED**'s reactivity, the influence of monofunctional **PyBD** on Aβ aggregation was also examined. Disaggregation studies investigated the

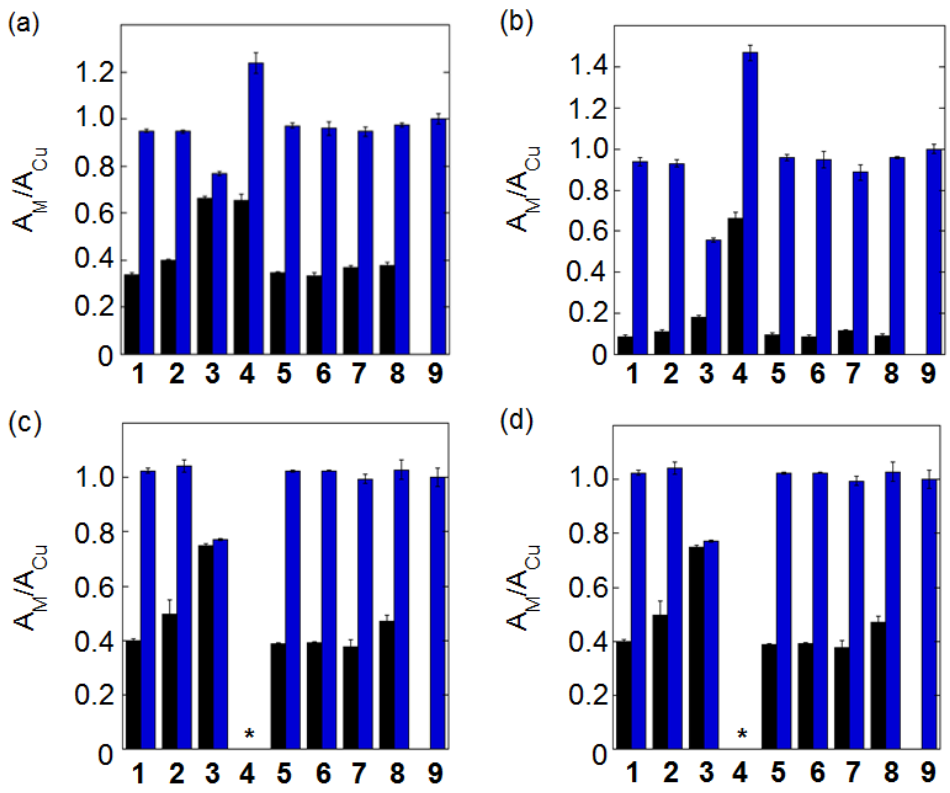

Figure 5.5. Metal selectivity studies of **PyBD** (50 μM) in HEPES buffer (20 mM, pH 7.35; NaCl 150 mM). Blue bars represent the addition of $CuCl_2$ (**9**) to solutions containing the ligand and another divalent metal ion (black bars; **1**, $CaCl_2$; **2**, $CoCl_2$; **3**, $FeCl_2$; **4**, $FeCl_3$; **5**, $MgCl_2$; **6**, $MnCl_2$; **7**, $NiCl_2$; **8**, $ZnCl_2$) in a ratio of 1:1 (a and b) and 25:1 (c and d) MCl_2 or MCl_3:$CuCl_2$ followed by 30 min incubation at room temperature. Absorbance at 285 nm (a and b), 305 nm (b and d) were used for the calculation of A_M/A_{Cu}. The observed higher absorbance after Cu^{2+} addition to solution containing ligand and another metal ion compared to that of the control (ligand and Cu^{2+} only) may be due to the absorbance from ligand binding to another metal ion at the wavelength selected for analysis. * Indicates precipitation in the solution or interference with unidentified species in spectra.

ability of both **PyED** and **PyBD** to structurally alter preformed metal-free Aβ and metal-treated Aβ aggregates (Figures 5.6 and 5.7), while inhibition experiments probed the compounds' ability to control the formation of metal-free and metal-triggered Aβ aggregates (Figures 5.8 and 5.9). The resultant Aβ species were characterized using gel electrophoresis followed by Western blot with an anti-Aβ antibody (6E10), and their morphologies were monitored by transmission electron microscopy (TEM).[11-13,15-17]

In the disaggregation studies, **PyED** and **PyBD** presented different reactivity toward preformed metal-free and metal-associated $Aβ_{40}$ and $Aβ_{42}$ aggregates (Figures 5.6 and 5.7). In the case of Zn^{2+}– and Cu^{2+}–$Aβ_{40}$ samples treated with **PyED**, Aβ species with an increasing range of molecular weight (MW) are observed at both 37 and

43 °C between 2 and 8 h, while a decrease in signal intensity occured between 8 and 24 h for samples incubated at 37 °C (Fig. 5.6a, lanes 5 and 8). Interestingly, at 43 °C, variable reactivity of **PyED** with preformed, Zn^{2+}–treated $A\beta_{40}$ aggregates was detected. Addition of **PyED** to Zn^{2+}–$A\beta_{40}$ presented an increasing distribution of MW throughout the time course (lane 5). In contrast, treatment of metal−$A\beta_{40}$ samples with **PyBD** led to the generation of lower MW species (MW ≤ 25 kDa) over the 24 h period (Fig. 5.6a, lanes 6 and 9). These data suggest that **PyBD** slightly affects the transformation of preformed metal–Aβ aggregates, indicating that the introduction of radical formation upon metal binding by **PyED** may be a key factor in the generation of metal-associated Aβ species exhibiting a different array of MW. Furthermore, the reduction of gel band intensity in Cu^{2+}–$A\beta_{40}$ samples incubated with **PyED** for 24 h may imply the occurrence of further aggregation over time. No reactivity was observed for either **PyED** or **PyBD** in metal-free conditions, except for $A\beta_{40}$ samples incubated with **PyED** at 8 h at 43 °C (Figure 5.6a, lanes 2, 3, and 8). The results suggest that **PyED** in the absence of metal ions may possibly go through radicalization with extended incubation and at higher temperature, generating Aβ species with an array of MW. The disappearnace of the gel band at 24 h may suggest further aggregation occurred (lane 8).

The trends in the gel analysis are consistent with TEM images of preformed metal–$A\beta_{40}$ aggregates treated with **PyED**. At 37 °C, TEM images of metal−$A\beta_{40}$ show a mixture of fibrillar and amorphous structure types, while at 43 °C, amorphous Aβ morphologies are dominant. In comparison, parallel samples incubated with **PyBD** exhibit fibrillar structures similar to those under compound-free conditions at both temperatures (Figure 5.6b and c). Since **PyED** and **PyBD** show minimal change in the morphology of metal-free $A\beta_{40}$ aggregates relative to compound-untreated samples, this suggests that variations in the fibrillar morphology may be derived from compound's functionality (*i.e.*, chelation and chelation-induced radical formation) (Figure 5.6b and c).

The ability of **PyED** and **PyBD** to transform preformed $A\beta_{42}$ aggregates was also examined (Figure 5.7). Relative to analogous $A\beta_{40}$ samples, a similar trend in both **PyED** and **PyBD** reactivity with $A\beta_{42}$ was confirmed by gel electrophoresis. $A\beta_{42}$ species with a wide distribution of MW are observed with **PyED**-treated metal-added Aβ

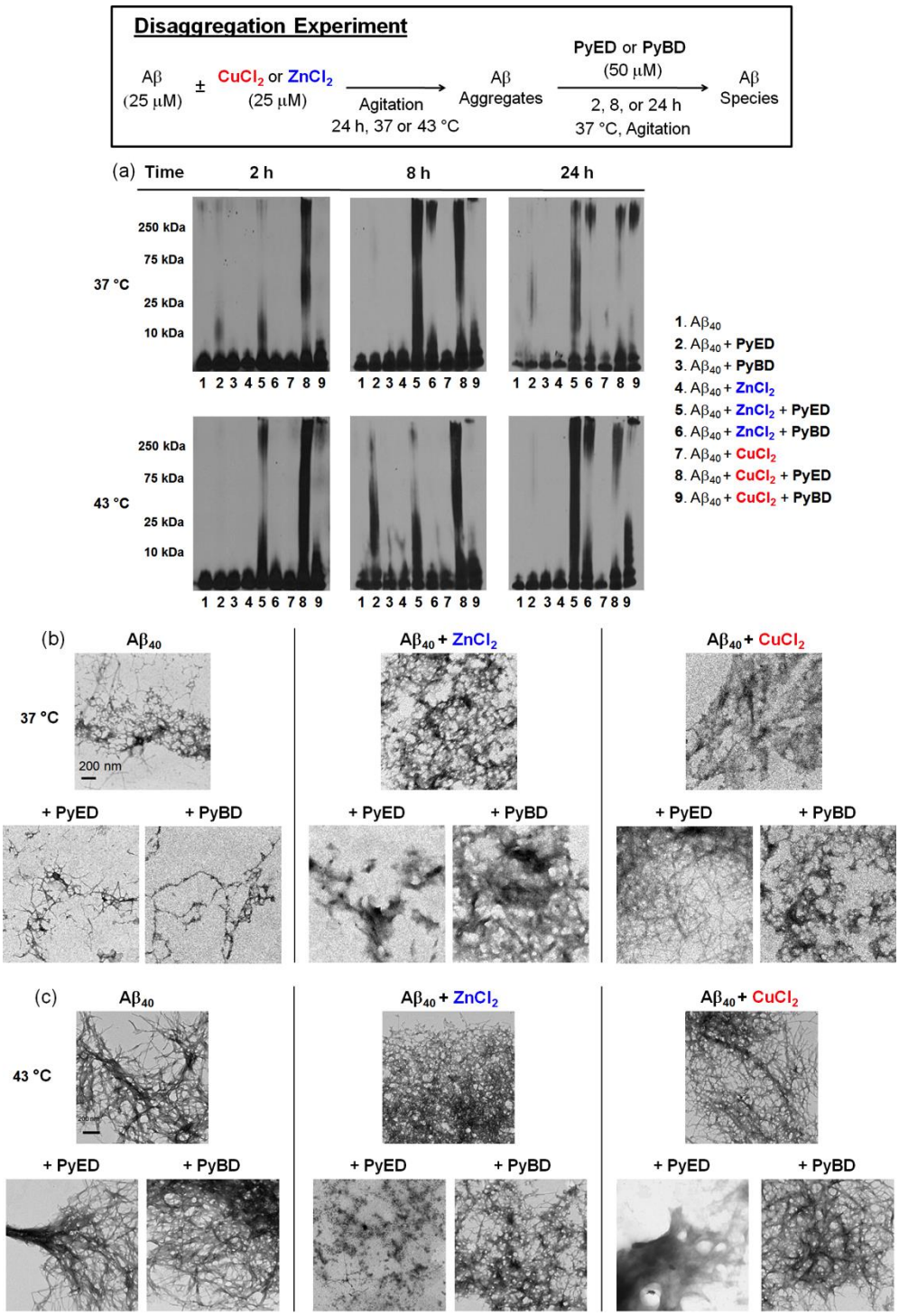

Figure 5.6. Disaggregation experiment: disassembly of preformed, metal-free or metal-induced $A\beta_{40}$ aggregates (scheme, top) by **PyED** and **PyBD**. (a) Analysis of the size distribution of the resulting $A\beta_{40}$ species by gel electrophoresis with Western blot using an anti-Aβ antibody (6E10) at either 37 or 43 °C. (b) Visualization of the morphologies of the $A\beta_{40}$ species from samples that were incubated with **PyED** or **PyBD** for 24 h by TEM at 37 °C. (c) Visualization of the morphologies of the $A\beta_{40}$ species from samples that were incubated with **PyED** or **PyBD** for 24 h by TEM at 43 °C. Conditions: [$A\beta_{40}$] = 25 μM; [$CuCl_2$ or $ZnCl_2$] = 25 μM; [compound] = 50 μM (compound = **PyED** or **PyBD**; pH 6.6 (for Cu^{2+} samples) or 7.4 (for metal-free and Zn^{2+} samples); various inhibition time; 37 or 43 °C; constant agitation.

aggregates over the course of 24 h at both temperatures (Figure 5.7a, lanes 5 and 8), while low reactivity is visualized with metal−Aβ_{42} aggregates incubated with **PyBD** (lanes 6 and 9). In the case of metal-free conditions, Aβ_{42} species with slightly different array of MW are produced upon addition of **PyED** or **PyBD** (lanes 2 and 3) relative to compound-free samples (lane 1). In addition to these trends, the TEM images reveal that **PyED** treatment to metal−Aβ_{42} samples induces changes in the morphology of preformed aggregates. Metal-treated Aβ_{42} aggregates exposed to either **PyED** or **PyBD** show thinner fibrils of various lengths (37 and 43 °C), as well as more amorphous species (37 °C) than observed in compound-free samples (Figure 5.7b and c). As demonstrated for Aβ_{40}, no significantly distinct morphology changes are observed in the metal-free Aβ_{42} aggregates treated with either compound when compared to the compound-untreated sample, indicating the potential importance of metal chelation in the disaggregation pathway.

In conjunction with the disaggregation studies, the ability of **PyED** and **PyBD** to control Aβ aggregation was also investigated (Figures 5.8 and 5.9). Upon incubation of Zn^{2+} and Aβ_{40} with **PyED**, an increasing dispersion of various MW was visualized by gel analysis over prolonged incubation (Figure 5.8a, lane 5). In comparison, samples containing Cu^{2+}, Aβ_{40}, and **PyED** generate different smearing patterns than those of Zn^{2+}–Aβ_{40} samples (lanes 5 and 8). Similar to the disaggregation results, the gel band intensity of the Cu^{2+}–Aβ_{40} samples also decreases between 8 and 24 h incubation time at both 37 and 43 °C. **PyBD** presented slight modulation of the metal-induced aggregation (lanes 6 and 9), while exposure of metal-free Aβ_{40} to either **PyED** or **PyBD** results in little to no activity (lanes 2 and 3). Thus, similar to the disaggregation results, these data indicate that **PyED** demonstrates greater inhibition of metal-induced Aβ aggregation compared to **PyBD**. Additionally, further progression of peptide aggregation may be occurring in Cu^{2+}–Aβ_{40} samples treated with **PyED** for 24 h under hyperthermic conditions. These findings are supported by TEM images of Aβ_{40} samples, incubated at 43 °C, that reveal smaller, amorphous Aβ species in the presence of divalent metal ions and **PyED** (Figure 5.8b and c). Importantly, morphological changes are not observed noticeably in the metal-free Aβ samples exposed to either **PyED** or **PyBD** (Figure 5.8b

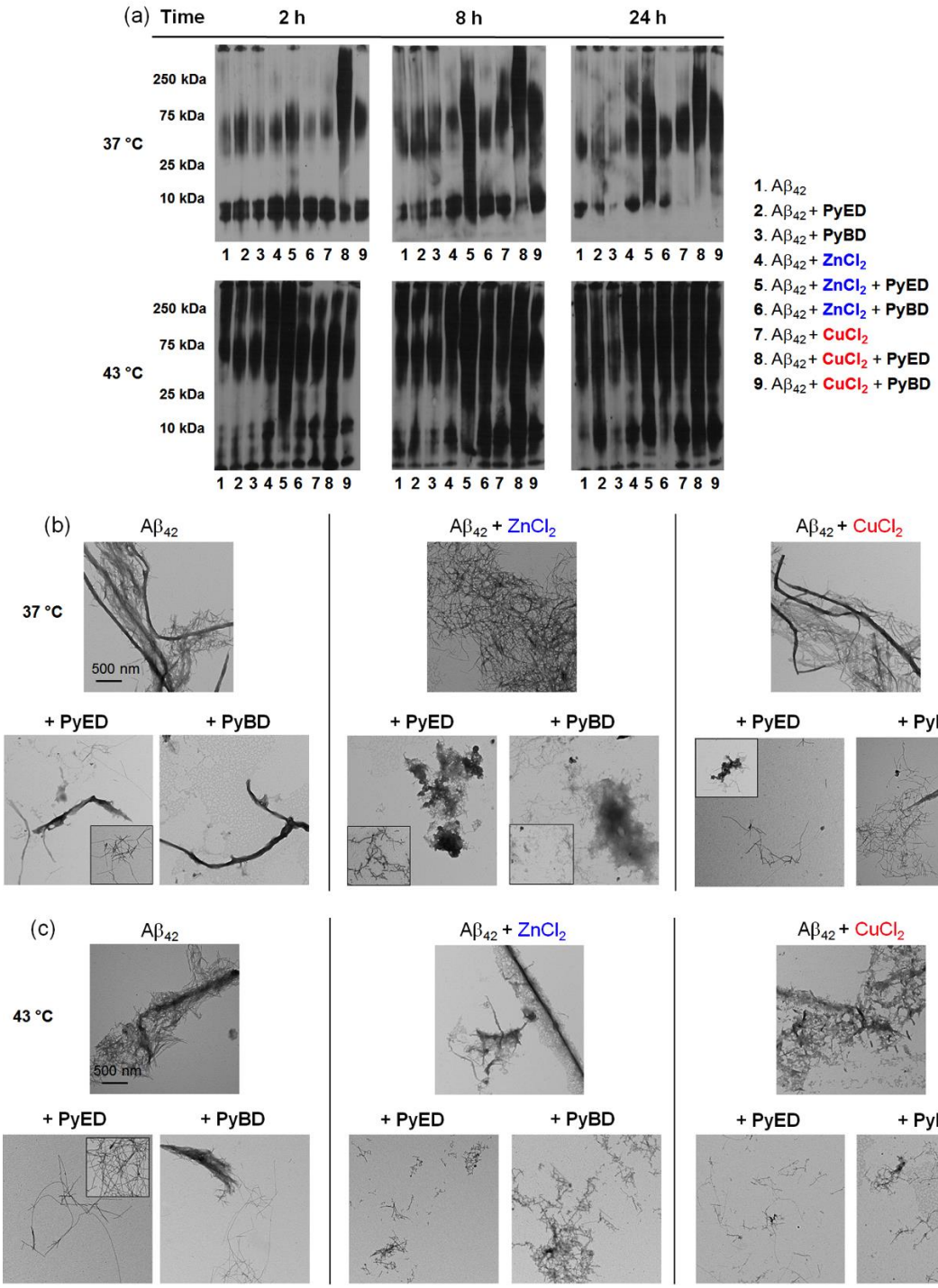

Figure 5.7. Disaggregation experiment: disassembly of preformed, metal-free or metal-induced $A\beta_{42}$ aggregates by **PyED** and **PyBD**. (a) Analysis of the size distribution of the resulting $A\beta_{42}$ species by gel electrophoresis with Western blot using an anti-Aβ antibody (6E10) at either 37 or 43 °C. (b) Visualization of the morphologies of the $A\beta_{42}$ species from samples that were incubated with **PyED** or **PyBD** for 24 h by TEM at 37 °C. (c) Visualization of the morphologies of the $A\beta_{42}$ species from samples that were incubated with **PyED** or **PyBD** for 24 h by TEM at 43 °C. Conditions: [$A\beta_{42}$] = 25 μM; [$CuCl_2$ or $ZnCl_2$] = 25 μM; [compound] = 50 μM (compound = **PyED** or **PyBD**; pH 6.6 (for Cu^{2+} samples) or 7.4 (for metal-free and Zn^{2+} samples); various inhibition time; 37 or 43 °C; constant agitation.

and c).

As expected, the trend in the inhibition of $A\beta_{42}$ aggregation upon addition of **PyED** or **PyBD** is comparable to that of $A\beta_{40}$ (Figure 5.9). Significant modification of the aggregation pathway is only visualized for metal-associated Aβ species treated with **PyED** (Figure 5.9a, lanes 5 and 8). Additionally, TEM images that reveal thinner fibrils and/or amorphous aggregates are generated in **PyED**-treated metal–$A\beta_{42}$ samples compared to compound-free conditions (Figure 5.9b and c). Taken together, the disaggregation and inhibition results demonstrate the enhanced ability of **PyED** (*versus* **PyBD**) to variably modulate metal-free and metal-induced Aβ aggregation.

5.2.4. Prediction of blood-brain barrier (BBB) permeability of PyED

To evaluate the drug-likeness of **PyED** and its potential to penetrate the blood-brain barrier (BBB), values for Lipinski's rules and the logBB were calculated (Table 5.1).[35-38] **PyED** is indicated to have drug-like characteristic as well as BBB permeability based on the calculated values (Table 5.1). In order to confirm the predicted the ability of **PyED** penetrate the BBB, an *in vitro* PAMPA-BBB assay was performed following literature procedure.[11,12,15-17,39] Using the empirical classification for BBB-permeable molecules, the measured permeability value, $-\log P_e$, for **PyED** ($-\log P_e = 4.9 \pm 0.1$) suggests that **PyED** is possibly penetrating the BBB.

5.3. Conclusion

An enediyne derivative, **PyED**, was investigated as a potential chemical tool that has the capability to target metal–Aβ species and alter metal-induced Aβ aggregation *in vitro*. UV-vis titration studies of **PyBD**, instead of **PyED** due to the tendency of **PyED** to undergo Bergman cyclization in metal-added conditions, in the absence and presence of Cu^{2+} indicate that the enediyne derivative could interact with Cu^{2+} from Cu^{2+}-bound Aβ species. Through biochemical and TEM studies, **PyED** is demonstrated to be able to modulate both metal-triggered $A\beta_{40}$ and $A\beta_{42}$ aggregation. Additionally, **PyED** shows the potential to be BBB permeable, which suggests its futher biological applicability. Taken

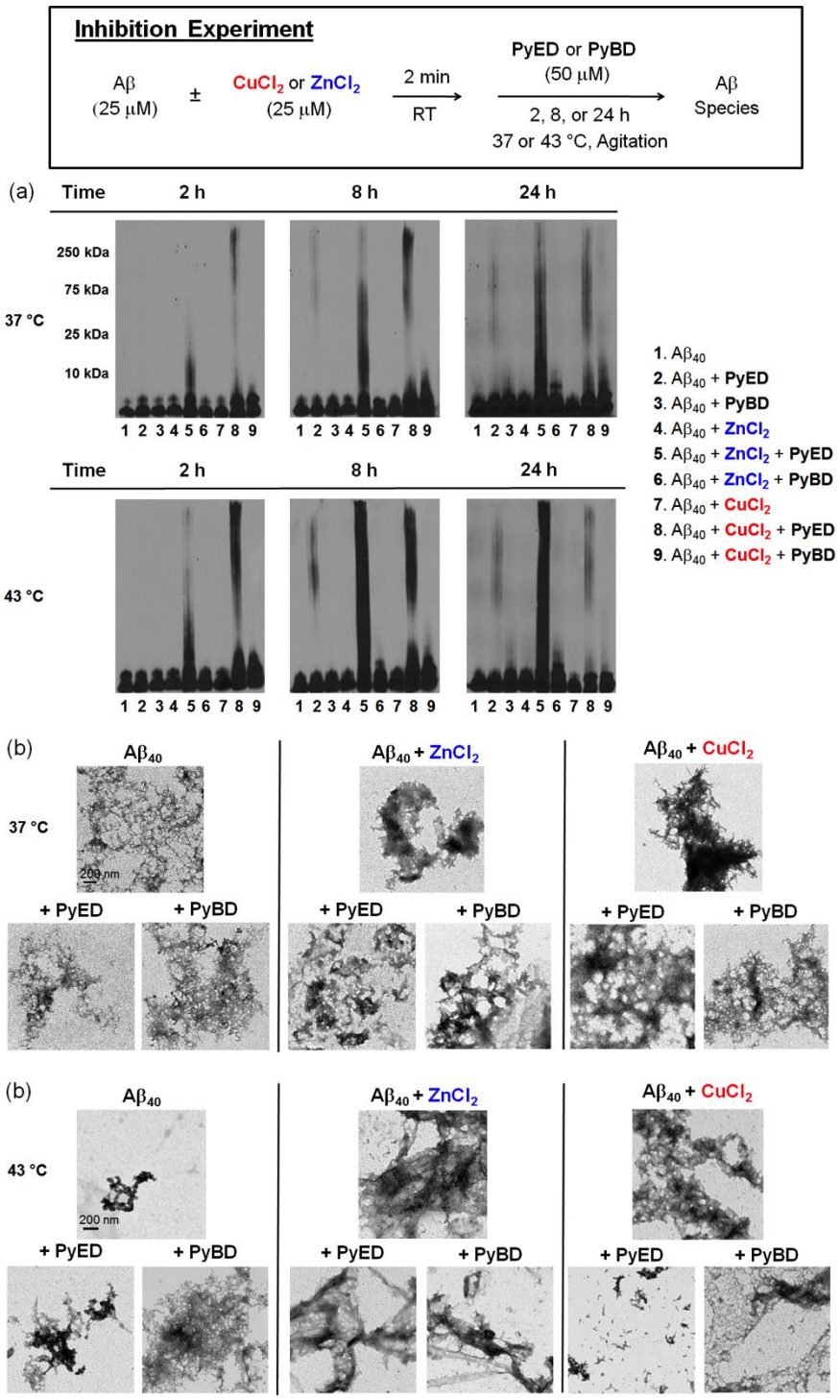

Figure 5.8. Inhibition experiment: modulation of $A\beta_{40}$ aggregate formation in the absence and presence of metal ions (scheme, top) by **PyED** and **PyBD**. (a) Analysis of the size distribution of the resulting $A\beta_{40}$ species by gel electrophoresis with Western blot using an anti-Aβ antibody (6E10) at either 37 or 43 °C. (b) Visualization of the morphologies of the $A\beta_{40}$ species from samples that were incubated with **PyED** or **PyBD** for 24 h by TEM at 37 °C. (c) Visualization of the morphologies of the $A\beta_{40}$ species from samples that were incubated with **PyED** or **PyBD** for 24 h by TEM at 43 °C. Conditions: [$A\beta_{40}$] = 25 μM; [$CuCl_2$ or $ZnCl_2$] = 25 μM; [compound] = 50 μM (compound = **PyED** or **PyBD**; pH 6.6 (for Cu^{2+} samples) or 7.4 (for metal-free and Zn^{2+} samples); various inhibition time; 37 or 43 °C; constant agitation.

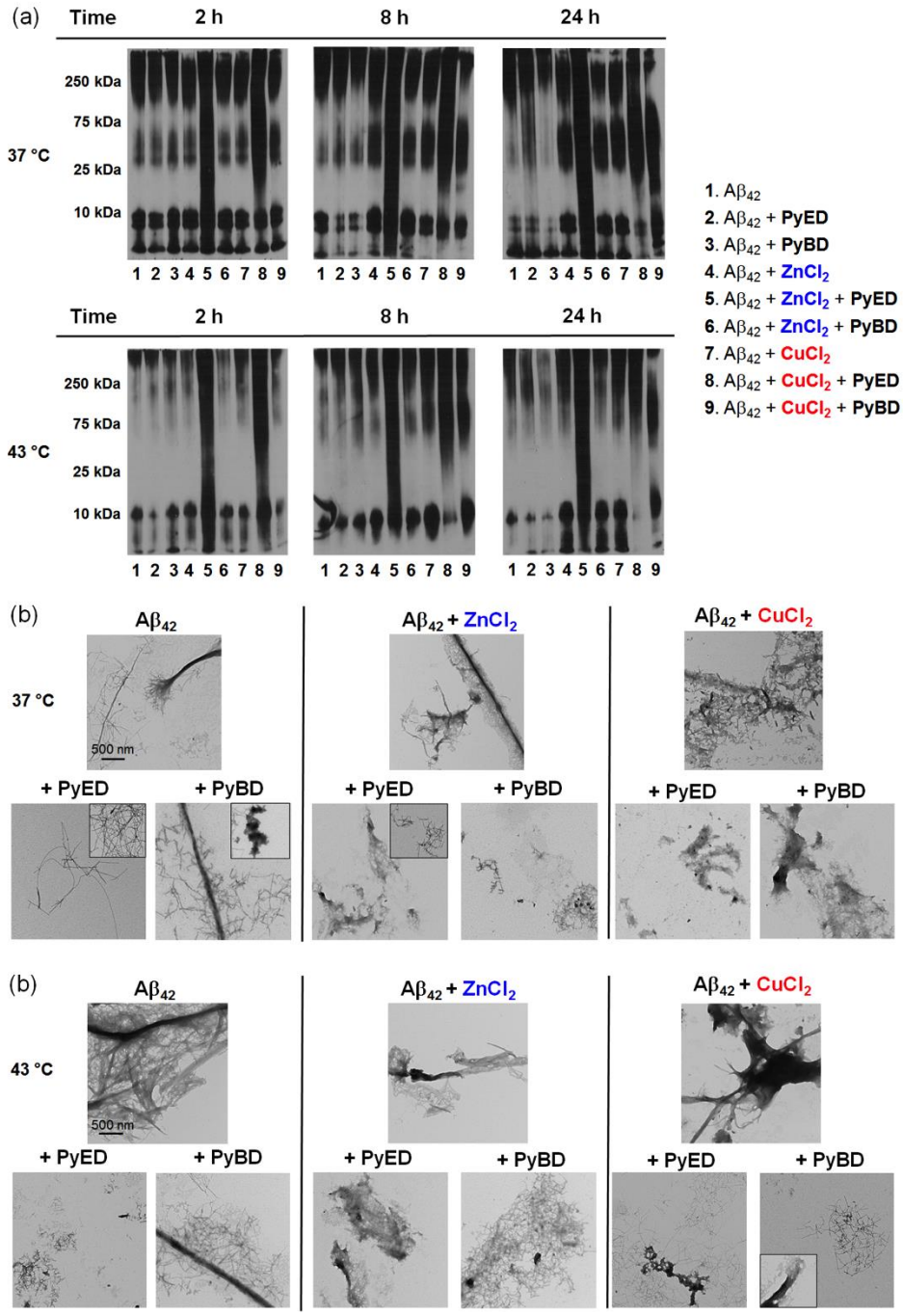

Figure 5.9. Inhibition experiment: modulation of $A\beta_{42}$ aggregate formation in the absence and presence of metal ions (scheme, top) by **PyED** and **PyBD**. (a) Analysis of the size distribution of the resulting $A\beta_{42}$ species by gel electrophoresis with Western blot using an anti-Aβ antibody (6E10) at either 37 or 43 °C. (b) Visualization of the morphologies of the $A\beta_{42}$ species from samples that were incubated with **PyED** or **PyBD** for 24 h by TEM at 37 °C. (c) Visualization of the morphologies of the $A\beta_{42}$ species from samples that were incubated with **PyED** or **PyBD** for 24 h by TEM at 43 °C. Conditions: [$A\beta_{42}$] = 25 μM; [$CuCl_2$ or $ZnCl_2$] = 25 μM; [compound] = 50 μM (compound = **PyED** or **PyBD**; pH 6.6 (for Cu^{2+} samples) or 7.4 (for metal-free and Zn^{2+} samples); various inhibition time; 37 or 43 °C; constant agitation.

Table 5.1. Values (MW, *c*logP, HBA, HBD, PSA, logBB, and –logP_e) of **PyED**.

Calculation[a]	**PyED**	Lipinski's rules & others
MW	312	≤ 450
*c*logP	1.01	≤ 5.0
HBA	4	≤ 10
HBD	0	≤ 5
PSA	50.5	≤ 90
logBB	−0.464	< −1.0 (poorly distributed in the brain.
–logP_e[b]	4.9 ± 0.01	
CNS +/− Prediction[c]	CNS+	–logP_e < 5.4 (CNS+) > 5.7 (CNS−)

[a] MW, molecular weight; *c*logP, calculated logarithm of the octonal-water partition coefficient; HBA, hydrogen-bond acceptor atoms; HBD, hydrogen-bond donor atoms; PSA, polar surface area; logBB = −0.0148 x PSA + 0.152 x *c*logP + 0.130. [b] The values of –logP_e were measured by the Parallel Artificial Membrane Permeability Assay adapted for BBB (PAMPA-BBB). [c] Compounds categorized as central nervous system, CNS+ have the ability to permeate through the BBB and target the CNS. In the case of compounds assigned as CNS− they have poor permeability through the BBB and therefore, their bioavailability into the CNS is considered to be minimal.

together, our studies present the framework of **PyED** could be utilized for developing novel chemical tools for investigating metal−Aβ species *in vitro* and further *in vivo*. This may warrant additional structural modifications (*e.g.*, incorporating a dimethylamino moiety that has been suggested to be essential for Aβ interaction)[12,13,15,16,40] in order to improve properties for interactions and reactivity with Aβ/metal−Aβ.

5.4. Experimental section

5.4.1. Materials and procedures

All reagents were purchased from commercial suppliers and used as received unless otherwise stated. The ligands (*Z*)-*N*,*N*'-bis[1-pyridin-2-yl-meth-(*E*)-ylidene]oct-4-ene-2,6-diyne-1,8-diamine (**PyED**) and pyridine-2-ylmethyl-(2-{[pyridine-2-ylmethylene)-amino]-methyl}-benzyl)-amine (**PyBD**) were synthesized according to previously published procedure.[33] $A\beta_{40}$ (DAEFRHDSGYEVHHQKLVFFAEDVGSNKGAIIGLMVGG VV) and $A\beta_{42}$ (DAEFRHDSGYEVHHQKLVFFAEDVGSNKGAIIGLMVGGVVIA) were purchased from AnaSpec (Fremont, CA). Absorbance measurements for the PAMPA-BBB assay were recorded on a SpectraMax M5 microplate reader (Molecular Devices, Sunnydale, CA). Mass spectrometry for interaction studies was conducted on a Waters

Synapt G2/S mass spectrometer. TEM images were recorded on JEOL 1010 transmission electron microscope (Electron Microscopy Center, Indiana University, Bloomington, IN) or a Philips CM-100 transmission electron microscope (Microscopy and Image Analysis Laboratory, University of Michigan, Ann Arbor, MI). Optical spectra were recorded on an Agilent 8453 UV-Vis spectrophotometer.

5.4.2. Solution speciation determination for PyBD and the Cu^{2+}–PyBD complex

UV-vis variable-pH titration was used to determine the pK_a values for **PyBD**.[12] A solution (100 mM NaCl, 10 mM NaOH, pH 12) of **PyBD** (50 μM) was titrated with small aliquots of HCl and at least 30 spectra were recorded in the pH range of 2–9. Additionally, Cu^{2+} binding to ligand at various pH values was investigated. A solution (100 mM NaCl, 10 mM NaOH, pH 10) containing **PyBD** (50 μM) and $CuCl_2$ (50 μM) was titrated with small aliquots of HCl and at least 30 spectra were recorded in the pH range of 3–8. The HypSpec program (Protonic Software, UK)[41] was used to calculate the acidity and stability constants and the HySS2009 program (Protonoc Software)[42] was used to model the speciation diagrams of ligand and its corresponding metal complex.

5.4.3. Metal binding and selectivity studies

The binding of **PyED** and **PyBD** with Cu^{2+} and Zn^{2+} was investigated by UV-vis.[12] A solution of ligand (20 μM, 1% v/v DMSO) was treated with $CuCl_2$ or $ZnCl_2$ (1 equiv). Solutions were incubated at 4 °C for 1 h and the optical spectrum of the resulting solution was recorded.

The metal selectivity of **PyBD** was examined by measuring the optical changes upon addition of $CuCl_2$ (1 equiv) to a solution of **PyBD** (50 μM, 1% v/v DMSO) previously treated with another metal chloride salt (1 or 25 equiv; $CaCl_2$, $CoCl_2$, $FeCl_2$, $FeCl_3$, $MgCl_2$, $MnCl_2$, $NiCl_2$, and $ZnCl_2$). The Fe^{2+} and Fe^{3+} solutions were prepared anaerobically and spectra recorded under nitrogen. The quantification of metal selectivity was calculated by comparing and normalizing the absorption values for the metal–ligand complexes at 285 and 305 nm to the absorption at these wavelengths before and after Cu^{2+} addition.

5.4.4. Aβ peptide experiments

Aβ experiments were performed according to previously published procedures with slight modifications.[11,12,17] $A\beta_{40}$ or $A\beta_{42}$ was dissolved in ammonium hydroxide (NH_4OH, 1% v/v, aq), aliquoted, lyophilized overnight, and stored at −80 °C. A stock solution was prepared by dissolving Aβ in 1% NH_4OH and diluted with ddH_2O. For the disaggregation experiment, Aβ (25 μM) with and without metal ions ($CuCl_2$ or $ZnCl_2$, 25 μM) was first incubated for 24 h at 37 or 43 °C with constant agitation. Afterward, a compound (50 μM, 1% v/v final DMSO concentration) was added and followed by an additional 2, 8, or 24 h incubation at 37 or 43 °C with constant agitation. For the inhibition experiment, Aβ (25 μM) was treated with or without metal ions ($CuCl_2$ or $ZnCl_2$; 25 μM) for 2 min, followed by addition of a compound (50 μM; 1% v/v final DMSO concentration). The resulting samples were incubated for 2, 8, or 24 h at 37 or 43 °C with constant agitation. Both studies were performed using a buffered solution (20 μM HEPES, pH 6.6 (for $CuCl_2$) or pH 7.4 (metal-free and $ZnCl_2$), 150 μM NaCl).

5.4.5. Gel electrophoresis

The Aβ peptide experiments described above were analyzed using gel electrophoresis followed by Western blotting with an anti-Aβ antibody (6E10, Covance, Princeton, NJ).[11,12,17] Each sample (10 μL) was separated using a 10–20% Tris-tricine gel (Invitrogen, Grand Island, NY). Following the separation, the proteins were transferred onto a nitrocellulose membrane and blocked with bovine serum albumin (BSA, 3% w/v, Sigma-Aldrich) in Tris-buffered saline (TBS) containing 0.1% Tween-20 (TBS-T) for 12 h ($A\beta_{40}$) or 2–3 h ($A\beta_{42}$) at ambient temperature. The membranes were incubated with an anti-Aβ antibody (1:2000) in 2% BSA (w/v in TBS-T) for 4 h at ambient temperature ($A\beta_{40}$) or overnight at 4 °C ($A\beta_{42}$). After washing, membranes were probed with the horseradish peroxidase-conjugated goat anti-mouse antibody (1:10,000) in 2% BSA for 1 h at ambient temperature. Thermo Scientific Supersignal West Pico Chemiluminescent Substrate (Thermo Scientific, Rockford, IL) was used to visualize protein bands.

5.4.6. Transmission electron microscopy (TEM)

Samples for TEM were prepared following a previously reported method ($A\beta_{40}$ samples; $A\beta_{42}$ samples).[11,12,17] Glow discharge grids (Formar/Carbon 300 mesh; Electron Microscopy Sciences, Hatfield, PA) were treated with 24 h incubated samples from either disaggregation of inhibition experiments (5 μL) for 5 min ($A\beta_{40}$ samples) or 2 min ($A\beta_{42}$ samples) at room temperature and excess sample was removed with filter paper. ($A\beta_{40}$ samples): Each grid was incubated with uranyl acetate (2% w/v ddH_2O, 5 μL, 5 min). Excess uranyl acetate was blotted and the grids were washed three time with ddH_2O (5 μL) and air-dried at room temperature. Images were acquired by a JEOL 1010 transmission electron microscope (80 kV, 25,000x magnification). ($A\beta_{42}$ samples): Grids were washed with ddH_2O three times. Each grid was stained with uranyl acetate (1% w/v ddH_2O, 5 μL). Excess uranyl acetate was blotted off and grids were air dried for 15 min at room temperature. Images were acquired by a Philips CM-100 transmission electron microscope (80 kV, 25,000x magnification).

5.4.8. Parallel Artificial Membrane Permeability Assay adapted for blood-brain barrier (PAMPA-BBB)

PAMPA-BBB experiments were carried out using the PAMPA Explorer kit (Pion Inc., Billerica, MA) using previously reported protocols with modifications.[12,17,35,36,39] Each stock solution was diluted with Prisma HT buffer (pH 7.4, Pion) to a final concentration of 25 μM (1% v/v final DMSO concentration). The resulting stock solution was added to wells of the donor plate (200 μL, number of replicates = 12). The polyvinylidene fluoride (0.45 μM) filter membrane on the acceptor plate was coated with the BBB-1 lipid formulation (5 μL, Pion) and placed on top of the donor plate, forming a sandwich. Brain sink buffer (200 μL, Pion) was added to each well of the acceptor plate. The sandwich was incubated at room temperature for 4 h without stirring. The UV-vis spectra of the solutions for reference, acceptor, and donor plates were measured using a microplate reader. The PAMPA Explorer software v.3.5 (Pion) was used to calculate the $-\log P_e$ for each compound. Designation of CNS± was assigned by comparison to those that were identified in previous reports.[35,36,39]

5.5. References

(1) Thies, W.; Bleiler, L. *Alzheimers Dement.* **2013**, *9*, 208.
(2) Kepp, K. P. *Chem. Rev.* **2012**, *112*, 5193.
(3) Faller, P.; Hureau, C. *Chemistry* **2012**, *18*, 15910.
(4) Scott, L. E.; Orvig, C. *Chem. Rev.* **2009**, *109*, 4885.
(5) Jakob-Roetne, R.; Jacobsen, H. *Angew. Chem., Int. Ed.* **2009**, *48*, 3030.
(6) Rauk, A. *Chem. Soc. Rev.* **2009**, *38*, 2698.
(7) DeToma, A. S.; Salamekh, S.; Ramamoorthy, A.; Lim, M. H. *Chem. Soc. Rev.* **2012**, *41*, 608.
(8) Savelieff, M. G.; Lee, S.; Liu, Y.; Lim, M. H. *ACS Chem. Biol.* **2013**, *8*, 856.
(9) Bush, A. I.; Tanzi, R. E. *Neurotherapeutics* **2008**, *5*, 421.
(10) Rodríguez-Rodríguez, C.; Sánchez de Groot, N.; Rimola, A.; Álvarez-Larena, Á.; Lloveras, V.; Vidal-Gancedo, J.; Ventura, S.; Vendrell, J.; Sodupe, M.; Gonzalez-Duarte, P. *J. Am. Chem. Soc.* **2009**, *131*, 1436.
(11) Hindo, S. S.; Mancino, A. M.; Braymer, J. J.; Liu, Y.; Vivekanandan, S.; Ramamoorthy, A.; Lim, M. H. *J. Am. Chem. Soc.* **2009**, *131*, 16663.
(12) Choi, J. S.; Braymer, J. J.; Nanga, R. P.; Ramamoorthy, A.; Lim, M. H. *Proc. Natl. Acad. Sci. U. S. A.* **2010**, *107*, 21990.
(13) Braymer, J. J.; Choi, J.-S.; DeToma, A. S.; Wang, C.; Nam, K.; Kampf, J. W.; Ramamoorthy, A.; Lim, M. H. *Inorg. Chem.* **2011**, *50*, 10724.
(14) Sharma, A. K.; Pavlova, S. T.; Kim, J.; Finkelstein, D.; Hawco, N.; Rath, N. P.; Kim, J.; Mirica, L. M. *J. Am. Chem. Soc.* **2012**, *134*, 6625.
(15) Pithadia, A. S.; Kochi, A.; Soper, M. T.; Beck, M. W.; Liu, Y.; Lee, S.; DeToma, A. S.; Ruotolo, B. T.; Lim, M. H. *Inorg. Chem.* **2012**, *51*, 12959.
(16) Liu, Y.; Kochi, A.; Pithadia, A. S.; Lee, S.; Nam, Y.; Beck, M. W.; He, X.; Lee, D.; Lim, M. H. *Inorg. Chem.* **2013**, *52*, 8121.
(17) Lee, S.; Zheng, X.; Krishnamoorthy, J.; Savelieff, M. G.; Park, H. M.; Brender, J. R.; Kim, J. H.; Derrick, J. S.; Kochi, A.; Lee, H. J.; Kim, C.; Ramamoorthy, A.; Bowers, M. T.; Lim, M. H. *J. Am. Chem. Soc.* **2014**, *136*, 299.
(18) Ono, K.; Yoshiike, Y.; Takashima, A.; Hasegawa, K.; Naiki, H.; Yamada, M. *J. Neurochem.* **2003**, *87*, 172.
(19) Rezai-Zadeh, K.; Shytle, D.; Sun, N.; Mori, T.; Hou, H.; Jeanniton, D.; Ehrhart, J.; Townsend, K.; Zeng, J.; Morgan, D.; Hardy, J.; Town, T.; Tan, J. *J. Neurosci.* **2005**, *25*, 8807.
(20) Hyung, S. J.; DeToma, A. S.; Brender, J. R.; Lee, S.; Vivekanandan, S.; Kochi, A.; Choi, J. S.; Ramamoorthy, A.; Ruotolo, B. T.; Lim, M. H. *Proc. Natl. Acad. Sci. U. S. A.* **2013**, *110*, 3743.
(21) Yang, F.; Lim, G. P.; Begum, A. N.; Ubeda, O. J.; Simmons, M. R.; Ambegaokar, S. S.; Chen, P. P.; Kayed, R.; Glabe, C. G.; Frautschy, S. A.; Cole, G. M. *J. Biol. Chem.* **2005**, *280*, 5892.
(22) Zhang, C.; Browne, A.; Child, D.; Tanzi, R. E. *J. Biol. Chem.* **2010**, *285*, 28472.
(23) Baum, L.; Ng, A. *J. Alzheimers Dis.* **2004**, *6*, 367.
(24) Jones, G. B.; Fouad, F. S. *Curr. Pharm. Des.* **2002**, *8*, 2415.
(25) Joshi, M. C.; Rawat, D. S. *Chem. Biodivers.* **2012**, *9*, 459.
(26) Zein, N.; Sinha, A. M.; McGahren, W. J.; Ellestad, G. A. *Science* **1988**, *240*, 1198.

(27) Schreiner, P. R. *J. Am. Chem. Soc.* **1998**, *120*, 4184.
(28) Warner, B. P.; Millar, S. P.; Broene, R. D.; Buchwald, S. L. *Science* **1995**, *269*, 814.
(29) König, B.; Hollnagel, H.; Ahrens, B.; Jones, P. G. *Angew. Chem., Int. Ed.* **1995**, *34*, 2538.
(30) Konig, B.; Pitsch, W.; Thondorf, I. *J. Org. Chem.* **1996**, *61*, 4258.
(31) Coalter, N. L.; Concolino, T. E.; Streib, W. E.; Hughes, C. G.; Rheingold, A. L.; Zaleski, J. M. *J. Am. Chem. Soc.* **2000**, *122*, 3112.
(32) Benites, P. J.; Rawat, D. S.; Zaleski, J. M. *J. Am. Chem. Soc.* **2000**, 7208.
(33) Rawat, D. S.; Zaleski, J. M. *J. Am. Chem. Soc.* **2001**, *123*, 9675.
(34) Faller, P.; Hureau, C. *Dalton Trans.* **2009**, 1080.
(35) Di, L.; Kerns, E. H.; Fan, K.; McConnell, O. J.; Carter, G. T. *Eur. J. Med. Chem.* **2003**, *38*, 223.
(36) Avdeef, A.; Bendels, S.; Di, L.; Faller, B.; Kansy, M.; Sugano, K.; Yamauchi, Y. *J. Pharm. Sci.* **2007**, *96*, 2893.
(37) Lipinski, C. A.; Lombardo, F.; Dominy, B. W.; Feeney, P. J. *Adv. Drug Delivery Rev.* **2001**, *46*, 3.
(38) Clark, D. E.; Pickett, S. D. *Drug Discovery Today* **2000**, *5*, 49.
(39) *BBB Protocol and Test Compounds; Pion Inc.; Wolburn, MA, 2009*.
(40) Leuma Yona, R.; Mazères, S.; Faller, P.; Gras, E. *ChemMedChem* **2008**, *3*, 63.
(41) Gans, P.; Sabatini, A.; Vacca, A. *Ann. Chim.* **1999**, *89*, 45.
(42) Alderighi, L.; Gans, P.; Ienco, A.; Peters, D.; Sabatini, A.; Vacca, A. *Coord. Chem. Rev* **1999**, *184*, 311.

Chapter 6: A Novel Hybrid of 6-Chlorotacrine and Metal-Amyloid-β Modulator for Inhibition of Acetylcholinesterase and Metal-Induced Amyloid-β Aggregation

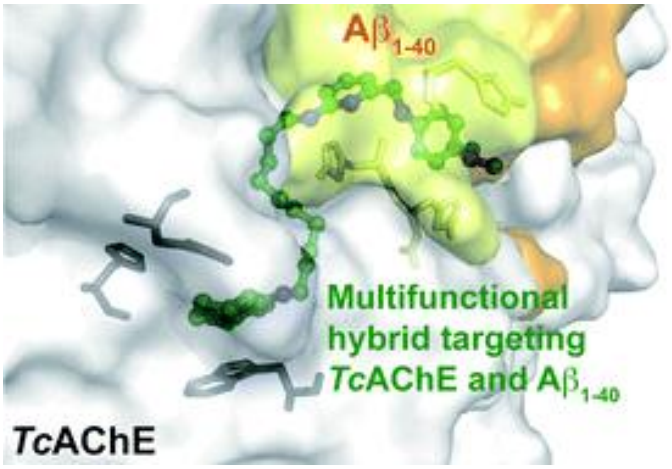

The results presented in this chapter for 6-chlorotacrine derivatives were previously published (Kochi, A.;‡ Eckroat, T. J.;‡ Green, K. D.; Mayhoub, A. S.; Lim, M. H.; Garneau-Tsodikova, S. *Chem. Sci.* **2013**, *4*, 4137-4145. ‡ Equal contribution.). We thank Professor Sylvie Garneau-Tsodikova, Dr. Keith Green, Dr. Abdelrahman Mayhoub and Dr. Todd Eckroat for the analysis of AChE/BChE activity, docking studies, and synthesis of compounds, respectively. Michael Beck conducted Zn^{2+} binding studies. In the present work, I contributed to metal binding studies, the gel and TEM analyses of Aβ aggreaton studies, and *in vitro* PAMPA assay. In addition to that, I was also involved in manuscript writing for metal binding, Aβ aggregation studies, and blood-brain barrier (BBB) permeability sections.

6.1. Introduction

Alzheimer's disease (AD) is an age-related, neurodegenerative disorder estimated to affect over 5 million people in the United States alone.[1] AD is progressive and ultimately fatal with symptoms ranging from cognitive dysfunction to psychiatric and behavioural disturbances. As the population ages, the prevalence of AD is expected to increase dramatically in the coming years and places an increasing burden on society. Many pathological hallmarks of the disease have been documented, yet the exact cause remains unknown. Current treatments for AD act mainly by inhibiting acetylcholinesterase (AChE). While these acetylcholinesterase inhibitors (AChEis) are moderately effective in treating cognitive symptoms, they are incapable of stopping or reversing disease progression.[2]

Tacrine was the first AChEi approved by the FDA.[3] Though its clinical use has been limited by hepatotoxicity,[4] tacrine remains an important starting point in research towards developing new drugs for AD due to its straightforward synthesis and comparatively low cost.[5,6] In fact, tacrine hybrids, bifunctional molecules where tacrine has been chemically linked to another molecule with beneficial anti-AD properties, have been well characterized in the literature. For example, tacrine-8-hydroxyquinoline hybrids, tacrine-ferulic acid hybrids, and tacrine-mefenamic acid hybrids have all shown promising results.[7-11] The role of the linker in inhibitory activity of these hybrids towards AChE has also been investigated.[12]

The presence and possible role of amyloid-β (Aβ) peptide aggregates in the brains of AD patients have been well documented.[13-17] These aggregates provide an interesting pharmacological target in that drugs capable of disrupting already formed Aβ aggregates or preventing Aβ aggregation may be capable of halting or inverting the progression of AD.[14,16] While AChE and butyrylcholinesterase (BChE) are important in AD because they control ACh levels, they also interact with Aβ.[18-20] Structurally, AChE consists of a catalytic active site (CAS) and a peripheral anionic site (PAS) connected by a 20-Å gorge.[21-23] AChE is known to promote Aβ aggregation through interaction at the PAS, and it is often found to be entangled in Aβ plaques along with BChE.[18,24] Thus, tacrine hybrids with the ability to simultaneously bind to the CAS and PAS by virtue of a

chemical linker spanning the active site gorge have the potential to disrupt Aβ aggregation.[25,26]

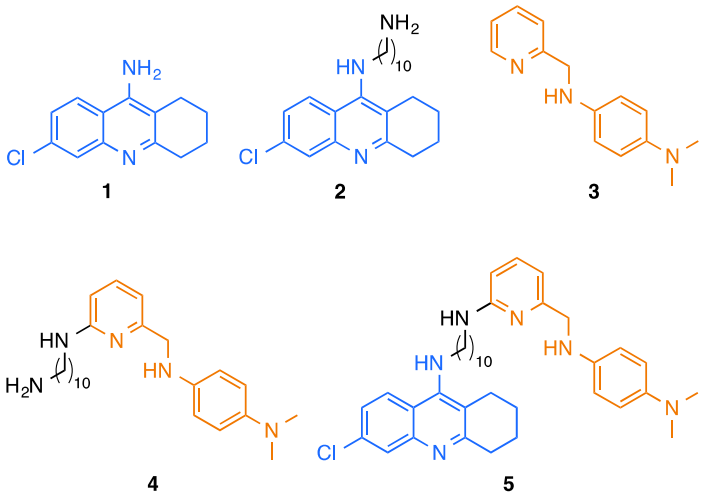

Figure 6.1. Structures of 6-chlorotacrine (**1**), 6-chlorotacrine linker (**2**), N^1,N^1-dimethyl-N^4-(pyridin-2-ylmethyl)benzene-1,4-diamine, metal–Aβ modulator (**3**), metal–Aβ modulator linker (**4**), and hybrid of 6-chlorotacrine-metal–Aβ modulator (**5**).

Metal ions such as Cu^{2+} and Zn^{2+} are known to interact with Aβ peptides and promote their aggregation, which has been suggested to be involved in neurotoxicity.[27-33] Given this fact, small molecules for modulation of metal–Aβ interaction and reactivity have been developed. For example, N^1,N^1-dimethyl-N^4-(pyridin-2-ylmethyl)benzene-1,4-diamine (**3**) (Figure 6.1) has shown the ability to chelate Cu^{2+} and Zn^{2+} and interact with Aβ, effectively regulating metal-induced Aβ aggregation and neurotoxicity *in vitro* and in human neuroblastoma cells.[34] We reasoned that chemically linking an AChEi with the metal–Aβ modulator **3** would create a hybrid molecule (**5**; Figure 6.1) potentially capable of multifunctionality (inhibition of AChE at the CAS, prevention of AChE–Aβ interaction by blocking the PAS, as well as alteration of the interaction between metal ions and Aβ with subsequent moderation of the reactivity of metal-associated Aβ species). Herein, we describe the design, synthesis, and initial biochemical evaluation of such a hybrid (**5**; Figure 6.1).

6.2. Results and discussion

6.2.1. Hybrid design and synthesis

Hybrid **5** (Figure 6.1) was designed to contain an AChEi moiety (blue), a linker region (black), and a metal–Aβ modulating moiety (orange). 6-Chlorotacrine (**1**), which was chosen as the AChEi moiety, has shown potent inhibition of AChE[5] and has been incorporated into other AChE-directed hybrid molecules with favourable results.[9] For comparison in biochemical studies, compound **1** was prepared by heating 2-amino-4-chlorobenzonitrile and cyclohexanone in the presence of anhydrous $ZnCl_2$ (Scheme 6.1a), as previously reported.[5,6] A decamethylene linker region was chosen due to its appropriate length to span the gorge of AChE and produce a compound capable of simultaneously interacting with the CAS and PAS.[9] This linker moiety was attached to 6-chlorotacrine to give analogue **2** as previously reported.[9] Compound **3** was chosen as

Scheme 6.1. Synthesis of (a) compound **1,** (b) compound **4** and **6**, and (c) compounds **5** and **7-9**

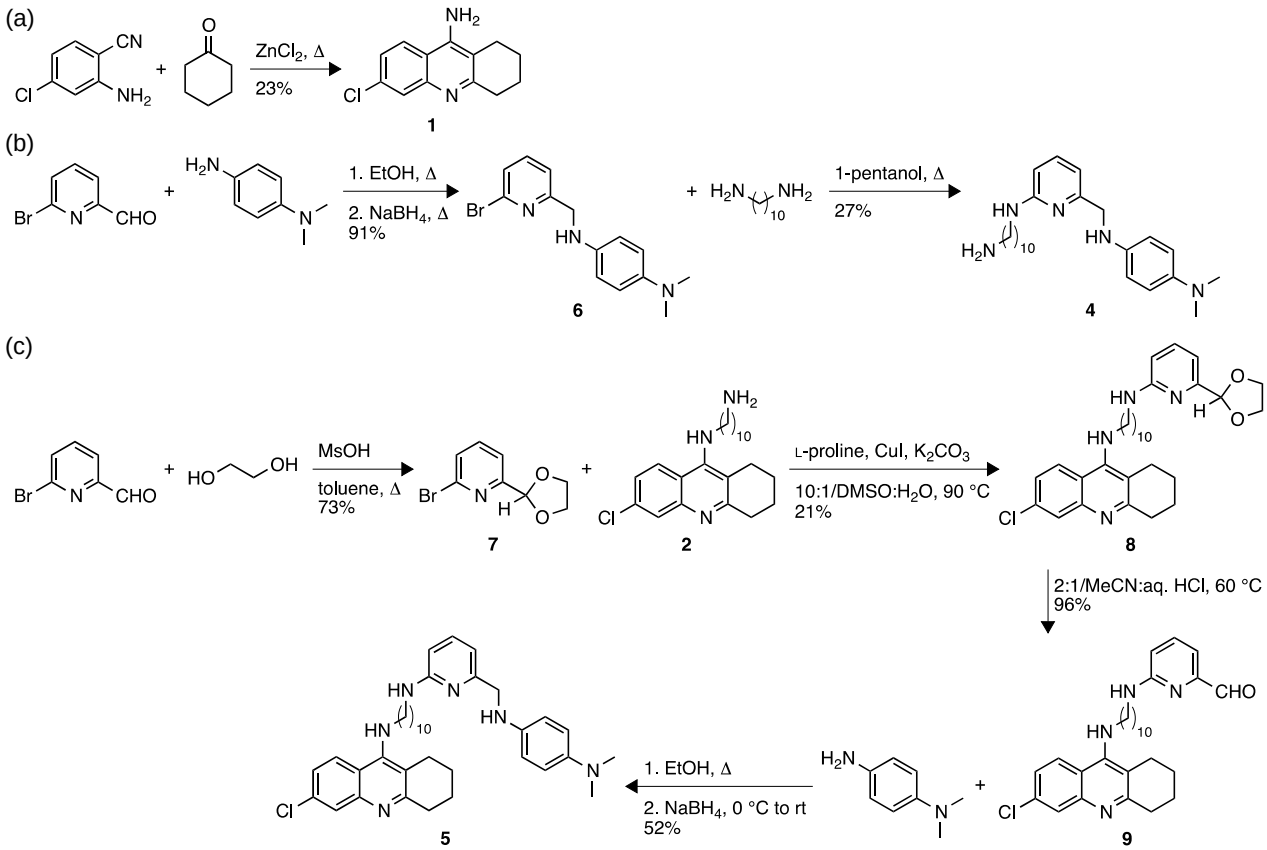

the metal–Aβ modulating moiety because of its ability to chelate metal ions (*i.e.*, Cu^{2+} and Zn^{2+}) as well as effectively interact with Aβ and was prepared as established in previous procedures.[34] For comparison in biochemical studies, metal–Aβ modulator linker **4** was prepared from 6-bromo-2-pyridinecarboxaldehyde *via* reductive amination with *N*,*N*-dimethyl-*p*-phenylenediamine followed by subsequent nucleophilic displacement of the bromo substituent by 1,10-diaminodecane (Scheme 6.1b). Hybrid **5** was prepared using a copper-catalyzed Ullmann-type reaction between **2** and the cyclic ethylene acetal-protected form of 6-bromo-2-pyridine carboxaldehyde. Subsequent deprotection and reductive amination with *N*,*N*-dimethyl-*p*-phenylenediamine gave the desired target hybrid **5** in 8% overall yield (Scheme 6.1c).

6.2.2. AChE inhibition

The AChE inhibitory properties of compounds **1**-**5** were assessed against AChE from *Electrophorus electricus* (*Ee*AChE) using the well established Ellman method[35] to determine IC_{50} (Table 6.1). We previously tested tacrine with AChE (Table 6.1).[9] However, since 6-chlorotacrine (**1**) is 25-fold more potent than tacrine itself, herein, we used it as the standard against which we compare all compounds. 6-Chlorotacrine (**1**) presented potent inhibition of AChE with an IC_{50} = 2.41 ± 0.48 nM, which is in good agreement with the literature value.[36] The IC_{50} of compound **2** has recently been reported,[12] and it also exhibited potent AChE inhibition. Metal–Aβ modulator **3** showed very poor inhibition (IC_{50} > 200 μM), which was expected given that it was not originally designed to interact with AChE. Introduction of the 1,10-diaminodecane moiety to **3**, however, provides a remarkable increase (> 200-fold) in potency (IC_{50} = 757 ± 279 nM for **4**). Hybrid **5** was observed to have an IC_{50} = 2.37 ± 0.29 nM, identical to that of **1**. Many tacrine hybrids reported in the literature showed an increase in potency compared to their parent compound. While this is not the case for **5** because the parent 6-chlorotacrine (**1**) is already highly potent, this compound is still of interest given its potential for metal chelation and Aβ interaction. In addition, the IC_{50} value of **5** is within the range reported for structurally similar metal/Aβ-targeted tacrine hybrids in the literature.[37-40]

The AChE inhibitory properties of compounds **1**-**5** were also assessed using a method described by Muraoka and Miura[41] to determine IC_{50} in the presence of reactive oxygen species (ROS IC_{50}, Table 6.1). Inflammation and oxidative stress from ROS are thought to play a role in AD, and tacrine-mefenamic acid hybrids have shown an increase in potency towards AChE in the presence of ROS, which may be beneficial for anti-AD compounds.[9] As such, we aimed to establish if the compounds of interest in this study displayed similar results. Unfortunately, only metal–Aβ modulator **3** showed a significant increase in potency in the presence of ROS. Although, even with this increase, **3** remains a relatively poor inhibitor. In the case of **4** and hybrid **5**, there was actually a reduction in potency. Compounds **1** and **2** indicated virtually no change between IC_{50} and ROS IC_{50}. To investigate the effect on enzyme inhibition of covalent linkage between the AChEi, linker, and metal–Aβ modulating moieties of hybrid **5**, we examined combinations of molecules (**2** + **3**, **1** + **4** in 1:1 equimolar mixtures) in each of our inhibition assays (Table 6.1). Results indicate that covalent linkage is not essential for hybrid **5** in terms of IC_{50} as the values for **5**, **2** + **3**, and **1** + **4** were nearly identical. Similar results have been observed for tacrine-mefenamic acid hybrids.[9,12] Interestingly, in terms of ROS IC_{50}, covalent linkage may actually be detrimental for hybrid **5** as it was outperformed by both mixtures in this assay. However, the covalent linkage may still be beneficial to simultaneously deliver all components of the hybrid to the same location in the brain.

6.2.3. BChE inhibition

BChE is also commonly associated with characteristic Aβ plaques. Thus, inhibition of BChE from equine serum (*es*BChE) by compounds **1**-**5** was also tested. With an IC_{50} = 2.41 ± 0.52 nM against BChE, 6-chlorotactine (**1**) showed inhibitory effect identical to that of AChE (2.41 ± 0.48 nM). Compounds **2** and **4** were found to be less active towards BChE than AChE with IC_{50} values of 13.6 ± 3.0 nM (13-fold diminution) and >200 μM, respectively. Meanwhile, as similarly observed with AChE, compound **3** exhibited no inhibitory activity with BChE and hybrid **5** demonstrated similar inhibition towards BChE (IC_{50} = 2.01 ± 0.12 nM) and AChE (IC_{50} = 2.37 ± 0.29 nM).

Table 6.1. Inhibition of *Ee*AChE and esBChE activity by compounds **1**-**5** and effect of M^{2+} and Aβ on IC_{50} of hybrid **5** under various conditions.

	EeAChE		esBChE	
Compound	IC_{50} (nM)	ROS IC_{50} (nM)	IC_{50} (nM)	ROS IC_{50} (nM)
Tacrine[a]	52.4 ± 7.3	183 ± 21	ND[e]	ND
1	2.41 ± 0.48	1.86 ± 0.37	2.41 ± 0.52	188 ± 43
2[b]	0.932 ± 0.220	2.18 ± 0.27	13.6 ± 3.0	2.18 ± 0.27
3	>200 □M	1858 ± 235	>200 □M	>200 □M
4	757 ± 279	1906 ± 490	>200 □M	0.162 ± 0.049
5	2.37 ± 0.29	96.5 ± 24.3	2.01 ± 0.12	1.51 ± 0.18
2 + **3**[c]	0.544 ± 0.123	1.13 ± 0.33	0.034 ± 0.007	0.012 ± 0.003
1 + **4**[c]	1.61 ± 0.19	1.93 ± 0.24	2.85 ± 0.71	0.604 ± 0.223
Effect of M^{2+} on IC_{50} of hybrid **5**				
	EeAChE		esBChE	
Conditions[d]	$CuCl_2$	$ZnCl_2$	$CuCl_2$	$ZnCl_2$
A	75.4 ± 12.4	2.46 ± 0.55	1.78 ± 0.22	0.713 ± 0.065
B	144 ± 11	2.08 ± 0.37	8.14 ± 1.00	1.28 ± 0.08
c	4.14 ± 0.43	6.99 ± 2.26	6.09 ± 0.54	2.76 ± 0.22
Effect of Aβ on IC_{50} of hybrid **5**				
	EeAChE		esBChE	
D	14.4 ± 5.2		0.554 ± 0.138	
E	2003 ± 647		1.02 ± 0.21	
f	7.26 ± 2.40		3.70 ± 0.48	
Effect of M^{2+} and Aβ on IC_{50} of hybrid **5**				
	EeAChE		esBChE	
	$CuCl_2$	$ZnCl_2$	$CuCl_2$	$ZnCl_2$
G	82.8 ± 8.3	8.80 ± 0.84	4.52 ± 1.54	2.38 ± 0.49
H	8.87 ± 1.22	9.42 ± 1.49	23.0 ± 3.2	4.70 ± 0.94
I	182 ± 66	111 ± 30	65.4 ± 6.7	41.5 ± 8.4

[a] Values from ref.[9] [b] Values from ref.[12] [c] Tested as 1:1 equimolar mixture. [d] Conditions: (a) Dilute compound **5**, add AChE or BChE, wait 10 min, add M^{2+}, wait 10 min, and initiate reaction. (b) Dilute compound **5**, add M^{2+}, wait 10 min, add AChE or BChE, wait 10 min, and initiate reaction. (c) Dilute compound **5**, add mixture of AChE or BChE and M^{2+}, wait 10 min, and initiate reaction. (d) Dilute compound **5**, add AChE or BChE, wait 10 min, add Aβ, wait 10 min, and initiate reaction. (e) Dilute compound **5**, add Aβ, wait 10 min, add AChE or BChE, wait 10 min, and initiate reaction. (f) Dilute compound **5**, add mixture of AChE or BChE and Aβ, wait 10 min, and initiate reaction. (g) Dilute compound **5**, add AChE or BChE, wait 10 min, add Aβ treated with M^{2+} for 2 min, wait 10 min, and initiate reaction. (h) Dilute compound **5**, add Aβ treated with M^{2+} for 2 min, wait 10 min, add AChE or BChE, wait 10 min, and initiate reaction. (i) Dilute compound **5**, add mixture of AChE or BChE, Aβ, and M^{2+}, wait 10 min, and initiate reaction.[e] ND = not determined.

As with AChE, the inhibitory effect of compounds **1**-**5** on BChE was also examined under a ROS environment. With the exception of compounds **1** and **4**, the introduction of ROS seemed to have little effect on the inhibition of BChE. Compound **1** showed *ca.*75-fold reduction in activity while compound **4** displayed vastly improved inhibitory properties (IC_{50} = 0.162 ± 0.049 nM) suggesting that in the absence of the tacrine moiety, the oxidized form of compound **4** may block enzymatic turnover of BChE at an increased efficiency compared to other compounds. As with AChE, the covalent bond linkage requirement for inhibitory activity was investigated. While an equimolar combination of compounds **1** and **4** showed no improvement in inhibitory activity for BChE, an equimolar mixture of compounds **2** and **3** presented a 59-fold increase in activity over hybrid **5**. In the presence of ROS, equimolar mixtures of compounds **1** and **4** as well as **2** and **3** yield values 2.5-fold and 125-fold better, respectively, than those observed for the covalently linked hybrid **5**. Although the covalent link seems to have an adverse effect upon the inhibitory activity of BChE, it still may be purposeful in transporting both components to the same site. It is important to note that the current linker used has been optimized for AChE not BChE.

6.2.4. Effect of metals and Aβ on AChE inhibition

As previously mentioned, AChE is often found to be entangled in Aβ plaques, and aggregation of Aβ is promoted through binding at the PAS of AChE.[18,24] Additionally, metal ions, such as Cu^{2+} and Zn^{2+}, have been observed to interact with Aβ and promote peptide aggregation.[27-31] Composed of tacrine and a metal–Aβ modulating moiety, the hybrid **5** was envisioned to interact with AChE, Aβ, and Cu^{2+}/Zn^{2+} simultaneously within the complex environment of an AD-affected brain. However, interaction with Aβ and Cu^{2+}/Zn^{2+} could potentially be detrimental to the ability of **5** to function as an AChEi. The ability of hybrid **5** to inhibit AChE in the presence of M^{2+} (Cu^{2+} or Zn^{2+}) and Aβ was examined (Table 6.1). It is important to note that although other tacrine-derived hybrids have been shown to successfully co-inhibit cholinesterases and Aβ aggregation,[37-40] to our knowledge, the effects of metals and Aβ on cholinesterases inhibition have not been studied for these compounds. Various conditions (a-i, Table 6.1) were tested as it was anticipated that the order of interaction

with AChE, Aβ, and M^{2+} could affect the IC_{50} of **5**. For example, **5** could potentially interact with AChE before being exposed to M^{2+} (condition a), with M^{2+} before being exposed to AChE (condition b), or with AChE and M^{2+} simultaneously (condition c). Similarly, **5** could interact with AChE before being exposed to Aβ (condition d), with Aβ before being exposed to AChE (condition e), or with AChE and Aβ simultaneously (condition f). Finally, **5** could interact with AChE before being exposed to Aβ treated with M^{2+} (condition g), with Aβ treated with M^{2+} before being exposed to AChE (condition h), or with AChE, Aβ, and M^{2+} simultaneously (condition i).

In general, hybrid **5** retained good inhibition of AChE in the presence of M^{2+} and Aβ. With only one exception, **5** showed an IC_{50} < 200 nM under all conditions tested. The lone exception (condition e, Table 6.1) occurred when **5** was exposed to Aβ for 10 min before introduction of AChE. Under these conditions, **5** indicated a nearly 850-fold reduction in potency (IC_{50} = 2003 ± 647 nM), which was not unexpected given that interaction of **5** with Aβ could likely lead to a complex that simply cannot fit into the AChE binding site as before. Only slight increases in IC_{50} were seen in the presence of Aβ in other cases (conditions d,f).

Hybrid **5** showed moderate reduction in potency in the presence of Cu^{2+} in two cases (conditions a,b, Table 6.1) but virtually no change under condition c. Similar to the case seen with Aβ, the largest reduction in potency was seen when **5** was exposed to Cu^{2+} for 10 min before introduction of AChE (condition b). However, in contrast to the case seen with Aβ, the reduction was only around 60-fold (IC_{50} = 144 ± 11 nM). Interestingly, **5** presented essentially no change in IC_{50} in the presence of Zn^{2+} under the conditions tested (conditions a, b, c, Table 6.1).

Hybrid **5** exhibited varying IC_{50} values in the presence of M^{2+} and Aβ simultaneously (conditions g, h, i, Table 6.1). A moderate reduction in potency was indicated when **5** interacted with AChE before being exposed to Cu^{2+}-treated Aβ (IC_{50} = 82.8 ± 8.3 nM), but this effect is not seen with Zn^{2+}-added Aβ samples (condition g). Only slight increases in IC_{50} were visible when **5** interacted with Cu^{2+}/Zn^{2+}-treated Aβ before being exposed to AChE (condition h). These results are interesting given the observation for condition e (described above) and may indicate that compound **5**

interacts differently with Aβ and M^{2+}-treated Aβ. Moderate reductions in potency were observed when **5** interacted with AChE, Aβ, and M^{2+} simultaneously (condition i). In the presence of AChE/Aβ/Cu^{2+}, hybrid **5** showed a nearly 80-fold reduction (IC_{50} = 182 ± 66 nM). In the presence of AChE/Aβ/Zn^{2+}, the reduction was nearly 50-fold (IC_{50} = 111 ± 30 nM). The case of AChE/Aβ/Zn^{2+} should be noted in that, of all the conditions tested with Zn^{2+} present, it was the only one that showed a significant change in IC_{50}.

The fact that **5** maintains much of its inhibition potential when exposed to M^{2+}-treated Aβ prior to AChE but not when exposed to Aβ prior to AChE may have implications for future *in vivo* studies. However, it is difficult to predict the order of interaction between these components in complex living systems. Regardless, the results described above indicate that hybrid **5** remains a relatively potent AChEi when interacting with M^{2+} and Aβ.

6.2.5 Effect of metals and Aβ on BChE inhibition

The effect of Cu^{2+}, Zn^{2+}, Aβ, and M^{2+}-treated Aβ on BChE inhibition was also tested. In general, hybrid **5** maintained good inhibition of BChE, never losing more than 32-fold activity compared to compound alone. Interestingly, with BChE, Cu^{2+} never changed the IC_{50} value by more than 4-fold (BChE added to the Cu^{2+}-inhibitor complex), while with AChE, the presence of Cu^{2+} increased the IC_{50} value by up to 72-fold. On the other hand, Zn^{2+} actually improved the inhibitory activity by *ca.* 3-fold when added to the inhibitor-BChE complex.

Similarly to the addition of Zn^{2+}, the addition of Aβ to the inhibitor-BChE complex resulted a 4-fold increase in inhibitory activity (0.554 ± 0.138 nM) when compared to hybrid **5**. The IC_{50} value was decreased by a factor of 2 when BChE was added to the Aβ-inhibitor complex (1.02 ± 0.21 nM) and no relative change was observed when the Aβ and BChE were added simultaneously (3.70 ± 0.48 nM).

When Aβ was initially treated with M^{2+}, a larger shift occurred than with Aβ or metal alone. The effect on inhibition was minimal when metal-treated Aβ was added to the inhibitor-BChE complex. The inhibitory activity of hybrid **5** was decreased 11-fold (23.0 ± 3.2 nM) when Aβ was treated with Cu^{2+} and added to hybrid **5** followed by

addition of BChE. The worst perturbation of activity arose when the metal-treated Aβ and BChE were simultaneously added to hybrid **5**. The inhibitory activity was reduced 32-fold and 21-fold by Cu^{2+}- and Zn^{2+}-treated Aβ, respectively. While the inhibition of BChE is disturbed in the presence of Aβ and metal species, the resulting change is less severe than that observed with AChE.

6.2.6. Metal binding

The ability of compounds **1**, **2**, **4**, and **5** to bind Cu^{2+} and Zn^{2+} was studied by UV-visible (UV-vis) and nuclear magnetic resonance (NMR) spectroscopy (Figure 6.2a-d). The Cu^{2+} and Zn^{2+} binding properties of compound **3** were previously reported.[34,42] In addition to **3**, new optical bands were observed in the UV-vis spectra of compounds **1** and **2** upon the addition of $CuCl_2$ or $ZnCl_2$, suggesting that these compounds were able to interact with Cu^{2+}/Zn^{2+} (Figure 6.2a, b). More importantly, compound **4** and hybrid **5**, which were designed as metal chelators, showed promising metal binding properties. Upon incubation of $CuCl_2$ with ligand (**4** or **5**) in EtOH, new optical bands (*ca*. 450 nm and 440 nm for **4** and **5**, respectively) were indicated, implicating complex formation *via* metal chelation (Figure 6.2c, d). Moreover, **4** or **5** treated with $ZnCl_2$ displayed a new optical band at *ca.* 440 nm suggesting Zn^{2+} binding (Figure 6.2c, d). In addition, ^{1}H NMR investigation was used to examine possible interaction between compound **4** or **5** and Zn^{2+}. Distinguishable downfield chemical shifts of the pyridyl, methylene, and aromatic protons were seen in the resulting spectrum of **4** or **5** when incubated with Zn^{2+} (Figure 6.2c, d, right panel). This suggests that both compounds are able to bind Zn^{2+} through the N-donor atoms on the pyridine ring and amino group.

Furthermore, the interaction of hybrid **5** with Cu^{2+}/Zn^{2+} was examined by UV-vis in the presence of Aβ with or without AChE (Figure 6.3a, b). For solutions containing Aβ and Cu^{2+} or Zn^{2+} with or without AChE, optical changes upon addition of **5** were similar to those observed from the samples containing **5** incubated with Cu^{2+} or Zn^{2+} alone, which suggests that **5** has the ability to interact with Cu^{2+} or Zn^{2+} in the presence of Aβ and AChE. While other metal/Aβ-targeted tacrine hybrids have shown the ability to bind biometals,[8,37] this is the first instance where a tacrine-metal chelator hybrid has been

shown to bind Cu^{2+} or Zn^{2+} in the presence of Aβ and AChE. Overall, the UV-vis and NMR results demonstrate Cu^{2+} and Zn^{2+} interaction of compounds **1**, **2**, **4**, and **5**, as well

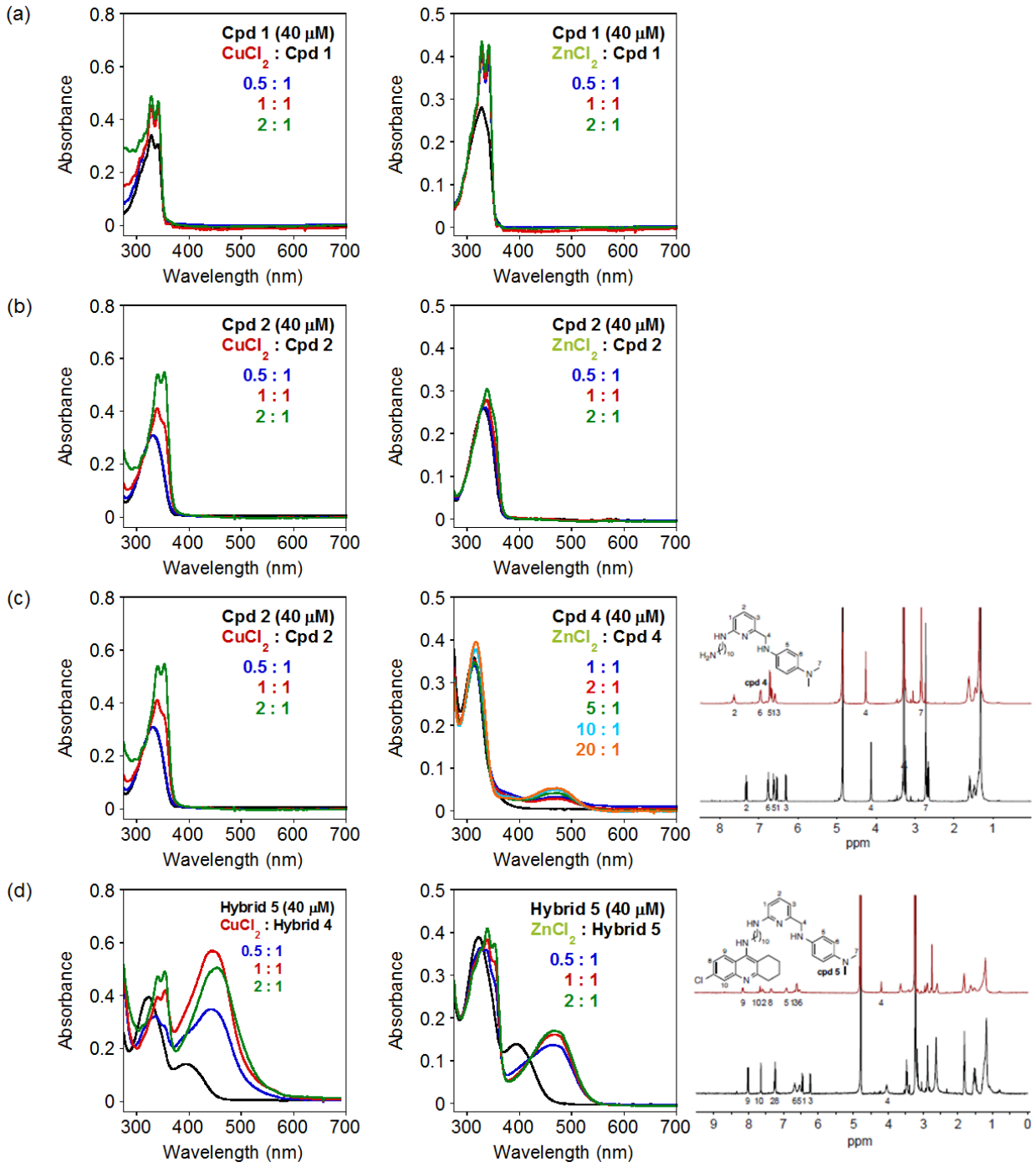

Figure 6.2. Metal binding studies of (a) cpd **1**, (b) cpd **2**, (c) cpd **4**, and (d) cpd **5** with $CuCl_2$ (left) or $ZnCl_2$ (middle) by UV-vis. Conditions: [compound] = 40 μM; [$CuCl_2$ or $ZnCl_2$] = 20–800 μM; 30 min incubation (4 h for Zn^{2+} binding for cpd **4**); room temperature. (c) and (d) right panel = Zn^{2+} binding of **4** or **5** by ^1H NMR. NMR spectra of **4** or **5** (black, 2.0 mM) with $ZnCl_2$ (red, 3.2 mM) in CD_3OD at room temperature.

as the potential interaction of **5** with Cu^{2+} and Zn^{2+} surrounded by Aβ and AChE. These results may correlate to the reactivity of the compounds towards metal–Aβ species *in vitro* (*vide infra*).

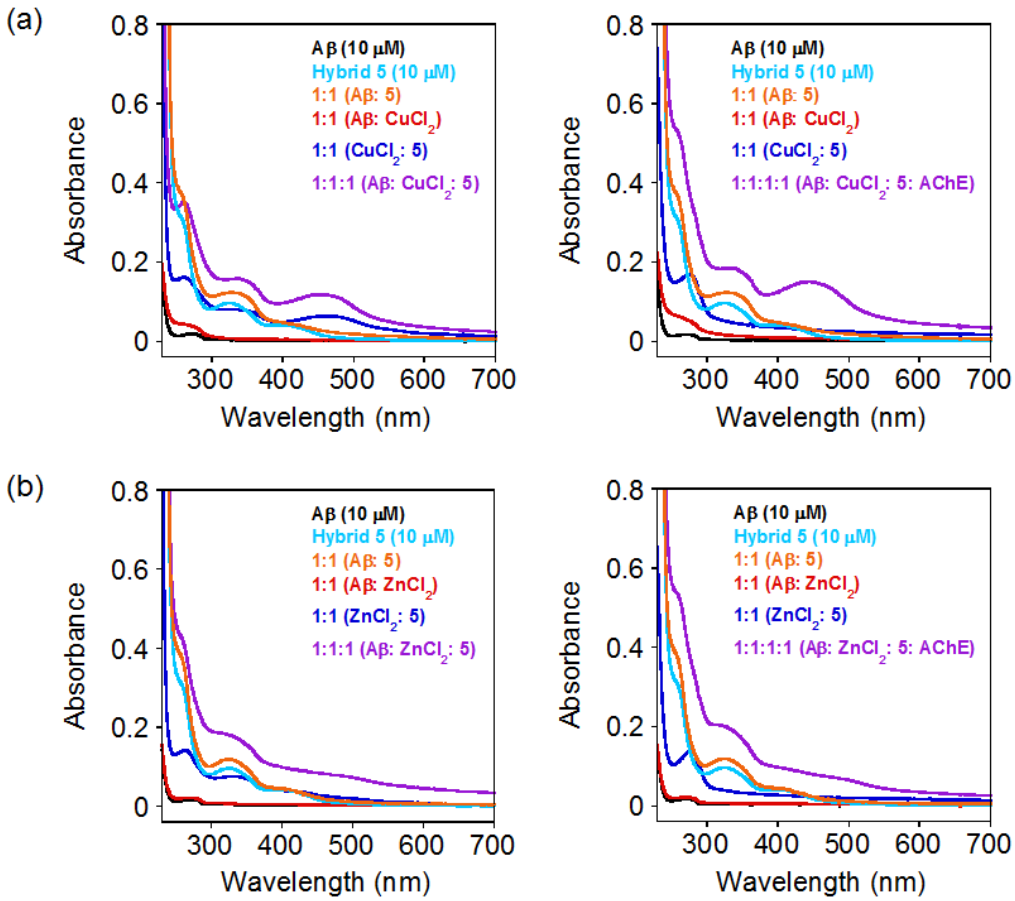

Figure 6.3. Metal binding studies of **5** with (a) $CuCl_2$ or (b) $ZnCl_2$ in the absence and presence of Aβ and/or AChE at pH 6.6 (Cu^{2+}) and 7.4 (Zn^{2+}), monitored by UV-vis. Spectra of Aβ, **5**, [Aβ + **5**], [Aβ + MCl_2], [MCl_2 + **5**], and [Aβ + MCl_2 + **5** ± AChE] are depicted in black, light blue, yellow, red, green, and blue, respectively. Conditions: [Aβ] = 10 μM; [$CuCl_2$ or $ZnCl_2$] = 10 μM; [AChE] = 10 μM; [**5**] = 10 μM (5% v/v DMSO); 20 mM HEPES, pH 6.6 (Cu^{2+}) and 7.4 (Zn^{2+}), 150 mM NaCl; room temperature.

6.2.7 Aβ aggregation inhibition

In addition to examining the AChE inhibitory activity and metal binding properties of hybrid **5**, its influence, compared to compounds **1**-**4**, on metal-free and metal-induced $Aβ_{40}$ aggregation in the absence and presence of AChE was studied *in vitro*. Two different Aβ aggregation studies were carried out: inhibition (Figure 6.4) and disaggregation (Figure 6.5). The distribution of various-sized Aβ species in both

experiments was analyzed by gel electrophoresis followed by Western blot with an anti-Aβ antibody (6E10), and morphologies of the resulting Aβ species were identified by transmission electron microscopy (TEM).

The inhibition experiment was conducted to determine whether compounds **1**-**5** were able to control the formation of metal-free and metal-associated Aβ aggregates in the absence and presence of AChE (Figure 6.4a-c). Aβ species having a dispersion of

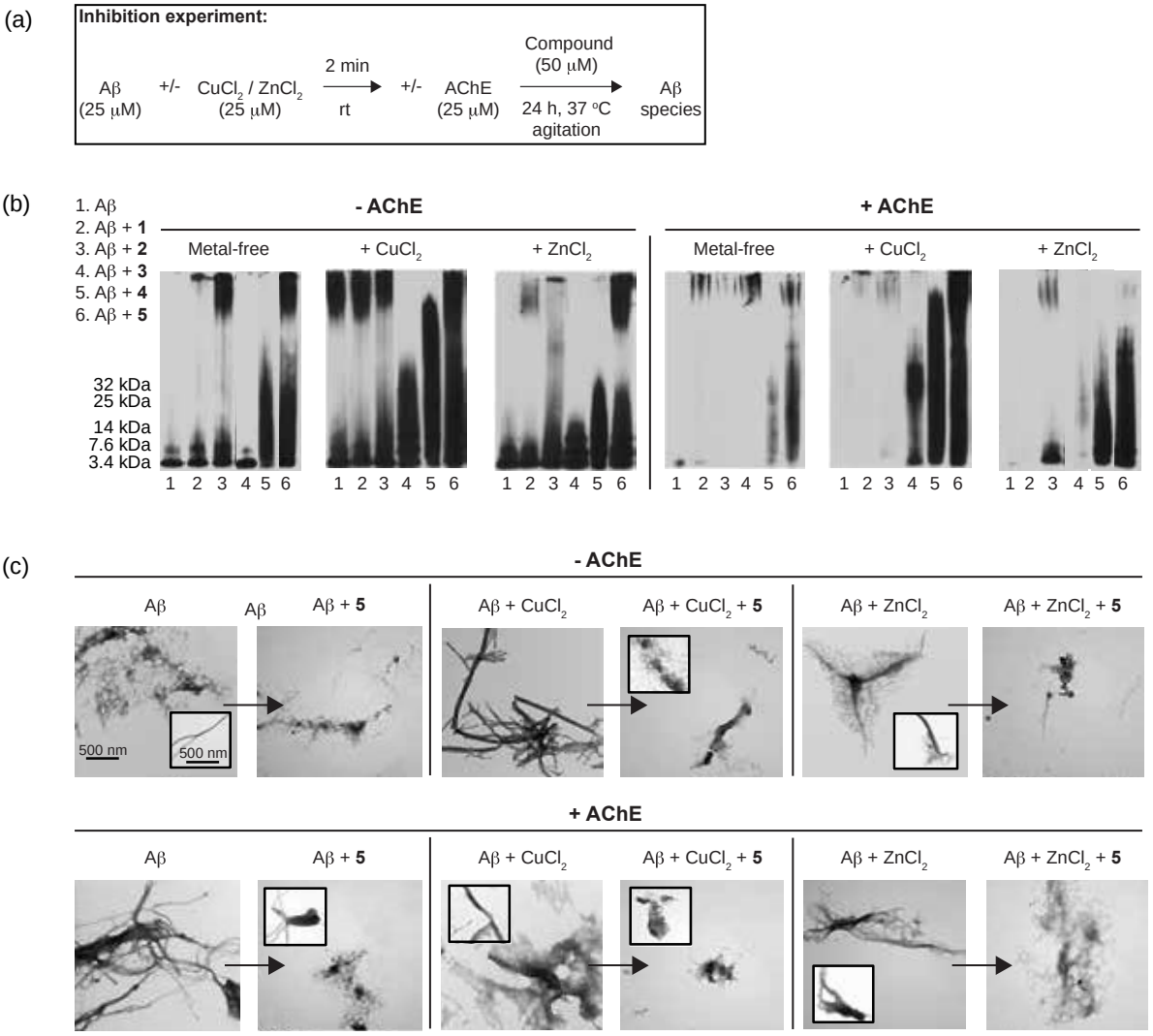

Figure 6.4. *In vitro* studies of the influence of **1**, **2**, **3**, **4**, and **5** on metal-free and metal-associated $A\beta_{40}$ aggregation with and without AChE. (a) Scheme of the inhibition experiment. (b) Visualization of various-sized Aβ species in the absence (left) and presence (right) of AChE by gel electrophoresis with Western blot (anti-Aβ antibody, 6E10). (c) TEM images of the 24 h incubated samples. Conditions: [Aβ] = 25 μM; [$CuCl_2$ or $ZnCl_2$] = 25 μM; [AChE] = 25 μM; [compound] = 50 μM; pH 6.6 (for Cu^{2+} samples) or 7.4 (for metal-free and Zn^{2+} samples); 24 h incubation; 37 °C; constant agitation.

molecular weight (MW) were observed with both metal-free and metal-treated conditions with and without AChE upon treatment with hybrid **5** (Figure 6.4b, lanes 6). Noticeable differences in the MW distribution of the generated Aβ species were indicated between Cu^{2+}-treated and Zn^{2+}-treated samples with and without AChE upon incubation with **5** (Figure 6.4b, lanes 6). In addition, TEM analysis of metal-free and metal-induced Aβ species with and without AChE upon treatment with hybrid **5** displayed a mixture of amorphous and structured peptide species distinct from those of untreated samples (Figure 6.4c). Metal/Aβ-targeted tacrine hybrids have been shown to inhibit self-induced and AChE-induced Aβ aggregation in previous studies.[37-39,43,44]

However, there exists little precedent for demonstrating modulation of metal-associated Aβ species among these hybrids making the results seen with **5** unique. The reactivity of metal–Aβ modulator linker **4**, which has the same metal chelation moiety and linker region as **5** minus the AChEi moiety, towards both metal-free and metal-triggered Aβ aggregation with and without AChE was similar to that of **5** (Figure 6.4b, lanes 5 and 6). However, metal–Aβ modulator **3**, which lacks the linker region and AChEi moiety, showed distinguishable reactivity with metal-treated samples with and without AChE compared to metal-free samples resulting in Aβ species that have MW ≤ 32 kDa (Figure 6.4b, lanes 4).[34] Comparing the results across all compounds of interest, the presence of the linker region in compounds **2**, **4**, and **5** gave greater reactivity towards metal-free and metal-associated Aβ species with and without AChE (Figure 6.4b, **2**/**5** *versus* **1** and **4**/**5** *versus* **3**). These results suggest the importance of the linker region, possibly by virtue of the increased hydrophobicity that it lends, for Aβ reactivity. Overall, hybrid **5** displayed the desired multifunctionality by presenting varying degrees of regulatory activity towards metal-free and metal-mediated Aβ aggregation with and without AChE *in vitro*. This activity may be resulted from combined properties of metal chelation, Aβ interaction, and hydrophobicity.

6.2.8. Disaggregation of Aβ aggregates

Disaggregation of preformed Aβ aggregates by other tacrine-derived hybrids has, to our knowledge, not been reported. Here, the disaggregation experiment was

performed to assess the ability of compounds **1**-**5** to disassemble preformed metal-free and metal-associated Aβ$_{40}$ aggregates in the absence and presence of AChE (Figure 6.5a, b). Similar to the results from the inhibition experiment, a wide array of both metal-free and metal-induced Aβ species in the absence of AChE were observed upon treatment with hybrid **5** (Figure 6.5b, lanes 6). However, in the presence of AChE, diverse-sized Aβ species generated by incubation with **5** were only visualized under metal-involved conditions. Also, as before, Aβ species having variable MW were detected between Cu^{2+}- and Zn^{2+}-treated samples with and without AChE upon treatment with **5** (Figure 6.5b, lanes 6). The overall reactivity of **4** towards preformed metal-free and metal-mediated Aβ aggregates with and without AChE was similar to that of **5** (Figure 6.5b, lanes 5). Relative to **5**, samples containing Aβ and **3** presented a smaller range of MW in both metal-free and metal-treated cases with and without AChE. (Figure 6.5b, lanes 4). Analogous to the inhibition results, compounds containing the linker region were shown to have the greater reactivity towards metal-free and metal-associated Aβ aggregates in the absence and presence of AChE (Figure 6.5b, in

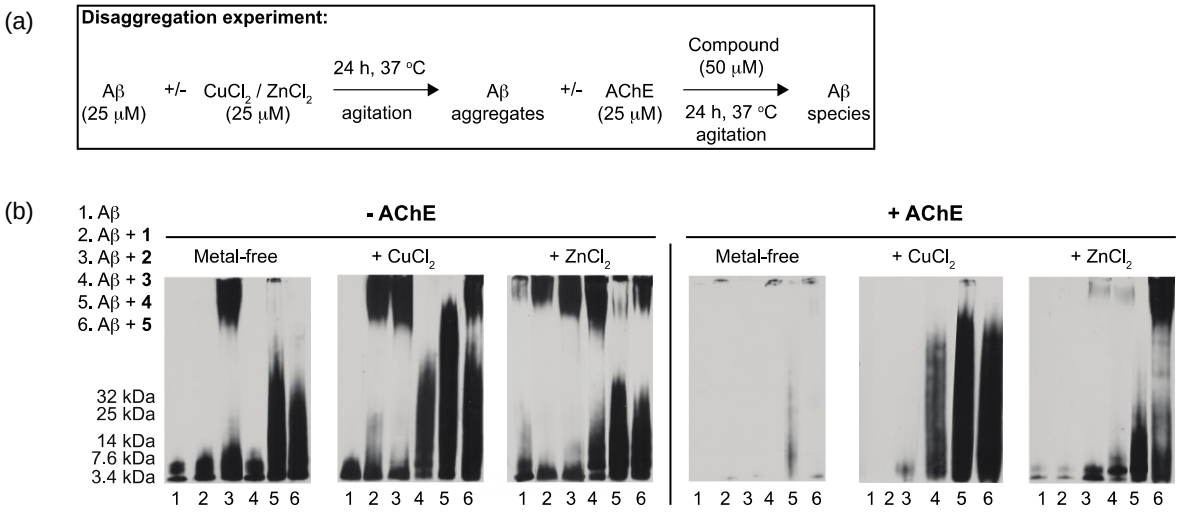

Figure 6.5. Disaggregation studies using **1**, **2**, **3**, **4**, and **5** with and without AChE. (a) Scheme of the disaggregation experiment. (b) Visualization of various-sized Aβ$_{40}$ species in the absence (left) and presence (right) of AChE by gel electrophoresis with Western blot (anti-Aβ antibody, 6E10). Conditions: [Aβ] = 25 μM; [$CuCl_2$ or $ZnCl_2$] = 25 μM; [AChE] = 25 μM [compound] = 50 μM; pH 6.6 (for Cu^{2+} samples) or 7.4 (for metal-free and Zn^{2+} samples); 24 h incubation; 37 °C; constant agitation.

particular, **3** *versus* **4**). Taken together, these results suggest that hybrid **5**, in addition to

being able to modulate the formation of metal-free and metal-induced Aβ aggregates with and without AChE, has the ability to impact preformed metal-free and metal-triggered Aβ aggregates with and without AChE to different extents.

6.2.9 Molecular modelling

Molecular modelling was performed in an effort to visualize the interactions of hybrid **5** with AChE and Aβ. Modelling was performed with GOLD[45] using AChE from *Torpedo californica* (*Tc*AChE) and $A\beta_{40}$ (PDB codes: 1ACJ[46] and 2LFM,[47] respectively). Hybrid **5** was docked into the tacrine-binding site of an energy optimized $A\beta_{40}$-*Tc*AChE

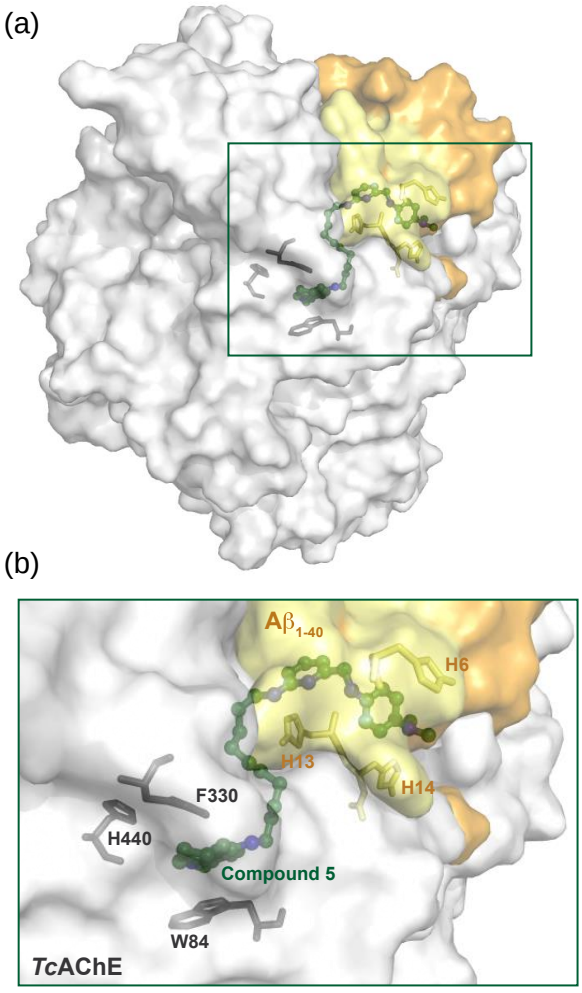

Figure 6.6. Hybrid **5** docked with $A\beta_{40}$-*Tc*AChE complex. (a) Interaction of **5** with *Tc*AChE (grey) and $A\beta_{40}$ (yellow/orange). (b) Close-up of important interactions between **5** and W84, H440, and F330 (grey) from *Tc*AChE and H6, H13, and H14 (yellow) form $A\beta_{40}$. Carbon and nitrogen atoms of **5** are shown in green and blue, respectively.

complex, and the first-ranked conformation is shown (Figure 6.6a, b). The energy optimized $A\beta_{40}$-*Tc*AChE complex showed a close association between the two components (Figure 6.6a). As expected, the 6-chlorotacrine moiety of **5** was positioned in the CAS of the enzyme with the quinoline ring system stacked between W84 and F330 and the nitrogen of the quinoline ring in close proximity to H440 (Figure 6.6b). The linker region of **5** was positioned such that it extended from the CAS to the PAS of the enzyme by spanning the gorge region. These modelling results are consistent with previous docking studies on tacrine-based linkers and hybrids with *Tc*AChE.[9,12,48,49] Of more interest is the predicted binding of the metal chelation moiety of **5** and its potential interactions with Aβ. This moiety was predicted to bind near the PAS of AChE and in close proximity to H6, H13, and H14 of $A\beta_{40}$ (Figure 6.6b). These residues are known to be important for interaction of M^{2+} with Aβ.[27-31,50] In addition, N-donor atoms from the pyridine ring and amino group of the metal chelation moiety of **5** were predicted to be in the correct geometry to coordinate M^{2+}.

6.2.10. Blood-brain barrier permeability

An essential characteristic for any anti-AD compound is the ability to cross the blood-brain barrier (BBB) and gain access to the central nervous system (CNS). BBB permeability for compounds **1**-**5** was first predicted based on the calculated values of Lipinski's rules and logBB (Table 2), which suggested that they might be able to cross the BBB.[30,51,52] Along with this theoretical prediction, the potential BBB penetration of **1**-**5** was verified by an *in vitro* Parallel Artificial Membrane Permeability-BBB (PAMPA-BBB) Assay (Table 2).[34,53] Permeability values ($-\log P_e$) of **1**-**5** were measured to be 5.1 ± 0.1 (for **1**, **2**, and **4**), 4.0 ± 0.1 (for **3**),[34] and 4.8 ± 0.1 (for **5**). Based on empirical classification of known BBB permeable molecules (*e.g.*, verapamil), our chemical scaffolds (in particular, hybrid **5**) could potentially be BBB permeable. Similar results have been seen in this type of assay with tacrine-8-hydroxyquinoline hybrids and pyrano[3,2-*c*]quinoline-6-chlorotacrine hybrids.[8,38] However, the PAMPA-BBB prediction only takes into account passive diffusion across the BBB. Permeability is likely more complex given the enzymes and efflux transporters (*e.g.*, P-glycoprotein) that are known to prevent xenobiotic entry into the CNS, and future studies will aim to elucidate how

hybrid **5** interacts with these biochemical barriers.

Table 6.2. Values (MW, *c*log*P*, HBA, HBD, PSA, logBB, and –logP_e) for **1**-**5**.

Calculation[a]	**1**	**2**	**3**[b]	**4**	**5**	Lipinski's rules and others
MW	233	388	227	398	613	500
*c*log*P*	4.08	7.76	1.76	5.10	10.7	≤ 5.0
HBA	2	3	3	5	6	≤ 10
HBD	2	3	1	4	3	≤ 5.0
PSA	38.9	50.9	28.2	66.2	65.1	≤ 90
logBB	0.174	0.555	–0.0197	–0.0744	0.785	< –1.0 (poor distribution in the brain)
–logP_e[c]	5.1 ± 0.1	5.1 ± 0.1	4.0 ± 0.1	5.1 ± 0.1	4.8 ± 0.1	
CNS+/– prediction[d]	CNS+	CNS+	CNS+	CNS+	CNS+	–logP_e < 5.4 (CNS+)
						–logP_e > 5.7 (CNS–)

[a] MW, molecular weight; *c*logP, calculated logarithm of the octonal-water partition coefficient; HBA, hydrogen-bond acceptor atoms; HBD, hydrogen-bond donor atoms; PSA, polar surface area; logBB = –0.0148 x PSA + 0.152 x *c*logP + 0.130. [b] The values for cpd 3 were previously reported.[34] [c] The values of –logP_e were measured by the Parallel Artificial Membrane Permeability Assay adapted for BBB (PAMPA-BBB). [d] CNS+/– prediction: prediction of compound penetration to the central nervous system (CNS). Compounds categorized as CNS+ could permeate through the BBB and target the CNS. In the case of compounds assigned as CNS–, they have poor permeability through the BBB and therefore, their bioavailability into the CNS is considered to be minimal.

6.3. Conclusion

In conclusion, a novel hybrid **5** of 6-chlorotacrine and metal–Aβ modulator has been synthesized and evaluated *in vitro*. This compound show potent inhibition of both AChE and BChE, and this potent inhibition was largely retained in the presence of ROS, M^{2+}, and Aβ. Additionally, **5** showed the ability to bind Cu^{2+} and Zn^{2+}, and it was able to effectively modulate the assembly of metal-free and metal-induced Aβ aggregates in the absence and presence of AChE. Furthermore, this compound presented the ability to transform preformed metal-free and metal-associated Aβ aggregates with and without AChE. Molecular modelling predicted that **5** was able to simultaneously interact with the CAS and PAS of AChE and with histidine residues known to be involved in M^{2+} binding in the Aβ peptide. A PAMPA-BBB assay predicted the BBB penetrability of **5**. Together, these results make hybrid **5** a worthy candidate for additional studies. As both a tacrine-8-hydroxyquinoline hybrid and a tacrine-melatonin hybrid have shown the ability to decrease Aβ deposits using an *in vivo* mouse model,[11,54] similar results would be

anticipated for hybrid **5**. However, due to the hepatotoxicity associated with tacrine, the next generation of hybrids capable of disaggregating metal-free and metal-triggered preformed Aβ aggregates as well as inhibiting cholinesterases and Aβ aggregation for *in vivo* studies will be composed of other currently used AD treatments, such as donepezil and galantamine. The synthesis and *in vitro* studies of such hybrids are currently underway in our laboratories.

6.4. Experimental section

6.4.1. Materials and instrumentation

Compounds **2**[9] and **3**[34] were prepared as previously reported. $A\beta_{40}$ (DAEFRHDSGYEVHHQKLVFFAEDVGSNKGAIIGLMVGGVV) was purchased from Anaspec (Fremont, CA). All reagents for chemical synthesis were purchased from Sigma-Aldrich (St. Louis, MO) and used without further purification. Reactions were monitored by TLC (Merck, Silica gel 60 F_{254}). Visualization was achieved using the following methods: UV absorption by fluorescence quenching or a ninhydrin stain (ninhydrin (1.5 g, *n*-butanol (100 mL), AcOH (3 mL)). Compounds were purified by SiO_2 flash chromatography (Dynamic Adsorbents Inc., Flash Silica Gel 32-63u). ^{1}H and ^{13}C NMR spectra were recorded on a Bruker Avance™ DPX 500 or Varian 400 MHz spectrometer. Liquid chromatography mass spectrometry (LCMS) was performed on a Shimadzu LCMS-2019EV equipped with a SPD-20AV UV-vis detector and a LC-20AD liquid chromatograph. HRMS was performed on a Micromass AutoSpec Ultima Magnetic sector mass spectrometer. Optical spectra for metal binding studies were obtained by using an Agilent 8453 UV-visible (UV-vis) spectrophotometer. Analyses by UV-vis assays (determination of IC_{50} values and Parallel Artificial Membrane Permeability blood-brain barrier penetration (PAMPA-BBB) Assay) were carried out on a multimode SpectraMax M5 plate reader (Molecular Devices, Sunnyvale, CA) using 96-well plates (Fisher Scientific). Transmission electron microscopy (TEM) images were recorded on a Philips CM-100 transmission electron microscope (Microscopy and Image Analysis Laboratory, University of Michigan, Ann Arbor, MI). Molecular modeling was performed using Sybyl-X and GOLD.[45]

6.4.2. Preparation of 6-chlorotacrine (1)

The known compound **1** was prepared in a manner similar to those previously established in the literature.[5,6] Briefly, 2-amino-4-chlorobenzonitrile (382 mg, 2.5 mmol, 1 equiv), cyclohexanone (1.26 mL, 12.2 mmol, 4.86 equiv), and anhydrous $ZnCl_2$ (750 mg, 5.5 mmol, 2.2 equiv) were combined and heated at 125 °C for 3 h. The reaction mixture was cooled to room temperature and treated with H_2O (50 mL). The remaining solid was collected by vacuum filtration, treated with 1 M aq. NaOH (50 mL), and heated to reflux for 16 h. The reaction mixture was then cooled to room temperature and extracted with $CHCl_3$ (3 x 50 mL). The combined organic layers were washed with brine (50 mL), dried ($MgSO_4$), filtered, and concentrated under reduced pressure to afford a crude yellow solid, which was purified by flash column chromatography (SiO_2, 9:1/EtOAc:MeOH, R_f 0.15) to yield 1 (135 mg, 23%) as an off-white solid: ^{1}H NMR ($(CD_3)_2SO$, 400 MHz) δ 8.18 (d, 1H, *J* = 9.0 Hz), 7.62 (d, 1H, *J* = 2.0 Hz), 7.28 (dd, 1H, J_1 = 9.0 Hz, J_2 = 2.0 Hz,), 6.48 (s, 2H), 2.81 (t, 2H, *J* = 5.4 Hz), 2.53 (t, 2H, *J* = 5.5 Hz), 1.81 (m, 4H); ^{13}C NMR ($(CD_3)_2SO$, 100 MHz) δ 158.8, 148.3, 147.0, 132.4, 126.4, 124.2, 122.7, 115.6, 109.4, 33.5, 23.6, 22.5, 22.4; LRMS *m/z* calcd for $C_{13}H_{13}ClN_2$: 232.08; found 233.00 $[M+H]^+$.

6.4.3. Preparation of *N*^{1}-[(6-bromopyridin-2-yl)methyl]-*N*^{4},*N*^{4}-dimethylbenzene-1,4-diamine (6)

6-Bromo-2-pyridinecarboxaldehyde (1 g, 5.38 mmol, 1 equiv), *N*,*N*-dimethyl-*p*-phenylenediamine (733 mg, 5.38 mmol, 1 equiv), and EtOH (40 mL) were combined and heated to reflux for 1 h. The reaction was cooled to room temperature, and $NaBH_4$ (1.1 g, 28.8 mmol, 5.4 equiv) was added. The reaction was again heated to reflux for 1 h before being cooled to room temperature, quenched with H_2O (100 mL), and extracted with Et_2O (3 x 50 mL). The combined organic layers were washed with brine (100 mL), dried ($MgSO_4$), filtered, and concentrated under reduced pressure to afford a crude brown oil, which was purified by flash column chromatography (SiO_2, 1:1/hexanes:EtOAc, R_f 0.43) to yield 6 (1.5 g, 91%) as a brown solid: ^{1}H NMR ($CDCl_3$, 400 MHz) δ 7.48 (t, 1H, *J* = 7.7 Hz), 7.35 (d, 1H, *J* = 7.8 Hz), 7.32 (d, 1H, *J* = 7.6 Hz),

6.76-6.58 (m, 4H), 4.41 (br s, 2H), 2.83 (br s, 6H); ^{13}C NMR ($CDCl_3$, 100 MHz) δ 161.5, 144.3, 141.6, 139.9, 139.1, 126.3, 120.3, 115.8, 114.5, 50.1, 42.2; LRMS *m/z* calcd for $C_{14}H_{16}BrN_3$: 305.05; found 305.75 $[M+H]^+$.

6.4.4. Preparation of *N*^{1}-{[6-((10-aminodecyl)amino)pyridin-2-yl]methyl}-*N*^{4},*N*^{4}-dimethylbenzene-1,4-diamine (4)

Compound **6** (136 mg, 0.443 mmol, 1 equiv), 1,10-diaminodecane (305 mg, 1.77 mmol, 4 equiv), and 1-pentanol (2 mL) were combined and heated to reflux for 14 h. The reaction was cooled to room temperature, diluted with CH_2Cl_2 (50 mL), and washed with 10% aq. KOH (2 x 50 mL), H_2O (2 x 50 mL), and brine (50 mL). The organic layer was dried ($MgSO_4$), filtered, and concentrated under reduced pressure to afford a crude yellow oil, which was purified by flash column chromatography (SiO_2, 7:3/CH_2Cl_2:MeOH with NH_4OH (7 mL/L of solvent), R_f 0.76). Further purification by flash column chromatography (SiO_2, 9:1/CH_2Cl_2:MeOH with NH_4OH (7 mL/L of solvent), R_f 0.23) removed remaining impurities and gave 4 (47 mg, 27%) as a dark yellow solid: ^{1}H NMR ($CDCl_3$, 400 MHz) δ 7.36 (t, 1H, *J* = 7.9 Hz), 6.73 (d, 2H, *J* = 8.8 Hz), 6.65 (d, 2H, *J* = 8.8 Hz), 6.58 (d, 1H, *J* = 7.3 Hz), 6.23 (d, 1H, *J* = 8.2 Hz), 4.56 (br t, 1H, *J* = 5.1 Hz), 4.19 (s, 2H), 3.22 (q, 2H, *J* = 6.6 Hz), 2.80 (s, 6H), 2.68 (t, 2H, *J* = 7.0 Hz), 1.61 (p, 2H, *J* = 7.2 Hz), 1.46-1.36 (m, 4H), 1.29 (s, 10H); ^{13}C NMR ($CDCl_3$, 100 MHz) δ 158.8, 157.4, 144.2, 141.0, 138.1, 116.0, 114.6, 110.4, 104.1, 50.4, 42.5, 42.4, 42.2, 33.5, 29.7, 29.63, 29.62, 29.53, 29.49, 27.2, 27.0; HRMS *m/z* calcd for $C_{24}H_{39}N_5$: 397.3205; found 398.3260 $[M+H]^+$

6.4.5. Preparation of 2-bromo-6-(1,3-dioxolan-2-yl)pyridine (7)

The known compound **7** was prepared by following a modified protocol of previously reported procedures.[55,56] A solution of 6-bromo-2-pyridinecarboxaldehyde (2.0 g, 10.8 mmol, 1 equiv), ethylene glycol (1.2 mL, 21.5 mmol, 2 equiv), and methanesulfonic acid (230 μL, 3.55 mmol, 0.33 equiv) in toluene (65 mL) was heated to reflux in a Dean-Stark apparatus for 24 h prior to being cooled to room temperature and neutralized with saturated aq. $NaHCO_3$. The organic layer was separated and the aqueous phase was extracted with Et_2O (3 x 50 mL). The combined organic layers were

washed with H_2O (3 x 50 mL) and brine (50 mL), dried ($MgSO_4$), filtered, and concentrated under reduced pressure to afford a crude yellow oil, which was purified by flash column chromatography (SiO_2, 1:1/hexanes:EtOAc, R_f 0.66) to yield 7 (1.81 g, 73%) as a pale yellow oil: ^{1}H NMR ($CDCl_3$, 500 MHz) δ 7.49 (t, 1H. *J* = 7.7 Hz), 7.38 (d, 1H, *J* = 7.3 Hz), 7.35 (d, 1H, *J* = 7.9 Hz), 5.68 (s, 1H), 4.06-3.99 (m, 2H), 3.97-3.90 (m, 2H); ^{13}C NMR ($CDCl_3$, 125 MHz) δ 158.3, 141.3, 139.0, 128.2, 119.3, 102.5, 65.4.

6.4.6. Preparation of N^1-[6-(1,3-dioxolan-2-yl)pyridin-2-yl]-N^{10}-(6-chloro-tacrine) decane-1,10-diamine (8)

Compound **7** (500 mg, 2.17 mmol, 1 equiv), compound **2** (1.25 g, 3.23 mmol, 1.5 equiv), CuI (21 mg, 0.109 mmol, 0.05 equiv), L-proline (25 mg, 0.217 mmol, 0.10 equiv), K_2CO_3 (45 mg, 0.326 mmol, 0.15 equiv), DMSO (8 mL), and H_2O (800 μL) were combined and stirred at 90 °C for 47 h. The reaction was cooled to room temperature, diluted with H_2O (150 mL), and extracted with CH_2Cl_2 (3 x 50 mL). The combined organic layers were washed with H_2O (3 x 50 mL) and brine (50 mL), dried ($MgSO_4$), filtered, and concentrated under reduced pressure to afford a crude brown oil, which was purified by flash column chromatography (SiO_2, 49:1/CH_2Cl_2:MeOH with NH_4OH (7 mL/L of solvent) to 19:1/CH_2Cl_2:MeOH with NH_4OH (7 mL/L of solvent), R_f 0.41 (9:1/CH_2Cl_2:MeOH with NH_4OH (7 mL/L of solvent))) to yield 8 (249 mg, 21%) as a yellow oil: ^{1}H NMR ($CDCl_3$, 400 MHz) δ 7.84 (d, 1H, *J* = 9.0 Hz), 7.83 (s, 1H), 7.39 (t, 1H, *J* = 7.8 Hz), 7.20 (dd, 1H, J_1 = 9.0 Hz, J_2 = 1.4 Hz), 6.73 (d, 1H, *J* = 7.3 Hz), 6.29 (d, 1H, *J* = 8.4 Hz), 5.63 (s, 1H), 4.65 (br t, 1H, *J* = 5.0 Hz), 4.13-4.05 (m, 2H), 4.02-3.96 (m, 2H), 3.94 (br s, 1H), 3.42 (br t, 2H), 3.15 (q, 2H, *J* = 6.6 Hz), 2.97 (br t, 2H), 2.60 (br t, 2H), 1.85 (br p, 4H), 1.59 (p, 2H, *J* = 7.0 Hz), 1.54 (p, 2H, *J* = 7.3 Hz), 1.32-1.29 (m, 4H), 1.23 (br s, 8H); ^{13}C NMR ($CDCl_3$, 100 MHz) δ 159.4, 158.8, 155.4, 150.8, 148.1, 138.0, 133.8, 127.5, 124.6, 124.0, 118.4, 115.6, 108.9, 106.0, 103.6, 65.3, 49.6, 42.3, 34.0, 31.7, 29.42, 29.38, 29.27, 29.26, 27.0, 26.8, 24.5, 22.9, 22.6; LRMS *m/z* calcd for $C_{31}H_{41}ClN_4O_2$: 536.29; found 537.35 $[M+H]^+$

6.4.7. Preparation of 6-{[10-((6-chloro-1,2,3,4-tacrine) amino)decyl]amino}picolin aldehyde (9)

A solution of compound **8** (91 mg, 0.170 mmol) in MeCN (2.2 mL) and 2 M aq. HCl (1.1 mL) was stirred at 60 °C for 23 h. The reaction was cooled to room temperature, slowly quenched with saturated aq. $NaHCO_3$, and extracted with CH_2Cl_2 (3 x 25 mL). The combined organic layers were washed with brine (50 mL), dried ($MgSO_4$), filtered, and concentrated under reduced pressure to yield 9 (81 mg, 96%) as a yellow oil, which was used without any further purification: ^{1}H NMR ($CDCl_3$, 400 MHz) δ 9.82 (s, 1H), 7.85 (d, 1H, J = 9.1 Hz), 7.84 (s, 1H), 7.48 (t, 1H, J = 7.8 Hz), 7.20 (dd, 1H, J_1 = 9.1 Hz, J_2 = 1.9 Hz), 7.15 (d, 1H, J = 7.2 Hz), 6.53 (d, 1H, J = 8.4 Hz), 4.86 (br t, 1H), 4.03-3.97 (m, 1H), 3.43 (t, 2H, J = 7.2 Hz), 3.27 (q, 2H, J = 6.7 Hz), 2.98 (br t, 2H), 2.61 (br t, 2H), 1.85 (br p, 4H), 1.62 (p, 2H, J = 7.2 Hz), 1.57 (p, 2H, J = 7.4 Hz), 1.34-1.30 (m, 4H), 1.24 (br s, 8H); ^{13}C NMR ($CDCl_3$, 100 MHz) δ 193.8, 159.4, 159.1, 151.3, 150.9, 148.0, 137.8, 133.9, 127.4, 124.7, 124.1, 118.3, 115.6, 112.0, 111.5, 49.6, 42.1, 34.0, 31.8, 29.5, 29.4, 29.31, 29.28, 27.0, 26.9, 24.6, 22.9, 22.6; *m/z* calcd for $C_{29}H_{37}ClN_4O$: 492.27; found 493.20 $[M+H]^+$.

6.4.8. Preparation of N^1-{[6-((10-((6-chloro-1,2,3,4-tetrahydroacridin-9-yl)amino) decyl)amino)pyridin-2-yl]methyl}-N^4,N^4-dimethylbenzene-1,4-diamine (5)

To a solution of compound **9** (64 mg, 0.129 mmol, 1 equiv) in EtOH (2.5 mL) was added *N*,*N*-dimethyl-*p*-phenylenediamine (18 mg, 0.129 mmol, 1 equiv). The reaction mixture was heated to reflux for 1 h and cooled to 0 °C prior to addition of $NaBH_4$ (33 mg, 0.864 mmol, 6.7 equiv). The reaction mixture was stirred at 0 °C for 5 min, warmed to room temperature, and stirred for an additional 30 min before quenching with H_2O (10 mL) and extracting with Et_2O (3 x 10 mL). The combined organic layers were dried ($MgSO_4$), filtered, and concentrated under reduced pressure to afford a crude yellow oil, which was purified by flash column chromatography (SiO_2, 19:1/CH_2Cl_2:MeOH with NH_4OH (7 mL/L of solvent), R_f 0.20) to yield 5 (41 mg, 52%) as a yellow oil: ^{1}H NMR ($CDCl_3$, 400 MHz) δ 7.888 (d, 1H, J = 1.5 Hz), 7.886 (d, 1H, J = 8.8 Hz), 7.35 (t, 1H, J = 7.7 Hz), 7.25 (dd, 1H, J_1 = 8.8 Hz, J_2 = 1.5 Hz), 6.73 (d, 2H, J = 8.6 Hz), 6.64 (d, 2H, J = 8.6 Hz), 6.58 (d, 1H, J = 7.3 Hz), 6.22 (d, 1H, J = 8.3 Hz), 4.56 (br t, 1H, J = 4.9 Hz), 4.19 (s, 2H), 3.97 (br s, 1H), 3.47 (t, 2H, J = 7.0 Hz), 3.22 (q, 2H, J = 6.6 Hz), 3.02 (br t, 2H), 2.80 (s, 6H), 2.65 (br t, 2H), 1.90 (br p, 4H), 1.64 (p, 2H, J = 7.1 Hz), 1.61 (p, 2H, J

= 7.4 Hz), 1.39-1.35 (m, 4H), 1.29 (s, 9H); ^{13}C NMR ($CDCl_3$, 100 MHz) δ 159.5, 158.7, 157.4, 150.9, 148.2, 144.1, 141.0, 138.1, 134.0, 127.6, 124.7, 124.2, 118.5, 115.9, 115.7, 114.6, 110.4, 104.1, 50.3, 49.7, 42.44, 42.36, 34.1, 31.9, 29.7, 29.5, 29.44, 29.39, 27.2, 27.0, 24.6, 23.0, 22.7; HRMS *m/z* calcd for $C_{37}H_{49}ClN_6$: 612.3707; found 613.3600 $[M+H]^+$.

6.4.9. *In vitro* acetyl- and butyrylcholinesterase (AChE and BChE) assay

Compounds of interest were dissolved in sodium phosphate (dibasic) buffer ((100 μL), 0.1 M, pH 8.0 adjusted at room temperature). AChE was added to the solution of inhibitors (50 μL, containing 0.08 U/mL (*ca.* 0.29 nM) AChE (final concentration) (Sigma-Aldrich cat #C2888 from eel) in sodium phosphate (dibasic) buffer (100 mM, pH 8.0 adjusted at room temperature)). The mixture of inhibitor and enzyme was incubated for 10 min before initiation with a DTNB:acetylthiocholine (ATC) (0.25 mM:0.5 mM final concentration, respectively) mixture (50 μL) in phosphate buffer (100 mM, pH 8.0 adjusted at room temperature). The reaction was monitored at 412 nm taking measurements every 30 sec for 20 min on a SpectraMax M5 plate reader. Data was corrected with the negative control (no ATC) and normalized to the positive control (no inhibitor) using the initial rates (first 2–5 min). All assays were performed in triplicate. The data was fitted to a Hill-plot and IC_{50} values calculated using KaleidaGraph 4.1.1. All IC_{50} values are reported in Table 6.1. All butyrylcholinesterase (BChE) experiments were performed using identical conditions substituting butyrylthiocholine (BTC) for ATC.

6.4.10. *In vitro* AChE and BChE inactivation assay in a ROS environment

In the wells of a 96-well plate, horseradish peroxidase (0.25 μM), H_2O_2 (100 μM), AChE (0.08 U/mL, *ca.* 0.29 nM), inhibitors (25 μM to 13 pM), and DETAPAC (100 μM) were dissolved in sodium acetate buffer (50 mM, pH 6.0 adjusted at room temperature) and incubated at 37 °C for 30 min. Note: all concentrations are reported as final concentrations. A DTNB:acetylthiocholine (ATC) (0.25 mM:0.5 mM final concentration, respectively) mixture in sodium phosphate (dibasic) buffer (50 mM, pH 7.4 adjusted at room temperature) was added to the AChE/inhibitor solution to initiate the reactions. The crude data was processed to obtain IC_{50} values as described in section 6.4.9. All

IC_{50} values are reported in Table 6.1. BChE experiments were done in an identical manner substituting BTC for ATC.

6.4.11. Metal binding studies by UV-vis and NMR spectroscopy

The interaction of compounds **1-5** with 0.5-2 equiv of Cu^{2+} or Zn^{2+} in EtOH was monitored by UV-vis ([compound] = 40 μM (1% v/v final DMSO concentration; incubation for 30 min (4 h for Zn^{2+} binding for cpd **4**); room temperature). Metal binding properties of compound **5** in the presence of Aβ and/or AChE were also studied by UV-vis. Aβ (10 μM) was treated for 2 min with $CuCl_2$ or $ZnCl_2$ (10 μM) in HEPES (20 mM, pH 6.6 (for Cu^{2+}) or pH 7.4 (for Zn^{2+}) and NaCl (150 mM). AChE (10 μM) was added to the solution containing Aβ and Cu^{2+} or Zn^{2+}. The resulting sample was incubated for 5 min at room temperature and treated with compound **5** (10 μM, 5% v/v final DMSO concentration) followed by 5 min incubation. For comparison, optical spectra of the samples generated from incubation of compound **5** (10 μM) with $CuCl_2$ or $ZnCl_2$ (10 μM) for 5 min were measured. The interaction of compounds **4** and **5** with $ZnCl_2$ was observed by ^1H NMR. Compound **4** or **5** (2 mM) was dissolved in CD_3OD and treated with 1 equiv of $ZnCl_2$. The resulting solution was incubated for 30 min prior to NMR measurement. Sequentially, 0.2 equiv of $ZnCl_2$ was added to this solution until no further change in the NMR spectrum or precipitation was observed.

6.4.12. Amyloid-β (Aβ) peptide experiments

To aliquot the $Aβ_{40}$ (1 mg), it was completely dissolved with the NH_4OH provided by the supplier, split into 5 aliquots, lyophilized, and stored at –80 °C. For assays, $Aβ_{40}$ solutions were prepared by addition of NH_4OH (10 μL, 1% v/v, aq) to the above aliquots and diluted with ddH_2O to obtain *ca.* 200 μM as determined by UV-vis (280 nm, room temperature). For both inhibition and disaggregation experiments, the buffer solution (20 μM HEPES, pH 6.6 (for Cu^{2+}) or pH 7.4 (for metal-free and Zn^{2+}), 150 μM NaCl) was used. For the inhibition experiment, Aβ (25 μM) was first treated with either $CuCl_2$ or $ZnCl_2$ (25 μM) for 2 min at room temperature followed by addition and incubation of AChE (25 μM) for 5 min (only for AChE-indicated samples). The resulting samples were

then incubated with compounds **1**-**5** (50 μM, 1% v/v final DMSO concentration) at 37 °C for 24 h with constant agitation. For the disaggregation experiment, Aβ (25 μM) was first incubated with $CuCl_2$ or $ZnCl_2$ (25 μM) at 37 °C for 24 h with continuous agitation. The samples were then treated sequentially with AChE (25 μM, only for AChE-indicated samples) for 5 min followed by addition of compounds **1**-**5** (50 μM; 1% v/v final DMSO concentration). These resulting solutions were incubated for an additional 24 h at 37 °C with constant agitation.

6.4.13. Gel electrophoresis with Western blot

The Aβ peptide experiments (described in section 6.5.12) were analyzed by gel electrophoresis with Western blot using anti-Aβ antibody (6E10).[34,57] Various Aβ species generated by both inhibition and disaggregation experiments were separated by a 10-20% Tris-tricine gel (Invitrogen). The gel was transferred to a nitrocellulose membrane and blocked for 2 h with BSA (Sigma, 3% w/v) dissolved in Tris-buffered saline (TBS, Fisher) containing 0.1% Tween-20 (TBS-T, Sigma). The membrane was treated with 6E10 (1:2,000; 2% BSA in TBS-T, Covance, Princeton, NJ) overnight at 4 °C with gentle agitation and probed with a horseradish peroxidase-conjugated goat anti-mouse secondary antibody (1:5,000; Cayman Chemical, Ann Arbor, MI) in 2% BSA in TBS-T solution for 1 h at room temperature. The protein bands were visualized by using the ThermoScientific Supersignal West Pico Chemiluminescent Substrate (Fisher).

6.4.14. Transmission electron microscopy (TEM)

TEM samples were prepared following a previously reported method.[34,57] Glow-discharged grids (Formar/Carbon 300-mesh, Electron Microscopy Sciences, Hatfield, PA) were treated with the samples (5 μL) from either the inhibition or disaggregation experiment for 2 min at room temperature. Excess sample was removed with filter paper. The grids were washed 5 times with ddH_2O, stained with uranyl acetate (1% w/v, ddH_2O, 5 μL) for 1 min, and dried for 15 min at room temperature. A Philips CM-100 transmission electron microscope (80 kV, 25,000x magnification) was used for obtaining TEM images of the samples.

6.4.15. Effect of metals and Aβ peptide on AChE and BChE inhibition by compound 5

The AChE inhibitor 5 (10 μM to 5 pM) was dissolved in phosphate buffer (100 μL, 100 mM final concentration, pH 8.0 adjusted at room temperature room temperature) and one of three conditions was followed. Conditions (a), (d), and (g): AChE (25 μL, 0.08 U/mL final concentration) was added to the inhibitor solutions (100 μL) and incubated for 10 min prior to addition of $CuCl_2$ or $ZnCl_2$ or Aβ peptide (25 μL, 10 μM final concentration). After 10 min, the reactions were initialized with a DTNB:ATC (0.25 mM:0.5 mM final concentration, respectively) mixture (50 μL) in phosphate buffer (100 mM final concentration, pH 8.0 adjusted at room temperature). Conditions (b), (e), and (h): $CuCl_2$ or $ZnCl_2$ or Aβ peptide (25 μL, 10 μM final concentration) were added to the inhibitor solutions (100 μL) and incubated for 10 min prior to addition AChE (0.08 U/mL final concentration). After 10 min, the reactions were initialized with a DTNB:ATC (0.25 mM:0.5 mM final concentration, respectively) mixture (50 μL) in phosphate buffer (100 mM final concentration, pH 8.0 adjusted at room temperature). Conditions (c), (f), and (i): A mixture (50 μL) of AChE (0.08 U/mL final concentration) and $CuCl_2$ or $ZnCl_2$ or Aβ peptide (10 μM final concentration) (50 μL total) was added to the inhibitor solutions (100 μL). After 10 min, the reactions were initialized with a DTNB:ATC (0.25 mM:0.5 mM final concentration, respectively) mixture (50 μL) in phosphate buffer (100 mM final concentration, pH 8.0 adjusted at room temperature). IC_{50} values were determined as described in section 3.1 and are reported in Table 1. Outside of using BTC in lieu of ATC, all BChE experiments were performed as AChE experiments.

6.4.16. Molecular modeling

Compound **5** was built using the Sybyl-X software and minimized to 0.01 kcal/mol by the Powell method, using Gasteiger-Hückel charges and the Tripos force fields. The coordinates of acetylcholinesterase (*Tc*AChE) and amyloid-beta ($A\beta_{40}$) were downloaded from the Protein Data Bank website (PDB codes: 1ACJ and 2LFM, respectively). The H_2O molecules and all other ligands were removed from the two proteins. Hydrogen atoms were added and the energy of both proteins was minimized

separately using the Amber force fields with Amber charges. Then, the energy-optimized ligand (compound **5**) was docked into the tacrine-binding site in the energy minimized tacrine-free *Tc*AChE using GOLD.[45] The parameters were set as the default values for GOLD. The maximum distance between hydrogen bond donors and acceptors for hydrogen bonding was set to 3.5 Å. After docking, the first-ranked conformation of compound **5** was merged into the corresponding tacrine-free *Tc*AChE (to determine the proper binding area for $A\beta_{40}$ binding).

The energy-optimized Aβ was then docked close to the surface of *Tc*AChE using GOLD. A distance constraint was applied between the H6 residue of $A\beta_{40}$ and the Gln74 of *Tc*AChE (that was chosen due its vicinity to the metal-chelator portion of compound **5** in the compound **5**–*Tc*AChE complex). Here again, the parameters were set as the default values for GOLD. The maximum distance between hydrogen bond donors and acceptors for hydrogen bonding was set to 3.5 Å. After docking, the first-ranked conformation of $A\beta_{40}$ was merged into the corresponding tacrine-free *Tc*AChE. The new $A\beta_{40}$–*Tc*AChE complex was subsequently subjected to energy minimization using the Amber force fields with Amber charges. During the energy minimization, the structure of $A\beta_{40}$ and residues within a 7-Å radius were allowed to move. The remaining residues were kept frozen in order to save calculation time. The energy minimization was performed using the Powell method with a 0.05 kcal/mol energy gradient convergence criterion and a distance dependent dielectric function. Compound 5 was then docked into the tacrine-binding site in the obtained energy optimized $A\beta_{40}$–*Tc*AChE complex as described above. The first-ranked conformation of compound 5 was merged into the tacrine-free $A\beta_{40}$–*Tc*AChE complex.

6.4.17. Parallel Artificial Membrane Permeability Assay adapted for blood-brain barrier (PAMPA-BBB)

Previously reported protocols with modification using the PAMPA Explorer kit (Pion, *Inc*.) were applied to our PAMPA-BBB experiment.[34,53,58,59] Each stock solution of the compounds was diluted to a final concentration of 10 μM (1% v/v final DMSO concentration) with pH 7.4 Prisma HT buffer (Pion). The resulting solution (200 μL) was

added to each of the wells of the donor plate (number of replicates per sample = 12). The BBB-1 lipid (Pion formulation, 5 μL) was used to coat the polyvinylidene fluoride (PDVF, 0.45 μM) filter membrane on the acceptor plate. The acceptor plate was placed on the top of the donor plate generating a "sandwich" and each well of the acceptor plate was filled with the brain sink buffer (200 μL, Pion). The sandwich was incubated at room temperature for 4 h without stirring. A microplate reader was used to obtain the optical spectra (250–500 nm) of the solutions in the reference, acceptor, and donor plates. The $-\log P_e$ for each compound was calculated using the PAMPA Explorer software c. 3.5 (Pion). CNS+/– assignment was determined in comparison to compounds identified previously.[53,58,59] Compounds categorized as CNS+ have the ability to permeate through the BBB and target the CNS. Compounds assigned as CNS– have poor permeability through the BBB and therefore, their bioavailability into the CNS is considered to be minimal.

6.6. Acknowledgment

This work was supported by the Life Sciences Institute (S.G.-T. and M.H.L.), the Department of Chemistry (M.H.L.), and the College of Pharmacy (S.G.-T.) at the University of Michigan as well as by startup funds from the University of Kentucky (S.G.-T.). The Alzheimer's Art Quilt Initiative (AAQI) is acknowledged for their support (S.G.-T.). Funding was also provided by the Ruth K. Broad Medical Foundation and the Alfred P. Sloan Foundation (M.H.L.). A.K. was supported in part by a Research Excellence Fellowship from the Department of Chemistry at the University of Michigan. We also thank Michael Beck for assistance with NMR studies for Zn^{2+} binding of **4** and **5**.

6.7. References

(1) Thies, W.; Bleiler, L. *Alzheimers Dement.* **2013**, *9*, 208.
(2) Schliebs, R.; Arendt, T. *J. Neural Transm.* **200**6, *113*, 1625.
(3) Davis, K. L.; Powchik, P. *Lancet* **1995**, *345*, 625.
(4) Ames, D. J.; Bhathal, P. S.; Davies, B. M.; Fraser, J. R. *Lancet* **1988**, *1*, 887.
(5) Recanatini, M.; Cavalli, A.; Belluti, F.; Piazzi, L.; Rampa, A.; Bisi, A.; Gobbi, S.; Valenti, P.; Andrisano, V.; Bartolini, M.; Cavrini, V. *J. Med. Chem.* **2000**, *43*, 2007.
(6) da Costa, J. S.; Pisoni, D. S.; da Silva, C. B.; Petzhold, C. L.; Russowsky, D.; Ceschi, M. A. *J. Braz. Chem. Soc.* **2009**, *20*, 1448.

(7) Fang, L.; Kraus, B.; Lehmann, J.; Heilmann, J.; Zhang, Y.; Decker, M. *Bioorg. Med. Chem. Lett.* **2008**, *18*, 2905.
(8) Fernandez-Bachiller, M. I.; Perez, C.; Gonzalez-Munoz, G. C.; Conde, S.; Lopez, M. G.; Villarroya, M.; Garcia, A. G.; Rodriguez-Franco, M. I. *J. Med. Chem.* **2010**, *53*, 4927.
(9) Bornstein, J. J.; Eckroat, T. J.; Houghton, J. L.; Jones, C. K.; Green, K. D.; Garneau-Tsodikova, S. *MedChemComm* **2011**, *2*, 406.
(10) Chen, Y.; Sun, J.; Fang, L.; Liu, M.; Peng, S.; Liao, H.; Lehmann, J.; Zhang, Y. *J. Med. Chem.* **2012**, *55*, 4309.
(11) Antequera, D.; Bolos, M.; Spuch, C.; Pascual, C.; Ferrer, I.; Fernandez-Bachiller, M. I.; Rodriguez-Franco, M. I.; Carro, E. *Neurobiol. Dis.* **2012**, *46*, 682.
(12) Eckroat, T. J.; Green, K. D.; Reed, R. A.; Bornstein, J. J.; Garneau-Tsodikova, S. *Bioorg. Med. Chem. Lett.* **2013**, *21*, 3614.
(13) Hardy, J. A.; Higgins, G. A. *Science* **1992**, *256*, 184.
(14) Wang, Y. J.; Zhou, H. D.; Zhou, X. F. *Drug Discovery Today* **2006**, *11*, 931.
(15) Haass, C.; Selkoe, D. J. *Nat. Rev. Mol. Cell Biol.* **2007**, *8*, 101.
(16) Jakob-Roetne, R.; Jacobsen, H. *Angew. Chem., Int. Ed.* **2009**, *48*, 3030.
(17) Kurz, A.; Perneczky, R. *J. Alzheimers Dis.* **2011**, *24 Suppl 2*, 61.
(18) Inestrosa, N. C.; Alvarez, A.; Perez, C. A.; Moreno, R. D.; Vicente, M.; Linker, C.; Casanueva, O. I.; Soto, C.; Garrido, J. *Neuron* **1996**, *16*, 881.
(19) Alvarez, A.; Alarcon, R.; Opazo, C.; Campos, E. O.; Munoz, F. J.; Calderon, F. H.; Dajas, F.; Gentry, M. K.; Doctor, B. P.; De Mello, F. G.; Inestrosa, N. C. *J. Neurosci.* **1998**, *18*, 3213.
(20) De Ferrari, G. V.; Canales, M. A.; Shin, I.; Weiner, L. M.; Silman, I.; Inestrosa, N. C. *Biochemistry* **2001**, *40*, 10447.
(21) Dvir, H.; Silman, I.; Harel, M.; Rosenberry, T. L.; Sussman, J. L. *Chem. Biol. Interact.* **2010**, *187*, 10.
(22) Rydberg, E. H.; Brumshtein, B.; Greenblatt, H. M.; Wong, D. M.; Shaya, D.; Williams, L. D.; Carlier, P. R.; Pang, Y. P.; Silman, I.; Sussman, J. L. *J. Med. Chem.* **2006**, *49*, 5491.
(23) Bourne, Y.; Radic, Z.; Kolb, H. C.; Sharpless, K. B.; Taylor, P.; Marchot, P. *Chem. Biol. Interact.* **2005**, *157-158*, 159.
(24) Bartolini, M.; Bertucci, C.; Cavrini, V.; Andrisano, V. *Biochem. Pharmacol.* **2003**, *65*, 407.
(25) Musial, A.; Bajda, M.; Malawska, B. *Curr. Med. Chem.* **2007**, *14*, 2654.
(26) Mehta, M.; Adem, A.; Sabbagh, M. *Int. J. Alzheimers Dis.* **2012**, *2012*, 728983.
(27) Pithadia, A. S.; Lim, M. H. *Curr. Opin. Chem. Biol.* **2012**, *16*, 67.
(28) Faller, P.; Hureau, C. *Dalton Trans.* **2009**, 1080.
(29) Drew, S. C.; Barnham, K. J. *Acc. Chem. Res.* **2011**, *44*, 1146.
(30) Scott, L. E.; Orvig, C. *Chem. Rev.* **2009**, *109*, 4885.
(31) Savelieff, M. G.; Lee, S.; Liu, Y.; Lim, M. H. *ACS Chem. Biol.* **2013**, *8*, 856.
(32) Hureau, C. *Coord. Chem. Rev.* **2012**, *256*, 2164.
(33) Hureau, C.; Dorlet, P. *Coord. Chem. Rev.* **2012**, *256*, 2175.
(34) Choi, J.-S.; Braymer, J. J.; Nanga, R. P.; Ramamoorthy, A.; Lim, M. H. *Proc. Natl. Acad. Sci. U. S. A.* **2010**, *107*, 21990.
(35) Ellman, G. L.; Courtney, K. D.; Andres, V., Jr.; Feather-Stone, R. M. *Biochem.*

Pharmacol. **1961**, *7*, 88.
(36) Gregor, V. E.; Emmerling, M. R.; Lee, C.; Moore, C. J. *Bioorg. Med. Chem. Lett.* **1992**, *2*, 861.
(37) Mao, F.; Huang, L.; Luo, Z.; Liu, A.; Lu, C.; Xie, Z.; Li, X. *Bioorg. Med. Chem.* **2012**, *20*, 5884.
(38) Camps, P.; Formosa, X.; Galdeano, C.; Munoz-Torrero, D.; Ramirez, L.; Gomez, E.; Isambert, N.; Lavilla, R.; Badia, A.; Clos, M. V.; Bartolini, M.; Mancini, F.; Andrisano, V.; Arce, M. P.; Rodriguez-Franco, M. I.; Huertas, O.; Dafni, T.; Luque, F. J. *J. Med. Chem.* **2009**, *52*, 5365.
(39) Luo, W.; Li, Y. P.; He, Y.; Huang, S. L.; Tan, J. H.; Ou, T. M.; Li, D.; Gu, L. Q.; Huang, Z. S. *Bioorg. Med. Chem.* **2011**, *19*, 763.
(40) Fernandez-Bachiller, M. I.; Perez, C.; Monjas, L.; Rademann, J.; Rodriguez-Franco, M. I. *J. Med. Chem.* **2012**, *55*, 1303.
(41) Muraoka, S.; Miura, T. *Life Sci.* **2009**, *84*, 272.
(42) Braymer, J. J.; Merrill, N. M.; Lim, M. H. *Inorg. Chim. Acta* **2012**, *380*, 261.
(43) Wang, Y.; Wang, F.; Yu, J. P.; Jiang, F. C.; Guan, X. L.; Wang, C. M.; Li, L.; Cao, H.; Li, M. X.; Chen, J. G. *Bioorg. Med. Chem.* 2012, *20*, 6513.
(44) Pi, R.; Mao, X.; Chao, X.; Cheng, Z.; Liu, M.; Duan, X.; Ye, M.; Chen, X.; Mei, Z.; Liu, P.; Li, W.; Han, Y. *PloS one* **2012**, *7*, e31921.
(45) Verdonk, M. L.; Cole, J. C.; Hartshorn, M. J.; Murray, C. W.; Taylor, R. D. *Proteins* **2003**, *52*, 609.
(46) Harel, M.; Schalk, I.; Ehret-Sabatier, L.; Bouet, F.; Goeldner, M.; Hirth, C.; Axelsen, P. H.; Silman, I.; Sussman, J. L. *Proc. Natl. Acad. Sci. U. S. A.* **1993**, *90*, 9031.
(47) Vivekanandan, S.; Brender, J. R.; Lee, S. Y.; Ramamoorthy, A. *Biochem. Biophys. Res. Commun.* **2011**, *411*, 312.
(48) Fernandez-Bachiller, M. I.; Perez, C.; Campillo, N. E.; Paez, J. A.; Gonzalez-Munoz, G. C.; Usan, P.; Garcia-Palomero, E.; Lopez, M. G.; Villarroya, M.; Garcia, A. G.; Martinez, A.; Rodriguez-Franco, M. I. *ChemMedChem* **2009**, *4*, 828.
(49) da Silva, C. H.; Campo, V. L.; Carvalho, I.; Taft, C. A. *J. Mol. Graph. Model.* **2006**, *25*, 169.
(50) Alies, B.; Bijani, C.; Sayen, S.; Guillon, E.; Faller, P.; Hureau, C. *Inorg. Chem.* **2012**, *51*, 12988.
(51) Lipinski, C. A.; Lombardo, F.; Dominy, B. W.; Feeney, P. J. *Adv. Drug Delivery Rev.* **2001**, *46*, 3.
(52) Clark, D. E.; Pickett, S. D. *Drug Discovery Today* **2000**, *5*, 49.
(53) Di, L.; Kerns, E. H.; Fan, K.; McConnell, O. J.; Carter, G. T. *Eur. J. Med. Chem.* **2003**, *38*, 223.
(54) Spuch, C.; Antequera, D.; Isabel Fernandez-Bachiller, M.; Isabel Rodriguez-Franco, M.; Carro, E. *Neurotox. Res.* **2010**, *17*, 421.
(55) Landa, A.; Minkkila, A.; Blay, G.; Jorgensen, K. A. *Chemistry* **2006**, *12*, 3472.
(56) Hamon, F.; Largy, E.; Guedin-Beaurepaire, A.; Rouchon-Dagois, M.; Sidibe, A.; Monchaud, D.; Mergny, J. L.; Riou, J. F.; Nguyen, C. H.; Teulade-Fichou, M. P. *Angew. Chem., Int. Ed.* **2011**, *50*, 8745.
(57) Hindo, S. S.; Mancino, A. M.; Braymer, J. J.; Liu, Y.; Vivekanandan, S.;

Ramamoorthy, A.; Lim, M. H. *J. Am. Chem. Soc.* **2009**, *131*, 16663.
(58) Avdeef, A.; DBendels, S.; Di, L.; Faller, B.; Kansy, M.; Sugano, K.; Yamauchi, Y. *J. Pharm. Sci.* b, *96*, 2893.
(59) *Pion Inc. BBB protocol and test compounds* 2009.

Chapter 7: Concluding Remarks and Perspectives

To understand the highly complex nature of the neuropathogenesis of Alzheimer's disease (AD), the fundamental understanding of how multiple factors (*i.e.*, Aβ, metal ions, proteins) intertwine together that lead to the onset and progression of the disease is critical. For this purpose, recent efforts have been made for the development of small molecules as chemical tools that have the potential to target these factors and modulate their reactivity. In literature, a wide range of libraries of small molecules with various molecular scaffolds has been utilized to illustrate some inkling of metal-peptide-protein interactons and their effects upon neurotoxicity leading to AD. Advancements in this particular area will be essential as AD etiology becomes slowly elucidated.

The studies presented in Chapters 2-6 of this dissertation demonstrate the feasibility of developing small molecules as chemical tools to understand the role of multiple factors play in AD neuropathogenesis. The small molecules investigated in this thesis were developed using a rational structure-based approach where critical moieties (*i.e.*, Aβ interaction, metal chelation, inhibition of protein activity) were designed into a single molecule. As shown in Chapters 2 and 3, **DPP** derivatives reveal a structure-reactivity-cytotoxicity relationship that explains the compounds' reactivity toward metal-associated Aβ (metal–Aβ) species. Tuning of reactivity (in particular, Aβ aggregation) *via* structural modifications allows us to understand that the balance of compounds' properties (*i.e.*, Aβ interaction and metal chelation) is necessary for achieving noticeable their reactivity with the target, metal–Aβ. Chapters 4 and 5 (**Gd-cur** and **PyED**, respectively) present alternative aspects of the framework, where small molecules could be used as a thernostic agent (**Gd-cur**) or a potential tool that could be used for Aβ clearance through radical formation (**PyED**). From these studies, both scaffolds show the ability to target metal–Aβ species and control Aβ aggregation as well, and we now can discern some nuances of how molecular structure could be designed to incorporate

other potential uses to study AD etiology. Hybrid **5**, presented in Chapter 6, displays interactions toward multiple facets (Aβ, metal ions, and acetylcholinesterase (AChE)) as well as abilities to modulate metal-induced Aβ aggregation with and without AChE, and to inhibit the activity of AChE, capable of breaking down the neurotransmitter acetylcholine (ACh), in the absence and presence of Aβ and/or metal ions under both normal and oxidative stress conditions. For hybrid **5**, the modulating framework, **L2-b**, for bifunctionality (Aβ interaction and metal chelation) was conjugated with tacrine moiety for AChE inhibition in order to target and regulate metal ions, Aβ/metal–Aβ, and AChE. All compounds (Chapters 2-6) are shown to modulate metal-induced Aβ aggregation to different extents in comparison to metal-free Aβ aggregation. Overall these studies provide us insight into the development of potential viable chemical tools to elucidate the multifaceted cause of AD.

The reactivity of presently investigated compounds with Aβ and metal–Aβ, however, has been observed to be limited *in vitro*, and therefore subsequent structural optimization for interacting with metal ions and Aβ species is necessary for their potential biological applicability. **DPP** derivatives show varying degrees of ability to control metal-induced Aβ aggregation; **DPP2** and **C2** (exhibiting cytotoxicity at low μM concentrations) exhibit the greatest reactivity toward Aβ/metal–Aβ, while **PA2** (relatively nontoxic up to high μM concentrations) demonstrates slight reactivity toward metal-triggered Aβ aggregation. The different metal binding affinities of these derivatives are suggested to have an impact in controlling the formation of Aβ aggregates. Therefore, the metal binding affinity of **DPP** series could be improved ($\geq 10^{-6}$ M) upon substitution with stronger donor atoms for metal binding as well as altering dencitiy, which could allow **DPP** derivatives to be applied for biological systems. Limitation of **Gd-cur** for its uses for brain applications comes from its BBB permeability properties. Scaffold modifications, such as lowering the MW or HBA of the compound by employing an alternate MRI agent (Gd^{III}DTPA contains 10 HBA with MW = 546) or changing the curcumin with the linker (contains 10 HBA; MW = 617), could provide a viable theranostic candidate for biological applications. **PyED**, though having metal chelating abilities, do not have an Aβ interaction moiety within the framework. Incorporation of a

dimethylamino moiety, which has been suggested to be essential for Aβ interaction,[1-3] may improve properties for interactions and reactivity toward Aβ/metal–Aβ direct its utilitzation in biological settings. Due to it solubility and hepatoxicity associated with the tacrine moiety, the next generation of hybrid **5** would be composed of a more hydrophilic linker (to improve compound solubility) for conjugation of a metal–Aβ modulating moiety and an AChE inhibiting moiety, as well as employing other current therapeutics employed for AD treatments (AChE inhibition). In addition, **L2-b** (metal–Aβ modulating moiety incorporated in hybrid **5**) has recently presented promising *in vivo* data toward Aβ species and its derivatives are being developed and investigated for greater bioavailability (*e.g.*, higher amount of neutral species at physiologically relevant pH (*i.e.*, 7.4), mitigation of compound's cytotoxicity in the presence of metal ions). Over the course of time, research in the AD field will highly benefit from the continuing development of small molecules as chemical reagents to aid in illustrating the complex, multifaceted cause of AD neuropathology, which may lead to discovery of diagnotics and therapeutics for AD. To contribute to this aspect, further tuning of chemical properties of present molecules and other lead compounds for optimization of biological applications (*e.g.*, solubility, BBB permeability, cytotoxicity) *via* structural refinement is essential.

References

(1) Pithadia, A. S.; Kochi, A.; Soper, M. T.; Beck, M. W.; Liu, Y.; Lee, S.; DeToma, A. S.; Ruotolo, B. T.; Lim, M. H. *Inorg. Chem.* **2012**, *51*, 12959.

(2) Liu, Y.; Kochi, A.; Pithadia, A. S.; Lee, S.; Nam, Y.; Beck, M. W.; He, X.; Lee, D.; Lim, M. H. *Inorg. Chem.* **2013**, *52*, 8121.

(3) Leuma Yona, R.; Mazeres, S.; Faller, P.; Gras, E. *ChemMedChem* **2008**, *3*, 63.

Appendix A: Reactivity of Triazole-Pyridine Derivatives Toward Metal-Associated Aβ Species

The work presented herein was conducted in collaboration with Dr. Matteo Tegoni at University of Parma, Italy. In this present work, I have contributed to studies of metal binding, docking, Aβ aggregation (gel/TEM), antioxidant activity, cytotoxicity, and *in vitro* blood-brain barrier (BBB) permeability.

A.1. Introduction

Alzheimer's disease is the most common form of dementia that is currently afflicting the aging population; cases of AD diagnosis has steadily risen, making it the sixth leading cause of death in the United States.[1] One of the hallmarks of AD is the accumulation of amyloid-beta (Aβ) peptide aggregates; through an amyloidogenic aggregation pathway, starts with the generation of monomers, which have the propensity to self-aggregate into higher MW Aβ species, such as oligomers, protofibrils and fibrils that ultimately form the senile plaques that are seen in AD brain.[2-8] Other multiple factors (*i.e.*, metal ion dyshomeostasis, oxidative stress) have been correlated to Aβ itself, where increased levels of metal ions (*i.e.*, Cu, Zn, and Fe) have been found within the senile plaques [2,4,6-8] and metal ions, upon binding to Aβ, facilitate peptide aggregation as well as enhance reactive oxygen species formation.[2,6-9]

To further illustrate the potential correlation between metal-associated (metal–Aβ) species in the onset and progression of the disease, efforts have been made in the development of chemical tools which have been designed to target metal–Aβ species, regulate the interaction between metal ions and Aβ, and modulate their reactivity.[6,7,9,10] Our laboratory has made strides in developing small molecules fashioned using a rational structure-based incorporation approach where a metal chelation site is integrated onto an Aβ interacting moiety.[11-18] Among them, reactivity of

triazole-pyridine derivatives toward metal–Aβ species were investigated and shown to have a modulating affect upon metal-induced Aβ aggregation.[15] In addition, triazoles have be incorporated into a wide variety of therapeutic drug frameworks due to observed its biological relevant properties, such as anti-inflammatory, anti-depressant, anticancer, and analgesic activities.[19-23] In particular, metal binding (specifically with copper through nitrogen/nitrogen or nitrogen/sulfur donor atoms) and antipoliferative activity of small molecules with 1,2,4-triazole-pyridine core framework have been studied.[21,24-27] Herein, we report the characterization of 1,2,4-triazole-pyridine derivatives (**PR1**, **PR2**, **PR3**, and **PR4**) toward Aβ, metal ions, metal–Aβ and reactivity toward metal-free and metal-induced Aβ aggregation (Figure A.1). Overall, the results indicate that the 1,2,4-triazole-pyridine scaffold may be a possible framework for chemical reagent development to study metal-associated Aβ species.

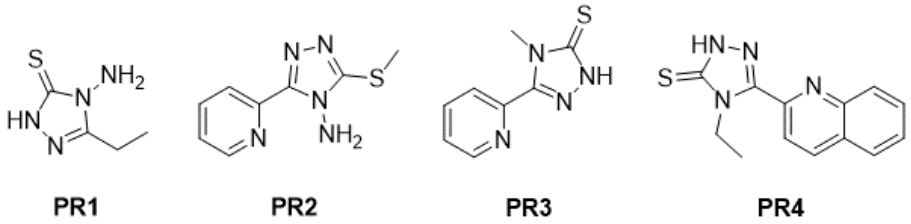

Figure A.1. Chemical structures of **PR1** (4-amino-5-ethyl-2,4-dihydro-3*H*-1,2,4-triazole-3-thione), **PR2** (3-(methylthio)-5-pyridin-2-yl)-4*H*-1,2,4-triazol-4-amine), **PR3** (4-methyl-5-(pyridin-2-yl)-2,4-dihydro-3*H*-1,2,4-triazole-3-thione, and **PR4** (4-ethyl-5-(quinolin-2-yl)-2-4-dihydro-3*H*-1,2,4-triazole-3-thione.

A.2. Results and discussion

A.2.1. Metal binding properties of PR1, PR2, PR3, and PR4

Cu^{2+} and Zn^{2+} binding was first examined by UV-vis and ^1H NMR spectroscopy, respectively (Figure A.2). Spectral changes, such as an appearance of a new optical band and/or variation in absorbance intensity, were observed upon the addition of $CuCl_2$ (1-5 equiv) to a ligand solution in EtOH, indicating Cu^{2+} interaction. Due to the minute optical shift displayed with Zn^{2+} treatment, Zn^{2+} binding of **PR1**, **PR2**, **PR3**, or **PR4** was investigated by ^1H NMR. Upon the addition of 2 equiv of $ZnCl_2$ to a solution of **PR1**, **PR2**, **PR3**, or **PR4** (in CD_3CN for **PR1**, **PR3**, or **PR4**; in CD_2OH for **PR2**), a slight

downfield shift of the pyridine protons (**PR2**, **PR3**, or **PR4**) or triazole proton (**PR1**, **PR3**, or **PR4**) was recorded, suggesting that the N donor atom from the pyridine ring (**PR2**, **PR3**, or **PR4**) or triazole ring (**PR1**, **PR3**, or **PR4**) may be involved in metal chelation (Figure A.2). Overall, the UV-vis and NMR studies implied that **PR1**, **PR2**, **PR3**, and **PR4** are capable of binding with Cu^{2+} and Zn^{2+}.

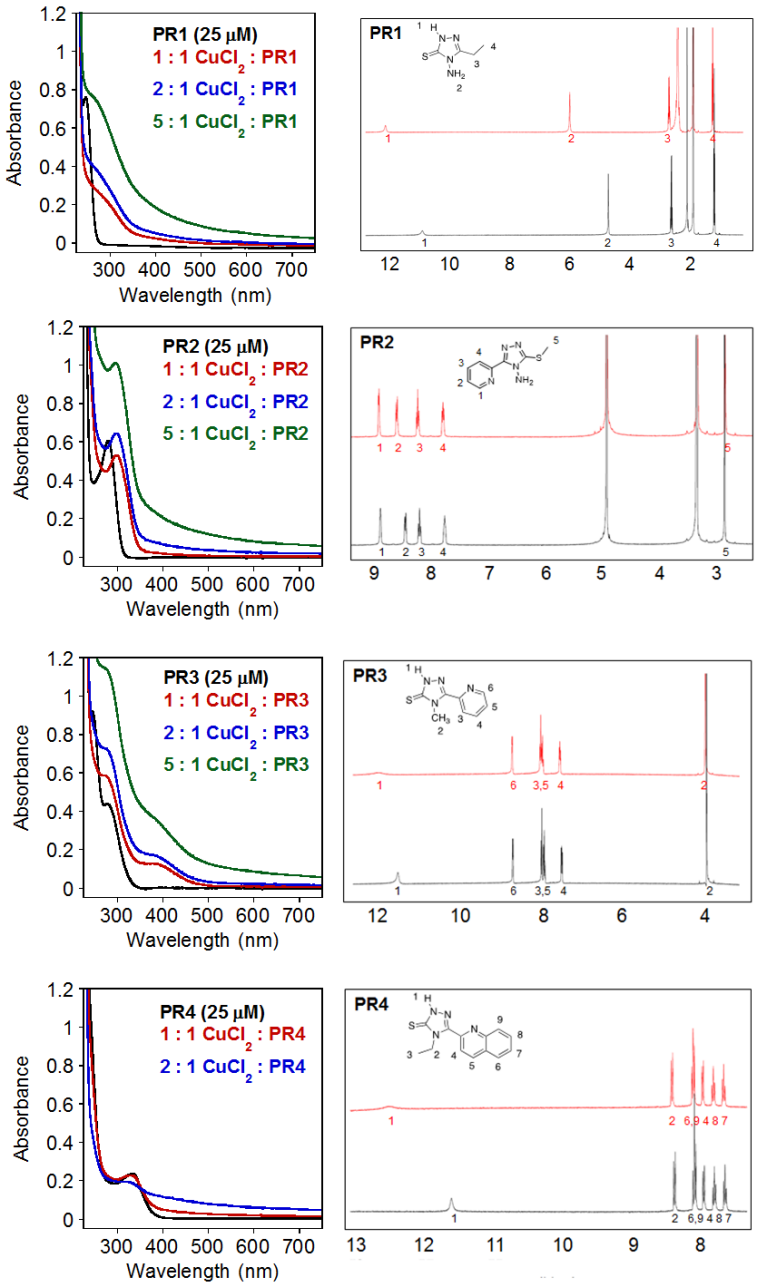

Figure A.2. Cu^{2+} or Zn^{2+} binding of **PR1**, **PR2**, **PR3**, and **PR4**. (a) UV-vis spectra of **PR1-4** with $CuCl_2$ (1–20 equiv) in EtOH at room temperature. (b) ^1H NMR spectra of **PR1-4** (black) with $ZnCl_2$ (red) in CD_3CN at room temperature ([compound] = 4 mM; [$ZnCl_2$] = 4 mM).

A.2.2. Influence of PR1, PR2, PR3, and PR4 on metal-free and metal-induced Aβ aggregation

The ability of **PR1**, **PR2**, **PR3**, and **PR4** to modulate Aβ aggregate formation (inhibition) and transform preformed Aβ aggregates (disaggregation) (Figure A.3) was investigated by gel electrophoresis followed by Western blot using an anti-Aβ antibody (6E10).[12,18,28]

As shown in Figure A.3a, for inhibition studies with $A\beta_{40}$, reactivity was not indicated for **PR1**, **PR2**, **PR3**, and **PR4** in metal-free and Zn^{2+}-treated conditions. $A\beta_{40}$ species (MW ≤ 20 kDa) was visualized upon the treatment with **PR1**, **PR3**, and **PR4** to Cu^{2+}–$A\beta_{40}$ species (Figure A.3a, lanes 2, 4 and 5). In the case of sample containing $A\beta_{42}$, similar to results observed (in metal-free conditions) in comparison to that of $A\beta_{40}$, where no reactivity was exhibited upon compound addition (Figure A.3a). Very slight reactivity was shown from the samples containing $A\beta_{42}$, Zn^{2+}, and **PR2** (lane 3). Minimal reactivity was indicated with **PR1**/**2**-treated Cu^{2+}–$A\beta_{42}$ species (lanes 2 and 3).

Disaggregation experiments were also conducted to verify the ability of **PR1**, **PR2**, **PR3**, and **PR4** to disassemble preformed Aβ aggregates (Figure A.3b). Similar to the inhibition experiment, no noticeable reactivity was observed for compounds in metal-free and Zn^{2+}-induced Aβ aggregation for $A\beta_{40}$. When **PR1** and **PR3** were incubated with Cu^{2+}-treated Aβ aggregates, $A\beta_{40}$ species having MW ≤ 20 kDa were detected (Figure A.3b, lanes 2 and 4). In the case of $A\beta_{42}$, no reactivity was indicated metal-free conditions, while nominal reactivity was shown for **PR1**/**3**-added metal-associated $A\beta_{42}$ species. Taken together, the inhibition and disaggregation results suggest that **PR1**, **PR2**, **PR3**, and **PR4** have the ability to slightly modulate Aβ aggregation to varying degrees.

A.2.3. Docking studies of PR1, PR2, PR3, and PR4

To visualize the possible interaction between $A\beta_{40}$ and **PR1**, **PR2**, **PR3**, or **PR4**, docking studies were performed using AutoDock Vina,[29] employing monomeric $A\beta_{40}$ NMR structure (PDB 2LFM)[30] (Figure A.4). The compounds and Aβ were predicted to interact through non-specific interactions, with most conformations exhibiting

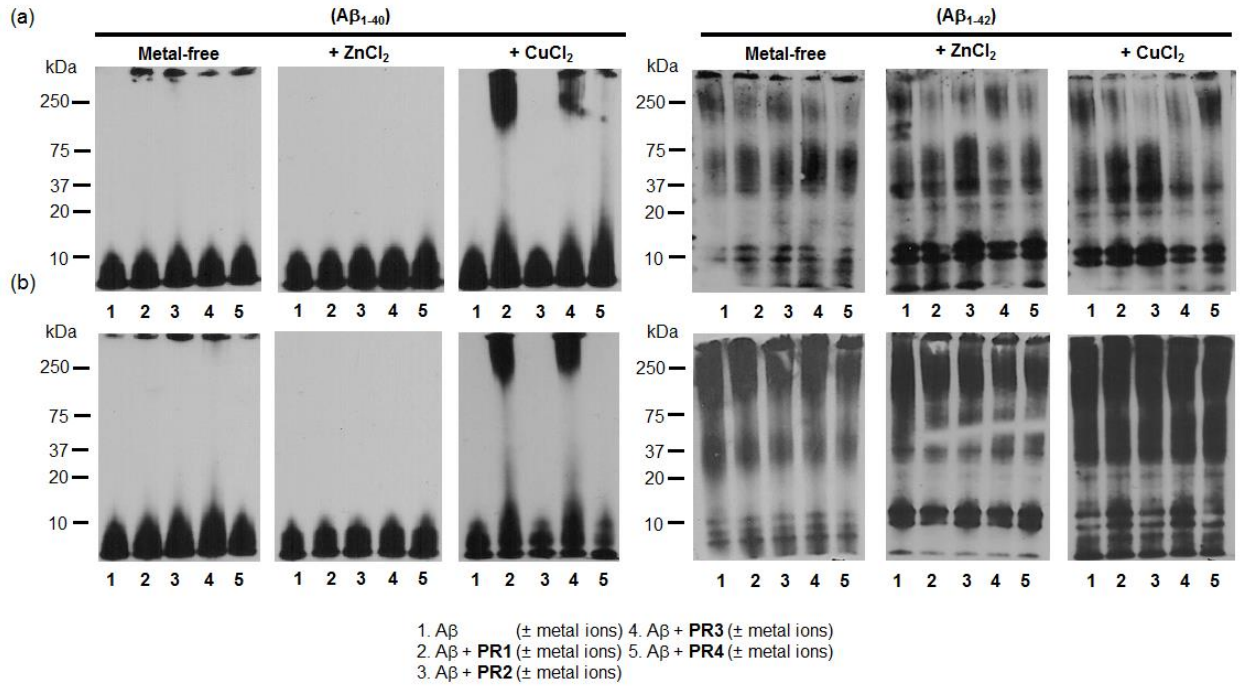

Figure A.3. Inhibition and disaggregation experiments (for $A\beta_{40}$ or $A\beta_{42}$). Analysis of various-sized Aβ species by gel electrophoresis with Western blot using an anti-Aβ antibody (6E10) for (a) inhibition experiment and (b) disaggregation experiment. Conditions: [Aβ] = 25 μM; [$CuCl_2$ or $ZnCl_2$] = 25 μM; [compound] = 50 μM; pH 6.6 (for Cu^{2+} samples) or 7.4 (for metal-free and Zn^{2+} samples); 24 h incubation; 37 °C; constant agitation.

compounds being docked between the α-helix and *N*-terminal random coil. These interactions had calculated to have binding energies ranging from –3.5 to –4.0, –4.5 to –5.1, –4.2 to –5.2, and –5.1 to –6.1 for **PR1**, **PR2**, **PR3**, and **PR4**, respectively. The ligands were shown to either be docked at different sites or be offset from each other when docked at similar sites on the peptide. Observations from the preliminary docking studies suggest that **PR1**, **PR2**, **PR3**, and **PR4** could interact with Aβ differently, which may result in the varying reactivity displayed toward Aβ aggregation *in vitro* (*vide supra*).

A.2.3. Isothermal titration calorimetry studies of PR3

Possible interactions of **PR3** with $A\beta_{40}$ was investigated by isothermal titration calorimetry (ITC) experiments.[31] The heat changes measured during the titration suggested possible interaction of **PR3** with $A\beta_{40}$. The titration data was fitted using a sequential binding model, where the best fit was achieved with N = 3; the thermodynamic values (binding constants (K_A), enthalpy changes (ΔH), entropy

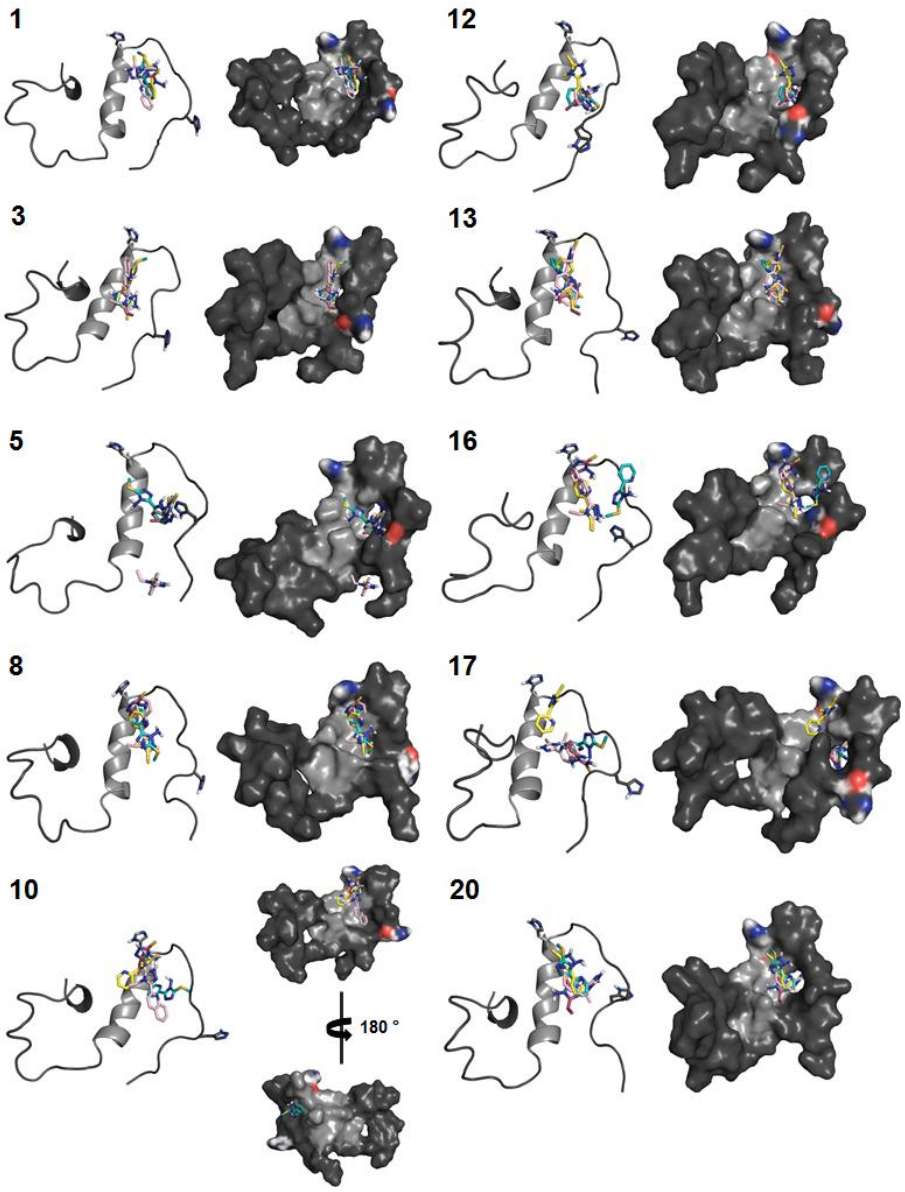

Figure A.4. Docking studies of **PR1**-**4**. Cartoon (left) and surface (right) versions of possible conformations of **PR1** (red), **PR2** (turquoise), **PR3** (yellow), and **PR4** (pink) docked with $A\beta_{40}$ (PDB 2LFM) by AutoDock Vina. The helical region of Aβ (H13-D23) in the surface representation is highlighted in color (light grey).

changes ($T\Delta S$), and Gibbs free energy (ΔG) were then determined, based on the binding model (Table A2.1). The first and third binding are entropically favorable, however enthapically unfavorable (Table A2.1), indicating that the binding may be driven by hydrophobic interactions. The second binding is enthalpically favored and entropically unfavored (Table A2.1), suggesting interaction may be occuring *via* hydrogen bonding. Overall, the ITC data demonstrate possible $A\beta_{40}$ interaction, which

may correspond to the reactivity observed with Aβ aggregation (*vide supra*; Figure A.3).

Table A2.1. Thermodynamic parameters for the interaction of **PR3** with $A\beta_{40}$ determined by isothermal titration calorimetry (ITC).

	Binding site 1	Binding site 2	Binding site 3
K_A (M^{-1})	$1.5 \times 10^4 \pm 9.7 \times 10^3$	$1.0 \times 10^5 \pm 7.3 \times 10^4$	$2.6 \times 10^5 \pm 1.8 \times 10^4$
ΔG (kJ/mol)	−23.8 ± 1.6	−28.6 ± 1.7	−30.9 ± 1.7
ΔH (kJ/mol)	9.89 ± 3.3	−3.70 ± 1.6	2.51 ± 1.2
$-T\Delta S$ (kJ/mol)	−33.7 ± 3.7	8.41 ± 15.9	−56.1 ± 12.4

A.2.5. Antioxidant capacity, cell toxicity, and BBB permeability of PR1, PR2, PR3, and PR4

To determine whether **PR1**, **PR2**, **PR3**, and **PR4** has biological applications, the antioxidant capacity of compounds were determined using a Trolox equivalent antioxidant capacity (TEAC) assay,[32,33] which measures the ability of compound to quench the generated ABTS cation radicals ($ABTS^{\bullet+}$; ABTS = 2,2'-azino-bis(3-ethylbenzothiazoline-6-sufonic acid)) in solution (Figure A.5). The compounds were less effective in scavenging free radicals in comparison to that of Trolox (a vitamin E analogue), but differences between the compounds were observed. **PR3** had the greatest activity followed by **PR1** < **PR4** < **PR2** (**PR2**; minimal if not any antioxidant capacity).

Cytotoxicity of **PR1**, **PR2**, **PR3**, and **PR4** was determined employing human neuroblastoma SK-N-BE(2)-M17 cells and assessed by the MTT assay.[11,12,18,28] The compounds themselves did not exhibit any cell toxicity (up to 100 μM; Figure A.6a). In the presence of Zn^{2+}, toxicity was not observed up to 50 μM. Upon addition of compound to Cu^{2+}-treated M17 cells, ≥ 80% cell viability was shown with **PR1** and **PR2** at 50 μM $CuCl_2$; however, **PR3** and **PR4** indicated *ca.* 60% or lower cell viability at 50 μM $CuCl_2$ (Figure A.6b).

The BBB permeability of **PR1**, **PR2**, **PR3**, and **PR4** was identified initially based

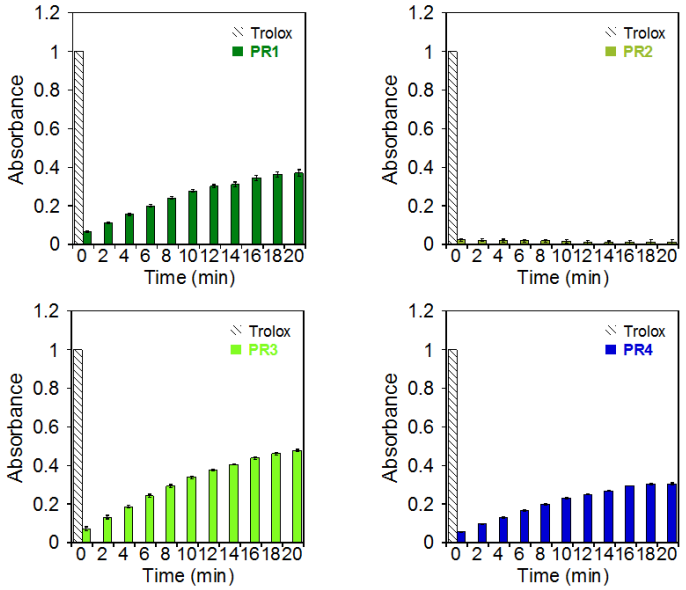

Figure A.5. Antioxidant activity of **PR1**, **PR2**, **PR3**, and **PR4** measured by the TEAC assay. The TEAC values are relative to Trolox, a vitamin E analogue (6-hydroxy-2,5,7,8-tetramethylchroman-2-carboxylic acid).

on the values of the Lipinski's rules and logBB.[34-37] The calculated values suggest that **PR1**, **PR2**, **PR3**, and **PR4** have drug-like characteristics and may be BBB permeable. An *in vitro* PAMPA-BBB assay was performed to verify the theoretical prediction for BBB permeability of our compounds. The permeability value ($-\log P_e$) of **PR1**, **PR2**, **PR3**, and **PR4** ($-\log P_e$ = 6.1 ± 0.1, 5.8 ± 0.1, 5.7 ± 0.1, and 4.9 ± 0.1, respectively; Table A2.2), along with the empirical classification of known molecules to permeate through the BBB (*e.g.*, verapamil),[34,35,38] indicated that **PR4** could potentially passively diffuse across the BBB membrane. Overall, our results to determine potential biological applicability suggest that **PR4** may be a possible candidate that is BBB permeable and not cytotoxic at lower copper concentration (*i.e.,* 5 μM)

A.3. Conclusion and future directions

Reactivity of triazole-pyridine derivatives was investigated toward Aβ, metal ions, and metal-associated Aβ species as a potential chemical reagent framework that could target and alter the interaction between the two factors (Aβ and metal ions) to alter their reactivity. Based on the data presented herein, **PR1**, **PR3**, and **PR4** show slight ability to modulate *in vitro* Cu^{2+}-induced Aβ aggregation, specifically $A\beta_{40}$ aggregation. As for

Table A2.2. Values (MW, *c*logP, HBA, HBD, PSA, logBB, and –logP_e) of **PR1**-**4**.

Calculation[a]	**PR1**	**PR3**	**PR4**	**PR5**	Lipinski's rules & others
MW	144	207	192	256	≤ 450
*c*logP	−0.225	0.693	−0.926	0.987	≤ 5.0
HBA	4	5	4	4	≤ 10
HBD	3	2	1	1	≤ 5
PSA	59.6	69.6	46.5	46.5	≤ 90
logBB	−0.786	−0.795	−0.699	−0.408	< −1.0 (poorly distributed in the brain.
–logP_e[b]	6.1 ± 0.1	5.8 ± 0.1	5.7 ± 0.1	4.9 ± 0.1	
CNS +/– Prediction[c]	CNS -	CNS -	CNS -	CNS +	–logP_e < 5.4 (CNS+) > 5.7 (CNS–)

[a]MW, molecular weight; *c*logP, calculated logarithm of the octonal-water partition coefficient; HBA, hydrogen-bond acceptor atoms; HBD, hydrogen-bond donor atoms; PSA, polar surface area; logBB = −0.0148 x PSA + 0.152 x *c*logP + 0.130. [b] The values of –logP_e were measured by the parallel artificial membrane permeability assay (PAMPA). [c] Compounds categorized as CNS+ have the ability to permeate through the BBB and target the CNS. In the case of compounds assigned as CNS− they have poor permeability through the BBB and therefore, their bioavailability into the CNS is considered to be minimal.

biological applicability, **PR1**, **PR3**, and **PR4** were observed to have modest antioxidant ability, relatively non-toxic in the absence of metal ions ($CuCl_2$ or $ZnCl_2$) and presence of $ZnCl_2$. Varying cell viability was observed in the presence of $CuCl_2$, with **PR1** and **PR2** being the least cytotoxic, and **PR4** predicted to be BBB permeable. Overall, our studies present a viable framework that could be used to develop chemical reagents to studying the correlation between Aβ and metal ions in AD. Furthermore modifications, such as the incorporation of a dimethylamino moiety, which has been suggested to be important for Aβ interaction,[12,16,39] could lead to better reactivity toward metal-free and metal-associated Aβ species.

A.4. Experimental section

A.4.1. Materials and procedures

All reagents were purchased from commercial suppliers and used as received unless otherwise stated. The compounds **PR1** (4-amino-5-ethyl-2,4-dihydro-3*H*-1,2,4-triazole-3-thione),[40] **PR2** (3-(methylthio)-5-pyridin-2-yl)-4*H*-1,2,4-triazol-4-amine),[24] **PR3** (4-methyl-5-(pyridin-2-yl)-2,4-dihydro-3*H*-1,2,4-triazole-3-thione,[41] and **PR4** (4-ethyl-5-(quinolin-2-yl)-2-4-dihydro-3*H*-1,2,4-triazole-3-thione)[42] were synthesized according to

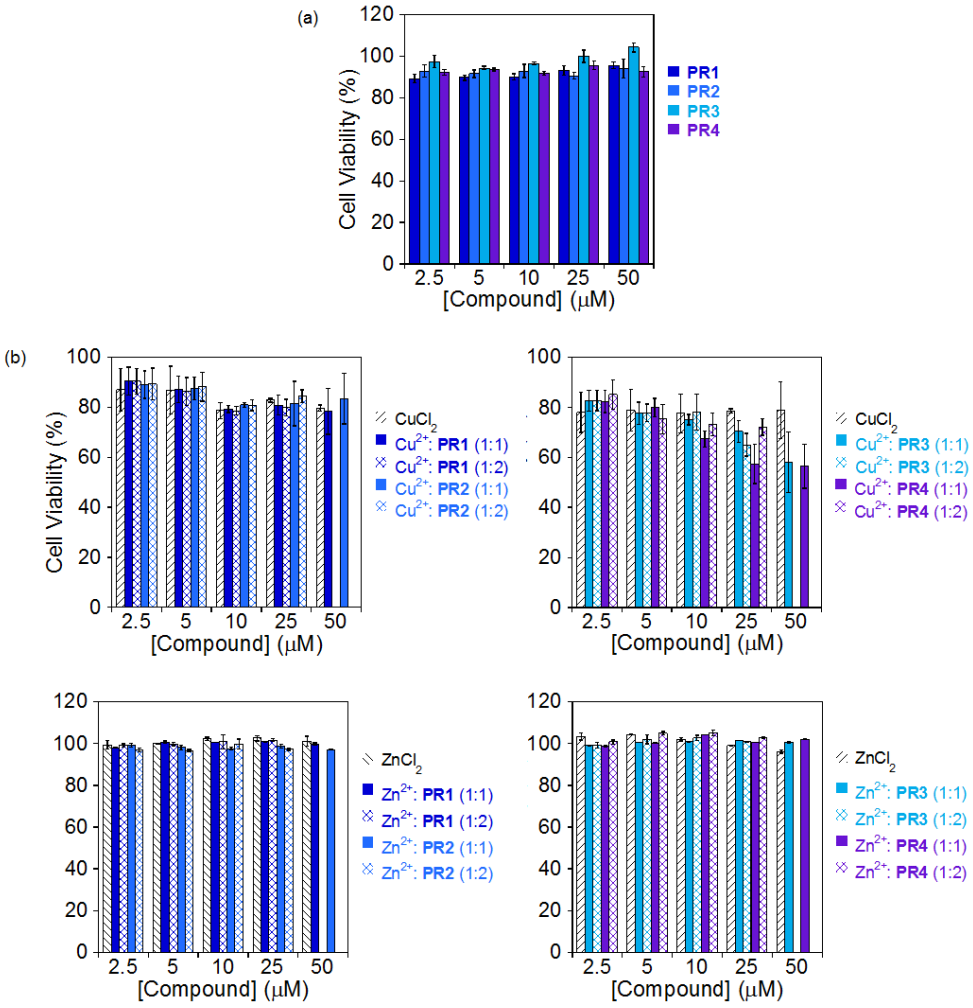

Figure A.6. Cytotoxicity of **PR1**, **PR2**, **PR3**, and **PR4** in SK-N-BE(2)-M17 neuroblastoma cells. (a) Cells were treated with various concentrations of compounds (2.5–50 μM) and (b) various concentrations of compound and metal chloride salts. ([cpd]:[M^{2+}] = 1:1 and 1:2 ratio; M^{2+} = $CuCl_2$ or $ZnCl_2$), incubated for 24 h. The cell viability was assessed by a MTT Assay. The values of cell viability (%) were calculated to cells treated with 1% v/v DMSO.

previous literature. $A\beta_{40}$ (DAEFRHDSGYEVHHQKLVFFAEDVGSNKGAIIGLMVGGVV) and $A\beta_{42}$ (DAEFRHDSGYEVHHQKLVFFAEDVGSNKGAIIGLMVGGVVIA) was purchased from AnaSpec (Fremont, CA). An Agilent 8453 UV-Visible (UV-Vis) spectrophotometer was used to measure the optical spectra. Nuclear magnetic resonance (NMR) spectra of small molecules and for Zn^{2+} binding studies were obtained by a Varian 400 MHz NMR spectrometer. Isothermal calorimetric titrations of $A\beta_{40}$ with compounds were carried out with a MicroCal VP-ITC isothermal titration calorimeter (Northhampton, MA). A SpectraMax M5 microplate reader (Molecular Devices, Sunnyvale, CA) was employed for the measurement of absorbance for 3-(4,5-

dimethylthiazol-2-yl)-2,5-diphenyltetrazolium bromide (MTT) and PAMPA-BBB assays.

A.4.2. Metal binding studies

The interaction of **PR1**, **PR2**, **PR3**, and **PR4** with Cu^{2+} and Zn^{2+} was determined by UV-vis and ^{1}H NMR spectroscopy, respectively, based on previously reported procedures.[11,12,18] A solution of ligand (25 μM in EtOH) was prepared, treated with 1 to 5 equiv of $CuCl_2$, and incubated at room temperature for 5 min. The optical spectra of the resulting solutions were measured by UV-vis. The interaction of **PR1**, **PR2**, **PR3**, or **PR4** with $ZnCl_2$ was observed by ^{1}H NMR. $ZnCl_2$ (1 equiv) was added to a solution of **PR1/3** (8 mM) or **PR4** (4 mM) in CD_3CN. Zinc binding (1 equiv) was performed for **PR2** (8 mM) in CD_3OH.

A.4.3. Isothermal calorimetry studies

Solutions of ligand (200 μM) and $A\beta_{40}$ (20 μM) HEPES buffer (20 μM, pH 7.4; NaCl 150 μM; 10% v/v DMSO) were prepared and degassed for 10 min prior to titration. The ligand solution (10 μL/injection) was injected over 1 s (25 times, with 200 sec interval between each injection) into a solution of $A\beta_{40}$ using a motor-driven 250 μL syringe (rotating speed of 310 rpm) at 25 °C. The heat of dilution was calculated by titrating ligand solution into buffer solution without the presence of $A\beta_{40}$. Heat values of binding were measured by subtracting the heat of dilution values from the experimental results. Titration data were analyzed by using MicroCal Origin, version 7.0 software. The binding curves were fitted with a one-site binding or sequential model, affording the overall heat values of thermodynamic parameters.[31]

A.4.4. Docking studies

Flexible ligand docking studies using AutoDock Vina[29] for **PR1**, **PR2**, **PR3**, and **PR4** were conducted against the $A\beta_{40}$ monomer from the previously determined aqueous solution NMR structure (PDB 2LFM).[30] Ten conformations were selected from 20 conformations within the PDB file (1, 3, 5, 8, 10, 12, 13, 16, 17, and 20). The MMFF94 energy minimization in ChemBio3D Ultra 11.0 was used to optimize the structures of the ligands for the docking studies. The structural files of **PR1**, **PR2**, **PR3**,

PR4, and the peptide were generated by AutoDock Tools and imported into PyRx,[43] which was used to run AutoDock Vina. The search space dimensions were set to contain the entire peptide. The exhaustiveness for the docking runs was set at 1024. Docked poses of the ligands were visualized with Aβ using Pymol.

A.4.5 Amyloid-β (Aβ) peptide

$A\beta_{40}$ was used in all Aβ experiments. $A\beta_{40}$ peptide (1 mg) was dissolved with ammonium hydroxide (NH_4OH, 1% v/v, aq), aliquoted, lyophilized, and stored at –80 °C. A stock solution (*ca*. 200 μM) was prepared by redissolving Aβ with NH_4OH (1% v/v, aq, 10 μL) followed by dilution with ddH_2O. All Aβ solutions were prepared following previously reported procedures.[11,12,18,28] The buffered solutions (20 μM HEPES, pH 6.6 (for Cu^{2+} samples) or pH 7.4 (for metal-free and Zn^{2+} samples), 150 μM NaCl) were used for both inhibition and disaggregation studies. For the inhibition experiment, Aβ (25 μM) was first treated with a metal chloride salt ($CuCl_2$ or $ZnCl_2$, 25 μM) for 2 min followed by addition of a compound (**PR1**, **PR2**, **PR3**, or **PR4**, 50 μM in DMSO, 1% v/v final DMSO concentration). The resulting samples were incubated at 37 °C for 24 h with constant agitation. For the disaggregation experiment, Aβ and a metal chloride salt ($CuCl_2$ or $ZnCl_2$) were initially incubated at 37 °C for 24 h with steady agitation. The compound was added afterwards followed by additional 24 h incubation at 37 °C with constant agitation.

A.4.6. Gel electrophoresis with Western blot

The Aβ peptide experiments (as described above) were analyzed by gel electrophoresis with Western blot using an anti-Aβ antibody (6E10).[11,12,18,28,44] Each sample containing 25 μM Aβ (10 μL) was separated using either a 10–20% gradient Tris-tricine gel (Invitrogen, Grand Island, NY). The gel was transferred to a nitrocellulose membrane and blocked overnight with bovine serum albumin (BSA, 3% w/v, Sigma, St. Louis, MO) dissolved in Tris-buffered saline (TBS, Fisher, Pittsburg, PA) containing 0.1% Tween-20 (TBS-T, Sigma). The membrane was treated with 6E10 (1:2,000; 2% BSA in TBS-T, Covance, Princeton, NJ) for 4 h at room temperature. The membrane

was probed with a horseradish peroxidase-conjugated goat anti-mouse secondary antibody (1:5,000; Cayman Chemical, Ann Arbor, MI) in 2% BSA in TBS-T solution for 1 h at room temperature. The protein bands were visualized using the Thermo Scientific Supersignal West Pico Chemiluminescent Subtrate (Rockford, IL).

A.4.7. Trolox Equivalence Antioxidant Capacity assay (TEAC)

The TEAC assay was used to determine the antioxidant ability based on the extent of decolorization of ABTS (2,2'-azino-bis(3-ethylbenzothiazoline-6-sulfonic acid) diammonium salt) cation radical relative to that of the vitamin E analogue, Trolox.[32] The assay was performed according to the previously reported method with slight modifications.[18,32,33,45] First, blue $ABTS^{+\bullet}$ cation radicals were generated by dissolving ABTS (19 mg, 7.0 mM) with potassium persulfate (3.3 mg, 2.5 mM) in 5 mL water and incubating for 16 h in the dark at room temperature. The resulting $ABTS^{+\bullet}$ solution was diluted with EtOH to an absorbance of *ca.* 0.7 at 734 nm. The assay was conducted in a clear 96 well plate to which 200 μL diluted $ABTS^{+\bullet}$ solution was added and incubated at 30 °C for 5 min in the plate reader. Each ligand was added from a stock solution prepared in DMSO (1% v/v) or in EtOH (for Trolox) and was incubated with the $ABTS^{+\bullet}$ solution at 30 °C for different time periods (2 min intervals up to 20 min). The percent inhibition was calculated according to the measured absorbance at 734 nm (% Inhibition = $100 \times (A - A_0)/A_0$) and was plotted as a function of ligand concentration. The TEAC value of compounds for each time point was calculated as a ratio of the slope of the standard curve of the compound to that of Trolox. The measurements were carried out in triplicate.

A.4.8. Cytotoxicity (MTT Assay)

The human neuroblastoma SK-N-BE(2)-M17 (M17) cell line was purchased from the American Type Cell Collection (ATCC, Manassas, VA, USA). M17 cells were maintained in media containing [1:1 Minimum Essential Media (MEM, Invitrogen)/Ham's F12 Nutrient Mixture (Invitrogen)], respectively, supplemented with 10% FBS (Atlanta Biologicals, Atlanta, GA, USA) and 100 U/mL penicillin and 100 mg/mL streptomycin (Invitrogen). The cells were grown in a humidified atmosphere with 5% CO_2 at 37 °C.

For the MTT assay (MTT = 3-(4,5-dimethyl-2-thiazolyl)-2,5-diphenyl-2H-tetrazolium bromide), M17 cells were seeded in a 96 well plate (15,000 cells/100 μL). The M17 cells were treated in parallel with only metal salts ($CuCl_2$ or $ZnCl_2$), **PR1**, **PR2**, **PR3**, and **PR4**, or metal/**PR1**, **PR2**, **PR3**, and **PR4** (1:2 metal/compound ratio). After incubation, 25 μL MTT (5 mg/mL in phosphate buffered saline (PBS, pH 7.4, Gibco, Grand Island, NY, USA) was added to each well and the plate was incubated for 4 h at 37 °C. Formazan produced by the cells was solubilized using an acidic solution of *N*,*N*-dimethylformamide (50%, v/v aq) and sodium dodecyl sulfate (SDS, 20%, w/v) overnight at room temperature in the dark. The absorbance was measured at 600 nm using a microplate reader. Cell viability was calculated relative to cells containing an equivalent amount of DMSO.

A.4.9. Parallel Artificial Membrane Permeability Assay adapted for blood-brain barrier (PAMPA-BBB)

PAMPA-BBB experiments were carried out using the PAMPA Explorer kit (Pion Inc. Billerica, MA) with modification to previously reported protocols.[12,34,35,38] Each stock solution was diluted with pH 7.4 Prisma HT buffer (Pion) to a final concentration of 25 μM (1% v/v final DMSO concentration) and 200 μL were added to the wells of the donor plate (number of replicates = 12). BBB-1 lipid formulation (5 μL, Pion) was used to coat the polyvinylidene fluoride (PVDF, 0.45 μM) filter membrane on the acceptor plate. The acceptor plate was placed on top of the donor plate forming a sandwich and the brain sink buffer (BSB, 200 μL, Pion) was added to each well of the acceptor plate. The sandwich was incubated for 4 h at ambient temperature without stirring. UV-vis spectra of the solutions in the reference, acceptor, and donor plates were measured using a microplate reader. The PAMPA Explorer software v. 3.5 (Pion) was used to calculate the $-\log P_e$ for each compound. CNS± designations were assigned by comparison to compounds that were identified in previous reports.[12,34,35,38]

A.5. References

(1) Thies, W.; Bleiler, L. *Alzheimers Dement.* **2013**, *9*, 208.
(2) Kepp, K. P. *Chem. Rev.* **2012**, *112*, 5193.

(3) Hardy, J. A.; Higgins, G. A. *Science* **1992**, *256*, 184.
(4) Jakob-Roetne, R.; Jacobsen, H. *Angew. Chem., Int. Ed.* **2009**, *48*, 3030.
(5) Rauk, A. *Chem. Soc. Rev.* **2009**, *38*, 2698.
(6) Scott, L. E.; Orvig, C. *Chem. Rev.* **2009**, *109*, 4885.
(7) DeToma, A. S.; Salamekh, S.; Ramamoorthy, A.; Lim, M. H. *Chem. Soc. Rev.* **2012**, *41*, 608.
(8) Savelieff, M. G.; Lee, S.; Liu, Y.; Lim, M. H. *ACS Chem. Biol.* **2013**, *8*, 856.
(9) Pithadia, A. S.; Lim, M. H. *Curr. Opin. Chem. Biol.* **2012**, *16*, 67.
(10) Rodríguez-Rodríguez, C.; Telpoukhovskaia, M.; Orvig, C. *Coord. Chem. Rev.* **2012**, *256*, 2308.
(11) Hindo, S. S.; Mancino, A. M.; Braymer, J. J.; Liu, Y.; Vivekanandan, S.; Ramamoorthy, A.; Lim, M. H. *J. Am. Chem. Soc.* **2009**, *131*, 16663.
(12) Choi, J. S.; Braymer, J. J.; Nanga, R. P.; Ramamoorthy, A.; Lim, M. H. *Proc. Natl. Acad. Sci. U. S. A.* **2010**, *107*, 21990.
(13) Braymer, J. J.; Choi, J.-S.; DeToma, A. S.; Wang, C.; Nam, K.; Kampf, J. W.; Ramamoorthy, A.; Lim, M. H. *Inorg. Chem.* **2011**, *50*, 10724.
(14) Choi, J.-S.; Braymer, J. J.; Park, S. K.; Mustafa, S.; Chae, J.; Lim, M. H. *Metallomics* **2011**, *3*, 284.
(15) Jones, M. R.; Service, E. L.; Thompson, J. R.; Wang, M. C.; Kimsey, I. J.; DeToma, A. S.; Ramamoorthy, A.; Lim, M. H.; Storr, T. *Metallomics* **2012**, *4*, 910.
(16) Pithadia, A. S.; Kochi, A.; Soper, M. T.; Beck, M. W.; Liu, Y.; Lee, S.; DeToma, A. S.; Ruotolo, B. T.; Lim, M. H. *Inorg. Chem.* **2012**, *51*, 12959.
(17) Liu, Y.; Kochi, A.; Pithadia, A. S.; Lee, S.; Nam, Y.; Beck, M. W.; He, X.; Lee, D.; Lim, M. H. *Inorg. Chem.* **2013**, *52*, 8121.
(18) Lee, S.; Zheng, X.; Krishnamoorthy, J.; Savelieff, M. G.; Park, H. M.; Brender, J. R.; Kim, J. H.; Derrick, J. S.; Kochi, A.; Lee, H. J.; Kim, C.; Ramamoorthy, A.; Bowers, M. T.; Lim, M. H. *J. Am. Chem. Soc.* **2014**, *136*, 299.
(19) Ashour, H. M.; Shaaban, O. G.; Rizk, O. H.; El-Ashmawy, I. M. *Eur. J. Med. Chem.* **2013**, *62*, 341.
(20) Varvaresou, A.; Siatra-Papastaikoudi, T.; Dalla Tsotinis, A.; Tsantili-Kakoulidou, A.; Vamvakides, A. *Farmaco* **1998**, *53*, 320.
(21) Tardito, S.; Bassanetti, I.; Bignardi, C.; Elviri, L.; Tegoni, M.; Mucchino, C.; Bussolati, O.; Franchi-Gazzola, R.; Marchio, L. *J. Am. Chem. Soc.* **2011**, *133*, 6235.
(22) Khan, I.; Ibrar, A.; Abbas, N. *Eur. J. Med. Chem.* **2013**, *63*, 854.
(23) Ferreira, V. F.; da Rocha, D. R.; da Silva, F. C.; Ferreira, P. G.; Boechat, N. A.; Magalhaes, J. L. *Expert Opin. Ther. Pat.* **2013**, *23*, 319.
(24) Dallavalle, F.; Gaccioli, F.; Franchi-Gazzola, R.; Lanfranchi, M.; Marchio, L.; Pellinghelli, M. A.; Tegoni, M. *J. Inorg. Biochem.* **2002**, *92*, 95.
(25) Ferloni, E.; Lanfranchi, M.; Marchio, L.; Metta, G.; Pellinghelli, M. A.; Tegoni, M. *Inorg. Chim. Acta* **2005**, *358*, 147.
(26) Gaccioli, F.; Franchi-Gazzola, R.; Lanfranchi, M.; Marchio, L.; Metta, G.; Pellinghelli, M. A.; Tardito, S.; Tegoni, M. *J. Inorg. Biochem.* **2005**, *99*, 1573.
(27) Tardito, S.; Bussolati, O.; Maffini, M.; Tegoni, M.; Giannetto, M.; Dall'asta, V.; Franchi-Gazzola, R.; Lanfranchi, M.; Pellinghelli, M. A.; Mucchino, C.; Mori, G.; Marchio, L. *J. Med. Chem.* **2007**, *50*, 1916.

(28) Hyung, S. J.; DeToma, A. S.; Brender, J. R.; Lee, S.; Vivekanandan, S.; Kochi, A.; Choi, J. S.; Ramamoorthy, A.; Ruotolo, B. T.; Lim, M. H. *Proc. Natl. Acad. Sci. U. S. A.* **2013**, *110*, 3743.
(29) Trott, O.; Olson, A. J. *J. Comput. Chem.* **2010**, *31*, 455.
(30) Vivekanandan, S.; Brender, J. R.; Lee, S. Y.; Ramamoorthy, A. *Biochem. Biophys. Res. Commun.* **2011,** *411*, 312.
(31) Wang, S. H.; Liu, F. F.; Dong, X. Y.; Sun, Y. *J. Phys. Chem. B* **2010**, *114*, 11576.
(32) Re, R.; Pellegrini, N.; Proteggente, A.; Pannala, A.; Yang, M.; Rice-Evans, C. *Free Radic. Biol. Med.* **1999**, *26*, 1231.
(33) Schugar, H.; Green, D. E.; Bowen, M. L.; Scott, L. E.; Storr, T.; Bohmerle, K.; Thomas, F.; Allen, D. D.; Lockman, P. R.; Merkel, M.; Thompson, K. H.; Orvig, C. *Angew. Chem., Int. Ed.* **2007**, *46*, 1716.
(34) Di, L.; Kerns, E. H.; Fan, K.; McConnell, O. J.; Carter, G. T. *Eur. J. Med. Chem.* **2003**, *38*, 223.
(35) Avdeef, A.; Bendels, S.; Di, L.; Faller, B.; Kansy, M.; Sugano, K.; Yamauchi, Y. *J. Pharm. Sci.* **2007**, *96*, 2893.
(36) Lipinski, C. A.; Lombardo, F.; Dominy, B. W.; Feeney, P. J. *Adv. Drug Delivery Rev.* **2001**, *46*, 3.
(37) Clark, D. E.; Pickett, S. D. *Drug Discovery Today* **2000**, *5*, 49.
(38) *BBB Protocol and Test Compounds; Pion Inc.; Wolburn, MA, 2009*.
(39) Leuma Yona, R.; Mazeres, S.; Faller, P.; Gras, E. *ChemMedChem* **2008**, *3*, 63.
(40) Cingi, M. B.; Lanfranchi, M.; Pellinghelli, M. A.; Tegoni, M. *Eur. J. Inorg. Chem* **2000**, 703.
(41) Gennari, M.; Giannetto, M.; Lanfranchi, M.; Marchio, L.; Pellinghelli, M. A.; Tegoni, M. *Polyhedron* **2004**, *23*, 1829.
(42) Keshk, E. M.; El-Desoky, S. I.; Hammouda, M. A. A.; Abdel-Rahman, A. H.; Hegazi, A. G. *Phosphorus, Sulfur, and Silicon* **2008**, *183*, 1323.
(43) Wolf, L. K. *Chem. Eng. News* **2009**, *87*, 31.
(44) Reinke, A. A.; Seh, H. Y.; Gestwicki, J. E. *Bioorg. Med. Chem. Lett.* **2009**, *19*, 4952.
(45) He, X.; Park, H. M.; Hyung, S. J.; DeToma, A. S.; Kim, C.; Ruotolo, B. T.; Lim, M. H. *Dalton Trans.* **2012**, *41*, 6558.